

# Characterization of hypertrophy-related effectors in *Ustilago maydis* induced tumor formation



**Inaugural-Dissertation**

**zur Erlangung des Doktorgrades der Naturwissenschaften**

**Dr.rer.nat.**

der Mathematisch-Naturwissenschaftlichen Fakultät

der Universität zu Köln

vorgelegt von

**Yoon Joo Lee**

aus Incheon, Korea

Köln, 2024



**Characterization of hypertrophy-related effectors in  
*Ustilago maydis* induced tumor formation**

**Inaugural-Dissertation**

**zur Erlangung des Doktorgrades der Naturwissenschaften**

**Dr.rer.nat.**

der Mathematisch-Naturwissenschaftlichen Fakultät

der Universität zu Köln

vorgelegt von

**Yoon Joo Lee**

aus Incheon, Korea

Köln, 2024

Die Untersuchungen zur vorliegenden Arbeit wurden von September 2019 bis Mai 2024 am Lehrstuhl für Terrestrische Mikrobiologie an der Universität zu Köln unter der Betreuung von Herrn Prof. Dr. Gunther Döhlemann durchgeführt.

**Erstgutachter:** Prof. Dr. Gunther Döhlemann

**Zweitgutachter:** Prof. Dr. Bart Thomma

**Tag der mündlichen Prüfung:** 11.07.24

## Summary

*Ustilago maydis*, a biotrophic corn smut fungus, secretes a cocktail of effectors in a spatiotemporal regulated manner to induce nutrient-rich tumors in all aerial parts of maize. By down-regulating genes linked to photosynthesis and increasing hexose accumulation in developing tumors, it manipulates the host's metabolic processes and alters the sink-source transition (Doehlemann et al., 2008a; Horst et al., 2008, 2010). Cell type-specific transcriptome profiling of *U. maydis* has revealed that a set of effectors are highly and specifically up-regulated in hypertrophy, leading to the enlargement of tumor cells through endoreduplication (Matei et al., 2018). This study focused on identifying and functionally characterizing *U. maydis* effectors involved in hypertrophy induction. Through various screening and selection methods, we have identified **h**ypertrophy-**a**ssociated **p**roteins 1-3 (Hap1-3) which are highly expressed at 2 days post infection (dpi) as potential hypertrophic mesophyll tumor cell (HTT) effectors. Pull-down of Hap effectors followed by mass-spectrometry analysis revealed that Hap effectors interact within the host cell, suggesting potential formation of effector complex. To gain insights into the cooperative mechanisms of Hap effectors, double and triple frameshift knockout mutants of *hap1*, *hap2*, and *hap3* were generated, and a large-scale mass spectrometry analysis was conducted. These analyses revealed that Hap1 is the dominant HTT-related virulence factor. Furthermore, Hap1 interacted with maize Snf1-related protein kinase 1 (SnRK1), a key regulator of cellular energy and nutrient homeostasis, which is activated by phosphorylation under energy deprivation. To explore Hap1's influence on the global gene expression within the host, RNA-seq analysis was performed. *Hap1* showed high expression levels of *AGPase3*, *SBEI*, and *Ae1* involved in starch biosynthesis. Conversely, the *hap1* frameshift knockout mutant exhibited high expression of WRKY transcription factors, wall-associated kinases, and lectin domain-containing receptor kinases, indicating that the frameshift knockout mutant of *hap1* induces a plant defense response. Quantitative phosphoproteomics analysis comparing Hap1 frameshift knockout mutants to wild-type infected plants revealed that SnRK1 and key metabolic enzymes are increased in phosphorylation in response to infection by the wild-type. Our findings support a model where *U. maydis*, in the presence of Hap1, targets the SnRK1 $\alpha$  subunit. This targeting prevents SnRK1 inhibition by high levels of T6P, thereby disrupting the antagonistic relationship between T6P and SnRK1 and reprogramming transcription required for starch metabolism and inhibiting sugar-induced immune signaling.

# Table of contents

<b>Summary</b> .....	<b>I</b>
<b>Table of contents</b> .....	<b>II</b>
<b>List of Abbreviations</b> .....	<b>VII</b>
<b>1. Introduction</b> .....	<b>1</b>
1.1 Plant pathogenic interactions .....	1
1.1.1 Pathogenic strategies of fungi in plant-pathogen interactions .....	1
1.1.2 Plant innate immunity .....	2
1.1.3 Effectors: The key factors in manipulating the host .....	5
1.1.4 Effectors: Unveiling antimicrobial strategies .....	8
1.1.5 Regulation and functions of SnRK1: a key player in plant energy homeostasis and immunity .....	8
1.2 <i>Ustilago maydis</i> – the causative agent of corn smut.....	10
1.2.1 The life cycle of <i>Ustilago maydis</i> .....	10
1.3 Maize physiology and its metabolic regulation by <i>Ustilago maydis</i> .....	13
1.3.1 C <sub>4</sub> metabolism of maize .....	13
1.3.2 <i>Ustilago maydis</i> induces changes in maize physiology .....	14
1.4 Effectors of <i>Ustilago maydis</i> .....	14
1.4.1 <i>Ustilago maydis</i> effectors involved in modulation of extracellular plant immunity .....	15
1.4.2 <i>Ustilago maydis</i> effectors involved in host metabolic regulation.....	16
1.4.3 Organ and cell type specificity in effectors.....	17
1.5 Aim of this study.....	19
<b>2. Results</b> .....	<b>20</b>
2.1 Functional characterization of HTT candidates in <i>Ustilago maydis</i> effectors.....	20
2.2 Identification of Hap effector targets .....	23
2.2.1 Hap effectors of <i>Ustilago maydis</i> interact with each other <i>in planta</i> .....	24
2.2.2 Hap effectors interact <i>in vivo</i> in split-luciferase complementation assay and co-immunoprecipitation .....	26
2.2.3 Hap1 is the key virulence effector among Hap effectors .....	28
2.3 Identification of maize targets upon <i>Ustilago maydis</i> infection .....	29

2.3.1 Hap1 interacts with all of the catalytic SnRK1 $\alpha$ subunits, a central metabolic regulator .....	29
2.3.2 Disrupting Hap effector network alters Hap1's host interaction partner .....	30
2.3.3 Hap1 interacts with the catalytic subunit of ZmSnRK1 in the split-luciferase complementation assay and co-IP .....	34
2.4 Phosphoproteomic analysis of maize upon <i>Ustilago maydis</i> infection .....	36
2.5 Hap1 is involved in the reprogramming of primary metabolism.....	41
2.5.1 Differential gene expression analysis in SG200 and SG200 $\Delta$ <i>hap1</i> infected leaves .....	41
2.5.2 Hap1 is required for starch accumulation .....	47
2.5.3 Hap1 is involved in altering sugar allocation in maize seedlings upon <i>Ustilago maydis</i> infection .....	49
<b>3. Discussion.....</b>	<b>52</b>
3.1. Hap effectors are essential for virulence.....	52
3.1.1 Hap effectors show maize line-specific regulation in <i>Ustilago maydis</i> virulence..	52
3.1.2 Hap1, 2, and 3 are forming a potential Hap effector complex .....	53
3.2. Hap1-host interaction in <i>Ustilago maydis</i> .....	54
3.2.1. Interaction of Hap1 with the central metabolic switch ZmSnRK1 .....	54
3.2.2. Disrupting Hap effector complex alters Hap1's host interaction partner.....	56
3.3. Phosphorylation profile of <i>Ustilago maydis</i> infected leaf tissue .....	57
3.3.1. The presence of Hap1 in <i>Ustilago maydis</i> alters ZmSnRK1 phosphorylation of ZmSnRK1 $\alpha$ , $\beta$ , and $\gamma$ subunits .....	57
3.3.2. The presence of Hap1 in <i>Ustilago maydis</i> alters ZmSnRK1 phosphorylation-mediated signaling .....	60
3.4. Hap1 regulates expression of key enzymes involved in starch biosynthesis.....	63
3.5. Hap1 is required for starch accumulation in <i>Ustilago maydis</i> -induced tumor cells .....	64
3.6. Enzymatic quantification of soluble sugars in <i>Ustilago maydis</i> -induced tumor cells ..	65
3.7. Working model of Hap1-SnRK1 interaction in starch metabolism .....	66
3.8. Perspective / future outlooks.....	67
<b>4. Material and Methods .....</b>	<b>69</b>
4.1 Material and Methods .....	69
4.1.1 Chemicals.....	69

4.1.2 Buffers and Solutions.....	69
4.1.3 Enzymes, antibodies, and IP trap beads .....	69
4.2 Media and cultivation methods for microorganisms .....	71
4.2.1 Media .....	71
4.2.2 Cultivation of <i>E. coli</i> .....	72
4.2.3 Cultivation of <i>A. tumefaciens</i> .....	73
4.2.4 Cultivation of <i>S. cerevisiae</i> .....	73
4.2.5 Cultivation of <i>U. maydis</i> .....	73
4.2.6 Measurement of cell density .....	73
4.3 Microbial strains, plasmids, and oligonucleotides.....	73
4.3.1 <i>E. coli</i> strains.....	73
4.3.2 <i>A. tumefaciens</i> strains.....	74
4.3.3 <i>S. cerevisiae</i> strains .....	74
4.3.4 <i>U. maydis</i> strains .....	74
4.3.5 Oligonucleotides .....	75
4.3.6 Plasmids .....	78
4.3.6.1 Plasmids for <i>U.maydis</i> transformation.....	78
4.3.6.2. Plasmids for the transformation of <i>S. cerevisiae</i> and yeast two-hybrid analysis .....	79
4.3.6.3. Plasmids for transient expression of proteins in <i>N. benthamiana</i> via.....	80
<i>A. tumefaciens</i> -mediated transformation .....	80
4.4 Standard microbiological methods .....	81
4.4.1 Competent cell preparation of <i>E. coli</i> .....	81
4.4.2 Heat-shock transformation of <i>E. coli</i> .....	82
4.4.3 Competent cell preparation and transformation of <i>A. tumefaciens</i> .....	82
4.4.4 Protoplast preparation of <i>U. maydis</i> .....	82
4.4.5 Transformation of <i>U. maydis</i> .....	83
4.4.6 Filamentous growth test for <i>U. maydis</i> .....	83
4.4.7 <i>In-vitro</i> impairment growth test for <i>U. maydis</i> .....	84
4.4.8 Competent cell preparation and transformation of <i>S. cerevisiae</i> .....	84
4.4.9 Dropout assay for <i>S. cerevisiae</i> .....	85
4.5 Molecular microbiological methods .....	85



4.5.1 Isolation of nucleic acids.....	85
4.5.1.1 Isolation of plasmid DNA from <i>E. coli</i> .....	85
4.5.1.2 Isolation of genomic DNA from <i>U. maydis</i> .....	85
4.5.1.3 Total RNA isolation from infected maize tissue.....	86
4.5.1.4. DNase treatment of isolated RNA.....	86
4.5.1.5 cDNA synthesis.....	87
4.5.1.6 Quantitative real-time PCR (qRT-PCR).....	87
4.5.2 Nucleic acid modification.....	87
4.5.2.1 Restriction enzyme digestion of DNA.....	87
4.5.2.2 Ligation of DNA fragments.....	88
4.5.2.3 Gibson assembly cloning.....	88
4.5.2.4 Site-directed mutagenesis.....	88
4.5.2.5 Polymerase chain reaction (PCR).....	88
4.5.3 Purification PCR fragments product.....	88
4.5.4 DNA sequencing and RNA sequencing.....	89
4.5.5 Agarose gel electrophoresis.....	89
4.5.6 Southern blot analysis.....	89
4.6 Protein methods and biochemical assays.....	91
4.6.1 Protein heterologous protein expression in <i>N. benthamiana</i> .....	91
4.6.2 Protein extraction from <i>S. cerevisiae</i> .....	91
4.6.3 Protein extraction from <i>Z. mays</i> or <i>N. benthamiana</i> .....	92
4.6.4 Co-immunoprecipitation assay in plant.....	92
4.6.4.1 Co-immunoprecipitation of proteins in maize and followed by Liquid chromatography-mass spectrometry/ mass spectrometry (LC-MS/MS).....	93
4.6.4.2 Total protein extraction for phosphoproteomic analysis.....	93
4.6.5 SDS polyacrylamide gel electrophoresis (SDS-PAGE).....	93
4.6.6 Western blot.....	94
4.6.7 Coomassie staining of proteins.....	96
4.7 Plant assays.....	96
4.7.1 <i>Zea mays</i> material.....	96

4.7.2 Cultivation of <i>Z. mays</i> .....	96
4.7.3 <i>U. maydis</i> infection of <i>Z. mays</i> .....	96
4.7.4 Cultivation of <i>N. benthamiana</i> .....	97
4.7.5 Split-luciferase complementation (split-LUC) assay .....	97
4.8 Tissue fixation, staining, quantification, and microscopy .....	97
4.8.1 Soluble sugar enzymatic quantification .....	97
4.8.2 Starch enzymatic quantification .....	98
4.8.3 Paraplast embedding of maize leaf tissue .....	98
4.8.4 Starch Lugol staining .....	99
4.8.5 Thunder microscopy .....	99
4.8.6 Confocal laser-scanning microscopy .....	99
4.9 Bioinformatics methods .....	99
4.9.1 RNA-Seq analysis .....	99
4.9.2 GO enrichment analysis .....	100
4.9.3 KEGG enrichment analysis .....	100
<b>5. Bibliography .....</b>	<b>101</b>
<b>6. Supplementary figures and tables .....</b>	<b>125</b>
<b>Erklärung zur Dissertation .....</b>	<b>136</b>
<b>Delimitation of own contribution .....</b>	<b>137</b>
<b>Acknowledgement .....</b>	<b>138</b>
<b>Curriculum Vitae .....</b>	<b>140</b>

## List of Abbreviations

°C	Degree Celsius		
x g	Gravitational acceleration on earth (9.81m/s <sup>2</sup> )	KOH	Potassium Hydroxide
µg	Microgram	LC/MS	Liquid chromatography–mass spectrometry
µl	Microliter	Lox3	Lipoxygenase 3
µm	Micrometer	LRR	Leucine-rich repeat
µM	Micromolar	LysM	Lysin motif
Adi3	AvrPto-dependent Pto-interacting protein 3	Lox3	Lipoxygenase 3
AFP1&2	Anti-fungal protein 1 & 2	M	Molar
AGPase	Adenosine 5' diphosphate-glucose pyrophosphorylase	MAMK	Mitogen activated protein kinase
AKIN	<i>A. thaliana</i> SNF1-related kinase	M	Mesophyll; mock
AMP	Antimicrobial peptide 2	MeOH	Methanol
AMPK	AMP-activated protein kinase	MgCl <sub>2</sub>	Magnesium chloride
AMY	Alpha-amylase	MgSO <sub>4</sub>	Magnesium sulphate
ANOVA	Analysis of variance	min	Minute(s)
ApB73	Apathogenic in B73	ml	Millilitre
Avr	Avirulence	mRNA	Messenger RNA
Ave1	Avirulence on ve1	NaCl	Sodium Chloride
BAK1	BR11-associated receptor kinase 1	NB	Nucleotide binding
bp	Base pair	ng	Nanogram
BIC	Biotrophic interfacial complex	nLUC	Amino-terminal half of luciferase
BAM	Beta-amylase	nm	Nanometer
BS	Bundle sheath	nt	Nucleotide
Carb	Carbenicillin	OD	Optical density
CBM	Carbohydrate-binding module	OG	Oligogalacturonide
CBS	Cystathionine-β synthase	Osp24	Orphan protein 24
Cbx	Carboxin	P	p-value
CC	Coiled-coil	PAGE	Polyacrylamide gel electrophoresis
Cce1	Cysteine-rich core effector	PAMP	Pathogen associated molecular pattern
CDPK	Calcium dependent protein kinase	PCA	Principle component analysis
Cda7	Chitin deacetylase 7	PCR	Polymerase chain reaction
CERK	Chitin elicitor receptor kinase 1	PCWDE	Plant cell wall degrading enzyme
CINV	Cell wall invertase	Pep1	Protein essential during penetration 1
cLUC	Carboxyl-terminal half of luciferase	PEP	Phosphoenol pyruvate

<b>Cmu1</b>	Chorismate mutase 1	<b>Pit2</b>	Protein involved in tumors 2
<b>Co-IP</b>	Co-immunoprecipitation	<b>PP2A&amp;C</b>	Protein phosphatase 2A&C
<b>Cryo-EM</b>	Cryo-electron microscopy	<b>PPP2CB</b>	Protein phosphatase 2 catalytic subunit beta
<b>CRISPR-cas9</b>	Clustered regularly interspaced short palindromic repeats and CRISPR-associated protein 9	<b>PRR</b>	Pattern recognition receptor
<b>DAMP</b>	Damage associated molecular pattern	<b>PTI</b>	Pattern-triggered immunity
<b>DBE</b>	Debranching enzyme	<b>PTPA</b>	Phosphotyrosyl phosphatase activator
<b>DEGs</b>	Differentially expressed genes	<b>QDR</b>	Quantitative disease resistance
<b>DMSO</b>	Dimethylsulfoxid	<b>qPCR</b>	Quantitative polymerase chain reaction
<b>DNA</b>	Deoxyribonucleic acid	<b>R5P</b>	Ribose-5-phosphate
<b>dNTP</b>	Deoxynucleoside triphosphates	<b>Rgt2p</b>	Regulator of glucose transport protein 2
<b>dpi</b>	Days post infection	<b>Rif</b>	Rifampicin
<b>DUF26</b>	Domain of unknown function	<b>RK</b>	Receptor kinase
<b>DTT</b>	Dithiotreitol	<b>RLP</b>	Receptor-like protein
<b>EAR</b>	Ethylene-responsive element binding factor-associated amphiphilic repression	<b>ROS</b>	Reactive oxygen species
<b>EDTA</b>	Ethylenediaminetetraacetic acid	<b>RNA</b>	Ribonucleic acid
<b>EFR</b>	ET-Tu receptor	<b>rpm</b>	Revolutions per minute
<b>ELR</b>	Extensive loop region	<b>RT</b>	Room temperature
<b>EGB</b>	Early golden bantam	<b>Rsp3</b>	Repetitive secreted protein 3
<b>ER</b>	Endoplasmic reticulum	<b>s</b>	Seconds
<b>Erc1</b>	Enzyme required for cell-to-cell extension 1	<b>SBE</b>	Starch branching enzyme
<b>ET</b>	Ethylene	<b>SDS</b>	Sodium Dodecyl Sulphate
<b>ETI</b>	Effector-triggered immunity	<b>SEM</b>	Standard error mean
<b>EtOH</b>	Ethanol	<b>SPS1</b>	Sucrose phosphate synthase 1
<b>ETS</b>	Effector-triggered susceptibility	<b>SnAK1&amp;2</b>	(SnRK1)-activating kinase 1&2
<b>f.c.</b>	Final concentration	<b>SNF1</b>	Sucrose non-fermenting kinase 1
<b>FB1</b>	Fumonisin mycotoxins	<b>SnRK1</b>	Sucrose non-fermenting related kinase 1
<b>Flg22</b>	Bacterial Flagellin peptide 22	<b>Srt1</b>	Saccharose transporter 1
<b>Fly1</b>	Fungalysin 1	<b>SS</b>	Starch synthase
<b>FLS2</b>	Flagellin-sensitive 2&3	<b>Sts2</b>	Small tumor on seedlings 2
<b>FLZ</b>	FCS-like zinc finger	<b>Susy</b>	Sucrose synthase
<b>FW</b>	Fresh weight	<b>T3SS</b>	Type III secretion system
<b>FIMO</b>	Find individual motif occurrences	<b>T4SS</b>	Type IV secretion system
<b>g</b>	Gram	<b>T6P</b>	Trehalose-6-phosphate
<b>G1P</b>	Glucose-1-phosphate	<b>TCA</b>	Tricarboxylic acid
<b>G6P</b>	Glucose-6-phosphate	<b>TEMED</b>	Tetramethylethylenediamine

<b>GB</b>	Golden bantam	<b>Tin2</b>	Tumor inducing 2
<b>Gent</b>	Gentamycin	<b>TIR</b>	Toll/interleukin-1 receptor
<b>GRIK1 &amp; 2</b>	Geminivirus Rep interacting kinase	<b>TPL/TPR</b>	Topless / Topless related protein
<b>GBSS</b>	Granule-bound starch synthase	<b>TPP</b>	T6P synthase
<b>HAP1-3</b>	Hypertrophy associated protein 1-3	<b>TPS</b>	T6P phosphatase
<b>HPT</b>	Hyperplasic tumor cell	<b>TRE</b>	Trehalase
<b>HR</b>	Hypersensitive response	<b>U</b>	Unit (Enzyme activity)
<b>HST</b>	Host-selective toxin	<b>UBA</b>	Ubiquitin associated
<b>HTT</b>	Hypertrophic tumor cell	<b>UDPG</b>	Uridine diphosphate glucose
<b>HXK1</b>	Hexokinase 1	<b>V</b>	Volt
<b>Hxt1</b>	Hexose transporter 1	<b>VIGs</b>	Virus-induced gene silencing
<b>Hyg</b>	Hygromycin	<b>v/v</b>	Volume/volume
<b>IKI</b>	Iodine potassium iodide	<b>w/v</b>	Weight/volume
<b>JA</b>	Jasmonic acid	<b>WAK1</b>	Wall associated kinase 1
<b>KA1</b>	Kinase-associated domain	<b>WT</b>	Wild type
<b>Kan</b>	Kanamycin	<b>TOR</b>	Target of rapamycin
<b>kb</b>	Kilobases	<b>Y2H</b>	Yeast two-hybrid
<b>kDa</b>	Kilodalton		

# 1. Introduction

Plants are sessile organisms that constantly face attacks from a diverse range of destructive microorganisms, such as fungi, oomycetes, bacteria, and viruses. Plant diseases in crops, caused by phytopathogens, have shown an increase in both number and severity as the world is shifting towards a warming world (Bebber et al., 2013; Chaloner et al., 2021). This increase is responsible for global yield losses of up to 40% in five major calorie crops: maize, potato, rice, soybean, and wheat (Savary et al., 2019). In addition, the modern practice of monoculture has led to a decline in crop genetic diversity, creating ideal conditions for the rapid emergence of new invading pathogen variants, including fungi that pose significant economic threats (Steinberg & Gurr, 2020). Among these fungi, Basidiomycota represents a large division of the kingdom Fungi, such as rusts and smuts of economically important plant pathogens. Ustilaginales, belonging to the smut fungi, represent some of the most well-described and effective pathogens of gramineous plants, especially cereals (Kijpornyongpan et al., 2018). In a world where global food demand and the threat of plant diseases are rapidly increasing, understanding plant-microbe interactions, including the infection strategies of phytopathogenic fungi and how plants defend themselves, as well as gaining in-depth knowledge of disease mechanisms, is key to developing new strategies to combat and manage fungal diseases and improve plant resistance to these pathogens.

## 1.1 Plant pathogenic interactions

### 1.1.1 Pathogenic strategies of fungi in plant-pathogen interactions

Plants are photoautotrophs that can sustain themselves by carbon fixation, and these fixed carbons serve as an energy source for the myriad of phytopathogens. To obtain nutrients from plants, phytopathogens have developed diverse lifestyles and infestation strategies to successfully colonize their respective hosts. Based on the mode of nutrient acquisition, they are classified as biotrophs, hemibiotrophs, and necrotrophs (Lo Presti et al., 2015). Necrotrophs, such as *Botrytis cinerea* and *Sclerotinia sclerotiorum*, actively destroy host tissues using toxic metabolites called host-selective toxins (HSTs) and plant cell wall degrading enzymes (PCWDEs) to degrade plant materials and subsequently consume their organic compounds (Horbach et al., 2011; van Kan, 2006). On the contrary, biotrophic fungus *Ustilago maydis*, is dependent on living tissue and uses a combination of turgor pressure and PCWDEs

to invade the intercellular space and break through the loosened cell wall to obtain nutrients from the host (Fei & Liu, 2023; Kubicek et al., 2014). *U. maydis* is also capable of intracellular invasion, whereby intracellular hyphae are fully covered by the host plasma membrane, establishing an interaction interface to acquire nutrition (Djamei & Kahmann, 2012). Similarly, other biotrophic fungi, *Cladosporium fulvum* and *Puccinia graminis* penetrate host cells through open stomata and form specialized structure called haustoria to absorb nutrients without disturbing the host cell wall (Fei & Liu, 2023). Additionally, there are other phytopathogens whose lifestyle lies between necrotrophs and biotrophs. Hemibiotrophs, like *Magnaporthe oryzae* and *Colletotrichum* spp., initially develop biotrophic invasive hyphae and switch to necrotrophic hyphae at later stages of the disease (Lo Presti et al., 2015). Regardless of their classification, whether necrotrophs, biotrophs, or hemibiotrophs, all phytopathogens encounter various plant defense mechanisms to stop or restrict the growth of any phytopathogenic organisms.

### **1.1.2 Plant innate immunity**

In nature, plants have evolved to resist most pathogens by detecting various forms of danger and successfully defending themselves against the pathogen attack with constitutive physical and chemical barriers. Physical barriers, including waxy cuticles and rigid cell walls, serve as their first line of mechanical defense, while secondary metabolites such as flavonoids, glucosinolates, and other antimicrobial compounds act as chemical barriers (Frerigmann et al., 2014; Mierziak et al., 2014; J. Zhang et al., 2020). These two constitutive barriers restrict microbe attachment or entry to the host tissues. However, some successful pathogens have simultaneously evolved sophisticated strategies to evade or subvert these constitutive barriers, such as PCWDEs and fungal chitinase-modifying proteins (Rodriguez-Moreno et al., 2018; J. Zhang et al., 2020). Therefore, beyond constitutive barriers, plants have evolved a robust two-tiered innate immune system for pathogen recognition and defense.

The first layer of innate immunity is triggered when plasma membrane-localized pattern recognition receptors (PRRs), such as receptor kinases (RKs) and receptor-like proteins (RLPs), recognize pathogen- or microbe-associated molecular patterns (PAMPs/MAMPs; hereafter, referred to as PAMPs) (Boutrot & Zipfel, 2017; Dodds & Rathjen, 2010; Y. Wang et al., 2022; Zipfel, 2014) (**Fig. 1**). The most well-characterized PRRs contain leucine-rich repeat (LRR) domains. In Arabidopsis, perception of the 22-residue bacterial flagellin epitope (flg22) and the elf18 epitope of bacterial elongation factor-Tu (EF-Tu) by the PRRs FLAGELLIN

SENSITIVE 2 (FLS2) and EF-Tu receptor (EFR) activates the signal transducer brassinosteroid receptor BRI1-associated receptor kinase1 (BAK1) (Chinchilla et al., 2007; Gómez-Gómez & Boller, 2000; Heese et al., 2007; Zipfel et al., 2006). Other types of PRRs contain lysine motifs (LysM), such as chitin elicitor receptor kinase 1 (CERK1) and LysM-containing proteins, which bind to carbohydrate-based ligands found mostly in cell envelope components. (Cao et al., 2014; de Jonge et al., 2010; Iizasa et al., 2010; Miya et al., 2007; Willmann et al., 2011). In addition to PAMPs, PRRs also recognize damage-associated molecular patterns (DAMPs) released from host cells during pathogen invasion or disrupted plant cell wall polysaccharides due to physical injury (Boller & Felix, 2009; Hou et al., 2019) (**Fig. 1**). The wall-associated kinase 1 (WAK1), for example, is a transmembrane receptor that recognizes oligogalacturonides (OG) which are DAMPs derived from pectic polysaccharide (Brutus et al., 2010).

Upon recognition of PAMPs and DAMPs by PRRs, pattern-triggered immunity (PTI) is initiated, which contributes to basal plant immunity and resistance to most non-adapted pathogens during infection (Boller & Felix, 2009; Boutrot & Zipfel, 2017; Zipfel, 2014). The physiological immune responses of PTI involve a rapid influx of  $Ca^{2+}$  into the cytosol, leading to the generation of extracellular reactive oxygen species (ROS) (Bigeard et al., 2015; Kimura et al., 2017; P. Yuan et al., 2017). The rapid burst of ROS is facilitated by the plasma membrane-localized NADPH oxidase and cell wall peroxidases, which activates downstream signaling, including defense-related mitogen-activated protein kinase (MAPK) cascades and regulation of calcium-dependent protein kinases (CDPKs) (Bigeard et al., 2015; Boller & Felix, 2009; Boudsocq & Sheen, 2013; Couto & Zipfel, 2016). Moreover, chemical and mechanical responses imposed by PTI involve phytohormone regulation, biosynthesis of antibacterial compounds, cell wall reinforcement, and expression of pathogenesis-related (PR) genes (Ahuja et al., 2012; Berens et al., 2017; Couto & Zipfel, 2016; Lee et al., 2015; Pieterse et al., 2012). Although PTI provides robust defense mechanisms against most pathogens, these mechanisms may not be sufficient to defend against successful and host-adapted pathogens. To evade PTI, host-adapted pathogens secrete molecules known as effectors into the plant cell or the apoplast to suppress the abovementioned defense responses (**Fig. 1**). Therefore, the secretion of effector molecules results in the susceptibility of plants and ultimately leads to effector-triggered susceptibility (ETS) (Jones & Dangl, 2006).



In response to susceptibility induced by ETS, plants have evolved the second layer of innate immunity known as effector-triggered immunity (ETI). In ETI, some pathogen-specific effectors, also called avirulence proteins (Avrs), can be recognized either directly or indirectly by resistance (R) proteins (Cesari, 2018). Among R proteins, a subclass includes those consisting of cell surface LRR domain localized on the cell surface and membrane such as RLKs and RLPs (X. Yang et al., 2012). However, the majority of R proteins encode two conserved features: nucleotide-binding (NB) and C-terminal LRR domains. Additionally, they have a variable N-terminal domain containing either a coiled-coil (CC) or a Toll/interleukin-1 receptor (TIR) domain. Collectively, these components are referred to as NLRs (nucleotide-binding domain leucine-rich repeat-containing proteins) (Dangl & Jones, 2001; Duxbury et al., 2021).

The recognition of effectors results in a response similar to that elicited by PRRs but with more robust and rapid defense responses. During ETI, in addition to the PTI-triggered defense responses, the hypersensitive response (HR) plays a crucial role in restricting the growth and spread of biotrophic and hemibiotrophic pathogens through programmed cell death of host cells. However, as pathogens evolve simultaneously with plants, other successful pathogens secrete new effector molecules to evade ETI, which can be detected by new plant R genes (**Fig.1**). Furthermore, recent studies have reported substantial crosstalk between NLR-mediated ETI and PRR-mediated PTI through the MAPK and NADPH oxidase signaling pathways (Ngou et al., 2021; M. Yuan et al., 2021). The recognition of effectors by NLR receptors, such as RRS1, RPS2, and RPS4, leads to the upregulation of gene expression and the accumulation of proteins for PTI signaling components, including BAK1, RBOHD, and MPK3. These cascades initiate the defense responses independently of direct PTI involvement. However, the activation of ETI in the absence of concomitant PTI resulted in a reduction in cell death (Ngou et al., 2021; M. Yuan et al., 2021). This demonstrates that PTI and ETI act synergistically to potentiate and ensure a fully active state of plant immunity.

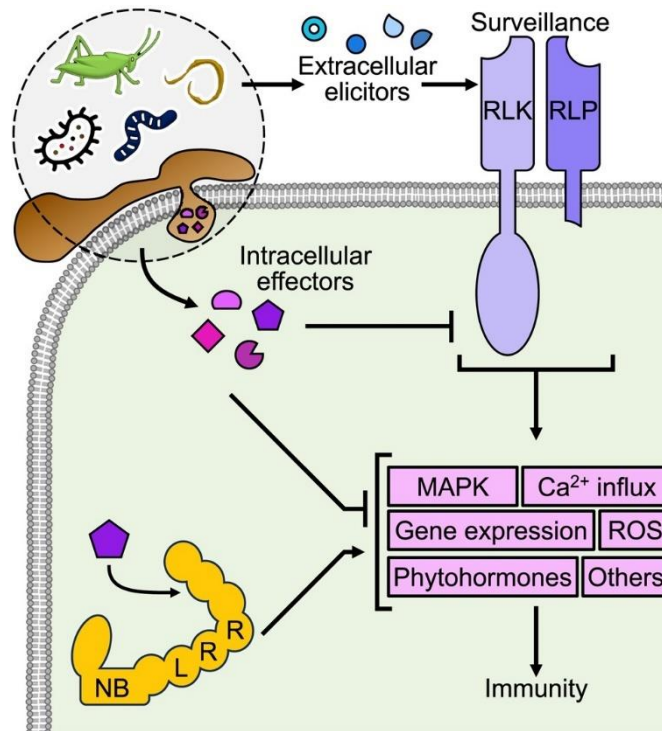


**Fig. 1 Schematic of representation of plant innate immunity.** Activation of the plant innate immune system upon pathogen attack involves three phases: immune recognition, signal integration, and defense execution. In the first phase, cell surface localized and membrane-resident immune receptors (PRRs) perceive PAMPs and DAMPs, while intracellular NLRs recognize microbial effectors released by pathogens. NLRs bind effectors directly or sense modulation of effector host targets. In the second phase, Ca<sup>2+</sup>, MAPK cascades, phytohormone signaling, etc are activated. In the last phase, plants execute effective cellular response responses such as cell wall reinforcement, reactive oxygen species (ROS) production, antimicrobial compound biosynthesis, and plant microbiota homeostasis. Collectively, the plant immune system facilitates an appropriate host response to microbial infection. Figure taken from (Dodds et al., 2024).

### 1.1.3 Effectors: The key factors in manipulating the host

Phytopathogens have diverse lifestyles to colonize their hosts, (Kourelis & Van Der Hoorn, 2018; Sánchez-Vallet et al., 2018) The success of colonization, irrespective of their specific lifestyle, relies on their ability to evade plant defense systems such as PTI and ETI (Lo Presti et al., 2015). To suppress plant immunity, phytopathogens secrete small molecules called effectors (Todd et al., 2022). Besides proteins, secreted small RNAs and secondary metabolites of necrotrophic and hemibiotrophic fungal pathogens can also act as effectors to avoid eliciting plant immunity and promote invasion (Collemare et al., 2019; Stergiopoulos et al., 2013; Wang et al., 2017; Weiberg et al., 2013). Effectors are highly diverse in sequence and structure, and their expression profile is tightly regulated to fine-tune different infection stages (Lo Presti et

al., 2015). Effectors can suppress plant immune responses and manipulate host cell physiology to establish a compatible interaction with the host and sequester necessary nutrients essential for their proliferation and reproduction (Lo Presti et al., 2015; Toruño et al., 2016).

Effectors are deployed in a spatial-temporal regulated manner within the host plant. They exist either in the apoplast as apoplastic effectors, which are rich in cysteine residues and stabilized by disulfide bridges to withstand the harsh apoplastic environment and to counteract plant proteases to suppress primary defense, or they are translocated into plant cells as cytoplasmic effectors, targeting different cellular compartments and interfering with host physiology (Doehlemann & Hemetsberger, 2013; Lo Presti & Kahmann, 2017; Toruño et al., 2016; Y. Wang & Wang, 2018). Depending on their subcellular localization within the host, either in the apoplast or cytoplasm, effector proteins employ diverse strategies to manipulate the host and facilitate the infection. Apoplastic effectors disrupt the recognition of the invaders by blocking and evading recognition of chitin by plant immune receptors, interfering with plant PR proteins, suppressing ROS generation and other secreted defense compounds (Hemetsberger et al., 2012; Sánchez-Vallet et al., 2013; R. Zhang et al., 2021). Meanwhile, cytoplasmic effectors manipulate plant immunity by reprogramming host metabolism, transcriptional regulation, cell cycle, and other intracellular signaling pathways (Boch et al., 2014; de Lange et al., 2013; Djamei et al., 2023; Redkar et al., 2015; Tanaka et al., 2014).

There are two different pathways for effector secretion. The first pathway involves the conventional secretory pathway, which the majority of fungal and oomycete effectors follow with an N-terminal signal peptide, proceeding through the endoplasmic reticulum (ER)-Golgi-dependent secretory pathway (Lo Presti et al., 2015; Saunders, 2023) On the contrary, the second pathway involves effectors that lack a typical signal peptide and are secreted unconventionally into plant cells. For example, AVRa10 and AVRk1 from *Blumeria graminis f. sp. hordei* and *M. oryzae* Pw12 and AVR-Pita are cytoplasmic effectors that are secreted unconventionally into plant cells via an unknown mechanism and the biotrophic interfacial complex (BIC) in a tRNA wobble U34 thiolation-dependent manner (Li et al., 2023; Ridout et al., 2006). In oomycetes, secreted effectors without secretion signal have evolved to share common N-terminal translocation motifs such as RxLR, crinkler (CRN), and CHxC. The RxLR (Arg-x-Leu-Arg) motif is located downstream of the secretory signal peptide, typically followed by a DEER (Asp-Glu-Glu-Arg) amino acid sequence (Anderson et al., 2015; Fabro, 2022; Rehmany et al., 2005). RxLR effectors from *Phytophthora infestans* and cytoplasmic

effectors of *M. oryzae* are translocated into plant cells through clathrin-mediated endocytosis (Oliveira-Garcia et al., 2023; Wang et al., 2023).

Pathogens are under continuous and high selection pressure from the host immune system (Derbyshire, 2020). The rapid evolution of the effector repertoire within pathogen genomes is crucial for effector diversification and effective virulence optimization to evade plant immunity (Lo Presti et al., 2015; Sánchez-Vallet et al., 2018). As a result of these processes, pathogens have evolved host-species and host-cultivar specificity through extensive chromosomal rearrangements in gene-sparse compartments, involving highly repetitive elements, loss or mutation of effector genes, diversion of gene expression of existing effector genes, as well as the gain of new effectors, which overall promotes gene diversity (Dutheil et al., 2016; Raffaele et al., 2010; Sánchez-Vallet et al., 2018; Todd et al., 2022).

Through similar mechanisms, pathogens have also evolved core effectors that are highly conserved and shared among closely or even distantly related species within a taxonomic family (Depotter & Doehlemann, 2020; Plissonneau et al., 2018; Sánchez-Vallet et al., 2018). In contrast to rapidly evolving accessory effectors, core effectors remain protected from mutation and play an indispensable role in virulence functions (Todd et al., 2022). In *Colletotrichum* fungi, approximately 20% of effectors are considered core effectors and are present across all *Colletotrichum* species (Lu et al., 2022). Moreover, the core effector NIS1, a necrosis-inducing protein, is not only widely found within the *Colletotrichum* genus but also shows conservation in Ascomycota and Basidiomycota (Irieda et al., 2019). Pep1 from *U. maydis*, known for its role as a plant peroxidases inhibitor, has been identified in several other Ustilaginaceae species, such as *Ustilago hordei*, *Sporisorium reilianum*, *Sporisorium scitamineum*, *Melanopsichium pennsylvanicum*. These orthologous effectors share a sequence homology ranging between 45–62% with the *U. maydis* Pep1 (Hemetsberger et al., 2015).

However, not all orthologous effectors that are conserved across different species exhibit the same function. Instead, they have evolved different functions to meet their specific needs (Todd et al., 2022). An effector avirulence protein 4 (Avr4) identified in *C. fulvum* is a chitin-binding lectin that protects fungal cell walls from plant chitinases. In addition, homologous proteins of Avr4 of *C. fulvum* can be found in Mycosphaerellaceae species (Kohler et al., 2016; Mesarich et al., 2018; Stergiopoulos et al., 2010). Apart from its avirulence function, Avr4 of *Cercospora flagellaris* is involved in cercosporin biosynthesis (Santos Rezende et al., 2020). Furthermore, in *Pseudocercospora fuligena*, a paralog of Avr4 known as PfAvr4-2 binds to highly de-

esterified pectin of the plant cell wall, thereby promoting the loosening of the cell wall. This facilitates the pathogen's colonization into the host tissues and synergizes with the activity of pathogen-secreted endo-polygalacturonases (L. H. Chen et al., 2021).

#### **1.1.4 Effectors: Unveiling antimicrobial strategies**

Effectors have been extensively studied in the context of host colonization, where they interfere with plant immunity to reduce plant fitness and induce physiological changes to manipulate host metabolic pathways, thereby facilitating successful microbial reproduction (Ökmen & Doehlemann, 2014; Toruño et al., 2016). However, studies have shown that effectors play a role beyond host colonization. The first effector of *Zymoseptoria tritici*, *Zte6*, has demonstrated dual functionality, exhibiting strong toxicity to other microorganisms while contributing to wheat cell death (Kettles et al., 2018). Similarly, small cysteine-rich effectors *VdAve1*, *AMP2*, and *VdAve1L2* from *Verticillium dahliae* exhibit antimicrobial activity by manipulating host microbial communities to suppress Sphingomonades and Actinobacteria to protect their niche and promote successful host colonization (Snelders et al., 2020, 2023). Furthermore, *Ribo1* from *U. hordei* showed cytotoxic activity to compete with host-associated bacteria during epiphytic development (Ökmen et al., 2023).

#### **1.1.5 Regulation and functions of SnRK1: a key player in plant energy homeostasis and immunity**

AMPK/SNF1/SnRK1 are heterotrimer complexes composed of a catalytic  $\alpha$  subunit, and regulatory  $\beta$  and  $\gamma$  subunits (Broeckx et al., 2016; Crepin & Rolland, 2019; Garcia & Shaw, 2017; Hulsmans et al., 2016). The  $\alpha$  subunit is composed of a Ser/Thr kinase domain at its N-terminus, which is linked to a regulatory domain at its C-terminus. The regulatory domain contains ubiquitin-associated (UBA) and kinase-associated (KA) domains that facilitate interaction with the  $\beta$  and  $\gamma$  regulatory subunits (Broeckx et al., 2016; Crepin & Rolland, 2019; Garcia & Shaw, 2017; Hulsmans et al., 2016). Complex activation is typically achieved by phosphorylating a conserved threonine residue located at the  $\alpha$  subunit's 'T-loop' by upstream activating kinases *SnAK1/GIRK2* and *SnRK2/GIRK1*, which complement yeast *Snf1*-activating kinases (*Pak1*, *Elm1*, and *Tos1*) (Crozet et al., 2010; Hey et al., 2007; Shen et al., 2009). The  $\beta$  subunits act as a scaffold protein consist of a myristoylated N-terminal domain, a central carbohydrate-binding module (CBM), and a C-terminal binding domain assisting interaction with  $\alpha$  and  $\gamma$  subunits, thereby promoting localization, and substrate specificity of the complex. The  $\gamma$  subunits consist of four conserved cystathionine- $\beta$  synthase (CBS) motifs

that can bind adenine nucleotides in mammals. Plants have a hybrid  $\beta\gamma$  subunit that is distinct from their canonical  $\gamma$  subunit due to the presence of an additional N-terminal CBM (Broeckx et al., 2016; Crepin & Rolland, 2019).

SnRK1 acts as a central energy regulator, controlling cellular metabolism for growth and development, and maintaining energy homeostasis, particularly in response to energy depletion. When SnRK1 is activated as a result of energy depletion, darkness, and stresses, it tightly regulates myriads of signaling and metabolic pathways by triggering energy-promoting catabolic processes to mobilize storage compounds, while repressing energy-anabolic processes (Baena-González & Hanson, 2017; Broeckx et al., 2016). In plants, SnRK1 plays more role not only regulating carbon and energy resource against stresses, but also optimizes nutrient partitioning between source and sink tissues, orchestrates various aspects of developmental phase transitions based on metabolic needs (Fichtner & Lunn, 2021; Gazzarrini & Tsai, 2014; Paul et al., 2017). In addition, SnRK1 has been implicated in modulating plant immunity against a variety of plant pathogens and as a target of various effector proteins (Hulsmans et al., 2016). In wheat, TaSnRK1 interacts with an orphan protein TaFROG of *Fusarium graminearum* to modulate the positive regulation of resistance by mediating proteasomal degradation of cytoplasmic effector Osp24 (Jiang et al., 2020). Overexpression of SnRK1A in rice enhanced its resistance to broad-spectrum hemibiotrophic and necrotrophic pathogens, such as *Xanthomonas oryzae* pv. *oryzae* (Xoo), *Magnaporthe oryzae*, *Cochliobolus miyabeanus*, and *Rhizoctonia solani* (Filipe et al., 2018). In Pepper, SnRK1 is involved in the effector protein AvrBsT-mediated suppression of the AvrBs1-specific hypersensitive response in *X. campestris* pv. *vesicatoria* (Szczesny et al., 2010). *Plasmodiophora brassicae*-specific and conserved effector, PBZF1 inhibits SnRK1.1-mediated resistance of *Arabidopsis thaliana* to clubroot disease (W. Chen et al., 2021).

SnRK1 activity is also regulated by various sugar metabolites, including glucose-1-phosphate (G1P), glucose-6-phosphate (G6P), trehalose-6-phosphate (T6P), and ribose 5-phosphate (R5P) (Nunes et al., 2013; Piattoni et al., 2011; Toroser et al., 2000). T6P inhibit SnRK1 most effectively and shows a synergistic effect with G1P and a cumulative effect with G6P in response to cellular energy status (Nunes et al., 2013). In most plants, T6P exists only in trace amount, but plays a crucial role in plant metabolism and growth (Paul et al., 2008, 2018). It is synthesized from UDP-glucose and G6P by T6P synthase (TPS) and is later broken down into trehalose by T6P phosphatase (TPP) and into glucose by trehalase (TRE) (Fichtner & Lunn, 2021).

## **1.2 *Ustilago maydis* – the causative agent of corn smut**

The biotrophic pathogen *U. maydis* is a soil-borne smut fungus that belongs to the family Ustilaginaceae (Kahmann et al., 2000). Smut fungi are characterized by their narrow host range and are known to infect economically important cereal crops such as maize, wheat, barley, sorghum, and sugarcane (Zuo et al., 2019). After infection, these fungi spread systemically throughout the plant, but cause disease only in the floral organs of the host by producing massive amounts of dark brown or black teliospores, which as a result affect host reproduction. In contrast to common smuts, *U. maydis* can infect all aerial parts of maize and teosinte (*Z. mays* sub.sp. *mexicana* and sp. *parvigluminis*), an ancestral plant of domesticated maize (Christensen, 1963; Doebley, 1992). Upon infection, it causes only the local formation of abnormal smut symptoms known as tumors. Subsequently, black teliospores develop and mature within these tumors, resulting in a distinctive black, sooty appearance (Zuo et al., 2019).

While *U. maydis* causes economic damage in many countries, it is generally less severe than many other smut pathogens that inflict devastating and extensive economic damage on major crops (Brefort et al., 2009; Dean et al., 2012). Conversely, in Mexican culture and cuisine, *U. maydis* is considered as iconic edible fungus called “huitlacoche” (Pataky & Chandler, 2003; Valverde et al., 1995; Villagrán et al., 2023). Due to its compact genome size of 20.5 Mb encoding 6902 genes, its amenability to genetic manipulation with fully sequenced and annotated genes, and its ease of cultivation in laboratory conditions with the solopathogenic SG200 strain that has been genetically engineered to filament without prior mating, *U. maydis* is a well-studied organism and serves as an important model for understanding the biology and function of effectors, the biotrophic fungal lifestyle, and plant immunity (Kahmann et al., 2000; Kämper et al., 2006; Zuo et al., 2019).

### **1.2.1 The life cycle of *Ustilago maydis***

*U. maydis* has a biphasic life cycle consisting of its saprophytic yeast haploid sporidia phase and a biotrophic phase (Gillissen et al., 1992; Kahmann et al., 1995) (Fig.2). Under favorable environmental conditions, such as an optimal temperature and ambient humidity, diploid teliospores germinate and undergo meiosis to form four haploid nuclei. The resulting haploid nuclei migrate into a promycelium, where each nucleus is separated by septa. Afterward, haploid cells bud off from the promycelium (Kahmann & Schirawski, 2007). Subsequently, the two compatible haploid cells recognize each other through the regulation of the a-locus

pheromone receptor system (Banuett & Herskowitz, 1994; Bölker et al., 1992; Fedler et al., 2009). The subsequent switch from budding to filamentous growth is initiated as the fused haploid cells undergo mitosis to form an infectious dikaryon (García-Muse et al., 2003; Snetselaar & Mims, 1992). The crucial step for initiation of the pathogenic phase is induced by the dimerization of two compatible homeodomain transcription factors, bEast (bE) and bWest (bW), to ultimately form the heterodimeric bE/bW complex encoded by the *b*-mating type locus (Brachmann et al., 2001; Gillissen et al., 1992; Kämper et al., 1995; Snetselaar & Mims, 1992). This complex initiates the transcriptional expression of the zinc-finger transcription factor Rbf1, which is a master regulator of pathogenic growth and development (Heimel et al., 2010; Kämper et al., 2006). During the early stage of infection, the dikaryotic hyphae with actively growing tips accumulate dikaryon in the cytoplasm of the hyphal tip, whereas the older parts become vacuolated and eventually separated by spaced septa (Freitag et al., 2011; Snetselaar et al., 1996). Upon sensing the hydrophobicity of the plant surface and the presence of fatty acids, hyphal growth is cell cycle arrested, which is regulated under the maintenance (Castanheira et al., 2014; Heimel et al., 2013; Mendoza-Mendoza et al., 2009; Snetselaar & Mims, 1992), 2009; Snetselaar & Mims, 1992). These filaments differentiate into infectious structures known as appressoria. In *U. maydis*, unlike other smut fungi, appressoria are inconspicuous, non-melanized, and are not dependent on high mechanical force like turgor pressure (de la Torre et al., 2020; Doehlemann et al., 2008b; Schirawski et al., 2005; Snetselaar & Mims, 1992). Instead, appressoria are formed in a localized area on the leaf surface where specific PCWDEs are secreted to breach the cell wall and penetrate the plant cuticle (Lanver et al., 2014). After appressoria penetrate the plant cuticle, cell cycle arrest is released and the host plasma membrane invaginates and tightly wraps around colonized intracellular hyphae, forming a biotrophic interaction zone that facilitates the exchange of signaling molecules and essential nutrients (Bauer et al., 2011; Doehlemann et al., 2009; Scherer et al., 2006). During the early phase of biotrophic development, fungal hyphae grow intra- and intercellularly and involve transcription factors such as Hdp2, Biz1, and Mzr1, which are responsible for inducing the expression of early effector genes (Flor-Parra et al., 2006; Lanver et al., 2014; Zheng et al., 2008). About 2-3 days post infection (dpi), the proliferated fungal hyphae branch intracellularly and move toward the vasculature, inducing overaccumulation of starch granules in the chloroplast (Snetselaar & Mims, 1994). At 4 dpi, the first morphological changes in cells become apparent due to the de novo cell division of bundle sheath cells. These lead to the formation of new cell walls within the bundle sheath cell, which tremendously increases the number of cells and facilitates easy access to water and nutrients for the fungus (Doehlemann



et al., 2008a; Redkar et al., 2015). Subsequently, these newly divided cells transform into hyperplastic tumor (HPT) cells, which originate from the bundle sheath within the infected regions of the leaf (Matei et al., 2018; Zuo et al., 2023). At 5-6 dpi, some hyperplastic cells along with mesophyll cells begin to enlarge and later transform into hypertrophic tumor (HTT) cells (Matei et al., 2018). These cells are linked with endoreduplication, a form of the cell cycle that doubles nuclear in volume without performing cell division (Callow, 1975; Nagl, 1976; Wildermuth, 2010). Upon tumor maturation, fungal hyphae aggregate within the apoplastic space of tumorous tissue, and the hyphal morphology undergoes substantial branching, fragmentation, and rounding to form teliospore (Snetselaar & Mims, 1994; Tollot et al., 2016). The teliospore formation is orchestrated by transcription factor Ros1, which induces the expression of late effector genes and downregulates the early effectors (Tollot et al., 2016). Finally, under suitable environmental conditions, massive tumors break open and release teliospores, spreading dark and highly melanized spores into the environment for the restart of the next life cycle.

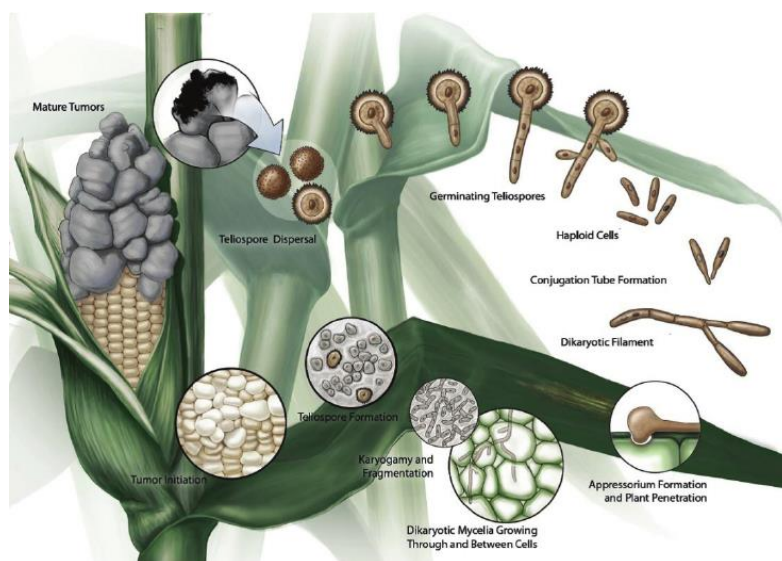


**Fig. 2 The life cycle of *Ustilago maydis*.** The dimorphic life cycle of *U. maydis* is divided into 1) a yeast-like saprophytic phase and 2) dikaryotic filamentous biotrophic phase. Under favorable environmental conditions, dispersed teliospores germinate and undergo meiosis to form haploid sporidia. These haploid sporidia encounter compatible mating types and form a conjugation tube, which leads to the development of infectious dikaryotic filaments. Subsequently, *U. maydis* forms appressoria for host penetration and grows inter- and intracellularly. Hyphae growing intercellularly invaginate plant plasma membranes and form a biotrophic interface. After colonization of plant, effectors are secreted to modulate plant defense and metabolism, eventually facilitating tumor formation on the host. Upon tumor maturation, the hyphal morphology undergoes karyogamy and fragmentation to form

teliospores. Again, as a restart of the next life cycle, massive tumors break open, releasing teliospores, spreading dark and highly melanized spores into the environment (Saville et al., 2012).

## **1.3 Maize physiology and its metabolic regulation by *Ustilago maydis***

### **1.3.1 C4 metabolism of maize**

Maize is a typical C4 plant with unique leaf functional properties during development, commonly referred to as Kranz anatomy (Haberlandt, 1904; Nelson & Langdale, 1992). This anatomical arrangement involves two distinct layers of bundle sheath (BS) cells known as “Kranz” (wreath-like arrangement of cells), surrounded by a concentric outer layer consisting of mesophyll (M) cells to achieve high rates of photosynthesis (Edwards & Walker, 1983). The differentiation of these two photosynthetic cell types involves specific characteristics: BS cells contains thick cell walls, centrifugally arranged chloroplasts with large starch granules, and unstacked thylakoid membranes, while M cells exhibit randomly arranged chloroplasts with minimal or no starch and stacked thylakoids (Edwards & Walker, 1983; Majeran et al., 2005). Initially, all photosynthetic cells follow the developmental pattern of the C3 photosynthesis by default. Later, in response to light, they transform to a C4 pattern and cell differentiation occurs, specifically for M cells under the influence of neighboring cells and for BS cells specialize from their procambial lineage and adjacent veins (Jankovsky et al., 2001; Nelson & Dengler, 1992; Smith et al., 1996). In C4 plant photosynthesis, atmospheric CO<sub>2</sub> is fixed in M cells by phosphoenol pyruvate (PEP) carboxylase, leading to formation of oxaloacetate. The oxaloacetate is then converted to malate, which is subsequently transported into BS cells for decarboxylation to pyruvate, releasing CO<sub>2</sub>. This released CO<sub>2</sub> is fixed by RubisCO and utilized in Calvin cycle to produce carbohydrates, while any excess carbohydrates are stored as starch. The produced pyruvate is then diffused back to M cells, where it regenerates PEP, completing the C4 cycle (Majeran et al., 2005). Proliferative capacity in maize leaf development is limited to immature tissue at the leaf base and is gradually lost as they enter post-mitotic cell differentiation (Gonzalez et al., 2012; Johnson & Lenhard, 2011; Wenzler & Meins, 1987). In addition, a study of the vascular anatomy and plastid development in intermediate veins of maize revealed minimal bundle sheath plastid development in the leaf base of the maize seedlings and in sections adjoining the source-sink boundary (Jung et al., 2008).

### **1.3.2 *Ustilago maydis* induces changes in maize physiology**

In accordance with leaf physiology, *U. maydis*-induced tumor formation in maize has been observed to be restricted to the young developmental meristematic sink tissue near the leaf base, where the region below the developing leaves (photosynthetic sink tissue) is comprised of actively dividing and enlarging cells (Smith et al., 2001; Sylvester et al., 1990; Wenzler & Meins, 1987). After initiation, *U. maydis* consistently alters the proliferative ability of maize tissues even in the absence of the fungus and the infected area tends to remain undifferentiated with the drastic transcriptional changes related to secondary metabolism and defense (Basse, 2005; Wenzler & Meins, 1987). Subsequent transcriptomic analysis of *U. maydis*-infected maize tumors showed induction of genes involved in glycolysis, the tricarboxylic acid (TCA) cycle, and lipid metabolism, while showing a reduction in photosynthesis and related genes. (Doehlemann et al., 2008a). Conforming to the *U. maydis*-infected maize tumors act as a sink, it was shown that carbohydrates and nitrogen assimilates from the source tissues are redirected to the tumors (Horst et al., 2009). Moreover, after light exposure, photosynthesis reduces free hexose content in sink tissues by converting it to sucrose. However, according to (Doehlemann et al., 2008a), there was a >20-fold increase in free hexose content in infected leaves compared to non-infected leaves, and increased expression of transcripts related to sucrose degradation. Interestingly, sucrose level remained constant between two tissues, demonstrating manipulation of *U. maydis* to impair sink-to-source transition. Overall, studies suggest that *U. maydis* reinitiates leaf proliferation and disrupts normal maturation, reallocating photoassimilates for tumor formation and maintaining sink metabolism in favor of the pathogen to utilize it as an easily accessible nutrition source for the fungus itself.

### **1.4 Effectors of *Ustilago maydis***

*U. maydis*, a biotrophic pathogen, establishes an intimate relationship with its living host for a successful infection process. To promote host colonization, it employs sophisticated strategies during infection process to suppresses plant immune responses (Brefort et al., 2009; Zuo et al., 2019). As a result, it induces a comprehensive reprogramming of plant metabolism to meet its own needs and modulate changes in physiological functions such as reprogramming of cell cycle for division of tumors (Djamei et al., 2011; Redkar et al., 2015; Tanaka et al., 2014; Zuo et al., 2023). A key aspect of *U. maydis*'s infection strategy involves a diverse array of effector proteins. It is predicted to encode 467 secreted effector proteins, 215 of which are novel and lack known functional domain (Kämper et al., 2006; Lanver et al., 2017, 2018; Schirawski et

al., 2010). Many effector genes are transcriptionally co-regulated and clustered, with 18.6% arranged in 12 clusters, and five of these clusters control *U. maydis* virulence (Kämper et al., 2006). For instance, gene cluster 10A encodes the Pleiades, ten effector proteins including Tay1 and Mer1, which function as ROS suppressors in distinct host cellular location (Navarrete et al., 2021). Gene cluster 6A encodes five Tip effectors that target TOPLESS/TOPLESS-related proteins (TPL/TPR) to influence auxin signaling (Bindics et al., 2022). In addition, while deletion of some effector clusters reduced or abolished virulence, the deletion of cluster 2A increased the virulence of *U. maydis* (Kämper et al., 2006). This suggests that effectors not only affect the host, but also contribute to the fitness of the pathogen itself. Furthermore, studies have shown that effectors can cooperate, achieving the synergistic effects and forming an effector complex (Alcântara et al., 2019; Ludwig et al., 2021; Sánchez-Vallet et al., 2020). These cooperative interactions of effectors were confirmed by a systematic yeast-two-hybrid analysis involving nearly 300 effector candidates, revealing 126 effectors that can interact with themselves or other effectors (Alcântara et al., 2019). A stable protein complex composed of five unrelated proteins (Stp1-3, core effectors Cce1 and Pep1) and two transmembrane proteins Stp5 and Stp6 has been identified (Doehlemann et al., 2009; Hemetsberger et al., 2012, 2015; Ludwig et al., 2021; Schipper, 2009; Seitner et al., 2018). This “Stp effector complex” is anchored in the fungal membrane and exposed to the cell surface of the host. It is proposed to be responsible for the effective delivery of effectors into the host, with each member in this complex playing an indispensable role in *U. maydis* virulence (Ludwig et al., 2021).

#### **1.4.1 *Ustilago maydis* effectors involved in modulation of extracellular plant immunity**

Upon secretion by pathogens, effectors overcome the physical barriers of the host and interfere with various biological processes related to defense responses in plants. *U. maydis* strategically employs individual effectors, such as Pep1, Cce1, Pit2, Rsp3, and Fly1, to enhance its pathogenicity by serving diverse range of molecular roles on the plant (Doehlemann et al., 2009, 2011; Ma et al., 2018; Mueller et al., 2013; Ökmen et al., 2018; Seitner et al., 2018). The core apoplastic proteins like Pep1 and Cce1 are involved in the initial establishment of fungal and host interactions (Doehlemann et al., 2009; Seitner et al., 2018). Pep1 is involved in the inhibition of maize peroxidase POX12 activity, a major generator of H<sub>2</sub>O<sub>2</sub>, thereby suppressing early immune responses (Hemetsberger et al., 2012, 2015). Cce1 has eight cysteine residues, which support its functions within the apoplast and are required at early stage of infection (Seitner et al., 2018). Deletion mutants of *pep1* and *cce1* are apathogenic and are arrested after

initial penetration, which is caused by ROS accumulation, local cell death, and callose deposition (Doehlemann et al., 2009; Seitner et al., 2018). In addition to the known function of Pep1 and Cce1, they are also members of Stp effector complex, as described in section 1.4. Another apoplastic effector Pit2 has a conserved inhibitory motif of 14 amino acids (PID14) and acts as an inhibitor of papain-like cysteine proteases (PLCPs) (Doehlemann et al., 2011; Misas Villamil et al., 2019; Mueller et al., 2013). This motif functions as a substrate mimicking molecule, with Pit2 being recognized by the host as substrate of host PLCPs. Cleavage by the proteases releases inhibitory PID14, resulting in the inactivation of PLCPs and subsequently prevent the triggering of SA-related defense (Misas Villamil et al., 2019). Rsp3 protects fungal hyphae during its early biotrophic stage by binding to the fungal cell wall through its N-terminal domain (Ma et al., 2018). Rsp3 interacts with maize mannose-binding AFP1 and AFP2 proteins. AFP1, containing the DUF26-domain, has an antifungal activity, that Rsp3 blocks for the virulence. Additionally, the *Rsp3* mutant in *U. maydis* lacks mannose binding activity (Ma et al., 2018). In response to *U. maydis* infection, maize genes encoding various chitinases are upregulated (Doehlemann et al., 2008a; Ökmen et al., 2018). Fly1, a fungal lysin metalloprotease, interacts with and cleaves chitinase ZmChiA. The cleavage, mediated by Fly1, reduces enzyme lytic activity by removing chitinase binding domain from the catalytic domain. Furthermore, Fly1 is associated with the activity of the endogenous chitinase UmCts1, an essential enzyme required for fungal cell separation (Ökmen et al., 2018).

#### **1.4.2 *Ustilago maydis* effectors involved in host metabolic regulation**

Translocated effectors in *U. maydis* play crucial roles in various host metabolic processes and development, interfering with plant cell machinery. They affect intracellular signaling pathway, transcription, and metabolic regulation to both suppress defense responses and induce tumor formation (Djamei et al., 2023). For example, Cmu1 interacts with maize chorismate mutase ZmCM1 in the cytoplasm, converting chorismate to prephenate. This leads to decreased chorismate levels for salicylic acid (SA) biogenesis (Djamei et al., 2011). Additionally, the Cmu1 protein features a unique additional  $\alpha$ -helix and an extensive loop region (ELR) that is recognized by a kiwellin-like protein, ZmKWL1, in maize. In the apoplast, ZmKWL1 recognizes Cmu1 homodimer and inhibits chorismate mutase activity by hindering substrate accessibility to the catalytic active site of Cmu1 (Han et al., 2019) Another effector that modulates the reprogramming of maize metabolic pathway is Tin2, a component of the largest fungal effector-cluster 19A (Brefort et al., 2014). Tin2 interacts with maize cytoplasmic serine/threonine protein kinase ZmTTK1, which hides the N-terminal phosphodegron-like

DSGxS motif from degradation and subsequent recognition by the plant ubiquitin-proteasome system. This results in the stabilization of ZmTTK1. Consequently, active ZmTTK1 redirects 4-coumaroyl CoA from the lignin biosynthesis pathway towards to anthocyanin production, which is facilitated by the transcription factor ZmR1 (Tanaka et al., 2014).

### **1.4.3 Organ and cell type specificity in effectors**

Most smuts, such as *S. reilianum* and *U. hordei* from Ustilaginales, typically spread disease systemically through the vascular system, causing symptoms exclusively in the inflorescences (Laurie et al., 2012; Schirawski et al., 2010). However, *U. maydis*, unlike majority of smuts, forms tumors in all aerial parts of maize, including seedlings, adult leaves, and tassels (Zuo et al., 2019). These maize organs exhibit substantial developmental differences and physiological variations. Therefore, the process of plant infection by *U. maydis* is associated with extensive transcriptional changes and coupled with a set of effectors that are tailored to colonize specific plant organs, overcoming plant defense mechanism and reprogramming host metabolism for its own benefit (Doehlemann et al., 2008a; Schilling et al., 2014; Skibbe et al., 2010). Parallel transcriptome analysis conducted on *U. maydis* and *U. maydis*-infected maize organs (seedling, adult leaf, and tassel) at different time points revealed that 21% of effectors were expressed in all maize organs, whereas 45% of fungal transcriptome showed organ-specific expression patterns as early as 3 dpi (Skibbe et al., 2010). Among organ-specific effectors, 24% exhibited specific expression in seedling leaves, with one third of them contributing to virulence, 73% in adult leaves, and 3% in tassels (Schilling et al., 2014; Skibbe et al., 2010). This suggests that *U. maydis* have undergone genetic adaptation to elicit specific responses in different parts of the host plant, resulting in the complex coordination of symptoms in the form of tumors. Moreover, mutant analyses revealed that gene clusters 5B and 19A played a key role in symptoms and development of tumors in seedling leaves, while clusters 2A, 9A, and 10A were essential for tumor formation in adult leaves and tassels (Skibbe et al., 2010).

Furthermore, a targeted transcriptomic analysis was conducted on specific tumors within the maize vasculature to gain a more detailed understanding of effector expression in each maize cell type, particularly those predominantly expressed in maize leaves (Fig.3). The analysis revealed cell type-specific effectors in bundle sheath and mesophyll tumor cells among the previously identified *U. maydis* leaf-specific effector candidates (Matei et al., 2018; Schilling et al., 2014). In this cell type-specific expression of effectors, two major biological processes are involved: the induction of hyperplasia in the bundle sheath and hypertrophy in the

mesophyll, as described in section 1.3.1. In HTT cells, 67 effectors were identified with significant expressions, including 10 that showed exclusive expressions. Meanwhile, in HPT cells, 43 effectors were found, and only 1 was exclusively expressed (Fig.3).

The See1 is the first effector characterized in *U. maydis* that contributes to hyperplastic tumor formation. It interacts with ZmSGT1, a cell cycle transition regulator, inducing the reactivation of DNA synthesis that is essential for cell division. SGT1, primarily studied in regulation of plant immunity, relies on phosphorylation by MAPK and is inhibited by See1. Another effector Erc1, is required for fungal cell to cell extension in bundle sheath and suppresses  $\beta$ -glucan mediated defense induction (Ökmen et al., 2022). Sts2, an intracellular effector contributing to hyperplastic tumor formation, which was found to be differentially regulated in different inbred lines upon *U. maydis* infection (Schurack et al., 2021; Zuo et al., 2023). In a recent study, Sts2 was shown to interact with ZmNECAP1, a plant transcriptional activator. This interaction leads to the activation of several regulators associated with leaf development, ultimately promoting tumor formation (Zuo et al., 2023). Furthermore, its ortholog in *S. reilianum*, SrSts2, cannot restore the deletion mutant of *U. maydis* Sts2 and is differentially regulated compared to *U. maydis* Sts2 during the infection of seedlings, suggesting functional diversity between these two closely related species (Zuo et al., 2021). Collectively, these studies provide insights into the tumorigenesis of *U. maydis* which involves the action of multiple effectors simultaneously at various points, resulting in rapid cell growth and proliferation upon infection (Zuo et al., 2019).

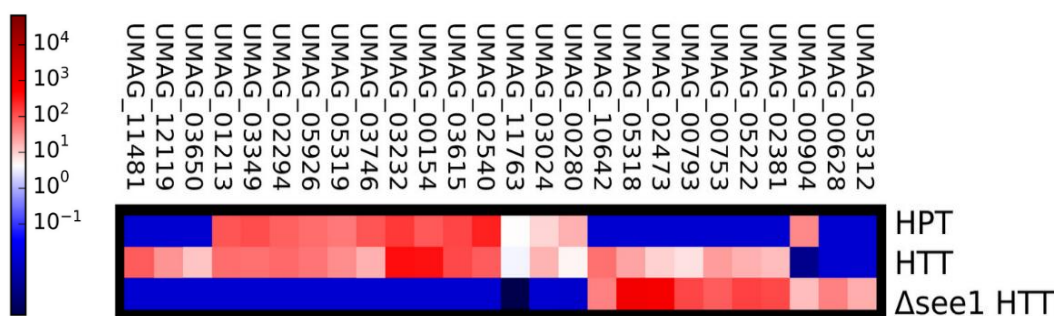


**Fig. 3 Cell type-specific effector gene expression from *Ustilago maydis*-infected maize tissue at 4dpi.** Heatmap depicts a strong cell type-specific gene expression pattern of *U. maydis* effector genes. P-value < 0.05 from DESeq analysis (Matei et al., 2018).

## 1.5 Aim of this study

In previous studies, several HPT-related effectors have been characterized to function in de novo cell division of bundle sheath tumor cells (Matei et al., 2018; Zuo et al., 2023). However, to date, HTT-related effectors still remain uncharacterized. Therefore, the aim of this study is to identify and functionally characterize the role of specific *U. maydis* effectors in hypertrophy induction. To address this aim, the study aimed to achieve the following objectives:

- 1) Identification of HTT-related effectors to define the set of effectors required for hypertrophy.
- 2) Identification of effector targets of HTT-related effectors to understand the potential formation of an effector complex upon *U. maydis* infection *in planta*.
- 3) Identification of maize targets of HTT-related effectors to unravel molecular mechanisms and their contribution to *U. maydis* full virulence.



## 2. Results

### 2.1 Functional characterization of HTT candidates in *Ustilago maydis* effectors

To understand how HTT-related effectors contribute to *U. maydis* virulence, we selected candidates from previous transcriptome data (Matei et al., 2018). The transcriptome data revealed ten effector genes (*UMAG\_02381* (*cda7*), *UMAG\_05222*, *UMAG\_00753*, *UMAG\_00793*, *UMAG\_02473*, *UMAG\_05318* (*sts2*), *UMAG\_10642*, *UMAG\_03650*, *UMAG\_12119*, *UMAG\_11484*) that were specifically and strongly upregulated in HTT cells in both SG200 and the SG200 $\Delta$ see1 mutant infected maize (Matei et al., 2018). Additionally, two paralogous genes of *UMAG\_00793* (*UMAG\_00792* and *UMAG\_00794*) were included for screening. Notably, *UMAG\_00792* and *UMAG\_00794* share 23% and 32% sequence similarity with *UMAG\_00793* (**Fig. S1A and Table 1**). Moreover, genomic analysis revealed that *UMAG\_00792* and *UMAG\_00793* are on chromosome 1 and share an intergenic region of promoter, sharing 352 bp out of a total of 848 bp, suggesting coordinated expression of these two genes (**Fig. 4A**). From hereafter, *UMAG\_02473*, *UMAG\_00792*, and *UMAG\_00793* will be referred to as Hap1, Hap2, and Hap3, respectively, standing for the **h**ypertrophy **a**ssociated **p**rotein.

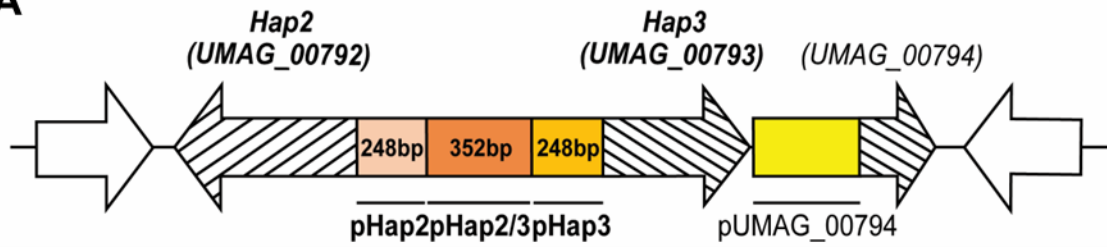
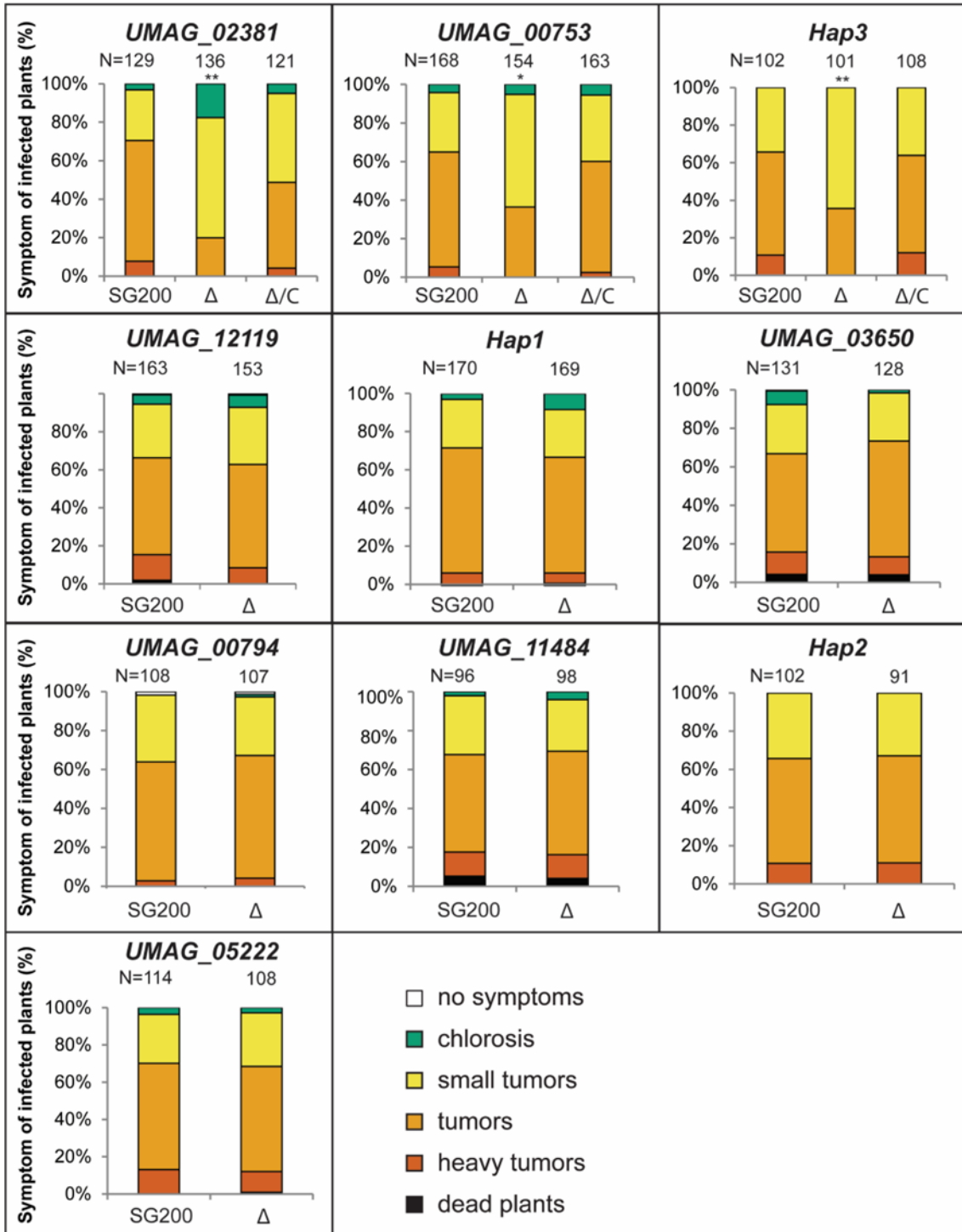
**Table 1) Overview of HTT-related effector candidates tested in this study**

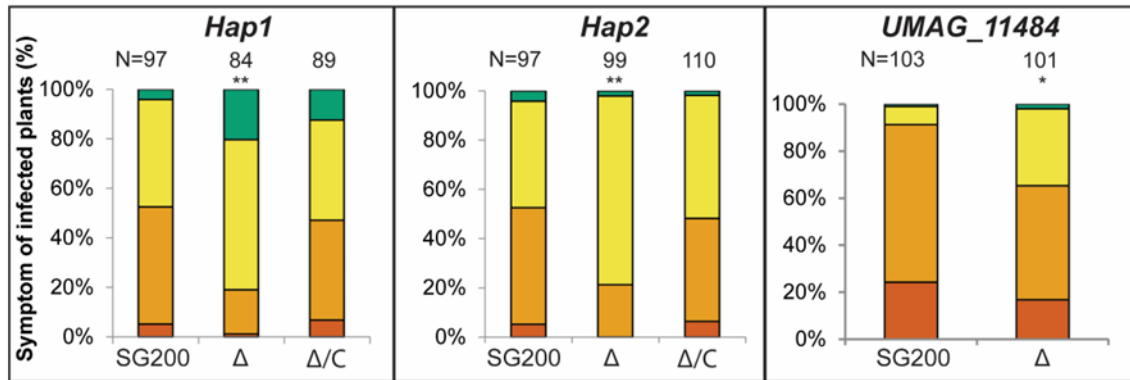
SP= signal peptide; TPMmax= the highest Transcripts Per Million, representing the highest expression level of *U. maydis* effector candidates observed at plant associated time points throughout the growth stages (Lanver et al., 2018). Effector relationship = indication of paralogous relationships among the HTT-related *U. maydis* effectors listed in the table.

Effector candidates with HTT specific expression									
Effector	Gene ID	SP	TPMmax	Effector relationship	Virulence in maize lines	Putative activity	Complementation	Reference	
Cda7	UMAG_02381	Y	12 dpi	-	Y	Chitin deacetylase	Y	Rizzi et al., 2021	
-	UMAG_05222	Y	1 dpi	-	N	-	-	-	
-	UMAG_00753	N	1 dpi	-	Y	-	Y	-	
Hap3	UMAG_00793	Y	2 dpi	Paralog	Y	-	Y	-	
Hap1	UMAG_02473	Y	2 dpi	-	Y	-	Y	-	
Sts2	UMAG_05318	Y	4 dpi	-	Y	Transcription activator	Y	Zuo et al., 2023	
-	UMAG_10642	N	0.5 dpi	-	N	-	-	-	
-	UMAG_03650	Y	6 dpi	-	N	-	-	-	
-	UMAG_12119	Y	1 dpi	-	N	-	-	-	
-	UMAG_11484	Y	6 dpi	-	Y	-	-	-	
Hap2	UMAG_00792	Y	2 dpi	Paralog	Y	-	Y	-	
-	UMAG_00794	N	6 dpi	Paralog	N	-	-	-	

To confirm HTT-related effector candidates, gene frameshift knockout mutants were generated in the solopathogenic strain SG200 background using CRISPR-Cas9 gene editing system. Subsequently, these mutants were inoculated into the maize line Golden Bantam (GB) and compared with the SG200 (wild type) strain for disease symptoms. Among the mutants, *UMAG\_02381*, *hap3*, and *UMAG\_00753* showed a significant reduction in virulence compared to SG200 in the GB maize line (**Fig. 4B**). Genes that did not exhibit virulence reduction in the GB maize line were tested in the VA35 maize line to observe the virulence reduction tendency of these effectors (**Fig. S1B**). Subsequently, only those that showed virulence reduction were tested in the maize line Early Golden Bantam (EGB). VA35 is more resistant to *U. maydis* infection compared to GB maize line. EGB line is derived from GB line bred for early maturation and predominantly used for *U. maydis*-maize pathosystem (Zuo et al., 2019). Here, we observed a significant reduction in virulence for *hap1*, *hap2*, and *UMAG\_11484* frameshift knockout mutants (**Fig. 4C**). Overall, these findings demonstrate that HTT-related effectors exhibit maize line specificity in virulence function.

After identifying candidate genes for HTT-related effectors that are essential for full virulence in one of the three maize lines, genetic complementation was performed for each mutant with their respective gene expressed under the control of the native promoter. Genetic complementation was performed into the ectopic *ip*-locus to validate that the observed virulence reduction was solely attributed to the deletion of the specific genes (**Fig. 4B and C**). The *ip*-locus contains the succinate dehydrogenase enzyme (*UMAG\_00844*, *sdh2*) which is commonly used for integrating the targeted/desired gene sequences in *U. maydis* genome through homologous recombination, thereby conferring carboxin resistance (Keon et al., 1991). The single integration event for each construct was confirmed by southern blot analysis (**Fig S1C-F**). Finally, complementation of frameshift knockout mutant that fully restored virulence were systematically selected, resulting in the identification of effectors *hap1*, *hap2*, and *hap3* as candidate genes for HTT-related effectors. Transcriptomic data revealed that these three candidate effectors showed the highest gene expression at 2 dpi (Lanver et al., 2018) (**Table 1**). *Cda7* and *Sts2* were excluded from further study due to their functional roles as chitin deacetylase and transcriptional activator (Rizzi et al., 2021; Zuo et al., 2023). *UMAG\_00753* was also excluded from further study due to the absence of a conventional N-terminal signal peptide (SignalP 6.0; Teufel et al., 2022) and it failed to exhibit secretion in a *in planta* secretion test (**Table 1 and Fig. S1G**). The generation of *UMAG\_10642* frameshift knockout mutant was not successful as it resulted in non-viable cells.

**A****B**

**C**

**Fig.4) Hap effectors are essential for full virulence in *Ustilago maydis*.** A) Organization of effectors on chromosome 1 of *U. maydis* encoding *hap2*, *hap3*, and *UMAG\_00794* genes. Dashed arrows represent three paralogous genes. Colored boxes represent promoters of effectors, with the identical dark orange color indicating the promoters of Hap2 and Hap3. White arrows represent flanking genes whose genes are not paralogous. B) Disease symptoms of frameshift knockout mutants and complementation of HTT-related effectors infected in the maize line GB seedlings compared to *U. maydis* SG200 at 12 dpi. C) Disease symptoms of frameshift knockout mutants and complementation of effectors infected in the maize line EGB compared to *U. maydis* SG200 at 12 dpi. The disease index of an average of three biological replications was used for the Student's t-test to calculate the P-value. n = number of infected plants; \*, p-value  $\leq 0.05$ .

## 2.2 Identification of Hap effector targets

To gain mechanistic insight of Hap1, Hap2, and Hap3, pull-down assay was performed to find their potential effector interactors. To achieve this, maize seedlings were infected with each of the  $\Delta$ Hap1,  $\Delta$ Hap2 or  $\Delta$ Hap3 strains expressing the respective 2xHA-tagged *hap1*, *hap2*, *hap3* genes (SG200 $\Delta$ Hap1-p*Pit2*::*hap1*-2xHA, SG200 $\Delta$ Hap2-p*Pit2*::*hap2*-2xHA, or SG200 $\Delta$ Hap3-p*Pit2*::*hap3*-2xHA) and, as a control, *U. maydis* SG200 expressing HA-tagged mCherry with a signal peptide (SG200-p*Pit2*::*SP*-mCherry-HA) under the control of the constitutive *Pit2* promoter (Fig. 5A). The *Pit2* promoter was chosen to ensure consistent and uniform expression of target proteins, as it has been shown to exhibit a constitutively high expression level during the biotrophic phase (Mueller et al., 2013). All maize-infected seedlings were collected at 3 dpi. Total protein extracts were then immunoprecipitated with HA beads to prepare samples for mass spectrometry (MS) analysis. Western Blot was performed to confirm the expression

of full-length proteins using both total extract lysate and HA-IP proteins of effectors (**Fig. S2**). After validation, the HA beads with bound effector proteins were then subjected to mass-spectrometry (MS) in collaboration with Dr. Hirofumi Nakagami (Max Planck Institute for Breeding, Cologne, Germany) to identify potential protein interactors.

### **2.2.1 Hap effectors of *Ustilago maydis* interact with each other *in planta***

In the pull-down experiment of Hap effectors, 56, 6, and 20 proteins were detected in Hap1, Hap2, and Hap3, respectively, using a cut-off of  $\text{Log}_2\text{FC} > 1$  and  $\text{FDR} < 0.05$  (**Fig. 5B**). From Hap1, Hap2, and Hap3 detected proteins, total of 32, 4, and 13 effector proteins were selected, respectively, using the list of 467 predicted secreted effectors proteins (**Table S1, S2, and S3**) (Kämper et al., 2006; Lanver et al., 2017). To identify effector proteins that are associated with HTT-related effectors in Table 1, EffectorP\_Fungi 3.0, SignalP 6.0, TPMmax, and InterproScan were employed to screen secreted cytoplasmic effectors that showed the highest expression at 2 dpi (Blum et al., 2021; Lanver et al., 2018; Sperschneider & Dodds, 2022; Teufel et al., 2022). In the Hap1 pull-down analysis, five cytoplasmic and dual-localized apoplasmic/cytoplasmic effectors were identified: UMAG\_10556 (Tin3), Hap1, Hap2, UMAG\_10823, and UMAG\_01802 (**Fig. 5B and Table S1**). In the Hap2 pull-down analysis, three cytoplasmic and dual-localized cytoplasmic/apoplasmic effectors were detected: UMAG\_01690, Hap1, and Hap3 (**Fig. 5B and Table S2**). In the Hap3 pull-down analysis, two cytoplasmic effectors were detected: UMAG\_01690 and Hap1 (**Fig. 5B and Table S3**). UMAG\_10556 (Tin3) effector belongs to cluster 19A and its single deletion mutant showed significant virulence reduction (Brefort et al., 2014). UMAG\_01690 is a leaf-specific effector required for full virulence in *U. maydis*, but it showed similar levels of HPT and HTT gene expression (Matei et al., 2018; Schilling et al., 2014). In conclusion, the pull-down experiments revealed the potential *in planta* interactions among Hap1, Hap2, and Hap3, suggesting a complex formation of Hap effectors. Moreover, given that Hap1 exclusively interacts with Hap2 and Hap3, it indicates the indispensable role of Hap1 as a dominant effector within the Hap interaction network. In light of these findings, our initial focus was on effector-effector interactions, with effector-host target interactions to be addressed subsequently.

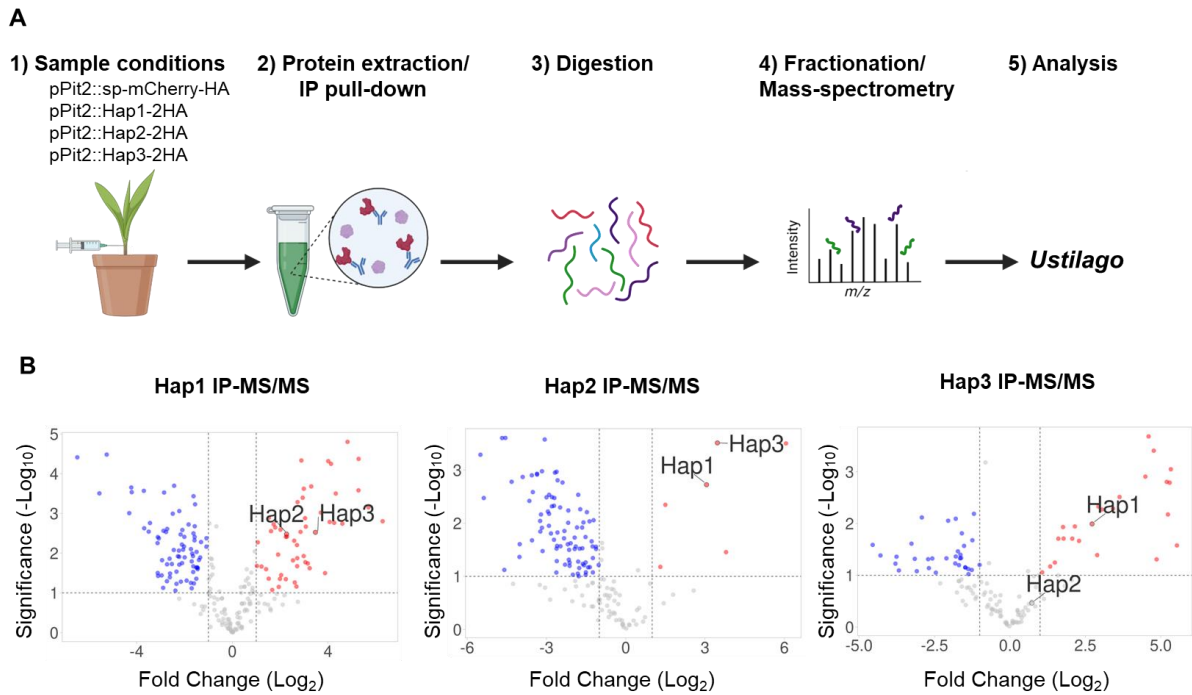


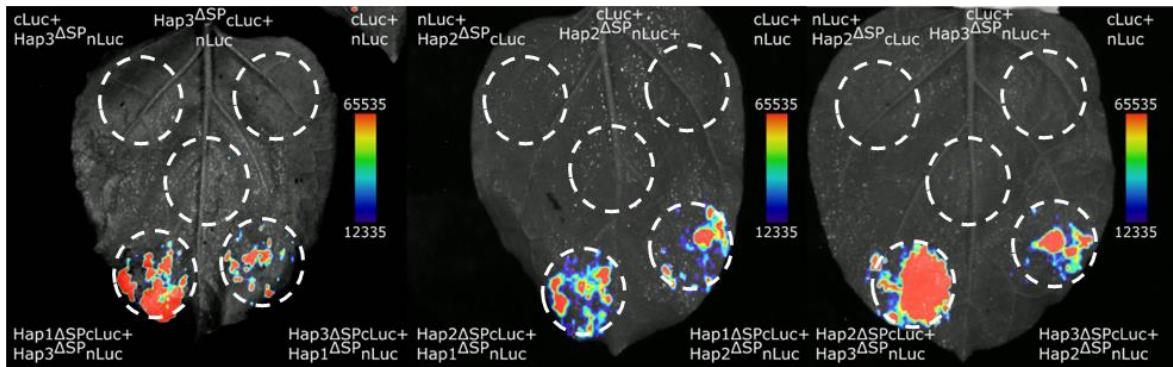
**Fig.5) Pull-down/MS analysis to unravel the interactome of Hap effectors.** **A)** Schematic overview of the pull-down/MS workflow, summarizing the experimental protocol and data analysis for effector target identification. (1) 7-day-old maize seedlings were infected with *U. maydis* SG200 strains expressing SG200-pPit2::SP-mCherry-HA, SG200ΔHap1-pPit2::Hap1-2xHA, SG200ΔHap2-pPit2::Hap2-2xHA, or SG200ΔHap3-pPit2::Hap3-2xHA and collected at 3 dpi. (2) Total maize proteins were extracted and immunoprecipitated with HA magnetic beads. (3) Proteins bound to HA magnetic beads were digested. (4) Digested protein peptides were fractionated and analyzed with MS. (5) The identified spectra are mapped against the *U. maydis* genome to search for potential interacting effector proteins. **B)** Volcano plots of Hap effector interacting proteins detected by LC/MS. The fold change (FC) values were calculated by dividing the LFQ intensity values of identified protein peptides in Hap1, Hap2, or Hap3 compared to the control. The x-axis represents Log<sub>2</sub>FC, and the y-axis represents high statistical significance (-Log<sub>10</sub> of P-values). Proteins with a Log<sub>2</sub>FC of >1.0 or -1 with p < 0.05 (from the Student's t-test) were selected for plotting. The red and blue dots, respectively, represent up- and down-regulated proteins. Gray dots represent proteins with no significant changes.

### 2.2.2 Hap effectors interact *in vivo* in split-luciferase complementation assay and co-immunoprecipitation

To verify the interaction among Hap effectors, a split luciferase complementation assay was performed. This assay employs the N-terminal (nLuc) and C-terminal (cLuc) domains of luciferase, which are fused with two proteins of interest. Upon interaction of these proteins and subsequent ligand binding, a detectable luminescent signal is produced (Azad et al., 2014). Hap1<sup>ΔSP</sup>-, Hap2<sup>ΔSP</sup>-, or Hap3<sup>ΔSP</sup>-nLuc was transiently co-expressed with Hap1<sup>ΔSP</sup>-, Hap2<sup>ΔSP</sup>-, or Hap3<sup>ΔSP</sup>-cLuc in *Nicotiana benthamiana* using *Agrobacterium*-mediated transformation. Empty-nLuc and -cLuc were used as a negative control. To test the autoactivation of either domain of the fused proteins of interest, Hap2<sup>ΔSP</sup>-, and Hap3<sup>ΔSP</sup>-nLuc or Hap2<sup>ΔSP</sup>-, and Hap3<sup>ΔSP</sup>-cLuc were co-infiltrated with empty-nLuc or -cLuc. A luminescence signal was exclusively detected when Hap effectors were co-expressed together, while no visible signal was observed when Hap effectors were co-expressed with either empty-cLuc or -nLuc control (**Fig. 6A**).

To further validate interaction among Hap effectors, co-immunoprecipitation (co-IP) assays were performed in *N. benthamiana*. *Agrobacterium* strains carrying Hap1<sup>ΔSP</sup>-GFP or Hap2<sup>ΔSP</sup>-4xMyc were co-infiltrated with Hap3<sup>ΔSP</sup>-6xHA or Hap1<sup>ΔSP</sup>-6xHA. As a negative control, *Agrobacterium* strains carrying eGFP or GFP-4xMyc were co-infiltrated with Hap3<sup>ΔSP</sup>-6xHA or Hap1<sup>ΔSP</sup>-6xHA. *N. benthamiana* leaves were collected 2-3 days post co-infiltration, and protein extraction was performed for Co-IP with  $\alpha$ -Myc or  $\alpha$ -GFP magnetic beads. Hap1<sup>ΔSP</sup>-GFP or Hap2<sup>ΔSP</sup>-4xMyc was co-immunoprecipitated with Hap1<sup>ΔSP</sup>-6xHA or Hap3<sup>ΔSP</sup>-6xHA, but not in either eGFP or GFP-4xMyc controls (**Fig. 6B**). In addition to the split-luciferase complementation assay and co-IP, Hap2 and Hap3 effector interactions were confirmed with the yeast-two-hybrid assay (**Fig. S3**). Collectively, these data indicate that Hap effectors interact with each other and form an effector complex *in vivo* (**Fig. 6C**).

**A**



**B**

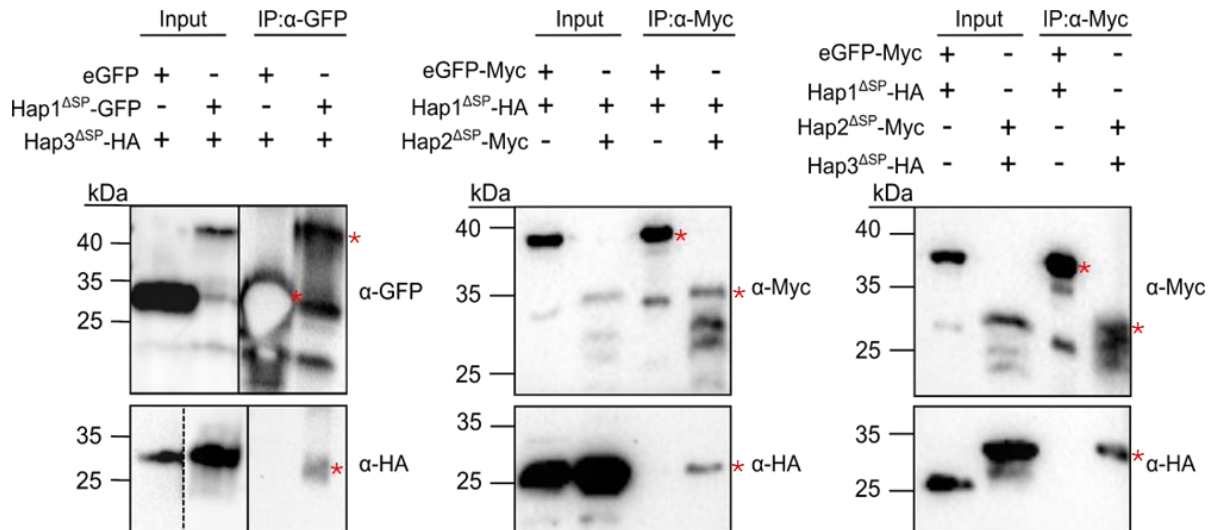


**Fig.6) Confirmation of Hap effector interaction using split-luciferase complementation assay and Co-IP.** **A)** Split-luciferase complementation assay of Hap effectors transiently co-expressed in *N. benthamiana*. Hap1<sup>ΔSP</sup>-nLuc, Hap2<sup>ΔSP</sup>-nLuc, Hap3<sup>ΔSP</sup>-nLuc, or empty-nLuc was transiently co-expressed with Hap1<sup>ΔSP</sup>-, Hap2<sup>ΔSP</sup>-, Hap3<sup>ΔSP</sup>-, or empty-cLuc. Luminescence was detected using Bio-Rad ChemiDoc™. The image depicts a representative picture obtained from three independent biological replicates. To enhance visualization, pseudo-fluorescence was applied using ImageJ software. **B)** Co-IP assay of Hap effectors in vivo. p2x35S-Hap1<sup>ΔSP</sup>-GFP or p2x35S-Hap2<sup>ΔSP</sup>-4xMyc with either p2x35S-Hap1<sup>ΔSP</sup>-6xHA or p2x35S-Hap3<sup>ΔSP</sup>-6xHA were transiently co-expressed in *N. benthamiana* for 2-3 days. As a control, p2x35S-Hap1<sup>ΔSP</sup>-6xHA with p2x35S-GFP or p2x35S-GFP-4xMyc were used. Proteins pulled-down with GFP or Myc magnetic beads were detected with anti-HA, anti-GFP, or anti-Myc antibodies. The expected size of proteins is as follows: Hap1<sup>ΔSP</sup>-GFP=40.05kDa; Hap2<sup>ΔSP</sup>-4xMyc=23.11kDa; Hap1<sup>ΔSP</sup>-6xHA=20.07kDa; Hap3<sup>ΔSP</sup>-6xHA=23.22kDa; GFP=27kDa; GFP-4xMyc=31.8 kDa.



### 2.2.3 Hap1 is the key virulence effector among Hap effectors

In the previous section, it was shown that Hap1, Hap2, and Hap3 interacted with each other *in vivo*. Therefore, it is intriguing to explore the potential additive effects or cooperative roles of these effectors in *U. maydis* virulence. To assess this, double- and triple frameshift knockout mutants of *hap2/3* and *hap1/2/3* were generated using CRISPR-Cas9 and subsequently performed maize infection. The double frameshift knockout mutants showed significant virulence reduction (13.3%), however, their virulence reduction was less pronounced compared to the single frameshift knockout mutant of *hap1* (27%). Furthermore, the triple frameshift knockout mutant showed a significant reduction in virulence similar to that observed in the single *hap1* frameshift knockout mutant (19.5%), suggesting that *hap1* is the dominant HTT-related effector contributing to *U. maydis* virulence, with *hap2* and *hap3* possibly displaying epistatic interaction with *Hap1* (Fig. 7A).

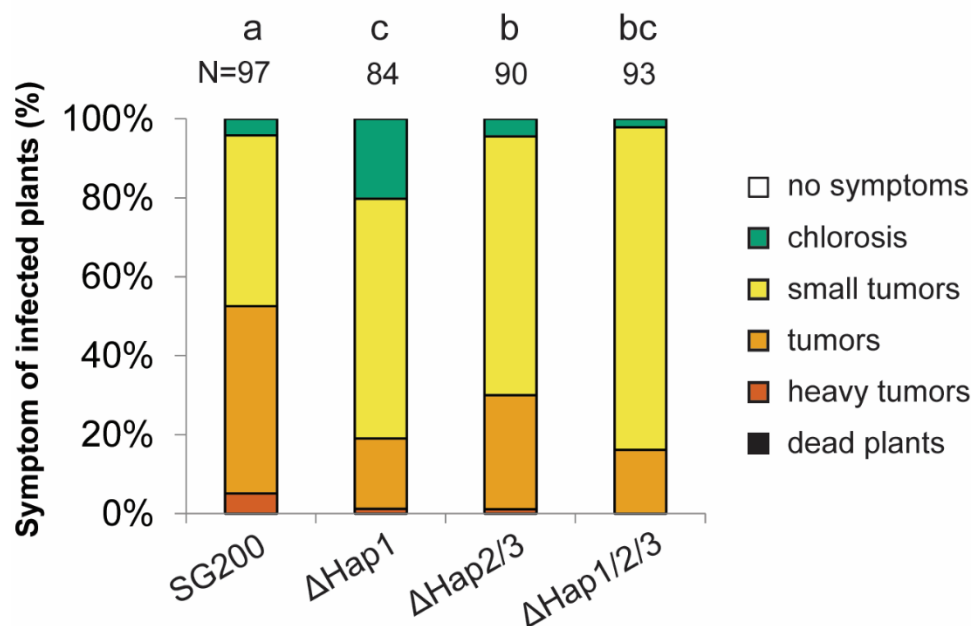


**Fig.7) Hap effectors are required for full virulence in *Ustilago maydis*.** A) Disease symptoms of *hap1* single, *hap2/3* double, and *hap1/2/3* triple frameshift knockout mutants infected in EGB maize seedlings compared to *U. maydis* SG200 at 12 dpi. The disease index of an average of three biological replications was used for the Student's t-test to calculate the P-value. n = number of infected plants. Statistics were performed using Tukey's hsd *post hoc* tests after one-way ANOVA,  $P < 0.05$ . Different letters represent significant differences between treatments.

## 2.3 Identification of maize targets upon *Ustilago maydis* infection

### 2.3.1 Hap1 interacts with all of the catalytic SnRK1 $\alpha$ subunits, a central metabolic regulator

Following the observation of Hap1's predominant role as a virulence effector among the three Hap effectors, we aim to elucidate potential maize interacting target(s) of Hap1 to unravel its molecular function in *U. maydis* virulence. To achieve this, a pull-down assay followed by MS analysis was conducted, as described in Section 2.2.1 (Fig. 8A). Maize extracts from Section 2.2.1. were utilized for the identification of possible Hap1 host targets. Proteins that were exclusively detected in Hap1-expressing samples were selected for further characterization. Additionally, to determine the biological processes of Hap1 interacting targets, Gene Ontology (GO) enrichment analysis was performed using PLAZAv5 and grouped the results into higher hierarchical terms with REVIGO. The analysis revealed that Hap1 targets are associated with protein phosphorylation and kinase activity, with particular emphasis on all isoforms of the Sucrose nonfermenting-1 (SNF1)-related protein kinase 1 (SnRK1)  $\alpha$  subunit. SnRK1 is a plant-specific signaling protein that plays a crucial role in carbon metabolism and energy homeostasis (Fig. 8B).

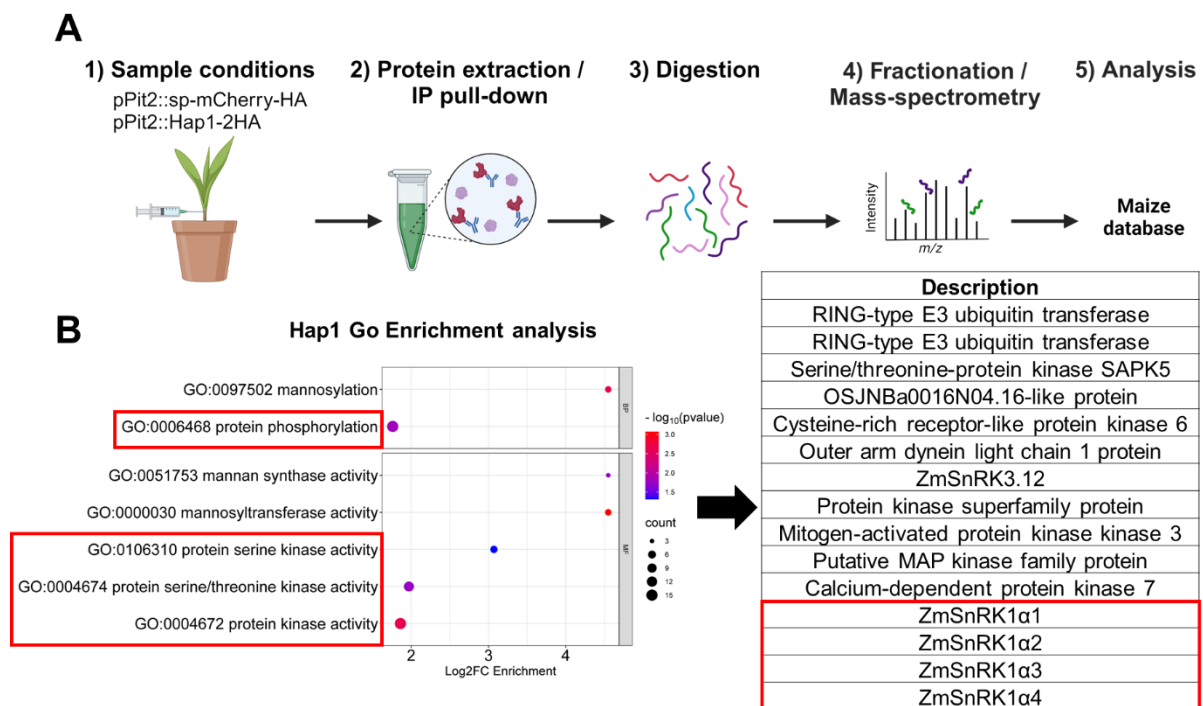


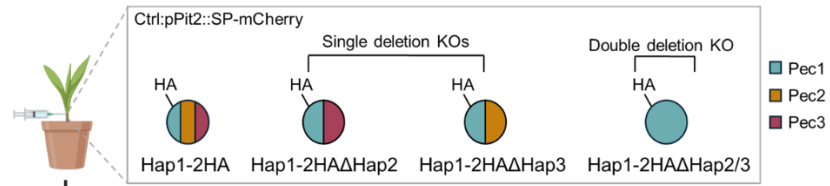
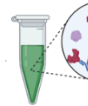
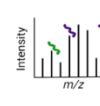
**Fig.8) IP/MS analysis to unravel the interactome of Hap1 host targets.** A) Schematic overview of the IP/MS workflow, summarizing the experimental protocol and data analysis for Hap1 host target identification. (1) 7-day-old maize seedlings were infected with *U. maydis*

SG200 strains expressing SG200 $\Delta$ Hap1-p*Pit2*::*Hap1-2xHA*, SG200 $\Delta$ Hap1-p*Pit2*::*Hap1-2xHA* $\Delta$ Hap2, SG200 $\Delta$ Hap1-p*Pit2*::*Hap1-2xHA* $\Delta$ Hap3, SG200 $\Delta$ Hap1-p*Pit2*::*Hap1-2xHA* $\Delta$ Hap2-3, or SG200-p*Pit2*::*SP-mCherry-HA* collected at 3 dpi. (2) Total maize proteins were extracted and immunoprecipitated with HA magnetic beads. (3) Proteins bound to HA magnetic beads were digested. (4) Digested protein peptides were fractionated and analyzed with MS. 5) Identified spectra are mapped against the *Z. mays* genome to search for potential interacting host proteins. **B)** Gene ontology enrichment analysis performed on the interactome of the Hap1 host target using PLAZAv5 and grouped into higher hierarchical terms with REVIGO. A list of proteins showing all biological processes related to protein kinase activity. The fold change (FC) values were calculated by dividing the LFQ intensity values of identified protein peptides in Hap1 compared to the control. Proteins with Log<sub>2</sub>FC of >1.0 with p < 0.05 (from the Student's t-test) were selected for GO enrichment. Red boxes indicate enrichment of proteins related to protein kinases and ZmSnRK1 $\alpha$ .

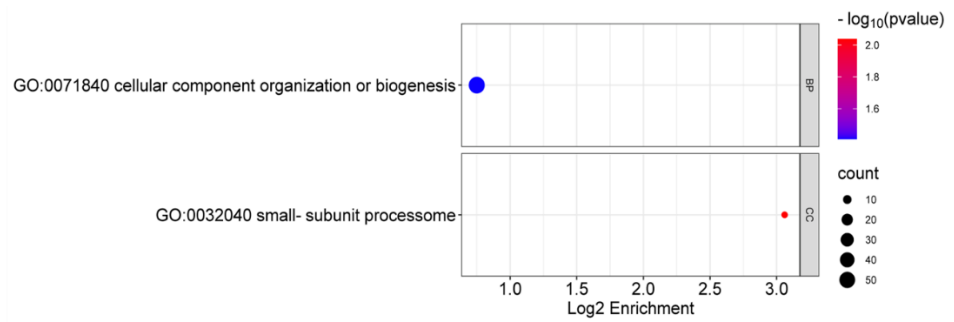
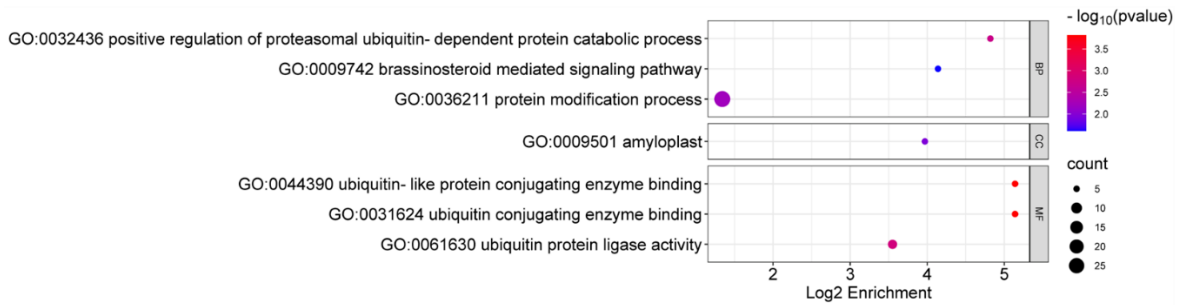
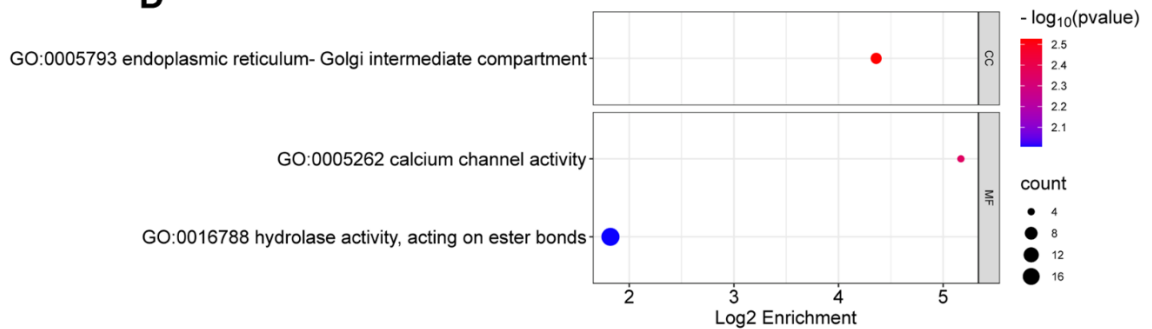
### 2.3.2 Disrupting Hap effector network alters Hap1's host interaction partner

Building upon our findings of interaction between Hap effectors and particularly Hap1's interaction with ZmSnRK1, we sought to explore potential alterations in host interacting partners with respect to frameshift knockout of Hap2 and Hap3. To address this, SG200 $\Delta$ Hap1-p*Pit2*::*Hap1-2xHA* was used as a background and the CRISPR-Cas9 harboring hygromycin cassette to generate single frameshift knockout mutants of *hap2* or *hap3* (SG200 $\Delta$ Hap1-p*Pit2*::*Hap1-2xHA* $\Delta$ *hap2* or SG200 $\Delta$ Hap1-p*Pit2*::*Hap1-2xHA* $\Delta$ *hap3*) and double frameshift knockout mutants of both *hap2* and *hap3* (SG200 $\Delta$ Hap1-p*Pit2*::*Hap1-2xHA* $\Delta$ *hap2-3*) was employed. Subsequently, we infected maize seedlings with knockout mutants alongside SG200-p*Pit2*::*SP-mCherry-HA* as a control for co-IP followed by MS analysis as described in Section 2.2.1. (**Fig. 9A**).

Proteins that were exclusively detected in Hap1 $\Delta$ Hap2, Hap1 $\Delta$ Hap3, or Hap1 $\Delta$ Hap2/3 expressing strains were selected for GO enrichment analyses using PLAZAv5. The analysis revealed that targets of Hap1 $\Delta$ Hap2 are associated with 'cellular components organization or biogenesis' in biological processes and 'small-subunit processome' in cellular components (**Fig. 9B**). For the Hap1 $\Delta$ Hap3 interacting proteins, GO enrichment included 'protein modification process', 'brassicasteroid mediated signaling pathway', and 'regulation of proteasomal ubiquitin-dependent catabolic processes' in biological processes, along with 'amyloplast' in cellular components and 'ubiquitin protein ligase' in molecular function (**Fig. 9C**). In Hap1 $\Delta$ Hap2/3 interacting proteins, 'ER-Golgi intermediate compartment' in the cellular component and 'calcium channel activity' and 'hydrolase activity' in molecular function were enriched (**Fig. 9D**).

**A****1) Sample conditions****2) Protein extraction / IP pull-down****3) Digestion****4) Fractionation / Mass-spectrometry****5) Analysis**

Maize database

**B****C****D**

**Fig.9) IP/MS analysis of Hap1ΔHap2, Hap1ΔHap3, and Hap1ΔHap2/3 host targets. A)** Schematic overview of the IP/MS workflow, summarizing the experimental protocol and data analysis for Hap1ΔHap2, Hap1ΔHap3, and Hap1ΔHap2/3 host target identification. (1) 7-day-old maize seedlings infected with *U. maydis* SG200 strains expressing SG200ΔHap1-p*Pit2*::*Hap1-2xHAA*ΔHap2, SG200ΔHap1-p*Pit2*::*Hap1-2xHAA*ΔHap3, SG200ΔHap1-p*Pit2*::*Hap1-2xHAA*ΔHap2-3, or SG200-p*Pit2*::*SP-mCherry-HA* were collected at 3 dpi. (2) Total maize proteins were extracted and immunoprecipitated with HA magnetic beads. (3) Proteins bound to HA magnetic beads were digested. (4) Digested protein peptides were fractionated and analyzed with MS. (5) Identified spectra are mapped against the *Z. mays* genome to search for potential interacting host proteins. **B)** Gene ontology enrichment analysis performed on the interactome of the Hap1ΔHap2 host targets. **C)** Gene ontology enrichment analysis performed on the interactome of the Hap1ΔHap3 host targets. **D)** Gene ontology enrichment analysis performed on the interactome of the Hap1ΔHap2/3 host targets. All GO analyses were performed using PLAZAv5 and grouped into higher hierarchical terms with REVIGO. The fold change (FC) values were calculated by dividing the LFQ intensity values of identified protein peptides in Hap1ΔHap2, Hap1ΔHap3, or Hap1ΔHap2/3 compared to the control. Proteins with Log<sub>2</sub>FC of >1.0 with p < 0.05 (from the Student's t-test) were selected for GO enrichment.

Subsequently following changes in the GO enrichment analysis after the frameshift knockout of Hap2 and/ or Hap3, we focused our search on kinases and SnRK1 substrates, as SnRK1α was the primary host target(s) of Hap1. Interestingly, we observed more abundant interaction with phosphatases across all Hap2 and Hap3 single- and double frameshift knockout mutant conditions, as well as trehalose-6-phosphate synthases, known SnRK1 substrates (**Table 2**). Particularly, Hap1ΔHap2 interacted with protein phosphatase 2C (PP2C), a regulator of signal transduction pathway, modulating receptor-like kinases and abscisic acid signaling (Schweighofer et al., 2004). It also interacted with phosphotyrosyl phosphatase activator (PTPA), which activates protein phosphatase 2A (PP2A). In addition, Hap1ΔHap2 and Hap1ΔHap2/3 demonstrated interaction with PPP2CB, a catalytic subunit of PP2A. PP2A is a major serine/threonine phosphatase that negatively regulates cell cycle progression, controlling the timing and coordination of cell division (Wlodarchak & Xing, 2016). The Hap1ΔHap3 showed interactions with enzymes involved in starch biosynthesis as well as kinases and phosphatases involved in the brassicasteroid signaling pathway. While Hap3 single and Hap2-3 double frameshift knockout mutants showed interaction with SnRK2, a kinase involved in stress and abscisic acid (ABA)-mediated signaling pathways, and fructose-2,6-biphosphatases, enzymes regulating glycolysis and gluconeogenesis (**Table 2**).

**Table 2) The list of proteins identified in the Hap2 and Hap3 single- and double frameshift knockout.**

Green: identically identified in both Hap2 and Hap2-3 frameshift knockout mutants. Pink: identically identified in both Hap3 and Hap2-3 frameshift knockout mutants. Blue: identically identified in Hap2 and Hap3 frameshift knockout mutants. Orange color: identically identified in all frameshift knockout mutant conditions. The listed proteins are exclusively present in SG200ΔHap1-p*Pit2*::*Hap1-2xHAA*ΔHap2, SG200ΔHap1-p*Pit2*::*Hap1-2xHAA*ΔHap3, or SG200ΔHap1-p*Pit2*::*Hap1-2xHAA*ΔHap2-3 mutants compared to the control, with a particular focus on kinases, phosphatases, SnRK1 substrates, and carbon metabolism.



Hap1-2HAΔHap2



Hap1-2HAΔHap3



Hap1-2HAΔHap2/3

<b>Kinases and phosphatases</b>		
PPP2CB	Serine/threonine phosphatases (BSL)	PPP2CB
PTPA	Serine_threonine-protein phosphatase	Serine threonine-protein phosphatase
Protein phosphatase 2C	Fructose-2,6-bisphosphatase	Fructose-2,6-bisphosphatase
RIO kinase 1	Protein kinase domain-containing protein	Protein kinase domain-containing protein
MAP3K-RAF	MAP3K-RAF	Serine_threonine protein kinase 3
Serine_threonine-protein phosphatase	SnRK2	SnRK2
Protein kinase superfamily protein	Protein kinase superfamily protein	Protein kinase superfamily protein
NAD kinase 2	NAD kinase 2	
	Uridine kinase	
	PTI1-like tyrosine-protein kinase 3	
<b>SnRK1 substrates and proteins in C metabolism</b>		
TPSII.3.1, 3.2	TPSII.3.1, 3.2	TPS13
Putative TPS7	Starch synthase 3	TPS5
	1,4-alpha-glucan branching enzyme	TPSII.2.1, 2.2

### 2.3.3 Hap1 interacts with the catalytic subunit of ZmSnRK1 in the split-luciferase complementation assay and co-IP

To confirm the interaction between Hap1 and ZmSnRK1 $\alpha$ , a split-luciferase complementation assay was conducted as described in Section 2.2.2. In this assay, ZmSnRK1 $\alpha$ 1-, ZmSnRK1 $\alpha$ 2-, or ZmSnRK1 $\alpha$ 3-nLuc was transiently co-expressed with Hap1 $\Delta$ SP-cLuc in *N. benthamiana* using *Agrobacterium*-mediated transformation. Empty-nLuc or -cLuc were used as a control. To test the autoactivation of either domain of the fused proteins of interest, ZmSnRK1 $\alpha$ 1-, ZmSnRK1 $\alpha$ 2-, or ZmSnRK1 $\alpha$ 3-nLuc or Hap1 $\Delta$ SP-cLuc were co-infiltrated with Empty-nLuc or -cLuc. Luminescence signal was exclusively observed when Hap1 $\Delta$ SP-cLuc and ZmSnRK1 $\alpha$ 2-nLuc are co-expressed, while no visible signal was observed when Hap1 $\Delta$ SP-cLuc is co-expressed with ZmSnRK1 $\alpha$ 1-nLuc, ZmSnRK1 $\alpha$ 3-nLuc, or empty-cLuc and -nLuc controls (**Fig. 10A**).

To further confirm the interaction between Hap1 with ZmSnRK1 $\alpha$ 1, ZmSnRK1 $\alpha$ 2, or ZmSnRK1 $\alpha$ 3, co-IP assays in *N. benthamiana* were conducted as described in Section 2.2.2. *Agrobacterium* strains carrying vector containing Hap1 $\Delta$ SP-6xHA were co-infiltrated with either ZmSnRK1 $\alpha$ 1-4xMyc, ZmSnRK1 $\alpha$ 2-4xMyc, or ZmSnRK1 $\alpha$ 3-4xMyc. As a negative control, *Agrobacterium* strain carrying vector containing GFP-4xMyc was co-infiltrated with Hap1 $\Delta$ SP-6xHA. Agroinfiltrated leaves of ZmSnRK1 $\alpha$ 1, ZmSnRK1 $\alpha$ 2, or ZmSnRK1 $\alpha$ 3 were co-immunoprecipitated by  $\alpha$ -Myc immunoprecipitation of Hap1 $\Delta$ SP-6xHA, but not in GFP-4xMyc control (**Fig. 10B**). In addition to the split-luciferase complementation assay and co-IP, ZmSnRK1 $\alpha$ 1, or ZmSnRK1 $\alpha$ 3 with Hap1 interactions were confirmed with the yeast-two-hybrid assay (**Fig. S4**). These results suggest that Hap1 interacts with catalytic subunits of ZmSnRK1.

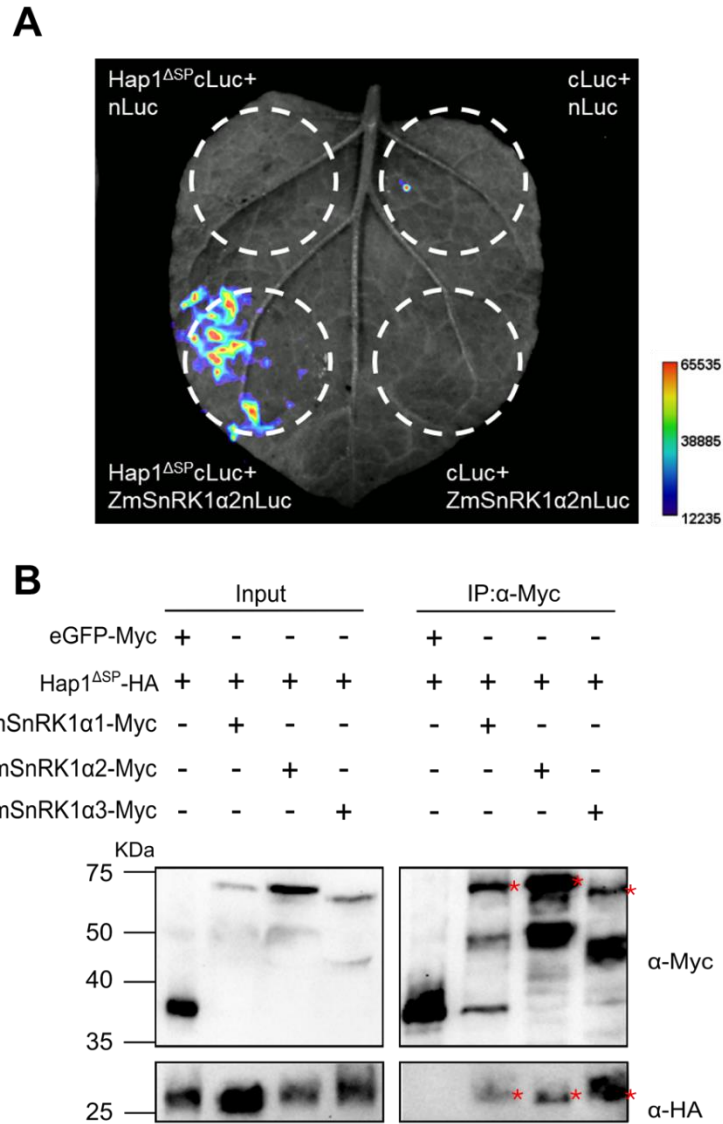


**Fig.10) Confirmation of Hap1 and ZmSnRK1 interaction using split-luciferase complementation assay and co-IP. A)** Split-luciferase complementation assay of Hap1 and ZmSnRK1α1, ZmSnRK1α2, or ZmSnRK1α3 in *N. benthamiana*. *Agrobacterium* carrying vector containing ZmSnRK1α1-, ZmSnRK1α2-, or ZmSnRK1α3-nLuc, empty-nLuc, was transiently co-expressed with Hap1<sup>ΔSP</sup>-cLuc or empty-cLuc. Luminescence was detected using Bio-Rad ChemiDoc™. The image depicts a preliminary result of two biological replicates. To enhance visualization, pseudo-fluorescence was applied using ImageJ software. **B)** Co-IP assay between Hap1 and ZmSnRK1α1, ZmSnRK1α2, or ZmSnRK1α3. p2x35S-ZmSnRK1α1-4xMyc, p2x35S-ZmSnRK1α2-4xMyc, or p2x35S-ZmSnRK1α3-4xMyc with p2x35S-Hap1<sup>ΔSP</sup>-6xHA were transiently co-expressed in *N. benthamiana* for 2-3 days. As a control, p2x35S-Hap1<sup>ΔSP</sup>-6xHA with p2x35S-GFP-4xMyc were used. Proteins pulled down with Myc magnetic beads were detected with anti-HA and anti-Myc antibodies. The expected size of proteins is as follows: ZmSnRK1α1-4xMyc=64.23kDa; ZmSnRK1α2-4xMyc=63.27kDa; ZmSnRK1α3-4xMyc=62.96kDa; Hap1<sup>ΔSP</sup>-6xHA=20.07kDa; GFP-4xMyc=31.8 kDa.



## 2.4 Phosphoproteomic analysis of maize upon *Ustilago maydis* infection

To investigate the phosphorylation profile of maize in response to *U. maydis* infection and whether the presence of Hap1 affects the SnRK1-dependent phosphorylation, a quantitative phosphoproteomic analysis on EGB maize seedlings infected with mock and *Ustilago* (SG200 and  $\Delta$ Hap1) strains was performed. Infected maize seedlings were collected at 3 dpi and subjected to protein extraction. The time point for 3 dpi was selected based on previous publication indicating the highest expression of Hap1 occurs at 2-3 dpi during early biotrophic development (Lanver et al., 2018). Afterwards, in collaboration with Dr. Hirofumi Nakagami (Max Planck Institute for Breeding, Cologne, Germany), the extracted proteins were then digested and enriched with titanium-dioxide for phospho-analysis by LC-MS/MS (**Fig. 11A**).

First, to distinguish proteins that are specifically enriched due to phosphorylation, rather than as a result of the general protein abundance, a Venn analysis of the phosphoproteome and total proteome in *Ustilago*-infected (SG200 or  $\Delta$ Hap1) compared to a mock sample using a cut-off of  $\text{Log}_2\text{FC} \geq 1$  or  $\leq -1$  and  $\text{FDR} < 0.05$  was performed. In the phosphoproteome analysis of the SG200-infected sample compared to mock (S vs M), 3618 proteins with increased phosphopeptides and 180 proteins with decreased phosphopeptides from 2237 and 148 proteins were identified, respectively. In the total proteome, S vs M analysis revealed 1535 enriched and 745 decreased proteins (**Fig. S5A and S5B**). Integration of these datasets using Venn diagram analysis resulted in 1983 unique proteins with increased phosphorylated proteins (**Fig. S5A**). Similarly, in the comparison between  $\Delta$ Hap1-infected compared to mock (dH vs M), phosphoproteome revealed 1480 increased and 117 decreased phosphopeptides from 1205 and 94 enriched and decreased proteins, respectively. In the total proteome of dH vs M, 1086 enriched and 567 decreased proteins have been identified, respectively (**Fig. S6C and S6D**). Integrating these datasets resulted in 1028 unique phosphorylated proteins (**Fig. S6C**). Interestingly, proteins with increased phosphorylation from S vs M sample identified approximately twice as many phosphorylated proteins as the dH vs M sample, suggesting the absence of Hap1 prevents the interaction with potential targets that are involved in post-translational modification.

Subsequently, to discern Hap1-dependent and Hap1-independent phosphorylation, uniquely increased or decreased phosphorylated proteins in S vs M and dH vs M were compared. The analysis revealed 1108 and 73 proteins with increased and decreased phosphopeptides in S vs M, respectively. In dH vs M, 153 and 22 increased or decreased phosphorylated proteins were

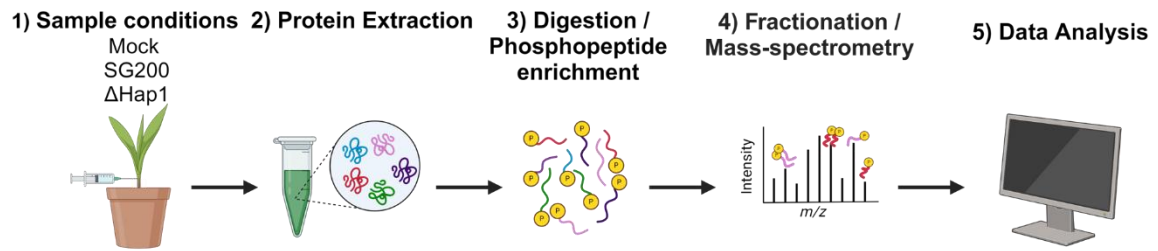
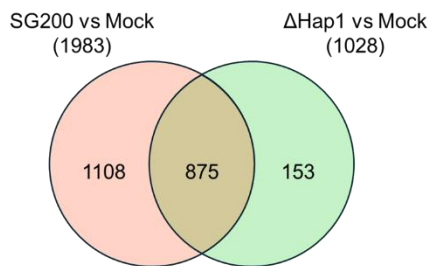
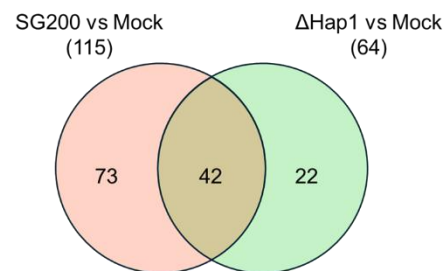
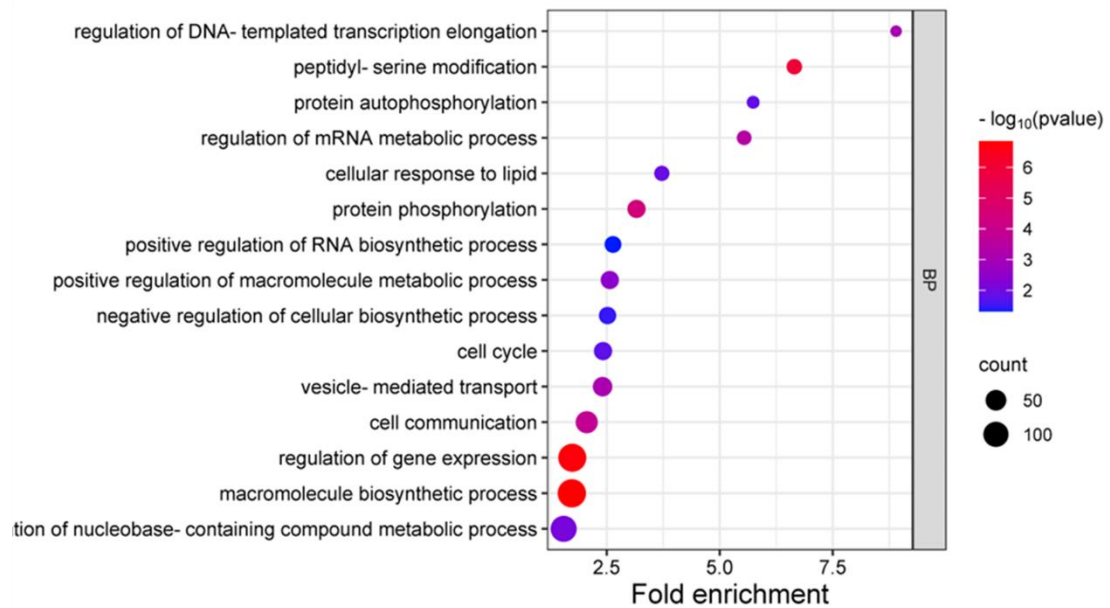
identified, respectively. Surprisingly, 85% (875) of phosphorylated proteins in the dH vs M sample overlapped with those in the S vs M sample. This indicates that SG200 and  $\Delta$ Hap1 have congruent regulatory responses and signaling events and that the absence of Hap1 has no discernible effect on these processes (**Fig. 11B and C**). To further study phosphorylation changes of maize upon infection, SG200 to  $\Delta$ Hap1 (S vs dH) was compared, resulting in 332 increased and 15 decreased phosphorylated proteins.

To study the biological implications of increased proteins containing phosphopeptides in S vs M, dH vs M, and S vs dH, GO enrichment overrepresentation analysis using PANTHER v18.0 was performed. In S vs M, enrichment analysis revealed ‘peptidyl-serine modification’, ‘negative regulation of metabolic process’, ‘protein autophosphorylation’, and ‘regulation of gene expression’ (**Fig. 11D**). Similarly, analysis of increased phosphorylated proteins in dH vs M revealed ‘RNA processing’ and ‘cellular response to stimulus’ (**Fig. 11E**). Furthermore, in S vs dH, ‘cell cycle’, ‘organelle organization’, and ‘rRNA processing’ were enriched.

Next, to investigate the phosphorylation status changes in response to *U. maydis* infection and its association with Hap1, we focused our search on the known SnRK1 consensus sequence and its substrates (**Table 3**). This motif consists of a 10-amino acid motif (phiXXXXS/TXXXphi), where phi represents hydrophobic residues (M, L, V, I, or F) at positions P-5 and P+4, and a basic residue at positions P-3 and P-4 relative to the serine/threonine residue (Broeckx et al., 2016) et al., 2016). Additionally, valine or serine at position P-2 and aspartic acid or asparagine at position P+3 of the human AMPK consensus motif was considered as selection criteria. Using the Find Individual Motif Occurrences (FIMO) database, the occurrence of SnRK1 consensus sequence on 1108 increased and 73 decreased unique to S vs M, and 153 increased and 22 decreased unique to dH vs M were searched. In addition, increased and decreased phosphorylated proteins from S vs dH were scanned to search for Hap1-dependent and independent phosphorylation. A total of 67 motifs matching the known SnRK1 consensus sequence among increased phosphorylated proteins and 6 motifs among the decreased phosphorylated proteins were found in S vs M, while in dH vs M, 13 increased and 1 among the decreased phosphorylated proteins were found. Finally, cross-referencing with phosphoproteomic data resulted in 10 proteins that perfectly matched the SnRK1 consensus sequence. When we relaxed the stringency of hydrophobic residues to only one of the two positions (P-5 or P+4) or containing only hydrophobic residues at (P-5 or P+4), 28 proteins were found to match the SnRK1 consensus sequence. However, it is important to interpret found motifs with caution since the SnRK1 consensus sequence is similar to the

phosphorylation motif of calcium-dependent protein kinases (CDPKs) (Broeckx et al., 2016; Nukarinen et al., 2016; Van Leene et al., 2022).

SnRK1 is a heterotrimeric serine-threonine kinase consisting of a catalytic  $\alpha$  subunit, a substrate interacting  $\beta$  subunit, and a regulatory  $\gamma$  subunit. It orchestrates myriads of transcriptional and metabolic reprogramming via direct phosphorylation of key transcription factors and metabolic enzymes to restrict energy-consuming anabolic processes under energy-limitation conditions and in turn promote energy-promoting catabolic processes (Baena-González & Hanson, 2017; Broeckx et al., 2016; Emanuelle et al., 2016; Peixoto et al., 2021). Interestingly, in our phosphoproteomic analysis we found that SnRK1 $\alpha$ 1,  $\beta$ 1 and  $\beta$ 2, and  $\gamma$  are highly phosphorylated in S vs M, but not in dH vs M. This suggests that the presence of Hap1 is indispensable for SnRK1 complex integrity and formation. However, it is important to note that the increased phosphopeptide identified in SnRK1 $\alpha$  did not align with the conventional SnRK1 T-loop phosphorylation site and was observed only in one of the four SnRK1 $\alpha$  subunits. Furthermore, our analysis of identified SnRK1 consensus-dependent sequences across different sample conditions revealed several enzymes that play a key role in primary metabolism. The proteins that were increased with phosphorylation in S vs M include sucrose synthase 7 (Susy 7) and Alkaline sucrose-specific invertase (CINV) that are involved in starch biosynthesis and breakdown of sucrose, respectively. The proteins that were decreased in S vs M identified transcription factor bZIP63, sucrose phosphate synthase1 (SPS1), poorly characterized phosphatase C (PP2C), and FCS-like zinc finger (FLZ) that have shown to be associated with sucrose biosynthesis and energy starvation, respectively. In S vs dH, the increased phosphorylated protein identified choline kinase, which is involved in lipid metabolism. (**Fig. 11F**).

**A****B** Increased phosphorylated proteins**C** Decreased phosphorylated proteins**D**

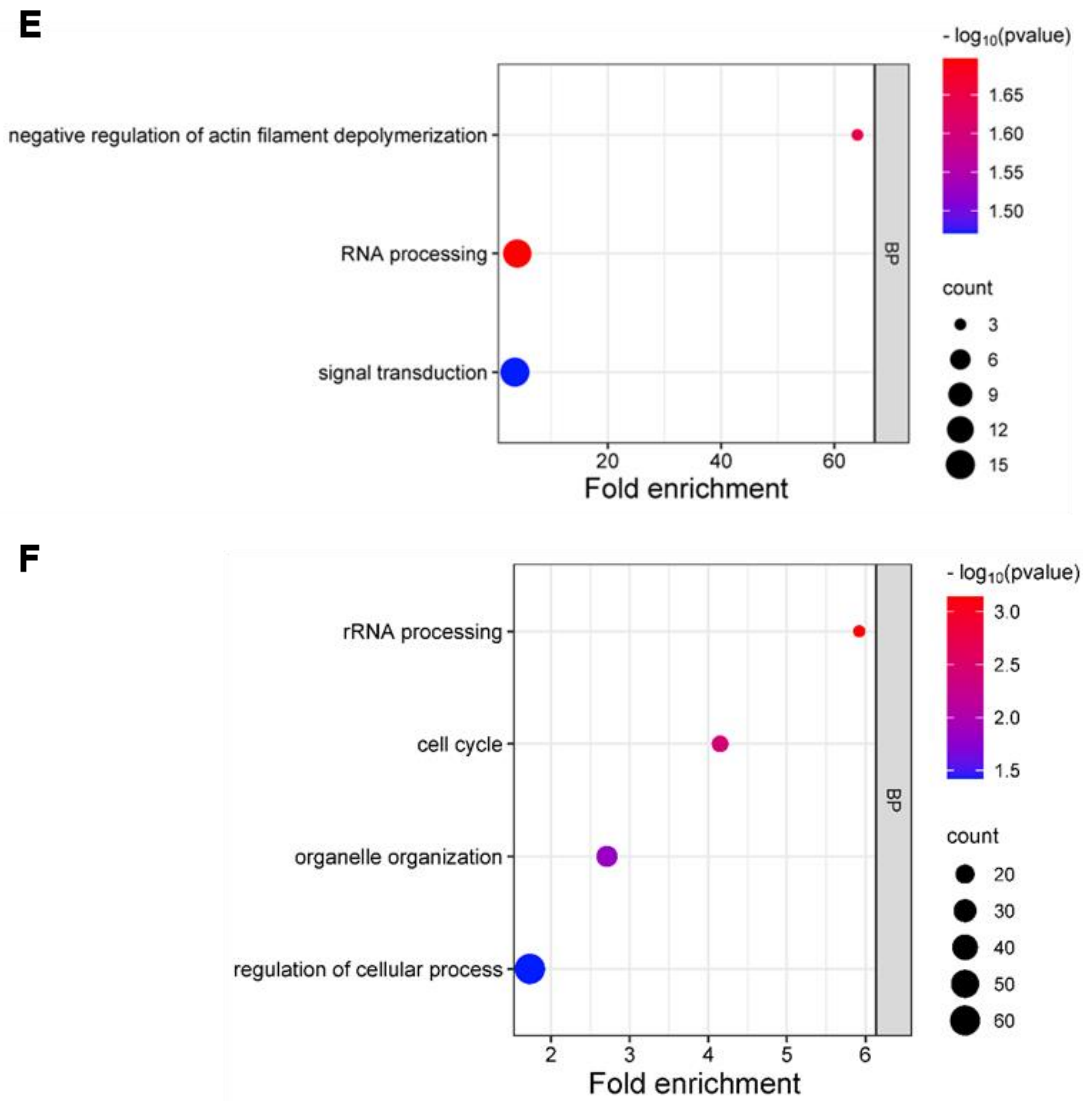


**Fig. 11) Phosphoproteomic analysis of maize infected with *Ustilago maydis* (SG200 and ΔHap1)** **A)** Schematic overview of phosphoproteomics experiment. (1) 7-day-old maize seedlings were infected mock, SG200, and *U. maydis* SG200 strains expressing SG200ΔHap1 collected at 3 dpi. (2) Total maize proteins were extracted and separated for total proteome and phosphoproteome (3) Digested protein peptides were phosphoenriched with titanium-dioxide. (4) Peptides were fractionated and analyzed with MS. 5) Identified spectra are mapped against the *Z. mays* genome to search for potential phosphorylation sites. **B)** Venn diagram depicting uniquely increased proteins with phosphorylation in SG200 and ΔHap1 in comparison to mock. **C)** Venn diagram depicting uniquely down-regulated proteins with phosphorylation in SG200 and ΔHap1 in comparison to mock.  $\text{Log}_2\text{FC} > 1$  or  $< -1$  and  $\text{FDR} < 0.05$  **D)** GO enrichment analysis of proteins with phosphorylation increased in SG200 to mock comparison. **E)** GO enrichment analysis of proteins with phosphorylation increased in ΔHap1 to mock comparison. **F)** GO enrichment analysis of proteins with phosphorylation increased in SG200 to ΔHap1 comparison. The significance of  $-\text{Log}_{10}(\text{P-value})$  values is represented from red to blue. Only up to 15 significant parental terms are illustrated.

**Table 3) Overview of the SnRK1-dependent consensus motif at P-5 and P+4 relative to phosphorylated Ser/Thr residues.**

The AMPK consensus phosphorylation sequence is colored in pink and blue at P-2 and P+3 positions, respectively.  $\text{Log}_2\text{FC} > 1$  or  $< -1$  and  $\text{FDR} < 0.05$ .

	Annotation	Position									Log2FC				
		-5	-4	-3	-2	-1	0	1	2	3	4	SG200 vs Mock	$\Delta\text{Hap1}$ vs Mock	SG200 vs $\Delta\text{Hap1}$	
SnRK1-related	SnRK1 $\beta$ 1	V	R	R	A	C	S	V	G	V	V	1.39			
	SnRK1 $\beta$ 2	V	R	R	A	C	S	V	G	V	V				
	TPSII.3.1	M	S	R	S	Y	T	N	L	L	D				1.08
	TPSII.3.2	M	S	R	S	Y	T	N	L	L	D				-1.73
	TPSII.5.3	L	P	R	V	M	S	V	A	S	P				2.45
Sucrose	SPS1	F	Q	R	N	F	S	D	L	T	V	-2.96	-1.71	-1.25	
	Susy2	L	D	R	N	P	S	I	R	D	R	3.08			
	Susy7	F	K	R	A	D	S	I	A	E	S	1.66			
	Alkaline sucrose-specific invertase (CIN)	M	R	K	A	S	S	Q	A	S	L	4.05			
Transcription factor	Transcription initiation factor1 IIB1	L	A	R	S	A	S	T	F	S	G	2.30			
	PBRP	L	A	R	S	A	S	T	F	S	G	2.30			
	BLHL	F	R	H	S	S	S	P	A	G	L	1.89			
	Bzip63	L	H	R	V	A	S	L	E	N	L	-1.25			
Lipid metabolism	Choline kinase	L	K	R	S	A	S	I	D	R	I	2.15		1.95	
Protein homeostasis /modification	GALT2	M	K	R	A	R	S	S	E	V	F	1.79			
	RING-type E3 ubiquitin transferase	F	P	R	I	I	S	S	S	T	M	1.77			
Vesicle trafficking	AGD7	M	R	R	N	Q	S	V	G	S	F	1.20			
Histone modification	JMJ703	I	A	D	E	D	S	D	A	E	V	1.43			
Microtubule	Kinesin	F	R	R	R	H	S	F	G	E	D	2.99			
Other	DUF632	I	R	K	G	R	S	G	E	A	P	1.00			
	Zinc finger (CCCH-type) family protein NCH1	L	K	E	S	L	S	P	V	L	D	1.02			
	Flowering time control protein	M	K	R	T	R	S	V	N	A	V	1.12			
	unknown	L	R	F	Q	Q	S	N	P	N	Y	1.73			
	unknown	L	H	S	L	S	S	A	A	S	V	5.00			
	PP2C	M	E	E	H	S	S	Q	G	L	V	2.20			
	FCS-like zink finger (FLZ)	V	S	T	E	S	S	I	F	E	I	-2.11			
	ACC1	M	R	R	T	T	S	M	T	E	F	-2.64			
	V	A	R	S	L	S	D	L	G	M	3.66	1.95			

## 2.5 Hap1 is involved in the reprogramming of primary metabolism

### 2.5.1 Differential gene expression analysis in SG200 and SG200 $\Delta\text{hap1}$ infected leaves

To study the impact of Hap1 and Hap2 on global gene expression in maize during *U. maydis* infection at the molecular level, transcriptome profiling via RNA sequencing (RNA-seq) was performed. EGB maize seedlings were infected with mock and *Ustilago* (SG200, SG200 $\Delta\text{hap1}$ , SG200 $\Delta\text{hap2}$ , and SG200 $\Delta\text{hap3}$  (positive control)) and collected samples at 3 dpi from three independent biological replicates. The time point for 3 dpi was selected based on previous publication indicating the highest expression of *hap1*, *hap2*, and *hap3* occurs at 2dpi during early biotrophic development (Lanver et al., 2018). SG200 $\Delta\text{hap3}$  was used as a positive control, as it showed virulence reduction only in the GB maize line, whereas *hap1* and

*hap2* showed in the EGB maize line. A principal component analysis (PCA) was performed to observe distinct grouping patterns among mock-infected and *Ustilago*-infected (SG200,  $\Delta hap1$ ,  $\Delta hap2$ , and  $\Delta hap3$ ) samples. The mock samples were clearly separated from the infected ones.  $\Delta hap1$  samples were distinct from mock, SG200, and  $\Delta hap3$  samples, while  $\Delta hap2$  closely clustered with SG200 and  $\Delta hap3$  (Fig. 12A). Thus, we focus on transcriptomic analysis of  $\Delta hap1$ .

Next, RNA-seq was analyzed using edgeR (Robinson et al., 2010) to dissect gene expression changes across different treatments. Pairwise comparisons were made between the *U. maydis*-infected (SG200 or  $\Delta hap1$ ) and the mock-infected treatments (i.e., S vs M and dH vs M), using a cut-off of  $\text{Log}_2\text{FC} > 1$  or  $< -1$  and  $\text{FDR} < 0.05$  to identify differentially expressed genes (DEGs). In the S vs M, 12,492 genes showed significantly differential expression, with 7,676 up-regulated and 4,816 down-regulated genes. In the dH vs M, 10,603 genes were differentially expressed, with 6,795 up-regulated and 3,808 down-regulated genes (Fig. 12B). Notably, 5,974 up-regulated and 3,072 down-regulated DEGs were commonly shared between the S vs M and dH vs M (Fig. 12C and D).

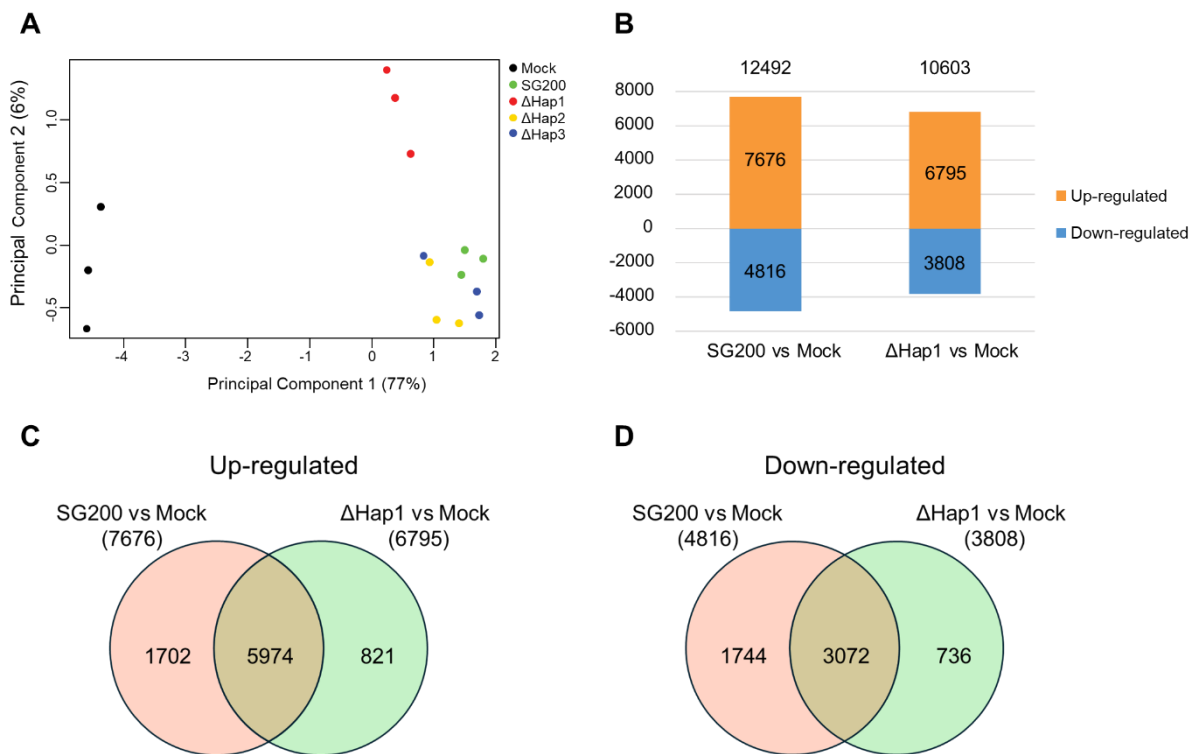


**Fig. 12) Differentially expressed genes in comparison of *Ustilago maydis*-infected (SG200 or  $\Delta hap1$ ) to mock-infected treatments. A) PCA illustrating different RNAseq sample distributions. Row counts were calculated for the contributions of the PCs. B) Pairwise bar graph depicting the number of up- and down-regulated DEGs in *U. maydis*-infected (SG200 or**

*Δhap1*) versus mock-infected treatments. DEGs =  $\text{Log}_2\text{FC} > 1$  or  $< -1$  and  $\text{FDR} < 0.05$ . **C and D**) Venn diagram depicting the number of commonly shared and unique DEGs of up- and down-regulated genes in *U. maydis*-infected (SG200 or *Δhap1*) versus mock-infected treatments, respectively.

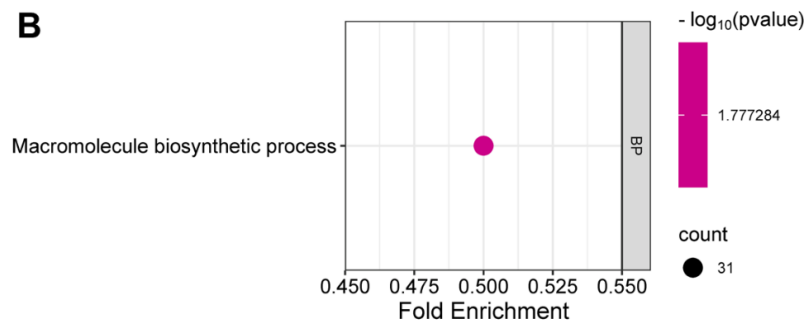
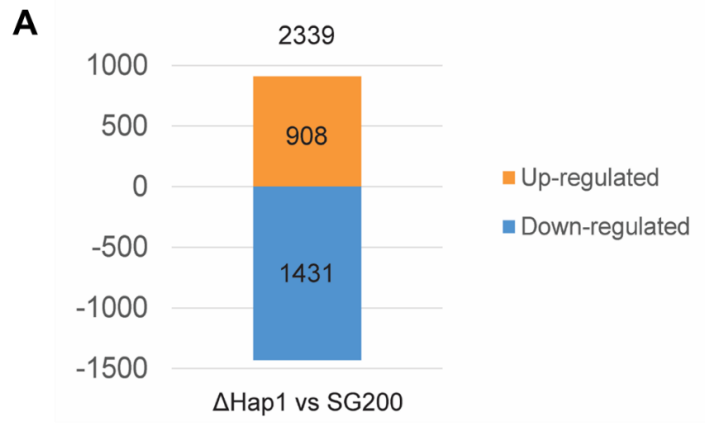
To understand the function of commonly shared DEGs, GO overrepresentation analysis was performed using PANTHER 18.0. The analysis is presented with GO in a hierarchy and reveals biological processes related to ‘regulation of primary metabolic process’, ‘carbohydrate derivative metabolic process’, and ‘carbohydrate catabolic process’. Additionally, and Kyoto Encyclopedia of Genes and Genomes (KEGG) pathway enrichment analysis (Kanehisa & Goto, 2000) was performed on 367 mapped KEGG pathways, displaying biosynthesis of secondary metabolites, starch and sucrose metabolism, and amino sugar and nucleotide sugar metabolism. Taken together, these data indicate that *U. maydis* affects cellular activities associated with the synthesis of complex molecules and the metabolism of carbohydrates and their derivatives within the host.

To further evaluate the impact of *hap1* in host transcriptional response to *U. maydis* infection, *Δhap1* and SG200 treatments were pairwise compared (i.e., dH vs S). This comparison resulted in 908 up-regulated and 1,431 down-regulated DEGs out of a total of 2,339 genes (**Fig. 13A**). Functional enrichment analysis of up-regulated (*Δhap1*) DEGs showed a biological process ‘macromolecule biosynthetic process’, while DEGs (presence of *hap1*) revealed genes associated with biological processes, such as ‘regulation of metabolic process’, ‘cell cycle phase transition, and ‘regulation of protein modification process’ (**Fig. 13B and C**). KEGG analysis was performed on 1,343 DEGs which resulted in the mapping of 217 KEGG pathways, including biosynthesis of secondary metabolites, starch and sucrose metabolism, amino sugar and nucleotide sugar metabolism, and glycolysis and gluconeogenesis. The aforementioned criteria were used for GO and KEGG enrichment analyses. These data suggest that *hap1* may play a role in promoting endoreduplication of mesophyll HTT cells by facilitating cell cycle transition from the mitotic phase to the synthesis phase of the cell cycle and this might be contingent upon the availability of carbon resources in the tumor.

In the previous section, we showed the interaction between Hap1 and SnRK1, a central metabolic switch. Additionally, phosphoproteomics analysis results revealed significant phosphorylation changes in enzymes essential for primary metabolism, especially in the starch biosynthesis pathway in different treatments. Furthermore, functional enrichment pathway analysis (GO and KEGG) between dH vs S treatments highlighted their integral role in primary



metabolism regulation and cell cycle, prompting us to investigate DEGs related to starch metabolism. Starch is an essential carbohydrate reserve in vegetative tissues, made up of  $\alpha$ -glucose polymers containing approximately 20-30% amylose and 70-80% amylopectin (MacNeill et al., 2017). Its synthesis involves multiple enzymes, such as adenosine 5' diphosphate-glucose pyrophosphorylase (AGPase), starch synthase (SS), granule-bound starch synthase (GBSS), starch branching enzyme (SBE), and debranching enzyme (DBE). In the production of starch, GBSS contributes to amylose biosynthesis, whereas SSs, SBEs, and DBEs are responsible for amylopectin biosynthesis (Keeling & Myers, 2010). Interestingly, upon closer examination of down-regulated DEGs in the dH vs S, increased expression levels of *AGPase3*, *SBE1*, and *Ael* were observed (**Fig. 13D**). This indicates that *Hapl* is involved in the regulation of gene expression of *SBEs*, which mainly act on amylopectin, a major component of starch, and facilitate the conversion of ADPG to starch by AGPase, as well as regulate the induction of starch degradation to a usable carbon source. On the contrary, in the up-regulated DEGs comparing the dH vs S, high expression levels of *WRKY17*, *WRKY27*, *WRKY29*, *WRKY73*, *WRKY74*, and *WRKY82* transcription factors involved in the signal transduction and stress responses were observed. *WRKY17* was shown to be up-regulated upon infection of *U. maydis* and interacts with the SWEET4b transporter in yeast-one-hybrid assay (Y. Wang et al., 2023). The Arabidopsis homolog of *WRKY17* activates SA-dependent defense genes and represses JA-regulated genes, fine-tuning plant defense response (Li et al., 2006). *WRKY82* regulates the phenolic pathway in maize (F. Yang et al., 2017). Not only WRKY TFs were identified, but also up-regulated genes related to cell surface receptor signaling pathways such as wall-associated kinases and lectin domain-containing proteins, which are important for plant immunity against pathogenic attack.



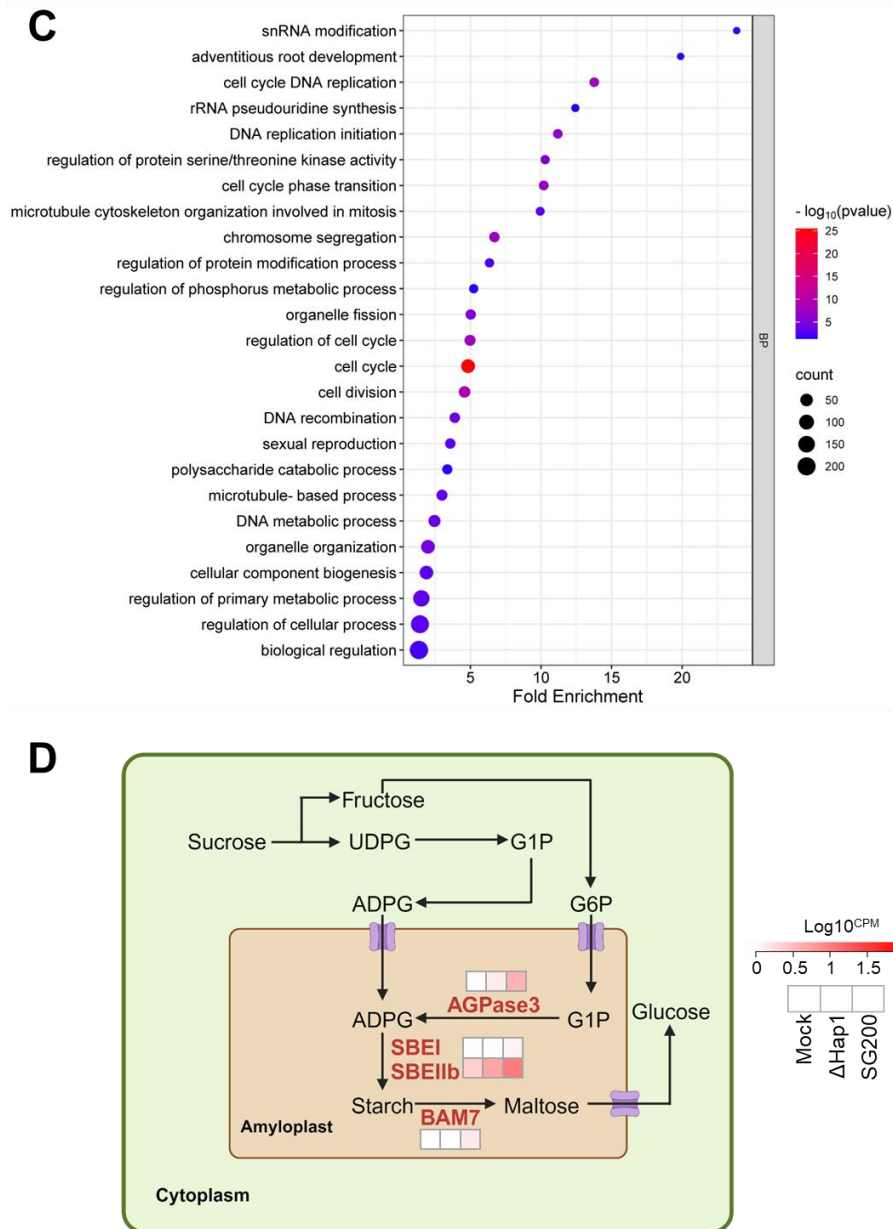


**Fig. 13) Differentially expressed genes compared between *Ustilago maydis*-infected treatment (SG200 and  $\Delta hap1$ ).** **A)** Pairwise bar graph of the number of up- and down-regulated DEGs in SG200 and  $\Delta hap1$  comparison. **B)** GO enrichment analysis of DEGs up-regulated in  $\Delta hap1$  and SG200 comparison. **C)** GO enrichment analysis of DEGs down-regulated in  $\Delta hap1$  and SG200 comparison. Only the parent terms of specific subclasses are shown. The significance of  $-\text{Log}_{10}(\text{P-value})$  values is represented from red to blue. **D)** Simplified diagram of sucrose and starch metabolic pathway. The differentially expressed genes in SG200 and  $\Delta hap1$  comparison in starch synthesis and degradation are colored in red. Gene counts were normalized using  $\text{Log}_{10}\text{CPM}$  (counts per million) of each gene across treatments. Boxes represent DEGs of mock,  $\Delta hap1$ , and SG200, arranged from left to right.

### 2.5.2 Hap1 is required for starch accumulation

Leaves infected with *U. maydis* display a high accumulation of starch (Doehlemann et al., 2008; Horst et al., 2008, 2010; Sosso et al., 2019). The chloroplast of infected plant cells begins to over-accumulate starch granules as early as 2 dpi (Snetselaar & Mims, 1994). After tumor formation is initiated, the level of starch increases particularly in mesophyll HTT cells, which are not a typical site for starch storage (Matei et al., 2018). Given the involvement of Hap1 in the starch synthesis-related genes, it became pertinent to investigate whether Hap1 is connected to starch distribution and accumulation in *U. maydis*-infected mesophyll HTT cells.

To address this question, maize seedlings were infected with mock and *U. maydis* (SG200 (WT), SG200 $\Delta$ hap1, SG200 $\Delta$ hap2, SG200 $\Delta$ hap1/2/3, and SG200 $\Delta$ sts2). SG200 $\Delta$ sts2 was used as a positive control since this effector is described as a transcription activator that induces *de novo* cell division in bundle sheath tumor cells (HPT) (Zuo et al., 2023). SG200 $\Delta$ hap2 and SG200 $\Delta$ hap1/2/3 were also included due to their interaction with Hap1 in planta, as previously mentioned in Section 2.2.2. The infected plant tissues were collected at 6 dpi and subjected to a series of paraplasm embeddings for thin cross-sectioning or enzymatic quantification for starch content. A collection time of 6 dpi was chosen based on prior observations indicating notable changes in starch distribution upon the establishment of tumors (Matei et al., 2018)

Enzymatic starch quantification of infected tissues revealed no significant difference across all sample conditions. Thus, microscopic quantification of starch by staining sections with Lugol's iodine solution (IKI) was performed. Lugol iodine staining (IKI) is a simple method for visualizing intracellular starch. Starch with a helical glucose traps iodine, resulting in the staining of starch granules a purple-black color (Kutík & Beneš, 1977). The sections stained with ddH<sub>2</sub>O displayed starch accumulation only within the bundle sheath, while SG200 displayed dispersed distribution and highly elevated accumulation only in mesophyll cells, consistent with previous findings (**Fig. 14A-B and G**). Notably, SG200 $\Delta$ hap1 and SG200 $\Delta$ hap1/2/3 exhibited significantly reduced starch accumulation compared to SG200 in mesophyll (**Fig. 14C-D and G**). On the contrary, SG200 $\Delta$ hap2 showed a significant reduction compared to SG200, however, showed no difference compared to SG200 $\Delta$ sts2 (**Fig. 14E and G**). SG200 $\Delta$ sts2 sections showed no significant difference in starch accumulation compared to SG200, indicating that reduced starch accumulation is a specific feature in *hap1* frameshift knockout mutant (**Fig. 14F and G**). Overall, these results demonstrate that the presence of

Hap1 is required for starch accumulation in mesophyll HTT cells upon *U. maydis* infection, with no impact on the reversal of typical C4 dimorphism even in the absence of Hap1.

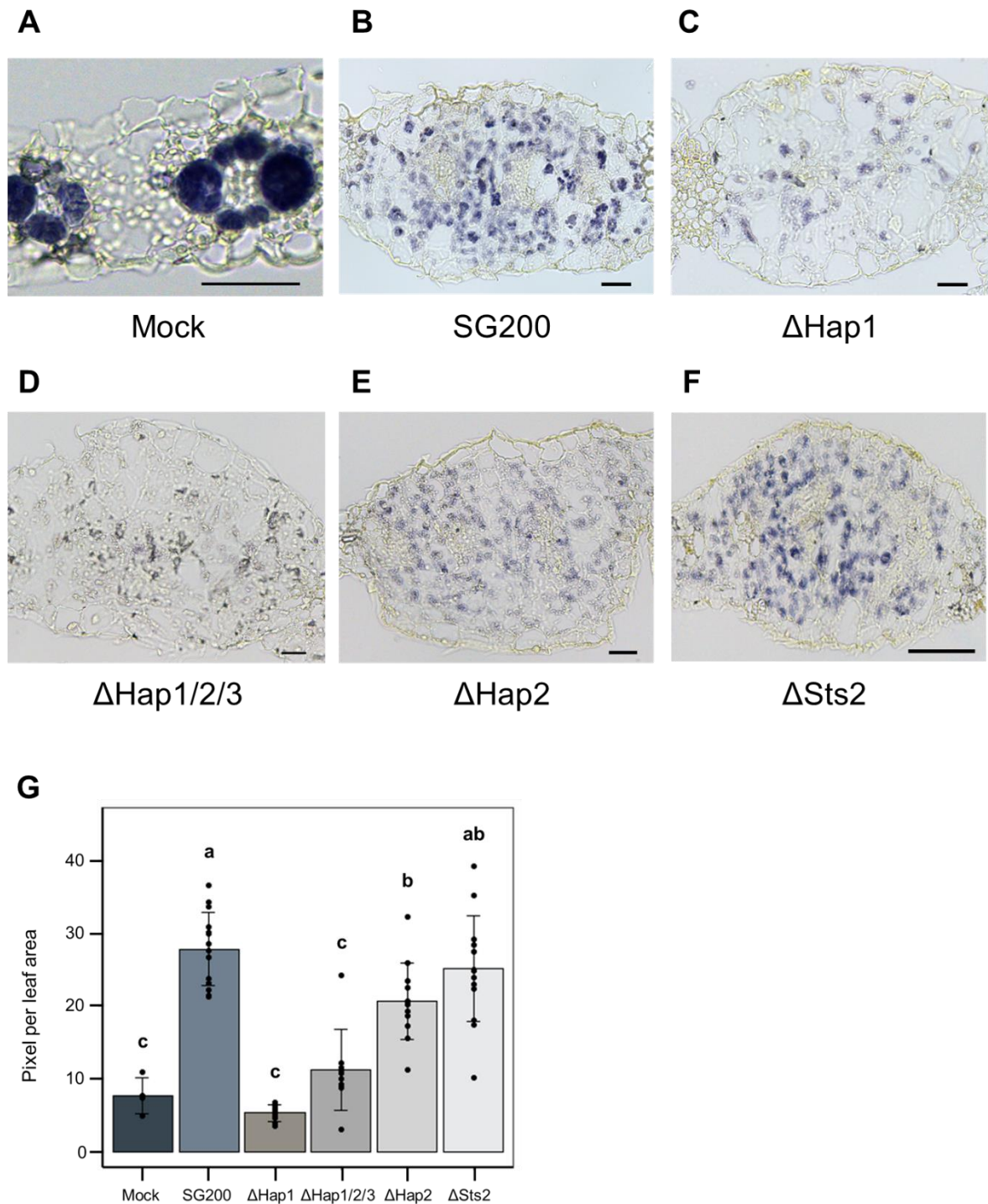


**Fig.14) Iodine staining for identification of starch allocation and its quantification in leaf tissue sections upon tumor formation** A) Lugol-stained ddH<sub>2</sub>O (mock)-infected leaf cross-sections at 6 dpi. B) Lugol-stained SG200-infected leaf cross-sections at 6 dpi. C) Lugol-stained SG200 $\Delta$ Hap1-infected leaf cross-sections at 6 dpi. D) Lugol-stained SG200 $\Delta$ hap1/2/3-

infected leaf cross-sections at 6 dpi. **E)** Lugol-stained SG200 $\Delta$ *hap2*-infected leaf cross-sections at 6 dpi. **F)** Lugol-stained SG200 $\Delta$ *Sts2*-infected leaf cross-sections at 6 dpi. The image depicts a representative picture obtained from three independent biological replicates. Scale bars = 50  $\mu$ m **G)** Quantification of Lugol-stained infected leaf cross-sections of A-E. Statistics were performed using Tukey's hsd *post hoc* tests after one-way ANOVA,  $P < 0.05$ . Different letters represent significant differences between treatments.

### **2.5.3 Hap1 is involved in altering sugar allocation in maize seedlings upon *Ustilago maydis* infection**

*U. maydis* infection is restricted to young meristematic sink tissue, resulting in the growth of extensive tumors (Smith et al., 2001; Sylvester et al., 1990; Wenzler & Meins, 1987). Tumorigenesis is achieved by redirecting hexoses to the tumors, which prevents the transition from sink to source to meet the metabolic needs of the *U. maydis* (Doehlemann et al., 2008a; Horst et al., 2008, 2010). Furthermore, leaves infected with *U. maydis*, including both seedling and adult leaves, showed an increased level of glucose, whereas fructose levels remained unchanged (Sosso et al., 2019). As previously demonstrated, the presence of Hap1 is required for starch accumulation in mesophyll HTT cells and its interaction with SnRK1. Thus, it is conceivable to hypothesize that Hap1 may also facilitate the changes in soluble sugar accumulation in maize in response to *U. maydis* infection. Soluble sugars, such as sucrose, glucose, and fructose, are important carbon sources in plants and have an impact on various physiological processes, including growth, development, and defense responses. To study the impact of Hap1 on changes in soluble sugar accumulation, maize seedlings were infected with mock, *Ustilago* (SG200 (WT), SG200 $\Delta$ *hap1*, SG200 $\Delta$ *hap2*, SG200 $\Delta$ *hap1/2/3*, and SG200 $\Delta$ *Sts2* (positive control)). All infected leaf tissues were collected at 4 dpi and 9 dpi, both at night (5 a.m.; before the long day period starts) and during the day (4 p.m.), and then subjected to enzymatic soluble sugar quantification. Samples were collected at different time points and times of the day to evaluate the correlation between tumor growth, the indicator of disease progression, and diurnal fluctuations in soluble sugar accumulation over time upon *U. maydis* infection.

For the soluble sugar quantification assays, mock-infected seedling leaves were compared with *Ustilago*-infected (SG200, SG200 $\Delta$ *hap1*, SG200 $\Delta$ *hap2*, SG200 $\Delta$ *hap1/2/3*, and SG200 $\Delta$ *Sts2*) leaves. Sucrose levels of *Ustilago*-infected leaves did not increase significantly compared to mock-infected samples at 4 dpi during the day and night, as well as 9 dpi (preliminary result) during the day (**Fig. 15A and B**). However, *Ustilago*-infected leaves contained more than 2-7

times higher sucrose when samples were collected at 4 dpi at night and 9 dpi during the day compared to mock-infected samples (**Fig. 15B and C**). Furthermore, at 9 dpi at night, only  $\Delta hap1$  and  $\Delta hap1/2/3$  infected samples showed significant increase in sucrose level (**Fig. 15D**). Although the elevated sucrose levels of samples collected at 9 dpi at night were not significant, owing to variability of samples, they demonstrated a trend towards higher sucrose content in *Ustilago*-infected leaves compare to mock-infected tissue.

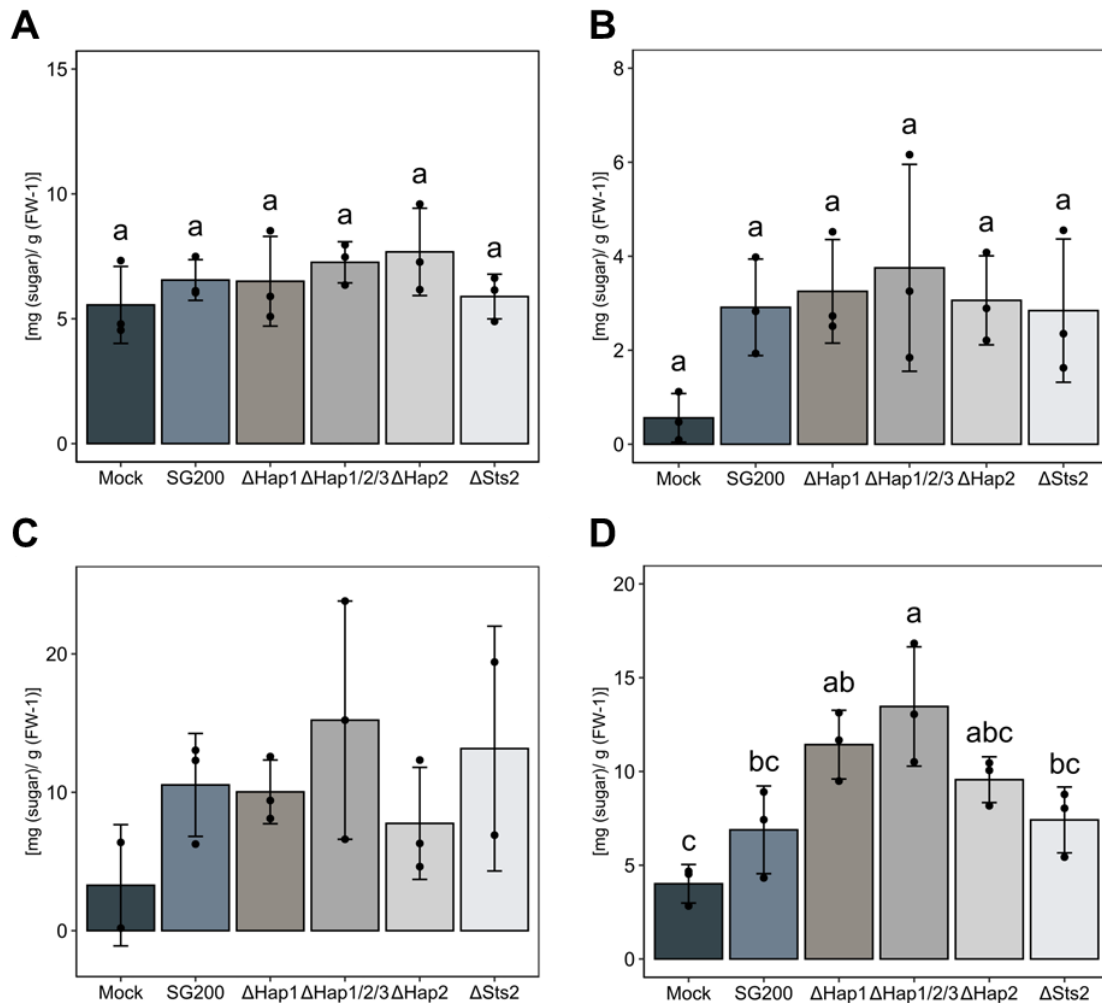


**Fig. 15) Enzymatic sucrose quantification of *Ustilago maydis* infected maize tissue**

**A)** Sucrose quantification of infected maize leaves at 4 dpi during the daytime. **B)** Sucrose quantification of infected maize leaves at 4 dpi at nighttime. **C)** Sucrose quantification of infected maize leaves at 9 dpi during the daytime (n=2) **D)** Sucrose quantification of infected maize leaves at 9 dpi at nighttime. Data represent mean sucrose levels  $\pm$  standard error of the mean (SEM); n = 3 biological replicates. Statistical significance was determined by one-way ANOVA with Tukey's hsd *post hoc* tests ( $P < 0.05$ ). Different letters represent significant differences between treatments. FW, Fresh weight.

With regards to glucose level, we observed significantly increased levels of glucose in *Ustilago*-infected leaves ( $\Delta hap2$ ,  $\Delta hap1-3$ ,  $\Delta sts2$ ) at 4 dpi during the day and all *Ustilago*-infected samples at night (**Fig. 16A and B**). However, at 9 dpi, during the day, only  $\Delta hap1/2/3$  showed twofold elevated glucose levels, while at night, all *Ustilago*-infected samples exhibited approximately two- to ninefold higher accumulation of glucose relative to mock-infected sample (**Fig. 16C and D**). 9 dpi sample collected during the day is preliminary result.

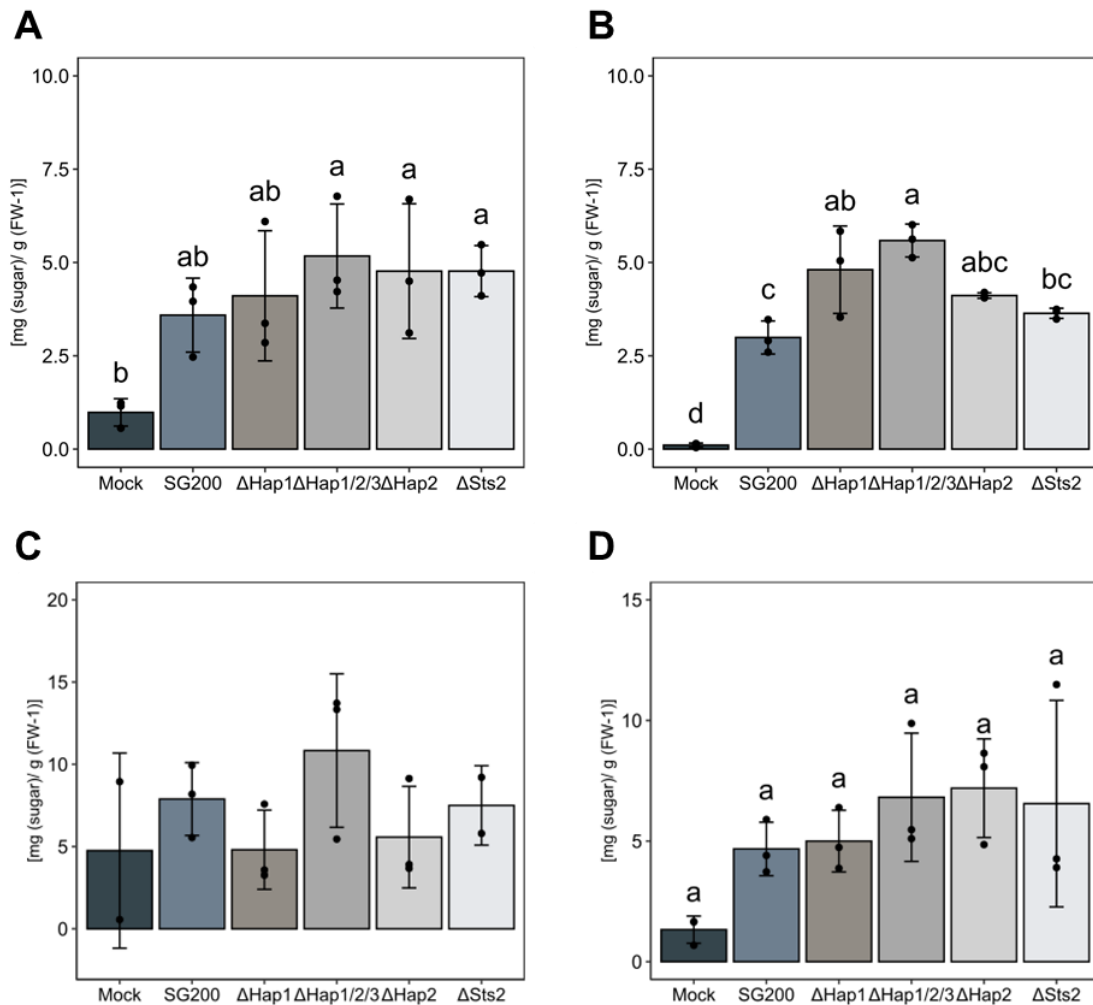


**Fig. 16) Enzymatic glucose quantification of *Ustilago maydis* infected maize tissue** **A)** Glucose quantification of infected maize leaves at 4dpi during the daytime. **B)** Glucose quantification of infected maize leaves at 4 dpi at nighttime. **C)** Glucose quantification of infected maize leaves at 9 dpi during the daytime (n=2) **D)** Glucose quantification of infected maize leaves at 9 dpi at nighttime. Data represent mean glucose levels  $\pm$  standard error of the mean (SEM); n = 3 biological replicates. Statistical significance determined by one-way ANOVA with Tukey's hsd *post hoc* tests ( $P < 0.05$ ). Different letters represent significant differences between treatments. FW, Fresh weight.



### 3. Discussion

In the complex interplay of plant-microbe interactions, efficient nutrient acquisition from the host is critical for the survival and proliferation of fungal pathogens. Upon infection, *U. maydis* secretes a repertoire of effectors and modifies the host's metabolic processes, redirecting starch and glucose accumulation toward tumor growth, thereby transforming them into strong sinks (Doehlemann et al., 2008a; Horst et al., 2008, 2010). A comprehensive cell type-specific transcriptome profiling of *U. maydis* during tumorigenesis revealed a set of highly upregulated effectors that contribute to the enlargement of mesophyll cells through endoreduplication, resulting in hypertrophic tumor (HTT) cells (Matei et al., 2018). This study investigates the role of Hap (hypertrophy-associated protein) effectors in hypertrophy induction and identifies effector and host target(s) to unravel molecular mechanisms and their contribution to *U. maydis* full virulence.

#### 3.1. Hap effectors are essential for virulence

##### 3.1.1 Hap effectors show maize line-specific regulation in *Ustilago maydis* virulence

In our effort to elucidate the virulence mechanisms of HTT-related effectors of *U. maydis* on *Zea mays*, we identified that *hap1* and *hap2* are essential for full virulence in EGB, whereas *Hap3* plays an indispensable role in GB. This aligns with previous studies that have shown different susceptibility levels across maize lines to *U. maydis* infection (Schurack et al., 2021; Stirnberg & Djamei, 2016). EGB, an heirloom and open-pollinated sweet corn variety, is widely used to study the virulence of *U. maydis* due to its susceptibility, particularly with the solopathogenic strain SG200 (Zuo et al., 2019). The agglomerative hierarchical clustering of maize disease resistance revealed that EGB shows a moderate susceptibility and an even distribution of disease resistance levels compared to tropical-origin maize lines, such as CML322 and Ki3 (Schurack et al., 2021). EGB is derived from its progenitor, the GB line, which was selected for early maturation, resulting in a limited allelic variation between these lines (personal communication). In VA35, a yellow dent southern-adapted inbred maize line, *U. maydis* has successfully established an infection (van der Linde et al., 2011). VA35 exhibited increased resistance to *U. maydis* infection compared to EGB and GB maize lines, as indicated by minimal heavy tumor formation (personal communication). This finding is further corroborated by preliminary infection symptoms observed in *hap1*, *hap2*, and *hap3* frameshift knockout mutants in VA35 line, which showed increased virulence resistance

accompanied by chlorosis and small tumor formation. Like *hap1*, *hap2*, and *hap3*, the effector *Apathogenic in B73* (apB73) exhibited maize line-specific virulence function, which knockout mutant of this effector showed apathogenic in more resistant B73 inbred maize line, but only partial reduction in the relatively susceptible EGB maize line (Stirnberg & Djamei, 2016). Similarly, *UMAG\_02297* is required for full virulence in CML322 maize line, but not in the EGB maize line (Schurack et al., 2021). The disease resistance of different maize lines varies depending on the specific pathogen encountered. For example, unlike prior observations of the resistance against *U. maydis*, VA35 line is highly susceptible and hypersensitive to *Aspergillus flavus* (Kelley et al., 2012). Similarly, CML322 line, which is highly resistant to northern leaf blight and *U. maydis* showed high susceptibility to aphids (Meihls et al., 2013; Poland et al., 2011; Schurack et al., 2021). This suggests that the virulence variability observed across different maize lines involves complex and dynamic interplay, requiring a fine-tuned adaptation of the pathogen to the specific host genotype, as well as sophisticated manipulation to target specific pathways of the host by fungal effectors. Additionally, the variation in disease resistance of *hap1*, *hap2*, and *hap3* effectors in specific maize lines may be attributed to the nature of the *U. maydis*-maize interaction. Unlike other closely related smut fungi that exhibit gene-for-gene resistance, such as *U. hordei*-barley and *U. tritic*-wheat, *U. maydis* is governed by a polygenic and quantitative trait (Linning et al., 2004; Menzies, 2016; Menzies et al., 2003; Tapke, 1945). Quantitative disease resistance (QDR) encompasses a broad range of mechanisms, including classes that are not directly associated with disease resistance, such as metabolite transport and biosynthesis. Wheat hexose transporters, *Lr67/Yr46/Pm46/Sr55*, confer partial resistance to wheat rust pathogen species and powdery mildew (Moore et al., 2015). *ZmCCoAOMT2* involved in lignin synthesis confers QDR to southern leaf blight and gray leaf spot of maize (Q. Yang et al., 2017). It is also possible that the expression patterns and impact of defense-related genes vary among plant genotypes due to allelic variations, as well as there may be variation in the quantitative disease resistance (QDR) across maize lines due to some specific allelic variants expressing at higher levels or with more effective timing (Niks et al., 2015). Therefore, it is speculated that the virulence phenotype observed for *hap1*, *hap2*, and *hap3* in EGB and GB lines, despite their limited allelic variations, may be attributed to selection for early maturation traits that inadvertently affected QDR, resulting in a distinct disease resistance profile of *hap1*, *hap2*, and *hap3* in GB and EGB.

### **3.1.2 Hap1, 2, and 3 are forming a potential Hap effector complex**

*U. maydis* infects strictly actively growing tissues on all aerial parts of maize, targeting meristematic tissue with dividing cells for tumor formation. It is predicted to encode 467 secreted effector proteins, of which 215 are novel effectors with no known functional domain, making their function difficult to predict (Kämper et al., 2006; Lanver et al., 2017, 2018; Schirawski et al., 2010). Therefore, using effective tools to find targets of *U. maydis* effectors is important (Varden et al., 2017). The IP/MS approach is a commonly used method for identifying host/effector partners and has been extensively applied to identify targets in *U. maydis*-maize interaction. Using this method, the Stp effector complex in *U. maydis*, consisting of Stp1, Stp3, Stp4, and Pep1, was identified (Ludwig et al., 2021). This complex is anchored in the fungal membrane and exposed to the host cell surface, which is proposed to be responsible for the effective delivery of effectors into the host cell (Ludwig et al., 2021). Effector complex is a common mechanism in bacteria for delivering effectors into host cells. *Pseudomonas syringae* and *Salmonella typhimurium* use type III secretion system (T3SS) and *A. tumefaciens* use type IV secretion system (T4SS), a needle-like structure used to inject bacterial effector proteins directly into the host cell cytoplasm (Lucke et al., 2020). However, the effector complex that translocates into the host cytoplasm has not been identified. Using the same IP/MS approach, hypertrophy-related effectors Hap1, Hap2, and Hap3 were pulled down *in planta*. Hap1, Hap2, and Hap3 are predicted to localize in cytoplasm and have the same highest expression at 2 dpi. The interaction of Hap1, Hap2, and Hap3 was validated via Co-IP and split-luciferase complementation. In addition, Y2H assays showed interaction between Hap2 and Hap3. Taken all together, these results suggest that Hap1, Hap2, and Hap3 are forming a potential complex to facilitate the *Ustilago*'s colonization in the host and induce tumor expansion in the mesophyll cell.

## **3.2. Hap1-host interaction in *Ustilago maydis***

### **3.2.1. Interaction of Hap1 with the central metabolic switch ZmSnRK1**

Hap1 was found to interact with *Z. mays* SnRK1 (**S**ucrose-**n**on-fermenting-1-**r**elated protein **k**inase1)  $\alpha$  subunit in *in vivo* IP/MS. The interaction of Hap1 and SnRK1.1-1.3 was confirmed via co-immunoprecipitation and preliminarily in split-luciferase complementation for SnRK1.2 in *N. benthamiana*. Additionally, Y2H assays confirmed the interaction between Hap1 and ZmSnRK1.1 or ZmSnRK1.3 only under medium stringency selection and also showed asymmetric interactions (with ZmSnRK1.1 in the GAL4 binding domain and ZmSnRK1.3 in the GAL4 activation domain of yeast). The variability in these interactions might be due to a

fused reporter protein causing steric hindrance that affects the interaction between the two proteins. In addition, incorrect, or no post-translational protein modification within the host system might cause misfolding or influence the exposure of the protein interaction domain, leading to negative interactions or the false positive growth of auxotrophic yeast on specific selection media.

Plant biotrophic fungi obtain their nutrition from their host and are closely interconnected with the metabolic processes of host cells. For instance, upon infection, *U. maydis* induces transcriptional and metabolic reprogramming in infected leaves. This includes a decrease in the expression of photosynthesis-related genes, as indicated by the reduced chlorophyll content in infected tissue and alterations in sink to source transition with increased levels of free hexoses in tumorous tissue (Doehlemann et al., 2008a; Horst et al., 2008; Matei et al., 2018). Free hexoses serve as a readily accessible nutrient for fungal growth and contribute to establishing an osmotic pressure necessary for tumor cell expansion (Doehlemann et al., 2008a; Horst et al., 2008). Similarly, the redirection of nitrogen-rich amino acids, previously thought to be involved in defense, serves as nutrients for the *Ustilago* (Horst et al., 2010; Kretschmer et al., 2017). Nutrient transporters, especially sugar will eventually be exported transporters (SWEETs), play a key role in the *U. maydis*-maize interaction. Many pathogens target these transporters to export sugars from the host cell to the apoplast for their growth. Upon *U. maydis* infection, the expression of *SWEET4a* and *SWEET4b* in seedlings, and *SWEET11a* in adult leaves was significantly up-regulated (Skibbe et al., 2010; Sosso et al., 2019). In our transcriptomics study, *SWEET4c*, which shares more than 80% sequence similarity with *SWEET4a* and *SWEET4b*, and *SWEET11a* are upregulated by 3- and 9-fold in both SG200 and *Δhap1* samples compared to Mock, respectively. *SWEET4c* facilitates the transport of hexoses across the endosperm during grain filling (Sosso et al., 2015). Sucrose and hexoses exported to the apoplast are transported to *U. maydis* via the fungal sucrose-specific saccharose transporter (Srt1) and monosaccharide transporter (Hxt1) (Schuler et al., 2015; Wahl et al., 2010). This suggests *U. maydis*'s ability to manipulate maize transporters and sink generation to ensure a steady supply of nutrients, independent of Hap1. It also demonstrates *U. maydis*'s employment of a wide array of effectors to modulate plant metabolic pathways in a comprehensive and coordinated manner. However, the interaction of Hap1 with SnRK1 suggests a more specific ability of the pathogen to modulate metabolic pathways through SnRK1. Given the central role of SnRK1 in plant energy homeostasis and the extensive metabolic reprogramming during *U.*

*maydis* infection, it is plausible that *U. maydis* tailors the metabolic status of host cells as a strategy to manipulate SnRK1's functions.

### **3.2.2. Disrupting Hap effector complex alters Hap1's host interaction partner**

To explore the impact of Hap2 and Hap3 effectors on Hap1 and its interaction target, single and double frameshift knockout mutants of *hap2* and *hap3* on the complemented  $\Delta hap1$  mutant background were generated using CRISPR-Cas9. A comprehensive *in vivo* IP-MS was performed and found that abolishing Hap1 interaction with Hap2 or Hap3 alters the interaction between Hap1 and host interacting partner. TPS, a downstream target of SnRK1, catalyzes the synthesis of T6P which has an antagonistic relationship with SnRK1 (Fichtner & Lunn, 2021; Nunes et al., 2013). Notably, TPS showed consistent interaction with Hap1, regardless of the absence of Hap2 and Hap3. This indicates a direct and independent interaction between Hap1 and TPS, thereby identifying Hap1's specific role in influencing host metabolic pathways regulated by TPS, such as the stress response and developmental processes through sugar signaling. However, it also shows that interaction between Hap1 and SnRK1 is conditional, suggesting that Hap2 and Hap3 may assist this interaction by stabilizing the effector protein or acting as scaffold proteins that physically bridge Hap1 and SnRK1, thereby enhancing their interaction. Moreover, interactions with phosphotyrosyl phosphatase activator (PTPA) and PPP2CB were observed in Hap1 $\Delta$ Hap2 and Hap1 $\Delta$ Hap2-3. PTPA activates PP2A activity by exchanging metal ions in the catalytic core of PP2A (Fellner et al., 2003). PPP2CB is the catalytic subunit of the PP2A core enzyme (B. Sun et al., 2021). PP2A is involved in the negative control of cell cycle progression, which regulates the timing and coordination of cell division (Wlodarchak & Xing, 2016). Considering the HTT-specific expression data from Matei et al., 2018, in which *Hap2* was not included, and the interaction between PTPA and PPP2CB with Hap1, independent of Hap2, suggests that Hap2 plays a role in the overall pathogenic strategy of *U. maydis* but its contribution to inducing hypertrophy in mesophyll is minimal. Hap1 $\Delta$ Hap2, Hap1 $\Delta$ Hap3, and Hap1 $\Delta$ Hap2/3 showed interaction with PP2C and SnRK2. In the upstream, the PP2C phosphatases ABI1 and PP2CA, repressors of ABA/SnRK2 signaling were found to dephosphorylate the SnRK1 T-loop (Rodrigues et al., 2013). The observed interactions suggest functional redundancy and compensatory mechanisms among the Hap effectors. The involvement of Hap effectors in a potential regulatory cascade further supports the hypothesis that Hap1, Hap2, and Hap3 form an effector complex within the host, acting as key modulators in the plant signaling network.

### 3.3. Phosphorylation profile of *Ustilago maydis* infected leaf tissue

#### 3.3.1. The presence of Hap1 in *Ustilago maydis* alters ZmSnRK1 phosphorylation of ZmSnRK1 $\alpha$ , $\beta$ , and $\gamma$ subunits

A phosphoproteomic approach revealed that *U. maydis* infection significantly alters host's phosphorylation profile in the presence and absence of Hap1 compared to mock (i.e., S vs M and dH vs M). Particularly, S vs M showed approximately twice as many phosphorylated proteins compared to dH vs M, indicating that *U. maydis* may modulate host phosphorylation processes, likely through Hap1, to disrupt host's cellular and biological processes. GO enrichment analysis in S vs M found biological processes related to phosphorylation, peptidyl serine modification, and regulation of gene expression. In contrast, in dH vs M, biological processes were related to 'RNA processing' and 'cellular response to stimulus'. Furthermore, in S vs dH, 'cell cycle', 'organelle organization', and 'rRNA processing' were found to be enriched. This finding is not surprising as it reflects Hap1's impact on the host by targeting ZmSnRK1. In the presence of Hap1, *U. maydis* facilitates post-translational modifications that modulate protein activities across signaling pathways and cellular processes, influencing the expression of genes important for defense, signaling, and metabolic adaptation. The S vs dH samples revealed enrichment in cell cycle and organelle organization, suggesting Hap1's role in transducing various signals to different organelles, such as the cytosol, membrane, and cellular compartments, aligning with *U. maydis*'s strategy to hijack the host's energy and nutrients by targeting photosynthetic and metabolic processes. Furthermore, Hap1 is one of effectors that may induce hypertrophy in mesophyll cells, hence can be supported by the enrichment of proteins altering the cell cycle leading to the facilitation of cell enlargement in tumors.

Using the SnRK1 and AMPK consensus sequences described in Section 2.4, we conducted a FIMO analysis and cross-referenced these proteins with the identified phosphopeptides. All SnRK1 subunits ( $\alpha$ 1,  $\beta$ 1,  $\beta$ 2, and  $\gamma$ ) showed increased phosphorylation in response to S vs M, but not in dH vs M. However, the phosphopeptide identified from SnRK1 $\alpha$ 1 was not located in the typical T-loop threonine residue, but in the  $\alpha$ -linker region. This region serves as a bridge between the ubiquitin-associated (UBA) domain and the kinase-associated domain (KA1) in the C-terminal domain, mediating interaction within the C-terminal domains of the  $\beta$  subunit and the N-terminus of the  $\gamma$  subunit. This suggests that in the presence of Hap1, *U. maydis* may target alternative phosphorylation sites within SnRK1 complex to manipulate its activation to promote infection and disrupt host energy regulation pathways. Pathogens targeting an

alternative phosphorylation site within the host to modify cellular processes is quite a common strategy. For example, in *U. maydis*, in the presence of the effector See1, phosphorylates Zm-SGT1 at the conserved phosphorylation site of some monocots. This inhibits MAPK-triggered phosphorylation, blocking the activation of downstream signaling (Redkar et al., 2015). However, it is important to note that the alternative phosphorylation site was found only in SnRK1 $\alpha$ 1 among the four alpha subunit isoforms, indicating that the interaction between Pec1 and SnRK1 might not be mediated through the phosphorylation of SnRK1.

Inconsistencies in the direct correlation between T-loop phosphorylation and SnRK1 kinase activity have been observed in various studies in plants (Baena-González et al., 2007; Coello et al., 2012; Fragoso et al., 2009; Ramon et al., 2019; Rodrigues et al., 2013). In Arabidopsis, it has been demonstrated that SnRK1 is resistant to T-loop dephosphorylation by phosphatases (Crozet et al., 2010; Emanuelle et al., 2015; Glab et al., 2017; Shen et al., 2009). The point mutation of the ATP-binding residues required for kinase activity K48 in AKIN10 (*A. thaliana* SNF1-related kinase 1.1) and K49 in AKIN11 (*A. thaliana* SNF1-related kinase 1.2) to a kinase-dead mutant (K48M) resulted in a significant reduction in T-loop phosphorylation of SnRK1, indicating that SnRK1 is autophosphorylated in leaf mesophyll protoplasts. (Baena-González et al., 2007; Ramon et al., 2019). In addition, the T-loop phosphorylation status of SnRK1 remained unchanged, although its kinase activity was altered in response to various treatments (Coello et al., 2012; Fragoso et al., 2009). Taken together, these findings support the hypothesis that *U. maydis* in the presence of Hap1 targets an alternative phosphorylation site identified in ZmSnRK1 $\alpha$ 1. However, experimental validation is required to confirm whether Hap1 alters SnRK1 kinase activity, and consequently affects the cellular and metabolic functions of the host.

The  $\beta$  subunits serve as a scaffold protein, facilitating interaction with  $\alpha$  and  $\gamma$  subunits, promoting complex localization, and substrate specificity (Baena-González & Hanson, 2017; Broeckx et al., 2016). The proper protein localization in specific subcellular compartments is crucial in plant cells as these compartments are structurally and functionally diverse. Correct localization of proteins provides appropriate physiological conditions and substrates needed for their activity. SnRK1 $\beta$ 1 and SnRK1 $\beta$ 2 proteins identified in S vs M comparison are homologous to Arabidopsis  $\beta$ 1 and  $\beta$ 2. The AKIN $\beta$ 2 is located close to the chloroplast and interacts with the outer membrane of the chloroplasts (Ávila-Castañeda et al., 2014). Most research on SnRK1/SNF1/AMPK has focused on the regulatory role of the  $\alpha$  subunit in controlling complex kinase activity. However, one study showed that phosphorylation of the

Ser<sup>108</sup> residue in human AMPK $\beta$ 1 resulted in a 60% reduction in AMPK activation due to salicylic acid preventing its T-loop dephosphorylation (Warden et al., 2001). The mutation at S<sup>24</sup>, S<sup>25</sup>, and S<sup>182</sup> in rat liver AMPK $\beta$ 1 released the myristoylation-membrane association of the complex to nuclear localization (Mitchell et al., 1997; Warden et al., 2001). Moreover, in Arabidopsis, the inhibition of a N-terminus myristoylation resulted in the relocation of AKIN $\beta$ 1 and AKIN $\beta$ 2 from the plasma membrane to the nucleus and the cytosol, respectively (Pierre et al., 2007). Additionally, a study on tomatoes indicated that AvrPto-dependent Pto-interacting protein 3 (Adi3) which is a nuclear suppressor of program cell death, can interact with SnRK1 $\alpha$ 1 and SnRK1 $\beta$ 1. Adi3 can also phosphorylate the S<sup>26</sup> residue of the  $\beta$  subunit SlGal83, which contributes to the inhibition of the tomato SnRK1 complex activity (Avila et al., 2012). Co-transfection of AKIN $\beta$  $\gamma$ /SnRK1 with the maize  $\beta$ 1 subunit in onion epidermal cells resulted in a stronger BiFC interaction and clear relocation of the signal to the cytoplasm (López-Paz et al., 2009). Taken all these findings together, the identification of increased phosphorylated peptides of ZmSnRK1 $\beta$ 1 and  $\beta$ 2 in the S vs M comparison, with matching SnRK1 consensus sequence, suggests that *U. maydis* influences the phosphorylation of ZmSnRK1 $\beta$  subunits in the presence of Hap1. This likely modulates the interaction between ZmSnRK1 $\alpha$  and ZmSnRK1 $\beta$ , stabilizing the activity of the SnRK1 complex and protecting it from being targeted by unknown upstream kinases. Moreover, phosphorylation of ZmSnRK1 $\beta$ 1 or  $\beta$ 2 may prevent the redistribution of the SnRK1 complex from the cytosol to other cellular compartments, ensuring that resources remain within the chloroplast to create a stable condition conducive to *U. maydis* growth by maintaining a nutrient-rich environment.

The  $\gamma$  subunits contain four conserved cystathionine- $\beta$  synthase (CBS) motifs that bind adenine nucleotides, regulating AMPK and SNF1 kinase activity (Mayer et al., 2011; Oakhill et al., 2012). Plant features two types of  $\gamma$  subunits:  $\gamma$  and  $\beta\gamma$  (Ramon et al., 2013). AKIN $\gamma$  interacts with AKIN $\beta$ 1, AKIN $\beta$ 2, and AKIN10 in Y2H assays (Bouly et al., 1999). In maize, AKIN $\beta\gamma$  interacted with SnRK1 $\alpha$  and  $\beta$  subunits in transfected cells through KIS/CBM and is specifically associated with SnRK1 activity (López-Paz et al., 2009). On the contrary, AKIN $\gamma$  does not complement a mutant of yeast  $\gamma$  subunit of SNF1 (*snf4*) in *in vitro* co-immunoprecipitation experiments or participate in the formation of a functional SnRK1 complex (Bouly et al., 1999; Emanuelle et al., 2015; Ramon et al., 2013). Moreover, *akiny* mutants did not exhibit changes in SnRK1-induced gene expression, suggesting a preference for AKIN $\beta\gamma$  in plants. *akiny* expression increased in the dark, but at a slower rate than *akin $\beta$ 1*, indicating its involvement in energy starvation signaling through sugar metabolites (Bouly et



al., 1999). The *akiny* subunit, despite not contributing to SnRK1 complex formation, has been found to interact with hexokinase 1 (HXK1) in the cytosol of leaf mesophyll protoplasts (Van Dingenen et al., 2019; Van Leene et al., 2022). HXK1 regulates cell proliferation and expansion during leaf development. The mutant leaves of *hxx1* exhibited increased cell numbers compared to wild-type leaves, suggesting the important role of HXK1 in restricting cell proliferation in sink tissues to regulate growth. Moreover, the *akiny* mutant displayed a slight enlargement in rosette size, while the *hxx1 akiny* double mutant demonstrated a growth defect under elevated light intensities similar to that of the *hxx1* single mutant. This suggests that AKIN $\gamma$  functions upstream of HXK1 and exerts a negative regulatory effect on it (Van Dingenen et al., 2019). The increased phosphorylation of the SnRK1 $\gamma$  peptide in the S vs M sample does not match the SnRK1 consensus recognition motif, suggesting a new interaction pathway. Building on previous findings, we can speculate that upon infection, SnRK1 $\gamma$  is targeted by *U. maydis* in the presence of Hap1, which impedes SnRK1 $\gamma$  from interacting with HXK1. This negatively impacts HXK1's role in cell proliferation and instead promotes cell expansion within the constant sink of tumor cells.

### **3.3.2. The presence of Hap1 in *Ustilago maydis* alters ZmSnRK1 phosphorylation-mediated signaling**

SnRK1 plays a crucial role in maintaining energy homeostasis in plants by phosphorylating key enzymes involved in carbon fluxes. Sucrose phosphate synthase (SPS) is required for sucrose synthesis in the cytosol and is mostly activated in the dephosphorylated state and is regulated by metabolites and reversible phosphorylation (Stitt et al., 1988). During the night, metabolites (glucose and maltose) are produced by the degradation of transient starch in the chloroplast. These metabolites are then transformed into hexose phosphates in the cytosol. The hexose phosphates (uridine diphosphate (UDP)-glucose and fructose-6-phosphate) are subsequently converted into sucrose by SPS (Strand et al., 2000). During the day, triose phosphates from the Calvin cycle are converted to fructose-1,6-bisphosphate and then to hexose phosphates (fructose-6-phosphate and glucose-6-phosphate) to the cytosol. Hexose phosphates are subsequently converted to sucrose via SPS (Strand et al., 2000). Our phosphoproteomics analysis revealed an increase in phosphorylation at S<sup>162</sup> residue in mock samples from S vs M and dH vs M comparisons, as well as in dH samples from dH vs S sample comparison. The S<sup>162</sup> residue is a conserved phosphorylation site of SPS among the five species (maize, sugar beet, rice, potato, and spinach) (Huber & Huber, 1996). Upon phosphorylation, sucrose phosphate synthase (SPS) activity is inhibited, resulting in reduced sucrose

biosynthesis (Worrell et al., 1991). An active SnRK1, phosphorylates SPS to conserve energy by restricting energy-intensive processes (Sugden et al., 1999). However, given the energy state of the mock sample, which was collected after 9-10 hours of illumination, it is unlikely that SPS activity is inhibited by an energy deficit in the plant. According to Stitt et al. (1988), SPS activity in leaves decreases when sucrose accumulates during the photoperiod, suggesting that phosphorylation of SPS serves as a feedback mechanism to prevent excessive sucrose accumulation which could disrupt cellular osmotic balance. Following this train of thought, the dephosphorylated state of SPS in the S sample is interesting as it indicates that SPS remains active only in the presence of Hap1. It maintains active sucrose synthesis in infected samples and promotes the formation of extensive sink tissues. This generation of massive sink is consistent with findings from previous studies demonstrating a correlation between increased sucrose availability and tumorous tissues (Doehlemann et al., 2008a; Horst et al., 2008; Sosso et al., 2019).

Sucrose synthase (Susy) cleaves sucrose into UDP-glucose and ADPG, a precursor of glycolysis, starch, and cellulose biosynthesis (Amor et al., 1995; Stein & Granot, 2019). SnRK1 phosphorylates Susy to convert metabolites into available nutrients that accumulate in the sink tissues, such as potato tubers (McKibbin et al., 2006; F. Wang et al., 2017). In the comparison between S and M, Susy7 showed increased phosphorylation in S. Susy2 also demonstrated increased phosphorylation in both S vs M and dH vs M comparisons, but the phosphorylation was more increased in S vs M than in dH vs M. The phosphorylation site of Susy in maize was mainly investigated in Susy1, specifically at residues S<sup>15</sup> and S<sup>170</sup> (Hardin et al., 2004). Susy1 is phosphorylated by SnRK1 and CDPK at these residues (Hardin et al., 2004; Huber & Huber, 1996). However, SnRK1 only phosphorylates S<sup>15</sup> to indirectly regulate sucrose degradation and starch biosynthesis activity. The identified phosphopeptide of Susy7 has phosphorylation sites at S<sup>12</sup> and S<sup>16</sup>, while Susy2 has a phosphorylation site at S<sup>11</sup>. The multiple alignment sequence of Susy2 and Susy7 was performed using the known sucrose phosphorylation site that has shown catalytic activities, such as ZmSuSy1 at S<sup>15</sup>, StSuSy1, and GmSuSy at S<sup>11</sup> (Hardin et al., 2004; Komina et al., 2002; Sauerzapfe et al., 2008). The result showed that S<sup>12</sup> of Susy7 and S<sup>11</sup> of Susy2 phosphorylation sites are conserved, indicating that these identified phosphorylation sites are potential targets for SnRK1. SnRK1 serves a distinct function in source and sink tissues. Overexpression of AKIN10 in potato increased starch accumulation, whereas it led to reduced starch levels in Arabidopsis seedlings (Jossier et al., 2009; McKibbin et al., 2006). Primarily, SnRK1 phosphorylates Susy in sink tissues of crops to facilitate starch

accumulation (Wurzinger et al., 2018). Nevertheless, we observed increased phosphorylation of Susy2 and Susy7 in *U. maydis*-infected samples when Hap1 is present. This indicates that tumor cells infected by *U. maydis* function as sink tissues and shows that Hap1 is required to modulate Susy activity, thereby increasing starch biosynthesis in tumorous tissue. These results are consistent with previous observations that *U. maydis* increases starch accumulation and induces its reallocation to infected tumorous mesophyll cells (Kretschmer et al., 2017; Matei et al., 2018).

The activity of SnRK1 is also regulated by different sugar metabolites, among which T6P inhibits SnRK1 most effectively. It shows a synergistic effect with G1P and a cumulative effect with G6P in response to cellular energy status (Nunes et al., 2013). T6P is synthesized from UDP-glucose and G6P by TPS (Fichtner & Lunn, 2021). In maize, T6P levels did not follow the typical pattern of a light/dark cycle following extended darkness, unlike sucrose and hexoses, suggesting that leaf cells may differentiate between imported sugars and those synthesized internally (Henry et al., 2014). In metabolite analysis of *U. maydis*-induced leaf tumors, the amount of G1P, G6P, and T6P increased starting from 2 dpi and peaked at 4 dpi (Horst et al., 2010). This correlates with the expression profile of effector Hap1 which peaks around 2-4 dpi (Lanver et al., 2018). The TPS family in plants is divided into two classes, class I and class II, both of which share a glucosyltransferase domain similar to that of *ScTPS1* from yeast (*S. cerevisiae*). Class I TPS enzymes are catalytically active and have demonstrated functionality by complementing the yeast  $\Delta tps1$  mutant. In contrast, class II TPS enzymes, although they contain some of the active site residues found in the glucosyltransferase domain, do not complement the  $\Delta sctps1$  mutant.

In the phosphoproteomic analysis we found increased phosphorylation of class II TPS proteins (TPSII 3.1, TPSII 3.2, TPSII 5.3). TPSII 3.1 and TPSII 5.3 showed increased phosphorylation in the S vs M comparison, whereas TPSII 3.2 showed decreased phosphorylation in the S vs M sample. The genome-wide analysis of maize TPSII showed that *ZmTPSII 3.3* (same clade as *ZmTPSII 3.1* and *ZmTPSII 3.2*) is expressed in leaf and *ZmTPSII 5.3* is expressed in both leaf and endosperm (Davidson et al., 2011; Sekhon et al., 2011). In addition, the expression patterns of *ZmTPSII 3.2* and *ZmTPSII 5.3* do not follow a circadian rhythm even under continuous light conditions and are rather regulated by the energy levels within the cell (Gibon et al., 2004). In Arabidopsis, SnRK1 phosphorylates and inhibits AtTPS5, -7, and -8. It was proposed that SnRK1 represses T6P synthesis by phosphorylating TPS7 and 8 to maintain its activity, however, at wild-type condition, TPS7 and 8 did not show a clear TPS function (Delatte et al.,

2011; Ramon et al., 2008). However, the increase in phosphorylation status of ZmTPSII3.1 and -3.2 in both infected and mock conditions makes it difficult to interpret the given data. It is possible that TPS has other, yet unknown regulatory roles, as high T6P levels do not respond to darkness despite SnRK1 being active in darkness. As the tumor tissue induced by *U. maydis* is believed to be in a non-photosynthetic and sink condition, it is possible that plants no longer sense T6P levels, regardless of TPS activity, leading to constant activation of SnRK1. However, the molecular basis of the T6P signaling mechanism and its regulation by plants remains largely unknown and requires further investigation. Finally, taking all phosphoproteomics data together, it is important to interpret found motifs with caution since the SnRK1 consensus sequence is similar to the phosphorylation motif of calcium-dependent protein kinases (CDPKs) (Bachmann et al., 1996; Broeckx et al., 2016; Cheng et al., 2002; Huang et al., 2001; Huang & Huber, 2001; Nukarinen et al., 2016; Van Leene et al., 2022).

### **3.4. Hap1 regulates expression of key enzymes involved in starch biosynthesis**

Principal component analysis of *Ustilago*-infected (SG200,  $\Delta hap1$ ,  $\Delta hap2$ , and  $\Delta hap3$ ) and Mock samples revealed three distinct clusters: mock,  $\Delta hap1$ , and a group comprising  $\Delta hap2$ ,  $\Delta hap3$ , and SG200. This led us to focus our transcriptome analysis primarily on  $\Delta hap1$ . GO and KEGG pathway analyses of DEGs in the presence of *Hap1* demonstrated up-regulation of key enzymes involved in starch biosynthesis and the cell cycle phase transition. Upon closer examination of DEGs involved in sucrose and starch pathways, ADP-Glucose pyrophosphorylase (*AGPase3*), starch branching enzyme (*SBEI*), and amylose extender (*Ae1*), were up-regulated in SG200 compared to  $\Delta hap1$  and mock. *AGPase3* is the first committed enzyme in the starch biosynthesis pathway, catalyzing the conversion of glucose-1-phosphate (G1P) to ADP-glucose and pyrophosphate. The ADP-glucose produced is then used to synthesize amylose and amylopectin. *SBEI* enhance amylopectin's solubility and determine its fine structure. *Ae1*, which encodes *SBEIIb*, a key enzyme involved in the branching of amylopectin were identified (K.-N. Kim et al., 1998; Tetlow & Emes, 2014). Starch composition in maize includes 20-30% amylose and 70-80% amylopectin (MacNeill et al., 2017). It is not surprising that pathogenic fungi trigger changes in the sugar metabolism of plants, transforming the infection site into a sink. *Spongospora subterranea f. sp. subterranea* is a soilborne protist that manipulates starch homeostasis to promote sporosorus development within the root galls (Kamal et al., 2024). It down-regulates genes for starch degrading enzymes in infected roots, while up-regulating genes involved in starch synthesis (Kamal et al., 2024).

This shows that manipulating starch synthesis is a commonly used mechanism for phytopathogens to acquire nutrients from the host. Moreover, there is a connection between starch, T6P, and SnRK1. In potato tuber, SnRK1 regulates the sucrose synthase gene and the redox activation of AGPase (Kolbe et al., 2005). The application of exogenous sucrose to potato tuber disc promoted AGPase redox activation, but this effect was not observed in the SnRK1 $\alpha$  antisense line (Tiessen et al., 2003). T6P has been proposed to indirectly activate AGPase in the chloroplast, promoting thioredoxin-mediated redox activation. In addition, an increase in sucrose levels in leaves resulted in a proportional increase in T6P levels. This led to AGPase in the chloroplast without changing the rate of photosynthesis, suggesting that T6P acts as a signaling molecule between cytosol and the chloroplast (Lunn et al., 2006; Ponnu et al., 2011).

Furthermore, upregulated DEGs were enriched in cell cycle phase transition, indicating *U. maydis* in the presence of *hap1* is involved in cell cycle modulation. Hypertrophy is the enlargement of tissue due to an increase in cell size (Chevalier et al., 2011). In *U. maydis*-induced tumors, hypertrophy is driven by endoreduplication, a cellular mechanism where DNA is replicated without cell division, resulting in increased nuclear DNA content (Matei et al., 2018). Endoreduplication is tightly linked to internal sugar levels in plants. It was shown that a high level of hexose in fruit cells creates an osmotic potential leading to cell water import and cell expansion (Ho, 1992). In addition, internal sugar level correlates with the phase transition of the cell cycle, which could trigger cell expansion (Van Dingenen et al., 2016). Thus, *U. maydis* might induce hypertrophy of mesophyll tumor cells in the presence of *Hap1*, leading to targeted starch accumulation.

### **3.5. Hap1 is required for starch accumulation in *Ustilago maydis*-induced tumor cells**

The change in carbon allocation from bundle sheath to mesophyll cells of *U. maydis*-induced tumor has been recorded by several publications (Kretschmer et al., 2017; Matei et al., 2018; Sosso et al., 2019). Our findings from Co-IP, RNA-seq analysis, proteomics, and phosphoproteomics in this study showed that Hap1 is required for starch biosynthesis in *U. maydis*-induced tumors. Lugol staining, which forms a blue-black complex when iodine reacts with the helical structure of starch, revealed that SG200 $\Delta$ *hap1* and SG200 $\Delta$ *hap1/2/3* showed significantly reduced starch accumulation compared to SG200 in mesophyll. SG200 $\Delta$ *hap2* exhibited a significant reduction compared to SG200, however, showed no difference compared to SG200 $\Delta$ *sts2*. SG200 $\Delta$ *sts2* displayed no significant difference in starch

accumulation compared to SG200, indicating that reduced starch accumulation is a distinct characteristic in the absence of *Hap1*. Plants use sugar transporters to move sugars to sink tissues, where high levels of sugars are stored as starch in plastids and act as signaling molecules to regulate metabolic processes based on their concentration (Loreti et al., 2001; N. Sun et al., 2023). However, fungi cannot directly utilize starch, a polysaccharide. Instead, they produce amylases that break down starch into glucose or maltose (B.-T. Wang et al., 2020). It is hypothesized that starch in tumor cells serves as an easily accessible resource for pathogens when they need it. However, one also can speculate that *U. maydis* alters the host's carbohydrate metabolism to enhance sugar availability while storing excess in tumorous tissues to manage the sugar concentration within the host cell and use it as a fuel to expand. This will minimize the osmotic and metabolic signals that could otherwise trigger the host's immune system in the apoplast.

### **3.6. Enzymatic quantification of soluble sugars in *Ustilago maydis*-induced tumor cells**

To investigate how Hap1 affects host metabolism, soluble sugars were quantified in infected maize seedlings. Sucrose levels in *Ustilago*-infected leaves showed no significant increase compared to mock-infected samples at 4 and 9 dpi during the day. Although not significant, at 4 dpi at night and 9 dpi during the day, *Ustilago*-infected leaves had sucrose levels 2-5 times higher than mock-infected samples. At 9 dpi, a significant increase in sucrose was observed only in  $\Delta hap1$  and  $\Delta hap1/2/3$  at night. Glucose levels were significantly higher in *Ustilago*-infected leaves ( $\Delta hap2$ ,  $\Delta hap1/2/3$ ,  $\Delta sts2$ ) at 4 dpi during the day and night. At 9 dpi, only  $\Delta hap1$  and  $\Delta hap1/2/3$  showed significantly elevated glucose levels compared to mock-infected sample. SG200 and  $\Delta hap1$ -infected samples showed no significant increase of glucose across all sampling time points and times of the day. The variability in results could be attributed to two reasons. First, the collection of a whole infected leaf section containing both infected and uninfected tissue rather than excising only the infected tumor area. Second, it is plausible that maize plants experienced physiological stress due to malfunctioning of the growth chamber and changes in the humidity conditions, although there were no observable stress symptoms on the maize leaves. Nevertheless, the trends towards increased sucrose and glucose at night compared to mock-infected samples are consistent with previously published data, suggesting that *U. maydis* induces a constant metabolic sink in infected cells and potentially alters the diurnal conversion of starch to sugar. However, more accurate and careful measurements are needed to confirm these results.

### 3.7. Working model of Hap1-SnRK1 interaction in starch metabolism

In this study, we investigated the role of Hap effectors in *U. maydis* virulence, with a particular focus on Hap1. Young maize seedlings, which are photosynthetic sink tissue, require large amounts of sugar metabolites for growth. Consequently, low sugar metabolites (T6P) in the cell activate SnRK1, initiating the catabolic process of transient starch breakdown by  $\alpha$ - and  $\beta$ -amylases (**Fig. 17**). Upon infection, *U. maydis* secretes Hap1 into the host cell, contributing to the creation of extensive sink tissue by increasing accumulation of T6P and enhancing nutrient flux that favors fungal colonization. Hap1 interacts with maize SnRK1 $\alpha$ , a central metabolic regulator, leading to the phosphorylation of SnRK1 downstream targets and the upregulation of key enzymes involved in starch biosynthesis during infection. This indicates that *U. maydis*, in the presence of Hap1, modulates starch biosynthesis by targeting ZmSnRK1 signaling pathways. The interaction of Hap1 and SnRK1 may also inhibit the immune signaling pathway induced by T6P present in the host cell, as sugars are actively converted into starch. Our findings support a model where *U. maydis* in the presence of Hap1, targets the SnRK1 $\alpha$  subunit. This targeting prevents inhibition of SnRK1 by high levels of sugar metabolites, thereby disrupting the antagonistic relationship between T6P and SnRK1 and reprogramming of transcription required for starch metabolism and sugar-induced immune signaling (**Fig. 17**). On the contrary, in the absence of Pec1, T6P may accumulate in the cell and inactivates SnRK1 to maintain energy homeostasis. Sugar metabolites, which also act as immunosignals, accumulate excessively in the host cell, potentially triggering immune responses by up-regulating gene expression of receptor kinases and transcription factors, resulting in less proliferation of *U. maydis* and a significant reduction in tumor formation (**Fig. 17**).

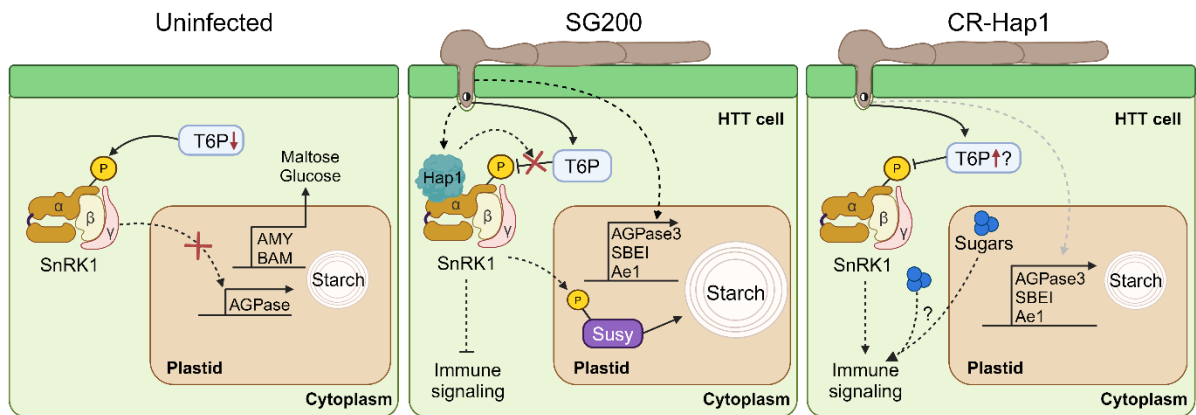


**Fig. 17) Hap1 disentangles T6P and SnRK1 antagonistic relationship and is required for starch metabolism.** The figure presents three different scenarios, which illustrate the role of Hap1 in *U. maydis* virulence. The first scenario depicts a young and healthy maize seedling (sink). A low level of T6P activates SnRK1. The activated SnRK1 induces starch degradation by down-regulating gene expression of *AGPase* and up-regulating  $\alpha$ -amylase (*AMY*) and  $\beta$ -amylase (*BAM*), thereby generating more energy in cells to maintain energy homeostasis. The second scenario depicts a young maize infected by *Ustilago*-containing Hap1 (sink). Upon infection, cells accumulate large amounts of T6P, and Hap1 binds to SnRK1. *Ustilago*-containing Hap1 phosphorylates SnRK1, thereby inhibiting the negative feedback loop of T6P and SnRK1 and inhibiting the sugar-induced immune signaling pathway. Active SnRK1 phosphorylates Susy7 (sucrose synthase 7) as well as *Ustilago* in the presence of Hap1 up-regulates *AGPase*, *SBEI*, and *Ae1*, key enzymes involved in starch biosynthesis, ultimately leading to starch accumulation in *U. maydis*-induced tumor cells. The third scenario depicts a young maize infected with *Ustilago* not containing Hap1. In the absence of Hap1, the T6P level upon infection may increase which leads to the inhibition of SnRK1 and a reduction in starch accumulation. The high level of T6P in turn induces sugar-induced immune signaling.

### 3.8. Perspective / future outlooks

To investigate the role of Hap1, it would be beneficial to obtain its crystal structure to predict its molecular function using cryo-electron microscopy (cryo-EM). Subsequently, to obtain direct evidence of the Hap effectors forming a complex, crystalizing Hap1, Hap2, and Hap3 together could reveal structural interactions and changes of Hap effectors within the host. Further exploration of SnRK1 and Hap effectors is needed to determine whether Hap2 and Hap3 stabilize and enhance the interaction between SnRK1 and Hap1. This would require the heterologous production of these proteins, which has been challenging in *E. coli* and *Pichia pastoris* for Hap1. Therefore, the collaboration with an established method to express proteins *in planta* and obtain crystal structure from the pull-down of proteins in planta would help us to understand the molecular mechanism behind Hap effectors and SnRK1.



*In vivo* kinase assays could elucidate how *U. maydis*, in the presence of Hap1, affects SnRK1 kinase activity, specifically by observing phosphorylation changes in SnRK1 and its downstream targets. Previous studies have demonstrated that SnRK1 phosphorylates class II TPS proteins and the delineation of the plant SnRK1 kinase signaling network has revealed the regulatory role of class II TPS proteins. In addition, comprehensive proteomic data from this study showed that the interaction with class II TPS is specific to Hap1. Therefore, it would be interesting to validate the interactions between SnRK1 and Hap effectors or class II TPS proteins using Co-IP. This would confirm the physical associations within these proteins complex. The investigation of SnRK's role in *U. maydis* induced tumor formation is important, however, the generation of transgenic lines takes a long time and is a laborious process. Although the CC9 overexpression line in transgenic maize has been successfully generated (van der Linde et al., 2012), a complete knockout of SnRK1 in maize could have detrimental effects, considering its function in maintaining energy homeostasis. Therefore, employing virus-induced gene silencing (VIGS) of SnRK1 in maize, or introducing point mutation in the ATP binding residues as previously done in Arabidopsis, to assess the response to *U. maydis* infection would be beneficial.

In addition, the application of exogenous sucrose to potato tuber discs was shown to facilitate redox activation of AGPase, suggesting that T6P may indirectly activate AGPase in the chloroplast through thioredoxin-mediated redox activation. It would be interesting to determine whether the application or overexpression of trehalose phosphate phosphatase (TPP), which converts T6P to trehalose, would reduce starch accumulation in *U. maydis*-induced tumor cells and disrupt the interaction between Hap1 and SnRK1. Moreover, it would be interesting to reconstitute starch accumulation in the  $\Delta hap1$  frameshift knockout mutant by replacing the promoter of Hap1 with that of Sts2, which induces de novo cell division in bundle sheath cells but showed no changes in starch accumulation compared to SG200.

To substantiate that Hap1 promotes endoreduplication in *U. maydis*-induced mesophyll cells, the established propidium iodide staining method to observe changes in nuclear size will be crucial, as our findings showed that frameshift knockouts of Hap2 and Hap3 from Hap1 alter Hap1's interaction partner to phosphatases that negatively regulate the cell cycle. Therefore, okadaic acid, a phosphatase inhibitor, could be instrumental in observing whether there is a change in nuclear doubling in *U. maydis*-induced tumor.

## 4. Material and Methods

### 4.1 Material and Methods

#### 4.1.1 Chemicals

All chemicals used in this study were purchased from Biozym (Hessisch Oldendorf, Germany), Difco (Augsburg, Germany), GE Healthcare Life Science (Freiburg, Germany), Invitrogen (Carlsbad, USA), Merck (Darmstadt, Germany), Roche (Mannheim, Germany), Roth (Karlsruhe, Germany), and Sigma-Aldrich (St. Louis, USA) unless stated otherwise.

#### 4.1.2 Buffers and Solutions

All buffers, media and solutions were prepared according to laboratory manual books (Ausubel et al., 1987; Sambrook et al., 1989) and autoclaved for 5 minutes at 121 °C unless stated in respective method section. Heat-sensitive solutions were filter-sterilized (0.2 µm pore size, GE Health Care Life Science, Freiburg, Germany).

#### 4.1.3 Enzymes, antibodies, and IP trap beads

All enzymes used in this study are summarized below in Table 4.1. Additionally used enzymes and a comprehensive list of the protein trap beads used in this study can be found in the respective method sections.

**Table 4.1 Chemical reagent and their purpose of use**

<b>Reagent/Purpose</b>	<b>Supplier</b>
Restriction enzymes	New England Biolabs (NEB, Frankfurt/Main, Germany) Thermo (Thermo Fisher Scientific Inc., Duesseldorf, Germany)
DNA polymerases	Phusion® Hot Start High-Fidelity DNA-Polymerase (Thermo Fisher Scientific Inc., Duesseldorf, Germany) Q5® High Fidelity DNA Polymerase (NEB, Frankfurt, Main) GoTaq® Green Master Mix (Promega, Walldorf, Germany)
DNA ligation	T4 DNA Ligase (NEB, Frankfurt, Main)
Enzymatic degradation of fungal cell walls	Novozyme 234 (Novo Nordisk, Copenhagen, Denmark)
Immunoprecipitation trap beads	GE Healthcare Life Science (Freiburg, Germany) and ChromoTek GmbH (München, Germany)

**Table 4.2 Commercial kits**

All commercial kits used in this study are summarized below in Table 4.2. Antibiotics and size markers used in this study are shown in Table 4.3 and Figure 4.1, respectively.

Purpose	Supplier
Plasmid DNA extraction	QIAprep® Mini Plasmid Kit (Qiagen, Hilden, Germany)
Purification of PCR products/ Extraction of nucleic acid from agarose gel	NucleoSpin® Gel and PCR Clean-up Kit (Macherey-Nagel, Düren, Germany)
Enzymatic degradation of DNA	TURBO DNA-free™ Kit (Ambion®/ Thermo Fisher Scientific Inc., Duesseldorf, Germany)
Enzymatic degradation of RNA	RNaseA (Serva, Heidelberg, Germany)
cDNA synthesis	RevertAid H Minus First Strand cDNA Synthesis Kit (Thermo Fisher Scientific Inc., Duesseldorf, Germany)
Gibson assembly	2x Hifi DNA assembly mix (NEB, Frankfurt/Main, Germany)
Site-directed mutagenesis	Quickchange II Kit (Agilent Technologies, Santa Clara, USA).
Chemiluminescence detection in western blot	SuperSignal™ West Pico PLUS Chemiluminescent Substrate SuperSignal™ West Femto Maximum Sensitivity Substrate (Thermo Fisher Scientific Inc., Duesseldorf, Germany)
Ni-NTA matrix for protein purification	Ni-Sepharose 6 Fast-Flow, GE-Healthcare; Freiburg, Germany
Protein desalting or buffer exchange	Zeba Spin Desalting Columns 7K MWCO (Thermo Fisher Scientific Inc., Duesseldorf, Germany)
Soluble sugar quantification	Sucrose/D-Fructose/D-Glucose Assay Kit (K-SUFRG) (Megazyme Ltd, Lansing Michigan, USA)
Starch quantification	Total Starch HK Assay Kit (K-TSHK) (Megazyme Ltd, Lansing Michigan, USA)

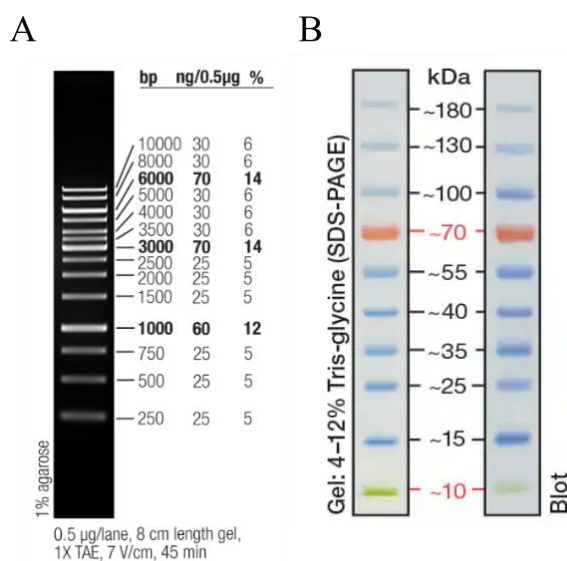


**Fig. 18 The standard markers used in this study.**

A) Thermo Scientific™ GeneRuler™ 1 kb DNA Ladder (Thermo Fisher Scientific Inc., Duesseldorf, Germany) was used for size determination of DNA fragments on agarose gels. B) PageRuler™ Prestained Protein Ladder, 10 to 180 kDa, used for SDS-PAGE electrophoresis. (Thermo Fisher Scientific Inc., Duesseldorf, Germany). Photos were obtained from the manufacturer's website.

**Table 4.3 Antibiotics**

Antibiotic	Usage	Working concentration [µg/ml]
Carbenicillin	<i>E. coli, A. tumefaciens</i>	100
Kanamycin	<i>E. coli</i>	40
Spectinomycin (Spec)	<i>E. coli</i>	50
Rifampicin (Rif)	<i>E. coli, A. tumefaciens</i>	40
Gentamicin (Gent)	<i>E. coli, A. tumefaciens</i>	50
Carboxin	<i>U. maydis</i>	2
Hygromycin	<i>U. maydis</i>	200
Zeocin	<i>E. coli, P. pastoris</i>	100

## 4.2 Media and cultivation methods for microorganisms

### 4.2.1 Media

**Table 4.4 Composition of media used in the study.**

Name	Ingredients	Note
Potato-Dextrose-Agar (PD)	3.9% (w/v) Potato-Dextrose Agar	in H <sub>2</sub> Obid
PDA- Charcoal	Addition of 1 % (w/v) Charcoal to PD-Agar media	in H <sub>2</sub> Obid
YEPSlight (modified from Tsukada et al., 1988)	1 % (w/v) Yeast extract 0.4% (w/v) Peptone 0.4% (w/v) Saccharose	in H <sub>2</sub> Obid
Regeneration Agar (Schulz et al., 1990)	1.5 % (w/v) Bacto Agar 1M Sorbitol 1 % (w/v) Yeast extract	in H <sub>2</sub> Obid

	0.4% (w/v) Peptone 0.4% (w/v) Saccharose	
dYT (Sambrook et al., 1989)	1.6% (w/v) Tryptone 1.0% (w/v) Yeast extract 0.5% (w/v) NaCl	dYT Agar addition of 1.5% (w/v) Bacto Agar
YT-Agar	0.8 % (w/v) Tryptone 0.5 % (w/v) Yeast extract 0.5 % (w/v) NaCl 1.3 % (w/v) Agar	in H <sub>2</sub> Obid
YPD	1 % (w/v) Yeast Extract 2 % (w/v) Peptone 0.003% (w/v) Adenine-Hemisulfate 2 % (w/v) Dextrose	Addition of 100 ml of sterile filtered 20 % (w/v) glucose after autoclaving
YPDA (-Agar)	1 % (w/v) Yeast extract 2% (w/v) Peptone 0.003% (w/v) Adenine-Hemisulfate 2% (w/v) Bacto Agar	Adjust the pH to 6.5 and after autoclaving add 2% (w/v) sterile filtered glucose
SD (-Agar) Synthetic Defined	0.67% (w/v) Yeast nitrogen base Without amino acids 0.06% (w/v) Dropout Solution [(- Ade, -His, -Leu, -Trp) or (-His, - Leu, -Trp, -Ura)] 2% (w/v) Bacto Agar	Adjust the pH to 5.8 and after autoclaving add 2% (w/v) sterile filtered glucose

#### 4.2.2 Cultivation of *E. coli*

*E. coli* strains were cultured at 37 °C either on dYT liquid and YT solid medium with shaking at 200 rpm. Glycerol stocks were prepared by adding 25% (v/v) glycerol to an overnight culture in a total volume of 1.5 ml and stored in a screw cap vial at -80 °C. For selection, media were supplied with carbenicillin, kanamycin, or spectinomycin according to Table 4.3.

### 4.2.3 Cultivation of *A. tumefaciens*

*A. tumefaciens* strains were cultured at 28 °C either on dYT liquid and YT solid medium with shaking at 200 rpm. Glycerol stocks were prepared by adding 25% (v/v) glycerol to an overnight culture in a total volume of 1.5 ml and stored in a screw cap vial at -80 °C. For selection, media were supplied with carbenicillin, rifampicin, or gentamicin according to Table 4.3.

### 4.2.4 Cultivation of *S. cerevisiae*

*S. cerevisiae* strain AH109 was grown in either YPD or SD liquid medium and cultivated on either YPD or SD solid medium. SD media supplemented with or without adenine, histidine, leucine, and tryptophan were used to select transformants. Liquid cultures were incubated at 28°C with continuous shaking at 200 rpm, while solid media were incubated under aerobic conditions at 28°C. Glycerol stocks were prepared by adding 25% (v/v) glycerol to an overnight culture in a total volume of 1.5 ml and stored in a screw cap vial at -80 °C.

### 4.2.5 Cultivation of *U. maydis*

*U. maydis* liquid cultures were cultivated in YEPSlight at 28 °C with shaking at 200 rpm. Solid cultures of *U. maydis* were cultivated on Potato Dextrose (PD) Agar at 28 °C. Glycerol stocks were prepared by adding 25% (v/v) glycerol to a culture with an OD<sub>600</sub>= 0.6-1.0 in a total volume of 1.5 ml and stored in a screw cap vial at -80 °C. After transformation of *U. maydis*, regeneration agar was used. For selection, the media was supplied with carboxin or hygromycin according to Table 4.3.

### 4.2.6 Measurement of cell density

To measure cell density, an absorption reading at 600 nm (OD<sub>600</sub>) on a Genesis 10S VIS spectrophotometer (Thermo Fisher Scientific, Waltham, USA) was used. The readings were taken using the respective medium as a reference. To ensure a linearity of the measurements, cultures were diluted to absorption values below 1.

## 4.3 Microbial strains, plasmids, and oligonucleotides

### 4.3.1 *E. coli* strains

For plasmid vector cloning procedures *E. coli* K-12 Top10: [FmcrAΔ (mrr-hsd RMS-mcrBC) Φ80lacZΔM15 ΔlacO74 recA1 araΔ139 Δ (ara98leu) 7697galU galK rpsL (StrR) endA1 nupG] (Invitrogen, Carlsbad, USA) (Grant et al., 1990) and *E. coli* K-12 DH5α: F- Φ80d lacZ ΔM15 Δ (lacZYA-argF) U169 deoR recA1 endA1 hsdR17(rK-, mK+) phoA supE44 λ- thi-lgyr A96 relA1](GibcoBRL, Eggenstein, Germany)(Hanahan, 1983) were used.

### 4.3.2 *A. tumefaciens* strains

*A. tumefaciens*-mediated transformation of *N. benthamiana* was performed using GV3101 (Koncz and Schell, 1986). This strain contains a chromosomal rifampicin resistance, the Ti-plasmid pMP90 with vir-genes and a gentamycin resistance, as well as a Ti-helper plasmid bearing a tetracycline resistance. All strains used for expression in *N. benthamiana* are listed in Table 4.11.

### 4.3.3 *S. cerevisiae* strains

The yeast two-hybrid assay was performed using the *Saccharomyces cerevisiae* AH109 (Clontech, Saint-Germain-en-Laye, France): (MATa, trp1-901, leu2-3, 112, ura3-52, his3-200, gal4Δ, gal80Δ, LYS2:GAL1<sub>UAS</sub>-GAL1<sub>TATA</sub>-HIS3, GAL2<sub>UAS</sub>-GAL2<sub>TATA</sub>-ADE2, URA3:MEL1<sub>UAS</sub>-MEL1<sub>TATA</sub>-lacZ). AH109 is derived from the PJ69-2A strain which contains the selectable marker ADE2 and HIS3 (James et al., 1996). MEL1 is an endogenous gene responsive to GAL4. The AH109 strain was constructed by introducing the lacZ reporter gene into PJ69-2A (A. Holtz, unpublished).

### 4.3.4 *U. maydis* strains

The solopathogenic strain SG200 was used as a reference for the wild type (Kämper et al., 2006). The other strains mentioned and generated in this study are listed in Table 4.5.

**Table 4.5** *U. maydis* strains used in this study.

Strain	Usage	Reference
SG200 reisolated	Maize infection	Kämper et al., 2006
SG200ΔUMAG_02381	Maize infection	This study
SG200ΔUMAG_00793	Maize infection	This study
SG200ΔUMAG_03650	Maize infection	This study
SG200ΔUMAG_12119	Maize infection	This study
SG200ΔUMAG_11484	Maize infection	This study
SG200ΔUMAG_00753	Maize infection	This study
SG200ΔUMAG_02473	Maize infection	This study
SG200ΔUMAG_00792	Maize infection	This study
SG200ΔUMAG_05222	Maize infection	This study
SG200ΔUMAG_00794	Maize infection	This study
SG200ΔUMAG_00793-ΔUMAG_00792::KOUMAG_02473#3	Maize infection	This study
SG200ΔUMAG_00793::KOUMAG_00792#16	Maize infection	This study
SG200Δ00793_pUm00793-cl 19	Maize infection, complementation	This study

SG200ΔUMAG_00792_NP::UMAG_00792-2HA #8	Maize infection, complementation	This study
SG200ΔUMAG_02473::NP-UMAG_02473-2HA #2	Maize infection, complementation	This study
SG200Δ00753_pUm00753/C-cl 7	Maize infection, complementation	This study
SG200Δ02381_pUm02381/C-cl 7	Maize infection, complementation	This study
SG200_pPit::SP02473-mCherry-HA	Maize infection, LC-MS	This study
SG200_pPit::SP00793-mCherry-HA	Maize infection, LC-MS	This study
SG200ΔUMAG_02473_pPit::UMAG_02473-2HA #5 MI	Maize infection, LC-MS	This study
SG200Δ00793_pPit2::Um00793-2xHA #6 MI	Maize infection, LC-MS	This study
SG200ΔUMAG_00792-pPit2::UMAG_00792-2HA #5 MI	Maize infection, LC-MS	This study
SG200ΔUMAG_00793::pPit2-UMAG_00793Δ02473 #2	Maize infection, LC-MS	This study
SG200ΔUMAG_00793::pPit2-UMAG_00793Δ00792 #1	Maize infection, LC-MS	This study
SG200ΔUMAG_02473::pPit2-UMAG_02473Δ00792 #2	Maize infection, LC-MS	This study
SG200ΔUMAG_02473::pPit2-UMAG_02473Δ00793 #10	Maize infection, LC-MS	This study
SG200ΔUMAG_00792::pPit2-UMAG_00792Δ00793 #2	Maize infection, LC-MS	This study
SG200ΔUMAG_00792::pPit2-UMAG_00792Δ02473 #10	Maize infection, LC-MS	This study
SG200ΔUMAG_02473::pPit2-UMAG_02473Δ00792-00793 #9	Maize infection, LC-MS	This study
SG200ΔUMAG_00792::pPit2-UMAG_00792Δ00793-02473 #4	Maize infection, LC-MS	This study
SG200ΔUMAG_00793::pPit2-UMAG_00793Δ00792-02473	Maize infection, LC-MS	This study

KO: Knockout; NP: Native promoter

#### 4.3.5 Oligonucleotides

All oligonucleotides utilized in this study were purchased from Sigma-Aldrich (St. Louis, USA). The names, sequences, and respective applications of the oligonucleotide are listed in Table 4.6, 4.7, and 4.8.



**Table 4.6 General oligonucleotides used in this study.**

<b>Name</b>	<b>Sequence</b>	<b>Plasmid # from Stammsammlung</b>
MOCLO 02473 F	TTGGTCTCAAATGGCAATGGCGCTA GAGCG	#2663/2840
MOCLO 02473 R	TTGGTCTCACGAAGCGAATTGTTTG GCGCACGATACCGTG	#2663/2840
MOCLO 00793 F	TTGGTCTCAAATGTGGTTCAATCAA CGCTT	#2619/2841
MOCLO 00793 R	AAGGTCTCACGAAGCCTTGTTGCA GAAGCAGTTCT	#2619/2841
00792-F	AGGCCTGGATCCTCGCGAGCGGTC AATGCGGGCTTT	#3049/3052/3248/3266/326 7
00792-R	GTGGTGATGGTGATGATGACTAGTA TCGTCTTTTGATACGGG	#3049/3052/3248/3266/326 7
00793-F	AGGCCTGGATCCTCGCGAGAAGAG ACGGCCACACAC	#3050/3053/3134
00793-R	GTGGTGATGGTGATGATGACTAGTC TTGTTGCAGAAGCAGTT	#3050/3053/3134
02473-F	AGGCCTGGATCCTCGCGAGCAATG GCGCTAGAGCGA	#3051/3052
02473-R	GTGGTGATGGTGATGATGACTAGTG AATTGTTTGGCGCACGA	#3051/3052
00793 pGBKT7-F	TCAGAGGAGGACCTGCATATGGAA GAGACGGCCACACACG	#2612
00793 pGBKT7-R	CCGCTGCAGGTCGACGGATCCCTA CTTGTTGCAGAAGCA	#2612
02473 pGBKT7-F	CAGAGGAGGACCTGCATATGGCAA TGCGCTAGAGCGA	#2694
02473 pGBKT7-R	GCCGCTGCAGGTCGACGGATCCCT AGAATTGTTTGGC	#2694
02473 pGADT7-F	GTACCAGATTACGCTCATATGGCAA TGCGCTAGAGCGAC	#2721
02473 pGADT7-R	CAGCTCGAGCTCGATGGATCCCTA GAATTGTTTGGCGCA	#2721
SnRK1 $\alpha$ 1-F	AGGCCTGGATCCTCGCGAATGGAT GGAAGTAGTAAAGG	#3566/3569/3578/3718
SnRK1 $\alpha$ 1-R	ATGGTGATGATGACTAGTTAGAACC CTAAGCTTGGTA	#3566/3569/3578/3718
SnRK1 $\alpha$ 2-F	AGGCCTGGATCCTCGCGAATGGAG GGAGCGGGAAGA	#3571/3574/3575/3618
SnRK1 $\alpha$ 2-R	GTGATGGTGATGATGACTAGTAAGA ACTCTCAGCTGAGTTAGAAAGGC	#3571/3574/3575/3618
SnRK1 $\alpha$ 3-F	AGGCCTGGATCCTCGCGAATGGAG GGGCAGGCAA	#3578/3579/3580/3717

SnRK1 $\alpha$ 3-R	GTGATGGTGATGATGACTAGTAAGA ACTCTCAGTTGAGTTAGAAAGGC	#3578/3579/3580/3717
--------------------	--	----------------------

**Table 4.7 Oligonucleotides used as sgRNA for CRISPR/Cas9-mediated KO in this study.**

Target gene	Sequence	Comments
UMAG_02381	<u>CAAAATTCCATTCTACAACGAGGGCCAGT</u> <u>CCGTGACCGCGTTTTAGAGCTAGAAATAG</u> C	pU6 Overhang
UMAG_00793	<u>CAAAATTCCATTCTACAACGGTGGCGACG</u> <u>ACCAGCAAGGGTTTTAGAGCTAGAAATAG</u> C	pU6 Overhang
UMAG_03650	<u>CAAAATTCCATTCTACAACGTTTCGTGCCAG</u> <u>GATCATGCTGTTTTAGAGCTAGAAATAGC</u>	pU6 Overhang
UMAG_12119	<u>CAAAATTCCATTCTACAACGATGAGACCA</u> <u>ACATTTGCGAGTTTTAGAGCTAGAAATAGC</u>	pU6 Overhang
UMAG_11484	<u>CAAAATTCCATTCTACAACGCGGCAGGAT</u> <u>GATCGGTGACGTTTTAGAGCTAGAAATAGC</u>	pU6 Overhang
UMAG_00753	<u>CAAAATTCCATTCTACAACGCGATCAACAA</u> <u>GCTCACCGGGTTTTAGAGCTAGAAATAGC</u>	pU6 Overhang
UMAG_02473	<u>CAAAATTCCATTCTACAACGCAGATGACT</u> <u>GCATCTGTGTGTTTTAGAGCTAGAAATAG</u> C	pU6 Overhang
UMAG_00792	<u>CAAAATTCCATTCTACAACGAAGTGCCGA</u> <u>AAGCGAGTGGGTTTTAGAGCTAGAAATAG</u> C	pU6 Overhang
UMAG_05222	<u>CAAAATTCCATTCTACAACGGTGGCTACGA</u> <u>GCTGCACCTGTTTTAGAGCTAGAAATAGC</u>	pU6 Overhang
UMAG_00794	<u>CAAAATTCCATTCTACAACGTTTCCAGGG</u> <u>TACGGAAGACGTTTTAGAGCTAGAAATAG</u> C	pU6 Overhang
UMAG_02473	<u>TCGAATCCCGTCTGGTCAAGCAGATGACT</u> <u>GCATCTGTGTGTTTTAGAGCTAGAAATAGC</u>	ptRNA <sup>Leu</sup> overhang
UMAG_00792	<u>TCGAATCCCGTCTGGTCAAGAAGTGCCGA</u> <u>AAGCGAGTGGGTTTTAGAGCTAGAAATAG</u> C	ptRNA <sup>Leu</sup> overhang
UMAG_00793	<u>TCGAATCCCGTCTGGTCAAGAGTACCGTG</u> <u>GTCGAGGCGGGTTTTAGAGCTAGAAATAG</u> C	ptRNA <sup>Leu</sup> overhang

sgRNA spacer sequence is underlined.

**Table 4.8 Oligonucleotides used for quantitative PCR in this study.**

Target gene	Name	Sequence
Zm_GAPDH	GAPDH_F	CTTCGGCATTGTTGAGGGTTTG
Zm_GAPDH	GAPDH_R	TCCTTGGCTGAGGGTCCGTC

### 4.3.6 Plasmids

#### 4.3.6.1 Plasmids for *U. maydis* transformation

All plasmids used in this study were tested via restriction enzyme digest. After amplifying gene of your interest by PCR, the newly generated sequence was verified via sequencing (Eurofins Genomics, Luxembourg, Luxembourg). For CRISPR/Cas9 plasmid construction, 59 nt oligomers containing the specific spacer sequence and an upstream 19 nt overlap to the corresponding promoter and a 20 nt overlap downstream to the scaffold sequence were assembled with the Cas9 plasmid backbone via Gibson assembly. The sgRNA spacer sequences were designed by ECRISP (<http://www.e-crisp.org/E-CRISP/>, Heigwer et al. 2014, Table 4.5) using the “medium” setting and purchased from Sigma-Aldrich (St. Louis, USA). The plasmid backbones used for cloning are listed below. The plasmids used for transformation of *U. maydis* are given in Table 4.9.

#### **p123 (Aichinger et al., 2003)**

This plasmid backbone was used to generate complementation constructs containing cbx resistance and to facilitate the integration of the gene of interest into the *U. maydis ip* locus via homologous recombination. The plasmids were linearized with SspI or AgeI prior to transformation into *U. maydis*.

#### **pMS73 (Schuster et al., 2016)**

The self-replicating plasmid contains the following elements: a codon-optimized Cas9 under the control of the *U. maydis* hsp70 promoter, the U6 promoter of *U. maydis* for sgRNA expression, and Cbx-resistance, which is used for the selection of *U. maydis* transformants. The transient expression of all CRISPR components from this plasmid allows efficient removal of Cas9 from transformed cells, reducing off-target mutations. For multiplexing sgRNAs, the *U. maydis* tRNA-Gly and tRNA-Leu promoters derived from pMS77 (Schuster et al. 2018) were used.

#### **pCas9HF1 (Zuo et al. 2020a)**

The self-replicating plasmid derived from pMS73 replacing Cas9 with the high-fidelity variant of Cas9HF1.

**Table 4.9 Plasmids used for transformation of *U. maydis*.**

Backbone	Construct	Reference
pCas9HF1	pCas9HF1_pU6::sgRNA_UMAG_02381	This study
pCas9HF1	pCas9HF1_pU6::sgRNA_UMAG_00753	Schurack dissertation

pCas9HF1	pCas9HF1_pU6::sgRNA_UMAG_00793	This study
pCas9HF1	pCas9HF1_pU6::sgRNA_UMAG_12119	This study
pCas9HF1	pCas9HF1_pU6::sgRNA_UMAG_11484	This study
pCas9HF1	pCas9HF1_pU6::sgRNA_UMAG_00792	This study
pCas9HF1	pCas9HF1_pU6::sgRNA_UMAG_00794	This study
pCas9HF1	pCas9HF1_pU6::sgRNA_UMAG_02473	This study
pCas9HF1	pCas9HF1_pU6::sgRNA_UMAG_03650	This study
pCas9HF1	pCas9HF1_pU6::sgRNA_UMAG_05222	This study
pCas9HF1	pCas9_pU6::sgRNA_UMAG_02473_ptRNALeu::sgRNA_UMAG_00792	This study
pCas9HF1	pCas9_pU6::sgRNA_UMAG_02473_ptRNALeu::sgRNA_UMAG_00793	This study
pCas9HF1	pCas9_pU6::sgRNA_UMAG_00793_ptRNALeu::sgRNA_UMAG_00792	This study
pCas9HF1	pCas9_pU6::sgRNA_UMAG_02473_ptRNALeu::sgRNA_UMAG_02473	This study
pCas9HF1	pCas9_pU6::sgRNA_UMAG_00792_ptRNALeu::sgRNA_UMAG_00793	This study
pCas9HF1	pCas9_pU6::sgRNA_UMAG_00792_ptRNALeu::sgRNA_UMAG_02473	This study
p123	p123_pUMAG_00793::UMAG_00793::Tnos	This study
p123	p123_pUMAG_02473::UMAG_02473-HA::Tnos	This study
p123	p123_pUMAG_00792::UMAG_00792-HA::Tnos	This study
p123	p123_pUMAG_00753::UMAG_00753::Tnos	This study
p123	p123_pUMAG_02381::UMAG_02381-HA::Tnos	This study
p123	p123- pPit2::sp00793-mcherry-HA::Tnos	This study
p123	p123- pPit2::sp02473-mcherry-HA::Tnos	This study
p123	p123- pPit2::UMAG_02473-2HA::Tnos	This study
p123	p123-pUMAG_00753-UMAG_00753-mCherry #6	This study
p123	p123- pPit2::UMAG_00793-2HA::Tnos	This study
p123	p123- pPit2::UMAG_00792-2HA::Tnos	This study
p123	p123- pPit2::UMAG_02473-2HAΔUMAG_00792::Tnos	This study
p123	p123- pPit2::UMAG_02473-2HAΔUMAG_00793::Tnos	This study
p123	p123- pPit2::UMAG_02473-2HAΔUMAG_00792-UMAG_00793::Tnos	This study

#### 4.3.6.2. Plasmids for the transformation of *S. cerevisiae* and yeast two-hybrid analysis

In yeast two hybrid assay, the genes of interest are integrated into the designed backbones of pGBKT7 and pGADT7. The pGBKT7 plasmid contains a DNA-binding domain (BD), while the pGADT7 plasmid contains an activation domain (AD).

#### **pGBKT7 (Clontech, Mountain View, USA)**

This plasmid was used in yeast two-hybrid analysis (bait vector) and served as a control plasmid (starting vector), as well as a template for starting gene fusions of various variants with the integrated effectors or SnRK1 Gal4 DNA binding domain and a cMyc tag fusion. It conveys kanamycin resistance and contains tryptophan (TRP) auxotrophy.

**pGADT7 (Clontech, Mountain View, USA)**

This plasmid was used in yeast two-hybrid analysis (prey vector) and served as a control plasmid (empty vector), as well as a template for starting gene fusions for various effectors or SnRK1 variants with the integrated Gal4 activation domain and an HA tag. It conveys Amp resistance and contains the Leucine (LEU) auxotrophic marker.

**Table 4.10 Plasmids used for *S. cerevisiae* transformation.**

Backbone	Construct	Reference
pGBKT7	pGBKT7-UMAG_00793-no SP #5	This study
pGBKT7	pGBKT7-UMAG_02473-no SP #5	This study
pGADT7	pGADT7-UMAG_02473 #5	This study
pGADT7	pGADT7-UMAG_00793 $\Delta$ sp	This study
pGADT7	pGADT7-UMAG_00792-no SP #3	This study
pGBKT7	pGBKT7-UMAG_00792-no SP #2	This study
pGADT7	pGADT7-ZM_SnRK1.1	This study
pGADT7	pGADT7-ZM_SnRK1.2	This study
pGADT7	pGADT7-ZM_SnRK1.3	This study
pGBKT7	pGBKT7-ZM_SnRK1.1	This study
pGBKT7	pGBKT7-ZM_SnRK1.2	This study
pGBKT7	pGBKT7-ZM_SnRK1.3	This study
pGBKT7	pGBKT7-p53	In lab
pGADT7	pGADT7-T	In lab
pGBKT7	pGBKT7	Clontech, Mountain View, USA
pGADT7	pGADT7	Clontech, Mountain View, USA

**4.3.6.3. Plasmids for transient expression of proteins in *N. benthamiana* via**

***A. tumefaciens*-mediated transformation**

**Table 4.11 Plasmids used for transient expression in this study.**

Backbone	Construct	Reference
pL1B	pL1B-F1::p2x35s-UMAG_02473-6XHA::35ster_NO SP #3	This study
pL1B	pL1B-F1::p2x35s-UMAG_00793-6XHA::35ster_NO SP # 4	This study

pL1B	pL1B-F1::p2×35s-UMAG_00792-4myc::Noster_NO SP	This study
pL1B	pL1B-F1::p2×35s-ZM_SnRK1.1-4myc::Noster	This study
pL1B	pL1B-F1::p2×35s-ZM_SnRK1.2-4myc::Noster	This study
pL1B	pL1B-F1::p2×35s-ZM_SnRK1.3-4myc::Noster	This study
pL1B	pL1B-F1::p2x35s-UMAG_00793-GFP::35ster_NO SP #1	This study
pL1B	pL1B-F1::p2x35s-UMAG_02473-GFP::35ster_NO SP #3	This study
pCAMBIA 1300	pCAMBIA 1300-nLUC-UMAG_00792-NO SP	This study
pCAMBIA 1300	pCAMBIA 1300-nLUC-UMAG_00793-NO SP	This study
pCAMBIA 1300	pCAMBIA 1300-nLUC-UMAG_02473-NO SP	This study
pCAMBIA 1300	pCAMBIA 1300-cLUC-UMAG_00792-NO SP	This study
pCAMBIA 1300	pCAMBIA 1300-cLUC-UMAG_00793-NO SP	This study
pCAMBIA 1300	pCAMBIA 1300-cLUC-UMAG_02473-NO SP	This study
pCAMBIA 1300	pCAMBIA 1300-cLUC-Zm_SnRK1.1	This study
pCAMBIA 1300	pCAMBIA 1300-cLUC-Zm_SnRK1.2	This study
pCAMBIA 1300	pCAMBIA 1300-cLUC-Zm_SnRK1.3	This study

## 4.4 Standard microbiological methods

### 4.4.1 Competent cell preparation of *E. coli*

A single colony of *E. coli* (Top10 or DH5α) cells was grown in 100 ml of dYT medium containing 10 mM MgCl<sub>2</sub> and MgSO<sub>4</sub> at 37 °C with shaking at 200 rpm until an approximate OD<sub>600</sub> of 0.6 was reached. Subsequently, the cells were cooled on ice for 30 minutes, collected by centrifugation at 3,000 rpm at 4 °C for 15 minutes, and resuspended in 33 ml of ice-cold RF1 solution. After 30 minutes of incubation at 4°C, the cells were collected again by centrifugation at 3,000 rpm and 4 °C for 15 minutes, and the supernatant was discarded. Afterwards, the cells were resuspended in 5 ml of RF2 and incubated at 4°C for a minimum of 30 minutes. Finally, 50 µl of the cells were aliquoted into pre-chilled 1.5-ml Eppendorf tubes, snap-frozen in liquid nitrogen, and stored at -80 °C until further use.

RF1 solution            100 mM RbCl  
                               50 mM MnCl<sub>2</sub>·4H<sub>2</sub>O  
                               30 mM potassium acetate

	10 mM CaCl <sub>2</sub> ·2H <sub>2</sub> O
	15% (w/v) Glycerol
	pH 5.8(adjusted with glacial acetic acid)
RF2 solution	10 mM MOPS
	10 mM RbCl
	75 mM CaCl <sub>2</sub> x 2 H <sub>2</sub> O
	15% (w/v) Glycerol
	pH 5.8(adjusted with NaOH)

#### 4.4.2 Heat-shock transformation of *E. coli*

Chemically competent cells of *E. coli* K-12 Top10/DH10 $\beta$  or *E. coli* K-12 DH5 $\alpha$  were used for transformation. To 50  $\mu$ l of competent cells, approximately 1-5 ng of plasmid DNA or the Gibson assembly ligation product was added, and the mixture was incubated on ice for 30 minutes. The cells were then subjected to heat treatment at 42°C, followed by cooling on ice for 2 minutes. Subsequently, the cells were incubated for one hour at 37°C with 200 rpm shaking in 200  $\mu$ l of dYT. Finally, the cells were plated on YT solid plates containing the appropriate antibiotics for selection and incubated overnight at 37°C for growth.

#### 4.4.3 Competent cell preparation and transformation of *A. tumefaciens*

The preparation and transformation of *Agrobacterium* were carried out according (Höfgen & Willmitzer, 1988) by (Höfgen & Willmitzer, 1988), with minor alterations. The medium used for this purpose was dYT, rather than the specified YEB. This was according to the recommendations set out in the original publication (Höfgen & Willmitzer, 1988). The transformation was carried out through electroporation, whereby 1  $\mu$ L of the target plasmid was mixed with 50  $\mu$ L of competent *Agrobacterium* cells, which were then transferred to a pre-chilled 1 mm electroporation cuvette. The cuvette was placed into the *E. coli* Pulser apparatus (Eppendorf, Hamburg, Germany) and subjected to 1440 volts for 5 seconds. Subsequently, 1 mL of dYT medium without antibiotics was added to the cuvette to suspend the cells. The cell suspension was then transferred to a 1.5 mL microcentrifuge tube and incubated at 28 °C with continuous shaking for 1 h. Finally, approximately 30  $\mu$ L of the cell suspension was plated on YT agar plates containing the appropriate antibiotics.

#### 4.4.4 Protoplast preparation of *U. maydis*

*U. maydis* cells were grown in 20 ml of YEPSlight medium at 28 °C with shaking at 200 rpm. The following day, the overnight culture was diluted to an OD<sub>600</sub> of 0.25 in 50 ml YEPSlight and incubated at 28 °C until an OD<sub>600</sub> of 0.6–0.8 was reached. Subsequently, the culture was centrifuged at 2,000 xg for 10 minutes. The resulting pellet was resuspended in 10 ml SCS and centrifuged again for 5 minutes at 2,000 xg. The pellet was then lysed by resuspension in 2 ml SCS containing 7 mg/ml of Novozyme 234 (Novo Nordisk, Copenhagen, Denmark) and sterile filtration. The cells were incubated at room temperature for 5-10 minutes, and their morphological changes were observed under a microscope until 30-40% of the cells formed protoplasts. The cells were then added to 10 ml of ice-cold SCS and centrifuged at 1,300 x g for 5 minutes at 4 °C. The resulting pellet was carefully resuspended in 10 ml of ice-cold SCS

and the cells were centrifuged at 1,300 xg for 5 minutes at 4 °C twice. The pellet was then resuspended in 10 ml of ice-cold STC and the cells were centrifuged again at 1,300 xg for 5 minutes at 4 °C. The pellets were resuspended in 500 µl of ice-cold STC and divided into 50 µl portions in pre-chilled reaction tubes and stored at -80°C.

SCS solution	20 mM Na-Citrate, pH 5.8 1 M Sorbitol, sterile filtered
STC solution	10 mM Tris-HCl, pH 7.5 100 mM CaCl <sub>2</sub> 1 M Sorbitol, sterile filtered
STC/PEG solution	15 ml STC 10 g PEG4000

#### **4.4.5 Transformation of *U. maydis***

For *U. maydis* protoplast transformation, the previously prepared protoplasts were thawed on ice and a maximum volume of 10 µl of linearized plasmid DNA (SspI or AgeI digested for homologous recombination, such as gene complementation) or non-linear plasmid DNA (for CRISPR/Cas9-mediated gene editing) was added. Additionally, 1 µl of heparin solution (1 mg/ml) was added and incubated on ice for 10 minutes. The protoplasts were then mixed with 500 µl of STC/PEG solution and incubated on ice for 15 minutes. Finally, the protoplasts were gently spread on regeneration agar plates that had been freshly prepared. The plates had a 10 ml bottom layer containing the 2x selection resistance marker and a 10 ml top layer without the selection marker. The plates were incubated at 28°C for 3-6 days until colonies grew. The transformants were then transferred to PD plates containing selective markers. For rigorous selection, individual colonies were transferred a second time to PD plates with the selectable marker and finally to plates without the resistance marker. The DNA from the colonies could then be extracted for gene sequencing or Southern blot analysis.

#### **4.4.6 Filamentous growth test for *U. maydis***

The *U. maydis* strain was cultured in YEPSlight liquid medium at 28°C with 200 rpm shaking until the optical density at 600 nm (OD<sub>600</sub>) reached approximately 0.8-1.0. The cells were then collected by centrifugation at 3500 rpm for 10 minutes, and the resulting pellet was resuspended in sterile water and washed once. The OD<sub>600</sub> of the culture was adjusted to 1.0 in sterile water. Approximately 5 µL of the suspension culture was then applied to a PD plate containing charcoal, and the plates were incubated at 28 °C for 2-3 days. The formation of white mycelium indicated successful filamentous growth.



#### 4.4.7 *In-vitro* impairment growth test for *U. maydis*

CRISPR knockout strains of *U. maydis* were subjected to a series of tests to assess their fitness and axenic survivability. Strains exhibiting an OD<sub>600</sub> of 0.6-0.8 were subjected to centrifugation at 2000 xg for 10 minutes, after which they were suspended in sterile water to achieve an OD<sub>600</sub> 1.0. Subsequently, a dilution series was prepared from 100 to 10<sup>-4</sup> in sterile H<sub>2</sub>O. Finally, 5µl of each dilution was spotted on CM plates containing components of different stress conditions. The plates were incubated for 2 days at 22°C.

CM media	2 g (0.25 %) (w/v) Casamino acids (Difco)
	0.8 g (0.1 %) (w/v) Yeast extract
	8 ml (1 %) (v/v) Vitamin solution (Holliday '74)
	50 ml (6.25 %) (v/v) Salt solution (Holliday '74)
	0.4 g (0.05 %) (w/v) DNA degradation free (Sigma)
	1.2 g (0.15 %) (w/v) NH <sub>4</sub> NO <sub>3</sub>
	10 ml (1 %) (v/v) 1 M Tris-HCl pH 8.0
	16 g (2 %) (w/v) Agar

#### 4.4.8 Competent cell preparation and transformation of *S. cerevisiae*

The competent cell preparation was performed according to the Clotech yeast two hybrid protocols. A single colony of *S. cerevisiae* AH109 cells was selected and inoculated in 5 mL of YPD medium. The colonies were vigorously shaken by vortex for five minutes and grown overnight at 28°C with 200 rpm shaking. On the following day, the overnight culture was diluted to an OD<sub>600</sub> of 0.2 in 50 ml of YPD and grown to an OD<sub>600</sub> of 0.4-0.6 after being shaken for 3-4 hours at 28°C. The cells were then collected by centrifugation at 1000xg for 5 minutes and washed once with sterile water or 1x TE solution. The yeast cells were then centrifuged once more, and the supernatant was discarded. The pellet was resuspended in 1.5 ml of a freshly prepared 1xTE/1xLiAc solution. In a new 2-mL reaction tube, 100 µL of the prepared cell suspension was gently mixed with 1 µg of plasmid (or 0.5 µg for the interaction test) and 0.1 mg of carrier DNA (denatured herring testes carrier DNA, 10 mg/mL), followed by 600 µL of sterilized PEG/LiAc, and thoroughly mixed. The cells were recovered by shaking at 200 rpm for 30 minutes at 30°C. Subsequently, 70 µl of dimethyl sulfoxide (DMSO) was added to the tubes and gently mixed, followed by incubation at 42°C for 30 minutes. The cells were then centrifuged at maximum speed for 15 seconds to remove the supernatant. Subsequently, the cells were resuspended in 100 µl of 0.9% NaCl solution, and 50 µl were spread on the appropriate selective medium and incubated at 28°C for 3-5 days. Finally, the yeast colonies grown on the screening plate were transferred to plates containing the selective markers and used for the assay.

PEG/LiAc solution	40% (w/v) PEG3350
-------------------	-------------------

(Polyethylene acetate)	glycol/lithium	1X LiAC 1X TE
Stock solutions		50% PEG 3350 100% DMSO (Dimethyl sulfoxide) 10X TE buffer: 0.1 M Tris-HCl, 10 mM EDTA, pH 7.5. Autoclave. 10X LiAc: 1 M lithium acetate Adjust to pH 7.5 with dilute acetic acid and autoclave.

#### 4.4.9 Dropout assay for *S. cerevisiae*

The yeast two-hybrid assay was performed according to manufacturer's protocol (Clontech, Saint-Germain-en-Laye, France). Yeast cells were cultured overnight at 28°C with continuous shaking at 200 rpm in 5 mL of SD-Leu-Trp medium. On the following day, the cell density was adjusted to an OD<sub>600</sub> of 0.2 using the same medium, and the cultures were incubated until they reached an OD<sub>600</sub> of 1.0. Thereafter, the culture was collected by centrifugation at 4000 rpm for 5 minutes and the pellet was washed twice with sterile distilled water. Finally, the pellet was resuspended in sterile distilled water to an OD<sub>600</sub> of 1.0, and four sequential dilutions (1:10, 1:100, 1:1000, and 1:10,000) were performed. A total of 5 µL of the suspension for dilution was transferred to low-stringency (SD-Leu-Trp), medium-stringency (SD-Leu-Trp-His), and high-stringency (SD-Leu-Trp-Ade-His) medium plates, respectively. The plates were incubated for 4-5 days at 28 °C.

## 4.5 Molecular microbiological methods

### 4.5.1 Isolation of nucleic acids

#### 4.5.1.1 Isolation of plasmid DNA from *E. coli*

The NucleoSpin® Plasmid Kit (Macherey-Nagel, Düren, Germany) was used to isolate plasmids from *E. coli* according to the manufacturer's recommendations.

#### 4.5.1.2 Isolation of genomic DNA from *U. maydis*

The isolation of genomic DNA (gDNA) from *U. maydis* was performed using a modified version of the protol (Höfgen & Willmitzer, 1988). Two milliliters of *U. maydis* overnight cultures were subjected to centrifugation at 1,2000 xg for two minutes in 2 ml Eppendorf tubes. The supernatant was discarded, and 200 µl of glass beads, 400 µl of *Ustilago* lysate buffer, and 500 µl of phenol/chloroform were added to the pellets. Subsequently, the mixture was agitated at 2,500 rpm for 10 minutes on a Vibrax-VXR shaker (IKA, Staufen, Germany), followed by centrifugation at 1,2000 rpm for 15-20 minutes. The extracted DNA was then transferred to a

new 1.5 ml tube, along with 400 µl of the upper aqueous phase. One milliliter of absolute ethanol or 0.7x isopropanol was added and mixed by inverting the tubes. After 10 minutes of centrifugation at 12,000 x g, the DNA pellets were obtained, and the supernatant was discarded. The precipitate was resuspended in 400 µL of 70% ethanol and centrifuged at 12,000 x g for 5 minutes. The supernatant was discarded, and the pellets were dried at room temperature for 10 minutes until the ethanol had completely evaporated. Finally, 100 µl of H<sub>2</sub>O was added to the pellet and incubated in a thermomixer (Eppendorf, Hamburg, Germany) at 55 °C for 30 minutes to dissolve DNA completely. The extracted DNA was stored at -20 °C until further use.

<i>Ustilago</i> lysis buffer	10 mM Tris-HCl, pH 8 100mM NaCl 1 mM Na <sub>2</sub> -EDTA 1% (w/v) SDS 2% (v/v) Triton x-100
Phenol / Chloroform	50% (v/v) Phenol (equilibrated in TE buffer) 50% (v/v) Chloroform

#### **4.5.1.3 Total RNA isolation from infected maize tissue**

To isolate total RNA, samples were pulverized with liquid nitrogen. One milliliter of TRIzol® reagent (Invitrogen, Darmstadt, Germany) was added to approximately 400 µl of powdered tissue in a 1.5 mL microcentrifuge tube. The mixture was vortexed and incubated at room temperature for 10 minutes. Subsequently, centrifugation at 13,000 rpm at 4°C for 10 minutes was performed, after which the supernatant was transferred to a new 1.5 mL centrifuge tube containing 0.2 mL of chloroform. The samples were mixed by inverting the tube and incubated for 3 minutes at room temperature. Afterwards, centrifugation at 13,000 rpm for 15 minutes at 4°C was performed. To precipitate RNA, the upper aqueous phase was transferred to an additional 1.5 mL Eppendorf tube and combined with 0.5 mL isopropanol. After 10 minutes of incubation at room temperature, the samples were centrifuged at 13,000 rpm for 10 minutes at 4°C. After removing the supernatant, the pellet was washed with 1 mL of 75% ethanol and dried at room temperature. The dried RNA pellet was then dissolved in 50 µL of RNase-free ddH<sub>2</sub>O for 10 min at 55 °C. The RNA concentration was subsequently measured and evaluated using a NanoDrop ND-1000 spectrophotometer (Thermo Fisher Scientific, Waltham, USA), and the RNA quality was evaluated on a 1% agarose gel. The total RNA was then stored at -20°C until use.

#### **4.5.1.4. DNase treatment of isolated RNA**

A digest of contaminating DNA was performed after RNA isolation using the Turbo DNA Free Kit from Ambion Life Technologies (Carlsbad, USA) according to the manufacturer's

protocol. Ten micrograms of total RNA were treated in a 50-microliter reaction containing five microliters of 10X TURBO DNase Buffer and one microliter of TURBO DNase. The reaction was incubated at 37 °C for 30 minutes. The DNase was inactivated by the addition of 5 µl of DNase Inactivation Reagent. After a 5-minute incubation at room temperature with intermittent mixing, the sample was centrifuged at 10,000 xg for 2 minutes, and 44 µl of the supernatant was transferred to a fresh reaction tube. RNA concentration was quantified by spectrophotometry using a NanoDrop ND\_1000 (Thermo Fisher Scientific, Waltham, USA), and quality was subsequently assessed by loading 1 µl of RNA onto a 1.5% agarose gel.

#### **4.5.1.5 cDNA synthesis**

The DNase-treated RNA was converted to cDNA using the Thermo Scientific RevertAid H Minus First Strand cDNA Synthesis Kit (Thermo Fisher Scientific, Waltham, USA) according to the manufacturer's protocol. A mixture of 1-5 µg RNA and 1 µl oligo(dT)18 primer was combined with nuclease-free water to a total volume of 12 µl and incubated at 65 °C for 5 minutes. Subsequently, a solution comprising 4 µl of 5x Reaction Buffer, 1 µl of RiboLock RNase Inhibitor (20U/µl), and 2 µl of 10 mM dNTP Mix was prepared. A total volume of 20 µl was prepared, comprising 1 µl of RevertAid H Minus M-MuLV Reverse Transcriptase (200 U/µl) and 1 µl of RiboLock RNase Inhibitor (20 U/µl). This was incubated at 42°C for 60 minutes. Subsequently, the reaction was terminated by heating to 70 °C for 5 minutes. The synthesized cDNA was stored at -80 °C until further use.

#### **4.5.1.6 Quantitative real-time PCR (qRT-PCR)**

A 1:20 dilution of the synthesized cDNA (described in chapter 4.5.1.5) was employed as a template for quantitative real-time PCR (qRT-PCR). The qRT-PCR reactions were conducted using GoTaq® qPCR Mastermix (Promega GmbH, Madison, USA) according to the manufacturer's protocol. A total of 5 µl of diluted cDNA was added to the reaction, with a total volume of 15 µl. All qRT-PCRs were carried out on an iCycler system (Bio-Rad, Hercules, USA) using the following program: The reaction was heated to 95 °C for two minutes, followed by a denaturation step at 95 °C for 30 seconds, annealing at 62 °C for 30 seconds, and extension at 72 °C for 30 seconds. This cycle was repeated 45 times. After completion of the qPCR run, a melting curve analysis was performed to confirm the specificity of the reaction. The threshold cycles were determined using the Bio-Rad software, and the relative expression values were calculated using the  $2^{-\Delta\Delta C_t}$  method.

### **4.5.2 Nucleic acid modification**

#### **4.5.2.1 Restriction enzyme digestion of DNA**

Restriction digestion of DNA was performed via type II restriction endonucleases (New England Biolabs, Ipswich, USA). The amount of digested DNA ranged from 1-5 µg. The restriction reaction was set up according to the manufacturer's instructions.

#### **4.5.2.2 Ligation of DNA fragments**

The ligation of DNA fragments was performed using the T4 DNA ligase (Thermo Fisher Scientific, Waltham, USA) according to the manufacturer's protocol with a minor adjustment. For sticky ends, the ligation was performed overnight at a temperature of 4 °C, or for a duration of 10 minutes at room temperature. For blunt ends or single-base overhangs, the ligation was conducted over the course of one night at a temperature of 4 °C, or for a duration of at least two hours at room temperature. Finally, the enzyme was inactivated at 65 °C for 10 minutes to prepare it for subsequent transformation.

#### **4.5.2.3 Gibson assembly cloning**

The Gibson assembly cloning method employs homologous recombination of DNA fragments (Gibson et al., 2009). The DNA fragments were designed to have 18-20 nt overlap with the DNA fragments to be assembled. The Gibson assembly was performed using the NEBuilder® HiFi DNA Assembly Master Mix (New England Biolabs, Ipswich, USA) according to the manufacturer's protocol. Following the assembly of the desired ratio, the samples were incubated in a thermocycler at 50 °C for 20 minutes for 2 or 3 fragment assemblies and for 60 minutes for 4-6 fragment assemblies. Following the incubation period, the samples were stored either on ice or at -20 °C for subsequent transformations.

#### **4.5.2.4 Site-directed mutagenesis**

Site-directed mutagenesis was conducted using the QuikChange Lightning Multi Site-Directed Mutagenesis Kit (Agilent, Waldbronn, Germany) for the insertion of single or multiple site-specific mutations into double-stranded plasmids. The procedure was performed according to the manufacturer's instructions.

#### **4.5.2.5 Polymerase chain reaction (PCR)**

Polymerase chain reaction (PCR) was performed in T100 Thermal cyclers from Bio-Rad Laboratories GmbH (Hercules; USA) for the amplification of DNA fragments. Depending on the purpose, different polymerases were employed. For analytic purposes, the GoTaq® Green Master Mix (Promega GmbH, Madison, USA) was used for initial screening. The Q5® High Fidelity DNA Polymerase (New England Biolabs, Ipswich, USA) were used for the amplification of long fragments or gene of your interest in vector construction. Reactions were performed using the supplied buffers and solutions according to the manufacturer's protocol.

#### **4.5.3 Purification PCR fragments product**

A polymerase chain reaction (PCR) thermocycler from Bio-Rad Laboratories (Hercules, USA) was used to amplify DNA fragments. The appropriate polymerase was selected based on the intended use of amplification. GoTaq® Green Master Mix from Promega (Madison, USA) was used to verify clonal transformation. Long fragment amplicon or gene of your interest amplicon for vector construction was carried out using either Phusion® High-Fidelity DNA Polymerase

or Q5® High-Fidelity DNA Polymerase from New England Biolabs (Ipswich, USA). The reagents were added according to the manufacturer's instructions.

#### **4.5.4 DNA sequencing and RNA sequencing**

The DNA sequencing was conducted by Eurofins (formerly GATC, Luxembourg, Luxembourg). Prior to sequencing plasmids or PCR fragments, the plasmid was isolated using the plasmid kit, and PCR fragments were purified using the Nucleospin® Gel and PCR Clean-up kit (Macherey-Nagel, Düren, Germany), as previously described in section 4.5.3. The DNA sequencing results were analyzed using Clone Manager 9 (Sci-Ed, Denver, USA). The mRNA was sequenced by Novogene (Beijing, China) using the Illumina NovaSeq 6000 (Illumina, San Diego, USA) For details about RNA seq, refer to Chapter 4.9.1.

#### **4.5.5 Agarose gel electrophoresis**

The concentration of agarose gel, 0.9% and 2% (w/v), was used depending on the size of the fragments to be separated. The agarose was boiled and dissolved in 1xTAE buffer solution, after which ethidium bromide (0.25 µg/ml) was added to the cooled agarose containing solution. The gel was prepared by pouring agarose solution into a gel casting tray and a suitable comb was inserted. After solidification, the comb was removed, and the gel was transferred to an electrophoresis running chamber filled with 1xTAE buffer. The samples were mixed with 6x DNA loading dye and added to the comb pocket. Electrophoresis was performed at a constant voltage of 90-120 V for 30-60 minutes. The separated DNA fragments were visualized under ultraviolet radiation (Peqlab/VWR, Radnor, USA). The desired band was excised, and the DNA fragments was purified and recycled using the NucleoSpin® Gel and PCR Clean-up Kit (Macherey Nagel, Düren, Germany) for further experimentation.

50x TAE-buffer	2 M Tris-Base
	2 M Acetic acid
	50 mM EDTA, pH 8.0 in in H <sub>2</sub> O
6x DNA loading dye	50%(w/v) Sucrose
	0.1% (v/v) Bromophenol blue
	in TE-Buffer

#### **4.5.6 Southern blot analysis**

The specific DNA sequence inserted in genomic DNA was confirmed by Southern Blot according to Southern, 1975. Initially, the DNA extracted in the preceding step (outlined in chapter 4.5.1.2) was subjected to overnight digestion with an appropriate endonuclease. In order to enhance the concentration and purity of the DNA, a solution comprising 1/10x volume of 3 M sodium acetate and 2x volumes of 100% ethanol was added to the sample, which was then incubated at -20 °C for one hour. Following this, centrifugation was performed for 30

minutes at 12,000 xg at 4 °C for the collection of the precipitated DNA. The pellet was then dissolved in 20 µl of 1x DNA loading dye and the DNA fragments were separated using gel electrophoresis on a 0.9% agarose gel at 110 V for 2 hours. To depurinate DNA in agarose gel, the gel was incubated with 0.25 M HCl for 15 minutes and subsequently neutralized in transfer buffer containing 0.4 M NaOH for 30 minutes. Subsequently, the DNA was transferred from the gel to a nylon membrane (GE Healthcare Life Sciences, Freiburg, Germany) using transfer solution for capillary blotting overnight. On the following day, the DNA fragments were fixed to the membrane using UV crosslinking (Amersham Biosciences, Little Chalfont, UK). The membrane was pre-hybridized in a hybridization oven (UVP HB-1000 Hybridizer, Ultra-violet Products Ltd., Cambridge, UK) with 20 mL of Southern hybridization buffer at 65°C for 2 hours. The detection of DNA was conducted using digoxigenin (DIG)-labeled DNA probes. Probes were synthesized using the PCR DIG Labeling Mix kit (Roche, Mannheim, Germany) according to the manufacturer's protocol. The probe-containing DIG-labeled PCR products and 20ml of hybridization buffer were boiled for 10 minutes to denature the DNA. The membrane was incubated in a probe-containing hybridization buffer with rotation at 65°C overnight, and washed three times with Southern wash buffer for 15 minutes at 65°C. Subsequently, the membrane was incubated with DIG wash buffer for five minutes, blocked with DIG buffer 2 for 30 minutes, and finally incubated with DIG antibody solution for one hour. All the aforementioned steps were performed at room temperature with rotation. Subsequently, the membrane was washed three times for 15 minutes with DIG wash buffer, equilibrated in DIG buffer 3 for 5 minutes, and incubated with 2.5 ml of CDP-star solution in a small autoclave bag for 10 minutes at 37°C. Finally, the membrane was visualized using ChemiDoc™ MP (Bio-Rad Laboratories GmbH, Hercules; USA) to detect the DIG-labeled DNA fragments.

Depurination solution	0.25 M HCl
Transfer buffer	0.25 M HCl 0.5 M NaOH 1.5 M NaCl
Southern hybridization buffer	0.5 M Na-phosphate buffer, pH 7 7% (w/v) SDS
Southern wash buffer	0.1 M 1M Na-phosphate buffer, pH 7 1% (w/v) SDS 0.1 M maleic acid
DIG buffer 1	0.15 M NaOH set pH to 7.5 with NaOH autoclave
DIG buffer 2	1% (w/v) skimmed milk powder in DIG1

	0.1 M Tris-HCl (pH 9.5)
DIG buffer 3	0.1 M NaCl
	0.05 M MgCl <sub>2</sub>
DIG wash buffer	0.3% (v/v) Tween-20 in DIG1
Southern antibody solution	Anti-Dioxigenin-AP antibody 1:10,000 in DIG2 (Roche, Mannheim, Germany)
CDP-star solution	CDP-Star 1:200 in DIG3 (Roche, Mannheim, Germany)
	1 M Na <sub>2</sub> HPO <sub>4</sub>
Na-phosphate buffer, 1 M (pH 7.0)	1 M NaH <sub>2</sub> PO <sub>4</sub> ·H <sub>2</sub> O Add NaH <sub>2</sub> PO <sub>4</sub> ·H <sub>2</sub> O to Na <sub>2</sub> HPO <sub>4</sub> until pH reaches 7.0 in in H <sub>2</sub> O bid

## 4.6 Protein methods and biochemical assays

### 4.6.1 Protein heterologous protein expression in *N. benthamiana*

*A. tumefaciens* GV3101 strains carrying the relevant plasmids of interest were infiltrated into *N. benthamiana* to transiently express heterologous proteins. The GV3101 strain with the desired plasmid was grown to an OD<sub>600</sub> of 1.0 in dYT medium containing appropriate antibiotics. The culture was centrifuged at 4000 rpm for 10 minutes and washed twice with ddH<sub>2</sub>O. Subsequently, the cell pellet was resuspended in MES buffer (10 mM MES, 10 mM MgCl<sub>2</sub>, 100 μM acetosyringone) to an OD<sub>600</sub> of 0.5. The GV3101 cell suspension was mixed according to the experimental design and infiltrated into the abaxial surface of the leaf using a 1 mL syringe. After 2-3 days, the infiltrated leaves were collected, and protein was extracted for western blot.

### 4.6.2 Protein extraction from *S. cerevisiae*

The protein extraction from yeast strains used in Y2H assays was performed following the protocol outlined by Kushnirov, 2000. A single colony of yeast strains was cultured overnight in YPD medium, and 2 mL of the culture were subjected to centrifugation for 5 minutes at 13,000 rpm. The resulting pellets were resuspended in 100 μL of distilled water and 100 μL of 0.2 M NaOH, centrifuged for 5 minutes at 2,000 rpm, and incubated at room temperature for 10 minutes. Thereafter, the pellets were resuspended in 50 μL of 1x sample buffer, boiled for 10 minutes, and centrifuged. The supernatant was stored at -20°C or used for subsequent experiments by loading it onto an SDS-PAGE gel.



### 4.6.3 Protein extraction from *Z. mays* or *N. benthamiana*

The maize leaves infected with *U. maydis* (chapter 4.7.3) or *N. benthamiana* leaves infiltrated with *Agrobacterium* (chapter 4.6.1) were frozen in liquid nitrogen. The frozen plant material was then finely ground to powder using liquid nitrogen. A total of 300mg of each ground plant powder was transferred to 2 mL. For the protein extraction, the aforementioned plant material was mixed with 1.5 mL of protein extraction buffer (EWB). The samples were incubated on ice for 30 minutes and centrifuged twice at 13,000 rpm for 30 minutes at 4°C to remove any plant debris. The resulting supernatant served as the total extracted protein and was utilized in subsequent experiments.

#### Extraction/Washing Buffer (EWB)

	Stock	100ml
50mM Tris pH 7.5	1M	5ml
150mM NaCl	5M	3ml
10% Glycerol	Glycerol 80%	12,5ml
2mM EDTA	0,5M	400µl
Water		79,1ml
<hr/>		
Add fresh to	Stock	10ml of EWB
5mM DTT	1M	50µl
1% Triton		100µl
cComplete Tablets (Roche)	1 tablet in 1ml	100µl

### 4.6.4 Co-immunoprecipitation assay in plant

For co-immunoprecipitation assays, specific antibody-conjugated magnetic beads were utilized to capture proteins of interest. Initially, 5-10 µL of trap beads were added into 1 mL of the previously extracted total plant protein (chapter 4.6.4) and incubated at 4°C with rotation for 1-2 hours. 50 µL of total extract protein was utilized as input without incubating the beads to assess protein expression. The magnetic stand was used to collect the beads, which were then washed three times with extraction buffer and three times with wash buffer. A volume of 50–80 µL of 2x loading buffer was added to the washed beads, which were then boiled at 95°C for 10 minutes. Samples were then detected by western blot, and immunoblotting was performed with the appropriate antibodies.

#### 4.6.4.1 Co-immunoprecipitation of proteins in maize and followed by Liquid chromatography-mass spectrometry/ mass spectrometry (LC-MS/MS)

Total proteins were extracted from maize leaves infected with *U. maydis* (Table 4.5) according to the protocol described in chapter 4.6.4. The HA magnetic beads (ThermoFisher) were equilibrated and incubated with total extracted protein at 4 °C for 1-2 hours as described in chapter 4.6.4. The magnetic beads were collected using a magnetic stand and washed three times with 700 µL of washing buffer. Subsequently, the protein-bound beads were subjected to LC-MS/MS analysis.

#### 4.6.4.2 Total protein extraction for phosphoproteomic analysis

The total proteins were extracted from maize leaves infected with *U. maydis* (Table 4.5) according to the protocol described in chapter 4.6.4. The extracted proteins were sent for phosphoenrichment and subsequent phosphoproteomic analysis.

#### 4.6.5 SDS polyacrylamide gel electrophoresis (SDS-PAGE)

Sodium dodecyl sulfate-polyacrylamide gel electrophoresis (SDS-PAGE) was employed to separate denatured and negatively charged proteins based on their molecular weight. Samples were boiled for 10 minutes at 99 °C in 2x SDS gel loading buffer containing 100 mM DTT to denature proteins. The gels for SDS-PAGE are composed of an upper stacking gel and a lower resolving gel. The gels were casted and placed in the chamber (Mini Protean System, Bio-Rad, Munich, Germany) filled with SDS running buffer. The protein samples, along with 4 µl of PageRuler Prestained Protein Ladder (Thermo Fisher Scientific), were loaded into the wells of the SDS gel and subjected to electrophoresis in 1x SDS running buffer at a constant voltage of 120-160V for 1 h. The SDS gel was then utilized for protein staining or immunoblotting.

	10 mL 1.5 M Tris-HCl pH 6.8
	30 mL glycerin
4× Sample buffer	6 mL 20 % SDS
	5 mg bromophenol blue
	3 g DTT (f. c. 400 mM)
	Fill up to 50 mL with H <sub>2</sub> O
	0.5 mL 0.5 M Tris-HCl pH 6.8
	0.333 mL 30 % Polyacrylamide (PAA)
Stacking gel (5%)	20 µL 10 % SDS
	20 µL 10 % Ammonium persulfate (APS)
	2 µL Tetramethylethylenediamine (TEMED)

	1.125 mL in H <sub>2</sub> O
	1.25 mL 1.5 M Tris-HCl pH 8.8
	2.49 mL 30 % Polyacrylamide (PAA)
Stacking gel (15 %)	50 µL 10 % SDS
	50 µL 10 % Ammonium persulfate (APS)
	5 µL Tetramethylethylenediamine (TEMED)
	1.17 mL H <sub>2</sub> O
	25 mM Tris-HCl, pH 8.0
SDS running buffer	192 mM glycine
	4 mM SDS dissolve in H <sub>2</sub> O

#### 4.6.6 Western blot

The proteins separated by SDS-PAGE was transferred to polyvinylidene fluoride (PVDF) nitrocellulose membranes (Amersham Hybond P 0.45 PVDF blotting membrane, GE Healthcare, Munich, Germany) using the semi-dry Trans-Blot Turbo transfer system from Bio-Rad (Munich, Germany). Prior to the transfer of proteins to PVDF, the PVDF membrane was activated with methanol and Whatman papers were placed in transfer buffer. The assembly was set up from bottom to top in the following order: a Whatman paper, a PVDF nitrocellulose membrane, an SDS-PAGE gel, and another Whatman paper. It was then gently rolled on Whatman paper to remove any air bubbles. The "Mixed MW (Turbo)" pre-program from Bio-Rad was used for proteins with a molecular weight between 5 and 150 kDa. The gels were transferred for 20 to 30 minutes at 1.3 A, 25 V (for one mini gel) or 2.5 A, 25 V (for two mini gels), depending on the size of the desired proteins. Subsequently, the membranes were incubated in blocking solution at room temperature for one hour. Thereafter, the blocking solution was replaced with a solution containing the primary antibody or HRP-conjugated antibody and the mixture was incubated at room temperature for one hour or at 4°C overnight. The dilution of antibodies was carried out according to Table 4.12. The membrane was washed three times with TBST buffer for ten minutes to remove any excess and unbound antibodies. Subsequently, the membranes were incubated with the secondary antibody (for the membrane incubated with primary antibody) in TBST buffer for one hour at room temperature, followed by another three washes with TBST buffer for ten minutes. Finally, the membrane was subjected to signal detection using either SuperSignal™ West Pico PLUS Chemiluminescent Substrate or SuperSignal™ West Femto Maximum Sensitivity Substrate (Thermo Fisher Scientific, Dreieich, Germany) on a ChemiDoc™ MP (Bio-Rad Laboratories GmbH, Hercules; USA).

	25 mM Tris-HCl, pH 10.4
Western transfer buffer	192 mM glycine
	15%(v/v) methanol
	50 Mm Tris-HCl, pH 7.5
TBST	150 mM NaCl
	0.1 % (v/v) Tween 20 dissolve in H <sub>2</sub> O
Blocking solution	5 % (v/v) skim milk powder in TBST
Antibody solution	Antibodies dilute in blocking solution

**Table 4.12 Antibodies used in this study.**

<b>Name</b>	<b>Organism</b>	<b>Supplier</b>	<b>Working ratio</b>
GFP	mouse	Roche	1:3000
HA	mouse	Sigma-Aldrich (St. Louis, USA)	1:30000
His	mouse	Thermo Fischer	1:3000
c-myc	mouse	Sigma-Aldrich (St. Louis, USA)	1:5000
GST	rabbit	Cell signaling technology	1:1000
His-HRP		QIAGEN	1:2000
GFP-HRP		Invitrogen	1:1000
HA-HRP		Roche	1:2000
rabbit IgG	goat	Cell signaling	1:3000
mouse IgG	goat	Cell signaling	1:3000

#### 4.6.7 Coomassie staining of proteins

The SDS-PAGE gel was visualized with Coomassie Brilliant Blue (CBB) dye. The SDS-PAGE gel was stained with CBB for 15-30 minutes or overnight. The stained gel was then washed with either ddH<sub>2</sub>O or CBB destaining solution to remove any excess dye.

	0.1% (W/V) Coomassie Brilliant Blue R250
Coomassie Brilliant Blue R-250	25% (V/V) Isopropanol
	10% (V/V) Glacial Acetic Acid
Coomassie Brilliant Blue Stain	10% (V/V) Glacial Acetic Acid
Destaining Solution	5% (V/V) Ethanol

#### 4.7 Plant assays

##### 4.7.1 *Zea mays* material

The maize lines used for *U. maydis* pathogenicity experiment in this study are *Zea mays* cv. Golden Bantam (Demeter International, Germany), *Zea mays* cv. Early Golden Bantam (Heirloom maize), and *Zea mays* cv VA35 (yellow dent southern-adapted inbred maize line)

##### 4.7.2 Cultivation of *Z. mays*

All maize plants were grown in a temperature-controlled greenhouse or walk-in chamber with a light-dark cycle of 16 hours at 28 °C and 8 hours at 22 °C.

##### 4.7.3 *U. maydis* infection of *Z. mays*

For inoculation experiments, 7-day-old maize seedlings were used. *U. maydis* strains were cultured according to the chapter 4.2.5 until OD<sub>600</sub> 0.8-1.0 was reached. Subsequently, the fungal cells were centrifuged at 2400xg for 10 minutes. The resulting pellet was resuspended in double-distilled water (ddH<sub>2</sub>O) to achieve an OD<sub>600</sub> 1 for disease phenotyping purposes, and an OD<sub>600</sub> 3 for microscopy, (phospho)proteomics, and RNAseq. A 1 mL aliquot of the *U. maydis* suspension was then inoculated at the base of the stem, approximately 1 cm from the soil, into 7-day-old seedlings. The disease symptoms on the maize seedlings were evaluated at 6 dpi and 12 dpi, following the scoring system described by Kämper et al., 2006, as outlined in Table 4.13.

**Table 4.13. Categorization of *U. maydis* disease symptom scoring in maize seedlings**

Symptoms	Description
No symptoms	No disease symptoms or sign of infection in the plant
Chlorosis	Chlorotic areas around the infection site on the infected leaf and younger leaves
Small tumors	Tumors around the infection area are $\leq 1$ mm on the infected leaf and younger leaves
Normal tumors	Tumors around the infection area are $\geq 1$ mm on the infected leaf and younger leaves
Heavy tumors	Altered growth axes or formed large tumors at the base of the stem
Dead	Death of plant due to <i>U. maydis</i> infection.

The disease index was assigned using the following scales: 9 for dead plants, 7 for heavy tumors, 5 for normal tumors, 3 for small tumors, 1 for chlorosis, and 0 for plants without symptoms. The average disease index was calculated by multiplying the number of infected plants by the abovementioned disease index and dividing the sum of the total number of plants used in infection. The average disease index from three independent biological replicates was used for statistical significance testing via a Student's t-test.

#### **4.7.4 Cultivation of *N. benthamiana***

Six-week-old plants grown in a greenhouse with a 16-hour light and 8-hour dark cycle at 22°C were used for the infiltration with *Agrobacterium*.

#### **4.7.5 Split-luciferase complementation (split-LUC) assay**

The split-luciferase assay was performed as described in Zhou et al., 2018. The gene of interest was cloned into either the nLuc or cLuc vector, and subsequently transformed *Agrobacterium*. *Agrobacterium* carrying the gene of interest was mixed and infiltrated into *N. benthamiana* leaves (chapter 4.6.1). Two to three days after infiltration, the leaves were harvested to measure the bioluminescence of luciferin. The abaxial side of the leaves was sprayed with a solution of 1 mM D-luciferin, and the leaves were incubated in the dark for 10 minutes. The luminescence signals were detected using a ChemiDoc (Bio-RAD) from at least three independent plants.

### **4.8 Tissue fixation, staining, quantification, and microscopy**

#### **4.8.1 Soluble sugar enzymatic quantification**

Samples of *U. maydis* or mock infection were harvested at 4 and 9 dpi at different time points and immediately frozen in liquid nitrogen. Frozen samples were ground to a fine powder with mortar and pestle in liquid nitrogen. Samples of 100-600mg were incubated with 1mL of 80% (v/v) ethanol at 80°C, with frequent and vigorous vortexing. Subsequently, the samples were

centrifuged for 10 min at 13,000g, and the supernatant was recovered. This process was repeated three times. The concentration of soluble sugars was quantified with the Suc/D-Glc/D-Fru Assay Kit protocol, UV method (Megazyme). The measurements were adapted to 96-well microtiter plates. Therefore, volumes of samples and all reagents were scaled down by a factor of 10 (1/10<sup>th</sup>) and glucose and sucrose standard curves were prepared to ensure the linearity of the assay.

#### **4.8.2 Starch enzymatic quantification**

The soluble sugar extracted from the samples in chapter 4.8.1 was utilized to recover starch. To extract starch, a section from the basic protocol 2: starch extraction and enzymatic degradation to glucose from Leach & Braun, 2016 was followed. Subsequently, starch was quantified with the Total Starch HK Assay Kit (K-TSHK) from Megazyme. Measurements were adapted to 96-well microtiter plates. Consequently, the volumes of samples and all reagents were reduced by a factor of 10 (1/10<sup>th</sup>), and a glucose standard curve was prepared using pure maize starch in order to ensure the linearity of the assay.

#### **4.8.3 Paraplast embedding of maize leaf tissue**

The embedding of Paraplast was performed according to Jackson (1991). The infected maize tissues (chapter 4.7.3) were harvested at the designated time points and infiltrated with the fixing solution (50 % EtOH, 3.7 % formaldehyde, 5 % glacial acetic acid, 0.5 % Triton X-100, 1 % DMSO, 39.8 % H<sub>2</sub>O). Vacuum infiltration was conducted three times at 250 mbar for 5 minutes, followed by ATM for 5 minutes. Samples were incubated overnight at 4 °C with rotation. The following day, ½ volume of the fixing solution was removed and replaced with cold 95 % ethanol. The samples were incubated with rotation at 4 °C and repeated twice with a minimum of 2 hours between changes. All remaining solution was replaced with cold 95% ethanol and incubated with rotation for at least 2 hours. At the end of the day, all solution was replaced with 100% ethanol and incubated overnight at 4 °C with rotation. The following day, ethanol was replaced with fresh, cold 100% ethanol and placed on a shaker at room temperature. Once the samples had reached room temperature, a gradual infiltration process was performed using HistoClear (Roti-Histol, Roth, Karlsruhe, Germany). This involved a two-hour incubation period for each step, with the EtOH being removed and replaced with a 1:3 HistoClear:EtOH solution, followed by a 1:1 HistoClear:EtOH solution. ½ of the volume was subsequently replaced with 100% HistoClear twice. At the conclusion of the day, all liquid was replaced with 100% HistoClear and incubated on a shaker overnight at room temperature. The following day, paraffin infiltration was performed by the addition of ¼ volume of paraplast (Surgipath®Paraplast®, Leica Biosystems, Richmond, IL, US). Samples were incubated on a shaker for at least 2 hours until the paraplast chips had partially dissolved. At the end of the procedure, an additional ¼ volume of Paraplast was added and incubated on a shaker overnight at room temperature. The following morning, the samples were transferred to a temperature of 65 °C until all of the paraplast had melted. ½ the volume of the melted paraplast was added and incubated at 65 °C for three hours. At the end of the day, all of the liquid was replaced with 100% melted paraplast and twice every 12 hours. The embedded tissue was arranged in molds for embedding (Tissue-Tek®Cryomold Sakura Finetek, VWR, Darmstadt, Germany).

Thereafter, the tissue samples were transversely sectioned with a thickness of 12  $\mu\text{m}$  using a Leica RM2235 manual rotary microtome. The tissue sections were mounted on a droplet of water on microscopy slides that had been heated on a slide heater at 45 °C. The slides were maintained on the slide heater for a minimum of two hours until all the water had evaporated. Prior to microscopy, the tissue sections were dewaxed by incubation in fresh 100% HistoClear for 30 minutes at room temperature, followed by an ethanol hydration gradient. For this purpose, the slides were incubated in an ethanol gradient solution for a duration of two minutes in each solution (2x 100 % EtOH, 95 % EtOH, 90 % EtOH, 80 % EtOH, 70 % EtOH, 50 % EtOH, 30 % EtOH, 2x H<sub>2</sub>O).

#### **4.8.4 Starch Lugol staining**

De-waxed paraplast embedded sections from (chapter 4.8.3) were immersed in IKI Lugol (Roth, Karlsruhe, Germany) for 5mins and in ddH<sub>2</sub>O for 2-3mins to rinse off residual Lugol solution.

#### **4.8.5 Thunder microscopy**

Lugol-stained paraplast embedded sections were analyzed using a Leica Thunder microscope and processed with Leica imaging LAS X software.

#### **4.8.6 Confocal laser-scanning microscopy**

All live cell imaging was performed using a TCS SP8 confocal laser scanning microscope (Leica, Bensheim, Germany). eGFP was excited at 488 nm and detected at 490-540 nm. mCherry was excited at 561 nm and detected at 580-660 nm. Image analysis was performed using Leica LASX software (LAS, Leica, Bensheim, Germany).

### **4.9 Bioinformatics methods**

#### **4.9.1 RNA-Seq analysis**

Maize seedlings infected by mock, *U. maydis* (SG200,  $\Delta\text{Hap1}$ ,  $\Delta\text{Hap2}$ ,  $\Delta\text{Hap3}$ ) at 3 dpi were harvested for total RNA extraction. RNA was prepared as described in chapter 4.5.1.3 and chapter 4.5.1.4. Each sample was collected with three independent replicates and sent to Novogene (Cambridge, UK) for library construction using an Illumina NovaSeq 6000 (Illumina) with 150-bp paired-end reads. Paired-end RNAseq reads were quality trimmed using Trimmomatic, selecting for a per-base quality score at the start and end of the reads  $\geq 20$ . Subsequently, reads were mapped to the *Z. mays* genome (B73 reference genome version 5.0) with bowtie2 in very-sensitive end-to-end mode (Langmead & Salzberg, 2012). Successfully mapped reads were sorted with samtools and counted with HTseq-count (Anders et al., 2015) using intersection-nonempty mode for unstranded reads. Statistical analysis of differentially regulated genes between the treatments and the respective control samples was performed with edgeR (Robinson et al., 2010), using a quasi-likelihood negative binomial generalized log-linear model to fit the count data. Genes with  $\log_2\text{FC} > 1$  and  $\text{FDR} < 0.05$  were considered as significant differentially expressed genes.



### **4.9.2 GO enrichment analysis**

Maize gene ontology (GO) terms were annotated to the B73.v5 reference genome using Plaza v5 (Ge et al., 2020). The Go enrichment overrepresentation test was performed using PANTHER v18 Significant enrichment of GO terms (FDR<0.05) was calculated for all gene subsets.

### **4.9.3 KEGG enrichment analysis**

Identified DEGs and phosphorylated proteins from 4.6.4.2 and 4.9.1 were uploaded in KEGG BlastKOALA (<https://www.kegg.jp/blastkoala/>) to annotate KO (K number) assignment using SSEARCH computation. A Subset of KEGG genes containing KEGG reference genomes and individual sequences linked from pubmed records of KO entries were mapped to identify enriched KEGG pathway.

## 5. Bibliography

- Ahuja, I., Kissen, R., & Bones, A. M. (2012). Phytoalexins in defense against pathogens. *Trends in Plant Science*, *17*(2), 73–90. <https://doi.org/10.1016/J.TPLANTS.2011.11.002>
- Alcântara, A., Bosch, J., Nazari, F., Hoffmann, G., Gallei, M., Uhse, S., Darino, M. A., Olukayode, T., Reumann, D., Baggaley, L., & Djamei, A. (2019). Systematic Y2H Screening Reveals Extensive Effector-Complex Formation. *Frontiers in Plant Science*, *10*, 473594. <https://doi.org/10.3389/FPLS.2019.01437/BIBTEX>
- Amor, Y., Haigler, C. H., Johnson, S., Wainscott, M., & Delmer, D. P. (1995). A membrane-associated form of sucrose synthase and its potential role in synthesis of cellulose and callose in plants. *Proceedings of the National Academy of Sciences*, *92*(20), 9353–9357.
- Anderson, R. G., Deb, D., Fedkenheuer, K., & McDowell, J. M. (2015). Recent progress in RXLR effector research. *Molecular Plant-Microbe Interactions*, *28*(10), 1063–1072. [https://doi.org/10.1094/MPMI-01-15-0022-CR/ASSET/IMAGES/LARGE/MPMI-01-15-0022-CR\\_F2.JPEG](https://doi.org/10.1094/MPMI-01-15-0022-CR/ASSET/IMAGES/LARGE/MPMI-01-15-0022-CR_F2.JPEG)
- Ausubel, F. M., Brent, R., Kingston, R. E., Moore, D. D., Seidman, J. G., Smith, J. A., & Struhl, K. (1987). Current protocols in molecular biology John Wiley & Sons. *New York*, 877.
- Avila, J., Gregory, O. G., Su, D., Deeter, T. A., Chen, S., Silva-Sanchez, C., Xu, S., Martin, G. B., & Devarenne, T. P. (2012). The  $\beta$ -Subunit of the SnRK1 Complex is phosphorylated by the plant cell death suppressor Adi3. *Plant Physiology*, *159*(3), 1277–1290. <https://doi.org/10.1104/pp.112.198432>
- Ávila-Castañeda, A., Gutiérrez-Granados, N., Ruiz-Gayosso, A., Sosa-Peinado, A., Martínez-Barajas, E., & Coello, P. (2014). Structural and functional basis for starch binding in the SnRK1 subunits AKIN $\beta$ 2 and AKIN $\beta$ 3. *Frontiers in Plant Science*, *5*, 82257.
- Azad, T., Tashakor, A., & Hosseinkhani, S. (2014). Split-luciferase complementary assay: applications, recent developments, and future perspectives. *Analytical and Bioanalytical Chemistry*, *406*(23), 5541–5560. <https://doi.org/10.1007/s00216-014-7980-8>
- Bachmann, M., Shiraishi, N., Campbell, W. H., Yoo, B.-C., Harmon, A. C., & Huber, S. C. (1996). Identification of Ser-543 as the major regulatory phosphorylation site in spinach leaf nitrate reductase. *The Plant Cell*, *8*(3), 505–517.
- Baena-González, E., & Hanson, J. (2017). Shaping plant development through the SnRK1–TOR metabolic regulators. *Current Opinion in Plant Biology*, *35*, 152–157. <https://doi.org/https://doi.org/10.1016/j.pbi.2016.12.004>
- Baena-González, E., Rolland, F., Thevelein, J. M., & Sheen, J. (2007). A central integrator of transcription networks in plant stress and energy signalling. *Nature* *2007* *448*:7156, *448*(7156), 938–942. <https://doi.org/10.1038/nature06069>
- Banuett, F., & Herskowitz, I. (1994). Morphological transitions in the life cycle of *Ustilago maydis* and their genetic control by the a and b loci. *Experimental Mycology*, *18*(3), 247–266. <https://doi.org/10.1006/EMYC.1994.1024>
- Basse, C. W. (2005). Dissecting defense-related and developmental transcriptional responses of maize during *Ustilago maydis* infection and subsequent tumor formation. *Plant Physiology*, *138*(3), 1774–1784. <https://doi.org/10.1104/PP.105.061200>

- Bauer, R., Oberwinkler, F., & Kalman, K. (2011). Ultrastructural markers and systematics in smut fungi and allied taxa. *Https://Doi.Org/10.1139/B97-842*, 75(8), 1273–1314. <https://doi.org/10.1139/B97-842>
- Bebber, D. P., Ramotowski, M. A. T., & Gurr, S. J. (2013). Crop pests and pathogens move polewards in a warming world. *Nature Climate Change* 2013 3:11, 3(11), 985–988. <https://doi.org/10.1038/nclimate1990>
- Berens, M. L., Berry, H. M., Mine, A., Argueso, C. T., & Tsuda, K. (2017). Evolution of Hormone Signaling Networks in Plant Defense. *Annurev-Phyto-080516-035544*, 55, 401–425. <https://doi.org/10.1146/ANNUREV-PHYTO-080516-035544>
- Bigeard, J., Colcombet, J., & Hirt, H. (2015). Signaling Mechanisms in Pattern-Triggered Immunity (PTI). *Molecular Plant*, 8(4), 521–539. <https://doi.org/10.1016/J.MOLP.2014.12.022>
- Bindics, J., Khan, M., Uhse, S., Kogelmann, B., Baggely, L., Reumann, D., Ingole, K. D., Stirnberg, A., Rybecky, A., Darino, M., Navarrete, F., Doehlemann, G., & Djamei, A. (2022). Many ways to TOPLESS – manipulation of plant auxin signalling by a cluster of fungal effectors. *New Phytologist*, 236(4), 1455–1470. <https://doi.org/10.1111/NPH.18315>
- Blum, M., Chang, H.-Y., Chuguransky, S., Grego, T., Kandasamy, S., Mitchell, A., Nuka, G., Paysan-Lafosse, T., Qureshi, M., & Raj, S. (2021). The InterPro protein families and domains database: 20 years on. *Nucleic Acids Research*, 49(D1), D344–D354.
- Boch, J., Bonas, U., & Lahaye, T. (2014). TAL effectors – pathogen strategies and plant resistance engineering. *New Phytologist*, 204(4), 823–832. <https://doi.org/https://doi.org/10.1111/nph.13015>
- Bölker, M., Urban, M., & Kahmann, R. (1992). The a mating type locus of *U. maydis* specifies cell signaling components. *Cell*, 68, 441–450.
- Boller, T., & Felix, G. (2009). A renaissance of elicitors: perception of microbe-associated molecular patterns and danger signals by pattern-recognition receptors. *Annual Review of Plant Biology*, 60(1), 379–406. <https://doi.org/10.1146/annurev.arplant.57.032905.105346>
- Boudsocq, M., & Sheen, J. (2013). CDPKs in immune and stress signaling. *Trends in Plant Science*, 18(1), 30–40. <https://doi.org/10.1016/J.TPLANTS.2012.08.008>
- Bouly, J., Gissot, L., Lessard, P., Kreis, M., & Thomas, M. (1999). *Arabidopsis thaliana* proteins related to the yeast SIP and SNF4 interact with AKINα1, an SNF1-like protein kinase. *The Plant Journal*, 18(5), 541–550.
- Boutrot, F., & Zipfel, C. (2017). Function, discovery, and exploitation of plant pattern recognition receptors for broad-spectrum disease resistance. *Annurev-Phyto-080614-120106*, 55, 257–286. <https://doi.org/10.1146/ANNUREV-PHYTO-080614-120106>
- Brachmann, A., Weinzierl, G., Kämper, J., & Kahmann, R. (2001). Identification of genes in the bW/bE regulatory cascade in *Ustilago maydis*. *Molecular Microbiology*, 42(4), 1047–1063. <https://doi.org/10.1046/J.1365-2958.2001.02699.X>
- Brefort, T., Doehlemann, G., Mendoza-Mendoza, A., Reissmann, S., Djamei, A., & Kallmann, R. (2009). *Ustilago maydis* as a Pathogen. *Annurev-Phyto-080508-081923*, 47, 423–445. <https://doi.org/10.1146/ANNUREV-PHYTO-080508-081923>

- Brefort, T., Tanaka, S., Neidig, N., Doehlemann, G., Vincon, V., & Kahmann, R. (2014). Characterization of the largest effector gene cluster of *Ustilago maydis*. *PLOS Pathogens*, *10*(7), e1003866. <https://doi.org/10.1371/JOURNAL.PPAT.1003866>
- Broeckx, T., Hulsmans, S., & Rolland, F. (2016). The plant energy sensor: evolutionary conservation and divergence of SnRK1 structure, regulation, and function. *Journal of Experimental Botany*, *67*(22), 6215–6252. <https://doi.org/10.1093/jxb/erw416>
- Brutus, A., Sicilia, F., Macone, A., Cervone, F., & De Lorenzo, G. (2010). A domain swap approach reveals a role of the plant wall-associated kinase 1 (WAK1) as a receptor of oligogalacturonides. *Proceedings of the National Academy of Sciences of the United States of America*, *107*(20), 9452–9457. <https://doi.org/10.1073/PNAS.1000675107/-/DCSUPPLEMENTAL/PNAS.201000675SI.PDF>
- Callow, J. A. (1975). Endopolyploidy in maize smut neoplasms induced by the maize smut fungus, *Ustilago maydis*. *New Phytologist*, *75*(2), 253–257. <https://doi.org/10.1111/J.1469-8137.1975.TB01394.X>
- Cao, Y., Liang, Y., Tanaka, K., Nguyen, C. T., Jedrzejczak, R. P., Joachimiak, A., & Stacey, G. (2014). The kinase LYK5 is a major chitin receptor in Arabidopsis and forms a chitin-induced complex with related kinase CERK1. *ELife*, *3*. <https://doi.org/10.7554/ELIFE.03766>
- Castanheira, S., Mielnichuk, N., & Pérez-Martín, J. (2014). Programmed cell cycle arrest is required for infection of corn plants by the fungus *Ustilago maydis*. *Development*, *141*(24), 4817–4826. <https://doi.org/10.1242/DEV.113415>
- Cesari, S. (2018). Multiple strategies for pathogen perception by plant immune receptors. *New Phytologist*, *219*(1), 17–24. <https://doi.org/10.1111/NPH.14877>
- Chaloner, T. M., Gurr, S. J., & Bebbler, D. P. (2021). Plant pathogen infection risk tracks global crop yields under climate change. *Nature Climate Change* *2021 11:8*, *11*(8), 710–715. <https://doi.org/10.1038/s41558-021-01104-8>
- Chen, L. H., Kračun, S. K., Nissen, K. S., Mravec, J., Jørgensen, B., Labavitch, J., & Stergiopoulos, I. (2021). A diverse member of the fungal Avr4 effector family interacts with de-esterified pectin in plant cell walls to disrupt their integrity. *Science Advances*, *7*(19). <https://doi.org/10.1126/SCIADV.ABE0809>
- Chen, W., Li, Y., Yan, R., Ren, L., Liu, F., Zeng, L., Sun, S., Yang, H., Chen, K., & Xu, L. (2021). SnRK1.1-mediated resistance of *Arabidopsis thaliana* to clubroot disease is inhibited by the novel *Plasmodiophora brassicae* effector PBZF1. *Molecular Plant Pathology*, *22*(9), 1057–1069.
- Cheng, S.-H., Willmann, M. R., Chen, H.-C., & Sheen, J. (2002). Calcium signaling through protein kinases. The Arabidopsis calcium-dependent protein kinase gene family. *Plant Physiology*, *129*(2), 469–485.
- Chevalier, C., Nafati, M., Mathieu-Rivet, E., Bourdon, M., Frangne, N., Cheniclet, C., Renaudin, J.-P., Gévaudant, F., & Hernould, M. (2011). Elucidating the functional role of endoreduplication in tomato fruit development. *Annals of Botany*, *107*(7), 1159–1169. <https://doi.org/10.1093/aob/mcq257>

- Chinchilla, D., Zipfel, C., Robatzek, S., Kemmerling, B., Nürnberger, T., Jones, J. D. G., Felix, G., & Boller, T. (2007). A flagellin-induced complex of the receptor FLS2 and BAK1 initiates plant defence. *Nature*, *448*(7152), 497–500. <https://doi.org/10.1038/nature05999>
- Christensen, J. J. (1963). Corn smut caused by *Ustilago maydis*. *Monograph, American Phytopathological Society*, *2*.
- Coello, P., Hirano, E., Hey, S. J., Muttucumaru, N., Martinez-Barajas, E., Parry, M. A. J., & Halford, N. G. (2012). Evidence that abscisic acid promotes degradation of SNF1-related protein kinase (SnRK) 1 in wheat and activation of a putative calcium-dependent SnRK2. *Journal of Experimental Botany*, *63*(2), 913–924.
- Collemare, J., O'Connell, R., & Lebrun, M. H. (2019). Nonproteinaceous effectors: the terra incognita of plant–fungal interactions. *New Phytologist*, *223*(2), 590–596. <https://doi.org/10.1111/NPH.15785>
- Couto, D., & Zipfel, C. (2016). Regulation of pattern recognition receptor signalling in plants. *Nature Reviews Immunology* *2016* *16:9*, *16*(9), 537–552. <https://doi.org/10.1038/nri.2016.77>
- Crepin, N., & Rolland, F. (2019). SnRK1 activation, signaling, and networking for energy homeostasis. *Current Opinion in Plant Biology*, *51*, 29–36. <https://doi.org/https://doi.org/10.1016/j.pbi.2019.03.006>
- Crozet, P., Jammes, F., Valot, B., Ambard-Bretteville, F., Nessler, S., Hodges, M., Vidal, J., & Thomas, M. (2010). Cross-phosphorylation between *Arabidopsis thaliana* sucrose nonfermenting 1-related protein kinase 1 (AtSnRK1) and its activating kinase (AtSnAK) determines their catalytic activities. *Journal of Biological Chemistry*, *285*(16), 12071–12077.
- Dangl, J. L., & Jones, J. D. G. (2001). Plant pathogens and integrated defence responses to infection. *Nature* *2001* *411:6839*, *411*(6839), 826–833. <https://doi.org/10.1038/35081161>
- Davidson, R. M., Hansey, C. N., Gowda, M., Childs, K. L., Lin, H., Vaillancourt, B., Sekhon, R. S., de Leon, N., Kaeppler, S. M., & Jiang, N. (2011). Utility of RNA sequencing for analysis of maize reproductive transcriptomes. *The Plant Genome*, *4*(3).
- de Jonge, R., Peter van Esse, H., Kombrink, A., Shinya, T., Desaki, Y., Bours, R., van der Krol, S., Shibuya, N., Joosten, M. H. A. J., & Thomma, B. P. H. J. (2010). Conserved Fungal LysM Effector Ecp6 Prevents Chitin-Triggered Immunity in Plants. *Science*, *329*(5994), 953–955. <https://doi.org/10.1126/science.1190859>
- de la Torre, A., Castanheira, S., & Pérez-Martín, J. (2020). Incompatibility between proliferation and plant invasion is mediated by a regulator of appressorium formation in the corn smut fungus *Ustilago maydis*. *Proceedings of the National Academy of Sciences*, *117*(48), 30599–30609. <https://doi.org/10.1073/pnas.2006909117>
- de Lange, O., Schreiber, T., Schandry, N., Radeck, J., Braun, K. H., Koszinowski, J., Heuer, H., Strauß, A., & Lahaye, T. (2013). Breaking the DNA-binding code of *Ralstonia solanacearum* TAL effectors provides new possibilities to generate plant resistance genes against bacterial wilt disease. *New Phytologist*, *199*(3), 773–786. <https://doi.org/https://doi.org/10.1111/nph.12324>
- Dean, R., Van Kan, J. A. L., Pretorius, Z. A., Hammond-Kosack, K. E., Di Pietro, A., Spanu, P. D., Rudd, J. J., Dickman, M., Kahmann, R., Ellis, J., & Foster, G. D. (2012). The Top

- 10 fungal pathogens in molecular plant pathology. *Molecular Plant Pathology*, 13(4), 414–430. <https://doi.org/10.1111/J.1364-3703.2011.00783.X>
- Delatte, T. L., Sedijani, P., Kondou, Y., Matsui, M., de Jong, G. J., Somsen, G. W., Wiese-Klinkenberg, A., Primavesi, L. F., Paul, M. J., & Schluepmann, H. (2011). Growth arrest by trehalose-6-phosphate: an astonishing case of primary metabolite control over growth by way of the SnRK1 signaling pathway. *Plant Physiology*, 157(1), 160–174.
- Depotter, J. R. L., & Doehlemann, G. (2020). Target the core: durable plant resistance against filamentous plant pathogens through effector recognition. *Pest Management Science*, 76(2), 426–431. <https://doi.org/10.1002/PS.5677>
- Derbyshire, M. C. (2020). Bioinformatic Detection of Positive Selection Pressure in Plant Pathogens: The Neutral Theory of Molecular Sequence Evolution in Action. *Frontiers in Microbiology*, 11, 503385. <https://doi.org/10.3389/FMICB.2020.00644/BIBTEX>
- Djamei, A., Depotter, J., Saridis, G., Prokchorchik, M., Barghahn, S., De Sousa, N., Silva, T. E., Zuo, W., Villamil, J. M., Doehlemann, G., Djamei, A., Prokchorchik, · M, Silva, · N D S T E, Depotter, J., Saridis, · G, Barghahn, · S, Zuo, · W, Villamil, · J M, & Doehlemann, · G. (2023). *Modulation of Host Immunity and Development by Ustilago maydis*. 3–30. [https://doi.org/10.1007/978-3-031-16503-0\\_1](https://doi.org/10.1007/978-3-031-16503-0_1)
- Djamei, A., & Kahmann, R. (2012). Ustilago maydis: Dissecting the Molecular Interface between Pathogen and Plant. *PLOS Pathogens*, 8(11), e1002955. <https://doi.org/10.1371/JOURNAL.PPAT.1002955>
- Djamei, A., Schipper, K., Rabe, F., Ghosh, A., Vincon, V., Kahnt, J., Osorio, S., Tohge, T., Fernie, A. R., Feussner, I., Feussner, K., Meinicke, P., Stierhof, Y. D., Schwarz, H., MacEk, B., Mann, M., & Kahmann, R. (2011). Metabolic priming by a secreted fungal effector. *Nature* 2011 478:7369, 478(7369), 395–398. <https://doi.org/10.1038/nature10454>
- Dodds, P. N., Chen, J., & Outram, M. A. (2024). Pathogen perception and signalling in plant immunity. *The Plant Cell*, koae020.
- Dodds, P. N., & Rathjen, J. P. (2010). Plant immunity: towards an integrated view of plant–pathogen interactions. *Nature Reviews Genetics*, 11(8), 539–548. <https://doi.org/10.1038/nrg2812>
- Doebley. (1992). Mapping the genes that made maize. *Trends in Genetics*, 8(9), 302–307.
- Doehlemann, G., & Hemetsberger, C. (2013). Apoplastic immunity and its suppression by filamentous plant pathogens. *New Phytologist*, 198(4), 1001–1016. <https://doi.org/10.1111/NPH.12277>
- Doehlemann, G., Reissmann, S., Aßmann, D., Fleckenstein, M., & Kahmann, R. (2011). Two linked genes encoding a secreted effector and a membrane protein are essential for Ustilago maydis-induced tumour formation. *Molecular Microbiology*, 81(3), 751–766. <https://doi.org/10.1111/J.1365-2958.2011.07728.X>
- Doehlemann, G., Van Der Linde, K., Aßmann, D., Schwammbach, D., Hof, A., Mohanty, A., Jackson, D., & Kahmann, R. (2009). Pep1, a Secreted Effector Protein of Ustilago maydis, Is Required for Successful Invasion of Plant Cells. *PLOS Pathogens*, 5(2), e1000290. <https://doi.org/10.1371/JOURNAL.PPAT.1000290>

- Doehlemann, G., Wahl, R., Horst, R. J., Voll, L. M., Usadel, B., Poree, F., Stitt, M., Pons-Kühnemann, J., Sonnewald, U., Kahmann, R., & Kämper, J. (2008a). Reprogramming a maize plant: transcriptional and metabolic changes induced by the fungal biotroph *Ustilago maydis*. *The Plant Journal*, *56*(2), 181–195. <https://doi.org/10.1111/J.1365-313X.2008.03590.X>
- Doehlemann, G., Wahl, R., Vranes, M., de Vries, R. P., Kämper, J., & Kahmann, R. (2008b). Establishment of compatibility in the *Ustilago maydis*/maize pathosystem. *Journal of Plant Physiology*, *165*(1), 29–40. <https://doi.org/10.1016/J.JPLPH.2007.05.016>
- Dutheil, J. Y., Mannhaupt, G., Schweizer, G., Sieber, C. M. K., Münsterkötter, M., Güdener, U., Schirawski, J., & Kahmann, R. (2016). A Tale of Genome Compartmentalization: The Evolution of Virulence Clusters in Smut Fungi. *Genome Biology and Evolution*, *8*(3), 681–704. <https://doi.org/10.1093/GBE/EVW026>
- Duxbury, Z., Wu, C. H., & Ding, P. (2021). A Comparative Overview of the Intracellular Guardians of Plants and Animals: NLRs in Innate Immunity and beyond. *Annual Review of Plant Biology*, *72*(Volume 72, 2021), 155–184. <https://doi.org/10.1146/ANNUREV-ARPLANT-080620-104948/CITE/REFWORKS>
- Edwards, G. E., & Walker, D. A. (1983). *C3, C4: Mechanism, and Cellular and Environmental Regulation, of Photosynthesis*. Blackwell Scientific Publications.
- Emanuelle, S., Doblin, M. S., Stapleton, D. I., Bacic, A., & Gooley, P. R. (2016). Molecular Insights into the Enigmatic Metabolic Regulator, SnRK1. *Trends in Plant Science*, *21*(4), 341–353. <https://doi.org/https://doi.org/10.1016/j.tplants.2015.11.001>
- Emanuelle, S., Hossain, M. I., Moller, I. E., Pedersen, H. L., Van De Meene, A. M. L., Doblin, M. S., Koay, A., Oakhill, J. S., Scott, J. W., & Willats, W. G. T. (2015). SnRK1 from *Arabidopsis thaliana* is an atypical AMPK. *The Plant Journal*, *82*(2), 183–192.
- Fabro, G. (2022). Oomycete intracellular effectors: specialised weapons targeting strategic plant processes. *New Phytologist*, *233*(3), 1074–1082. <https://doi.org/10.1111/NPH.17828>
- Fedler, M., Luh, K. S., Stelter, K., Nieto-Jacobo, F., & Basse, C. W. (2009). The a2 Mating-Type Locus Genes *lga2* and *rga2* Direct Uniparental Mitochondrial DNA (mtDNA) Inheritance and Constrain mtDNA Recombination During Sexual Development of *Ustilago maydis*. *Genetics*, *181*(3), 847–860. <https://doi.org/10.1534/GENETICS.108.096859>
- Fei, W., & Liu, Y. (2023). Biotrophic Fungal Pathogens: a Critical Overview. *Applied Biochemistry and Biotechnology*, *195*(1), 1–16. <https://doi.org/10.1007/S12010-022-04087-0/TABLES/4>
- Fellner, T., Lackner, D. H., Hombauer, H., Piribauer, P., Mudrak, I., Zaragoza, K., Juno, C., & Ogris, E. (2003). A novel and essential mechanism determining specificity and activity of protein phosphatase 2A (PP2A) in vivo. *Genes & Development*, *17*(17), 2138–2150. <https://doi.org/10.1101/GAD.259903>
- Fichtner, F., & Lunn, J. E. (2021). The role of trehalose 6-phosphate (Tre6P) in plant metabolism and development. *Annual Review of Plant Biology*, *72*, 737–760.

- Filipe, O., De Vleeschauwer, D., Haeck, A., Demeestere, K., & Höfte, M. (2018). The energy sensor OsSnRK1a confers broad-spectrum disease resistance in rice. *Scientific Reports*, 8(1), 3864.
- Flor-Parra, I., Vranes, M., Kämper, J., & Pérez-Martín, J. (2006). Biz1, a zinc finger protein required for plant invasion by *Ustilago maydis*, regulates the levels of a mitotic cyclin. *Plant Cell*, 18(9), 2369–2387. <https://doi.org/10.1105/TPC.106.042754>
- Fragoso, S., Espíndola, L., Páez-Valencia, J., Gamboa, A., Camacho, Y., Martínez-Barajas, E., & Coello, P. (2009). SnRK1 isoforms AKIN10 and AKIN11 are differentially regulated in Arabidopsis plants under phosphate starvation. *Plant Physiology*, 149(4), 1906–1916.
- Freitag, J., Lanver, D., Böhmer, C., Schink, K. O., Bölker, M., & Sandrock, B. (2011). Septation of Infectious Hyphae Is Critical for Appressoria Formation and Virulence in the Smut Fungus *Ustilago Maydis*. *PLoS Pathogens*, 7(5). <https://doi.org/10.1371/JOURNAL.PPAT.1002044>
- Frerigmann, H., Berger, B., & Gigolashvili, T. (2014). bHLH05 Is an Interaction Partner of MYB51 and a Novel Regulator of Glucosinolate Biosynthesis in Arabidopsis. *Plant Physiology*, 166(1), 349. <https://doi.org/10.1104/PP.114.240887>
- Garcia, D., & Shaw, R. J. (2017). AMPK: mechanisms of cellular energy sensing and restoration of metabolic balance. *Molecular Cell*, 66(6), 789–800.
- García-Muse, T., Steinberg, G., & Pérez-Martín, J. (2003). Pheromone-induced G2 arrest in the phytopathogenic fungus *Ustilago maydis*. *Eukaryotic Cell*, 2(3), 494–500. <https://doi.org/10.1128/EC.2.3.494-500.2003/ASSET/C609FC1D-CA9D-486F-84F1-D0003A5B93FC/ASSETS/GRAPHIC/EK0330212004.JPEG>
- Gazzarrini, S., & Tsai, A. Y.-L. (2014). Trehalose-6-phosphate and SnRK1 kinases in plant development and signaling: the emerging picture. *Frontiers in Plant Science*, 5. <https://www.frontiersin.org/journals/plant-science/articles/10.3389/fpls.2014.00119>
- Gibon, Y., Bläsing, O. E., Palacios-Rojas, N., Pankovic, D., Hendriks, J. H. M., Fisahn, J., Höhne, M., Günther, M., & Stitt, M. (2004). Adjustment of diurnal starch turnover to short days: depletion of sugar during the night leads to a temporary inhibition of carbohydrate utilization, accumulation of sugars and post-translational activation of ADP-glucose pyrophosphorylase in the following light period. *The Plant Journal*, 39(6), 847–862.
- Gibson, D. G., Young, L., Chuang, R.-Y., Venter, J. C., Hutchison, C. A., & Smith, H. O. (2009). Enzymatic assembly of DNA molecules up to several hundred kilobases. *Nature Methods*, 6(5), 343–345.
- Gillissen, B., Bergemann, J., Sandmann, C., Schroeer, B., Bölker, M., & Kahmann, R. (1992). A two-component regulatory system for self/non-self recognition in *Ustilago maydis*. *Cell*, 68(4), 647–657. [https://doi.org/10.1016/0092-8674\(92\)90141-X](https://doi.org/10.1016/0092-8674(92)90141-X)
- Glab, N., Oury, C., Guérinier, T., Domenichini, S., Crozet, P., Thomas, M., Vidal, J., & Hodges, M. (2017). The impact of *Arabidopsis thaliana* SNF 1-related-kinase 1 (Sn RK 1)-activating kinase 1 (SnAK 1) and SnAK 2 on Sn RK 1 phosphorylation status: characterization of a Sn AK double mutant. *The Plant Journal*, 89(5), 1031–1041.
- Gómez-Gómez, L., & Boller, T. (2000). FLS2: An LRR Receptor-like Kinase Involved in the Perception of the Bacterial Elicitor Flagellin in Arabidopsis. *Molecular Cell*, 5(6), 1003–1011. [https://doi.org/10.1016/S1097-2765\(00\)80265-8](https://doi.org/10.1016/S1097-2765(00)80265-8)



- Gonzalez, N., Vanhaeren, H., & Inzé, D. (2012). Leaf size control: complex coordination of cell division and expansion. *Trends in Plant Science*, 17(6), 332–340. <https://doi.org/10.1016/J.TPLANTS.2012.02.003>
- Haberlandt, G. (1904). *Physiologische Pflanzenanatomie* (3rd ed.). Wilhelm Engelmann.
- Han, X., Altegoer, F., Steinchen, W., Binnebesel, L., Schuhmacher, J., Glatter, T., Giammarinaro, P. I., Djamei, A., Rensing, S. A., Reissmann, S., Kahmann, R., & Bange, G. (2019). A kiwellin disarms the metabolic activity of a secreted fungal virulence factor. *Nature* 2019 565:7741, 565(7741), 650–653. <https://doi.org/10.1038/s41586-018-0857-9>
- Hardin, S. C., Winter, H., & Huber, S. C. (2004). Phosphorylation of the amino terminus of maize sucrose synthase in relation to membrane association and enzyme activity. *Plant Physiology*, 134(4), 1427–1438.
- Heese, A., Hann, D. R., Gimenez-Ibanez, S., Jones, A. M. E., He, K., Li, J., Schroeder, J. I., Peck, S. C., & Rathjen, J. P. (2007). The receptor-like kinase SERK3/BAK1 is a central regulator of innate immunity in plants. *Proceedings of the National Academy of Sciences of the United States of America*, 104(29), 12217–12222. [https://doi.org/10.1073/PNAS.0705306104/SUPPL\\_FILE/05306FIG6.JPG](https://doi.org/10.1073/PNAS.0705306104/SUPPL_FILE/05306FIG6.JPG)
- Heimel, K., Freitag, J., Hampel, M., Ast, J., Bölker, M., & Kämper, J. (2013). Crosstalk between the Unfolded Protein Response and Pathways That Regulate Pathogenic Development in *Ustilago maydis*. *The Plant Cell*, 25(10), 4262–4277. <https://doi.org/10.1105/TPC.113.115899>
- Heimel, K., Scherer, M., Vranes, M., Wahl, R., Pothiratana, C., Schuler, D., Vincon, V., Finkernagel, F., Flor-Parra, I., & Kämper, J. (2010). The Transcription Factor Rbf1 Is the Master Regulator for b-Mating Type Controlled Pathogenic Development in *Ustilago maydis*. *PLOS Pathogens*, 6(8), e1001035. <https://doi.org/10.1371/JOURNAL.PPAT.1001035>
- Hemetsberger, C., Herrberger, C., Zechmann, B., Hillmer, M., & Doehlemann, G. (2012). The *Ustilago maydis* Effector Pep1 Suppresses Plant Immunity by Inhibition of Host Peroxidase Activity. *PLOS Pathogens*, 8(5), e1002684. <https://doi.org/10.1371/JOURNAL.PPAT.1002684>
- Hemetsberger, C., Mueller, A. N., Matei, A., Herrberger, C., Hensel, G., Kumlehn, J., Mishra, B., Sharma, R., Thines, M., Hüchelhoven, R., & Doehlemann, G. (2015). The fungal core effector Pep1 is conserved across smuts of dicots and monocots. *New Phytologist*, 206(3), 1116–1126. <https://doi.org/10.1111/NPH.13304>
- Henry, C., Bledsoe, S. W., Siekman, A., Kollman, A., Waters, B. M., Feil, R., Stitt, M., & Lagrimini, L. M. (2014). The trehalose pathway in maize: conservation and gene regulation in response to the diurnal cycle and extended darkness. *Journal of Experimental Botany*, 65(20), 5959–5973. <https://doi.org/10.1093/jxb/eru335>
- Hey, S., Mayerhofer, H., Halford, N. G., & Dickinson, J. R. (2007). DNA sequences from *Arabidopsis*, which encode protein kinases and function as upstream regulators of Snf1 in yeast. *Journal of Biological Chemistry*, 282(14), 10472–10479.
- Ho, L. C. (1992). The possible effects of sink demand for assimilate on photosynthesis. In N. Murata (Ed.), *Proceedings of the IXth International Congress on Photosynthesis*, (pp. 729–736).

- Höfgen, R., & Willmitzer, L. (1988). Storage of competent cells for *Agrobacterium* transformation. *Nucleic Acids Research*, *16*(20), 9877.
- Horbach, R., Navarro-Quesada, A. R., Knogge, W., & Deising, H. B. (2011). When and how to kill a plant cell: Infection strategies of plant pathogenic fungi. *Journal of Plant Physiology*, *168*(1), 51–62. <https://doi.org/10.1016/J.JPLPH.2010.06.014>
- Horst, R. J., Doehlemann, G., Wahl, R., Hofmann, J., Schmiedl, A., Kahmann, R., Kamper, J., Sonnewald, U., & Voll, L. M. (2009). *Ustilago maydis* Infection Strongly Alters Organic Nitrogen Allocation in Maize and Stimulates Productivity of Systemic Source Leaves. *Plant Physiology*, *152*(1), 293–308. <https://doi.org/10.1104/PP.109.147702>
- Horst, R. J., Doehlemann, G., Wahl, R., Hofmann, J., Schmiedl, A., Kahmann, R., Kamper, J., Sonnewald, U., & Voll, L. M. (2010). *Ustilago maydis* Infection Strongly Alters Organic Nitrogen Allocation in Maize and Stimulates Productivity of Systemic Source Leaves. *Plant Physiology*, *152*(1), 293–308. <https://doi.org/10.1104/pp.109.147702>
- Horst, R. J., Engelsdorf, T., Sonnewald, U., & Voll, L. M. (2008). Infection of maize leaves with *Ustilago maydis* prevents establishment of C4 photosynthesis. *Journal of Plant Physiology*, *165*(1), 19–28. <https://doi.org/https://doi.org/10.1016/j.jplph.2007.05.008>
- Hou, S., Liu, Z., Shen, H., & Wu, D. (2019). Damage-associated molecular pattern-triggered immunity in plants. *Frontiers in Plant Science*, *10*, 453679. <https://doi.org/10.3389/FPLS.2019.00646/BIBTEX>
- Huang, J.-Z., Hardin, S. C., & Huber, S. C. (2001). Identification of a novel phosphorylation motif for CDPKs: phosphorylation of synthetic peptides lacking basic residues at P-3/P-4. *Archives of Biochemistry and Biophysics*, *393*(1), 61–66.
- Huang, J.-Z., & Huber, S. C. (2001). Phosphorylation of synthetic peptides by a CDPK and plant SNF1-related protein kinase. Influence of proline and basic amino acid residues at selected positions. *Plant and Cell Physiology*, *42*(10), 1079–1087.
- Huber, S. C., & Huber, J. L. (1996). Role and regulation of sucrose-phosphate synthase in higher plants. *Annual Review of Plant Biology*, *47*(1), 431–444.
- Hulsmans, S., Rodriguez, M., De Coninck, B., & Rolland, F. (2016). The SnRK1 energy sensor in plant biotic interactions. *Trends in Plant Science*, *21*(8), 648–661.
- Iizasa, E., Mitsutomi, M., & Nagano, Y. (2010). Direct binding of a plant LysM receptor-like kinase, LysM RLK1/CERK1, to chitin in vitro. *Journal of Biological Chemistry*, *285*(5), 2996–3004. <https://doi.org/10.1074/jbc.M109.027540>
- Irieda, H., Inoue, Y., Mori, M., Yamada, K., Oshikawa, Y., Saitoh, H., Uemura, A., Terauchi, R., Kitakura, S., Kosaka, A., Singkaravanit-Ogawa, S., & Takano, Y. (2019). Conserved fungal effector suppresses PAMP-triggered immunity by targeting plant immune kinases. *Proceedings of the National Academy of Sciences of the United States of America*, *116*(2), 496–505. [https://doi.org/10.1073/PNAS.1807297116/SUPPL\\_FILE/PNAS.1807297116.SAPP.PDF](https://doi.org/10.1073/PNAS.1807297116/SUPPL_FILE/PNAS.1807297116.SAPP.PDF)
- Jankovsky, J. P., Smith, L. G., & Nelson, T. (2001). Specification of bundle sheath cell fates during maize leaf development: roles of lineage and positional information evaluated through analysis of the tangled1 mutant. *Development*, *128*(14), 2747–2753. <https://doi.org/10.1242/DEV.128.14.2747>

- Jiang, C., Hei, R., Yang, Y., Zhang, S., Wang, Q., Wang, W., Zhang, Q., Yan, M., Zhu, G., Huang, P., Liu, H., & Xu, J.-R. (2020). An orphan protein of *Fusarium graminearum* modulates host immunity by mediating proteasomal degradation of TaSnRK1 $\alpha$ . *Nature Communications*, *11*(1), 4382. <https://doi.org/10.1038/s41467-020-18240-y>
- Johnson, K., & Lenhard, M. (2011). Genetic control of plant organ growth. *New Phytologist*, *191*(2), 319–333. <https://doi.org/10.1111/J.1469-8137.2011.03737.X>
- Jones, J. D. G., & Dangl, J. L. (2006). The plant immune system. *Nature*, *444*(7117), 323–329. <https://doi.org/10.1038/nature05286>
- Jossier, M., Bouly, J., Meimoun, P., Arjmand, A., Lessard, P., Hawley, S., Grahame Hardie, D., & Thomas, M. (2009). SnRK1 (SNF1-related kinase 1) has a central role in sugar and ABA signalling in *Arabidopsis thaliana*. *The Plant Journal*, *59*(2), 316–328.
- Jung, J. K., Kebrom, T. H., Turgeon, R., & Brutnell, T. (2008). *Anatomical differences in the bundle sheath and mesophyll cells of maize seedlings across a leaf developmental gradient*. [https://www.maizegdb.org/maize\\_meeting/abstracts/2008Program.pdf](https://www.maizegdb.org/maize_meeting/abstracts/2008Program.pdf)
- Kahmann, R., Romeis, T., Bölker, M., & Kämper, J. (1995). Control of mating and development in *Ustilago maydis*. *Current Opinion in Genetics & Development*, *5*(5), 559–564. [https://doi.org/10.1016/0959-437X\(95\)80023-9](https://doi.org/10.1016/0959-437X(95)80023-9)
- Kahmann, R., & Schirawski, J. (2007). Mating in the Smut Fungi: From a to b to the Downstream Cascades. *Sex in Fungi*, 377–387. <https://doi.org/10.1128/9781555815837.CH22>
- Kahmann, R., Steinberg, G., Basse, C., Feldbrügge, M., & Kämper, J. (2000). *Ustilago maydis*, the Causative Agent of Corn Smut Disease. *Fungal Pathology*, 347–371. [https://doi.org/10.1007/978-94-015-9546-9\\_12](https://doi.org/10.1007/978-94-015-9546-9_12)
- Kamal, H., Lynch-Holm, V., Pappu, H. R., & Tanaka, K. (2024). Starch Plays a Key Role in Sporosorus Formation by the Powdery Scab Pathogen *Spongospora subterranea*. *Phytopathology*®, *114*(3), 568–579.
- Kämper, J., Kahmann, R., Bölker, M., Ma, L. J., Brefort, T., Saville, B. J., Banuett, F., Kronstad, J. W., Gold, S. E., Müller, O., Perlin, M. H., Wösten, H. A. B., De Vries, R., Ruiz-Herrera, J., Reynaga-Peña, C. G., Snetselaar, K., McCann, M., Pérez-Martín, J., Feldbrügge, M., ... Birren, B. W. (2006). Insights from the genome of the biotrophic fungal plant pathogen *Ustilago maydis*. *Nature*, *444*(7115), 97–101. <https://doi.org/10.1038/nature05248>
- Kämper, J., Reichmann, M., Romeis, T., Bölker, M., & Kahmann, R. (1995). Multiallelic Recognition: Nonspecific-Dependent Dimerization of the bE and bW Homeodomain Proteins in *Ustilago maydis*. *Cell*, *81*, 73–83.
- Kanehisa, M., & Goto, S. (2000). KEGG: Kyoto Encyclopedia of Genes and Genomes. *Nucleic Acids Research*, *28*(1), 27–30. <https://doi.org/10.1093/nar/28.1.27>
- Keeling, P. L., & Myers, A. M. (2010). Biochemistry and Genetics of Starch Synthesis. *Annual Review of Food Science and Technology*, *1*(Volume 1, 2010), 271–303. <https://doi.org/https://doi.org/10.1146/annurev.food.102308.124214>
- Kelley, R. Y., Williams, W. P., Mylroie, J. E., Boykin, D. L., Harper, J. W., Windham, G. L., Ankala, A., & Shan, X. (2012). Identification of maize genes associated with host plant

- resistance or susceptibility to *Aspergillus flavus* infection and aflatoxin accumulation. *PLoS One*, 7(5), e36892.
- Keon, J. P. R., White, G. A., & Hargreaves, J. A. (1991). Isolation, characterization and sequence of a gene conferring resistance to the systemic fungicide carboxin from the maize smut pathogen, *Ustilago maydis*. *Current Genetics*, 19(6), 475–481. <https://doi.org/10.1007/BF00312739>
- Kettles, G. J., Bayon, C., Sparks, C. A., Canning, G., Kanyuka, K., & Rudd, J. J. (2018). Characterization of an antimicrobial and phytotoxic ribonuclease secreted by the fungal wheat pathogen *Zymoseptoria tritici*. *New Phytologist*, 217(1), 320–331. <https://doi.org/10.1111/NPH.14786>
- Kijpornyongpan, T., Mondo, S. J., Barry, K., Sandor, L., Lee, J., Lipzen, A., Pangilinan, J., LaButti, K., Hainaut, M., Henrissat, B., Grigoriev, I. V, Spatafora, J. W., & Aime, M. C. (2018). Broad Genomic Sampling Reveals a Smut Pathogenic Ancestry of the Fungal Clade Ustilaginomycotina. *Molecular Biology and Evolution*, 35(8), 1840–1854. <https://doi.org/10.1093/MOLBEV/MSY072>
- Kimura, S., Waszczak, C., Hunter, K., & Wrzaczek, M. (2017). Bound by Fate: The Role of Reactive Oxygen Species in Receptor-Like Kinase Signaling. *The Plant Cell*, 29(4), 638. <https://doi.org/10.1105/TPC.16.00947>
- Kohler, A. C., Chen, L. H., Hurlburt, N., Salvucci, A., Schwessinger, B., Fisher, A. J., & Stergiopoulos, I. (2016). Structural Analysis of an Avr4 Effector Ortholog Offers Insight into Chitin Binding and Recognition by the Cf-4 Receptor. *The Plant Cell*, 28(8), 1945–1965. <https://doi.org/10.1105/TPC.15.00893>
- Kolbe, A., Tiessen, A., Schlupepman, H., Paul, M., Ulrich, S., & Geigenberger, P. (2005). Trehalose 6-phosphate regulates starch synthesis via posttranslational redox activation of ADP-glucose pyrophosphorylase. *Proceedings of the National Academy of Sciences*, 102(31), 11118–11123.
- Komina, O., Zhou, Y., Sarath, G., & Chollet, R. (2002). In vivo and in vitro phosphorylation of membrane and soluble forms of soybean nodule sucrose synthase. *Plant Physiology*, 129(4), 1664–1673.
- Kourelis, J., & Van Der Hoorn, R. A. L. (2018). Defended to the Nines: 25 Years of Resistance Gene Cloning Identifies Nine Mechanisms for R Protein Function. *The Plant Cell*, 30(2), 285–299. <https://doi.org/10.1105/TPC.17.00579>
- Kretschmer, M., Croll, D., & Kronstad, J. W. (2017). Maize susceptibility to *Ustilago maydis* is influenced by genetic and chemical perturbation of carbohydrate allocation. *Molecular Plant Pathology*, 18(9), 1222–1237.
- Kubicek, C. P., Starr, T. L., & Glass, N. L. (2014). Plant Cell Wall–Degrading Enzymes and Their Secretion in Plant-Pathogenic Fungi. <https://doi.org/10.1146/annurev-phyto-102313-045831>, 52, 427–451. <https://doi.org/10.1146/ANNUREV-PHYTO-102313-045831>
- Kushnirov, V. V. (2000). Rapid and reliable protein extraction from yeast. *Yeast*, 16(9), 857–860.
- Kutík, J., & Beneš, K. (1977). Permanent slides after detection of starch grains with lugol's solution. *Biologia Plantarum*, 19(4), 309–312. <https://doi.org/10.1007/BF02923135>

- Lanver, D., Berndt, P., Tollot, M., Naik, V., Vranes, M., Warmann, T., Münch, K., Rössel, N., & Kahmann, R. (2014). Plant Surface Cues Prime *Ustilago maydis* for Biotrophic Development. *PLoS Pathogens*, 10(7). <https://doi.org/10.1371/JOURNAL.PPAT.1004272>
- Lanver, D., Müller, A. N., Happel, P., Schweizer, G., Haas, F. B., Franitza, M., Pellegrin, C., Reissmann, S., Altmüller, J., Rensing, S. A., & Kahmann, R. (2018). The Biotrophic Development of *Ustilago maydis* Studied by RNA-Seq Analysis. *The Plant Cell*, 30(2), 300–323. <https://doi.org/10.1105/TPC.17.00764>
- Lanver, D., Tollot, M., Schweizer, G., Lo Presti, L., Reissmann, S., Ma, L.-S., Schuster, M., Tanaka, S., Liang, L., Ludwig, N., & Kahmann, R. (2017). *Ustilago maydis* effectors and their impact on virulence. <https://doi.org/10.1038/nrmicro.2017.33>
- Laurie, J. D., Ali, S., Linning, R., Mannhaupt, G., Wong, P., Güldener, U., Münsterkötter, M., Moore, R., Kahmann, R., Bakkeren, G., & Schirawski, J. (2012). Genome Comparison of Barley and Maize Smut Fungi Reveals Targeted Loss of RNA Silencing Components and Species-Specific Presence of Transposable Elements. *The Plant Cell*, 24(5), 1733–1745. <https://doi.org/10.1105/TPC.112.097261>
- Leach, K. A., & Braun, D. M. (2016). Soluble sugar and starch extraction and quantification from maize (*Zea mays*) leaves. *Current Protocols in Plant Biology*, 1(1), 139–161.
- Lee, J., Eschen-Lippold, L., Lassowskat, I., Böttcher, C., & Scheel, D. (2015). Cellular reprogramming through mitogen-activated protein kinases. *Frontiers in Plant Science*, 6(OCTOBER), 940. <https://doi.org/10.3389/FPLS.2015.00940>
- Li, J., Brader, G., Kariola, T., & Tapio Palva, E. (2006). WRKY70 modulates the selection of signaling pathways in plant defense. *The Plant Journal*, 46(3), 477–491.
- Linning, R., Lin, D., Lee, N., Abdennadher, M., Gaudet, D., Thomas, P., Mills, D., Kronstad, J. W., & Bakkeren, G. (2004). Marker-Based Cloning of the Region Containing the UhAvr1 Avirulence Gene From the Basidiomycete Barley Pathogen *Ustilago hordei*. *Genetics*, 166(1), 99–111. <https://doi.org/10.1534/genetics.166.1.99>
- Lo Presti, L., & Kahmann, R. (2017). How filamentous plant pathogen effectors are translocated to host cells. *Current Opinion in Plant Biology*, 38, 19–24. <https://doi.org/10.1016/J.PBI.2017.04.005>
- Lo Presti, L., Lanver, D., Schweizer, G., Tanaka, S., Liang, L., Tollot, M., Zuccaro, A., Reissmann, S., & Kahmann, R. (2015). Fungal Effectors and Plant Susceptibility. *Https://Doi.Org/10.1146/Annurev-Arplant-043014-114623*, 66, 513–545. <https://doi.org/10.1146/ANNUREV-ARPLANT-043014-114623>
- López-Paz, C., Vilela, B., Riera, M., Pagès, M., & Lumberras, V. (2009). Maize AKIN $\beta\gamma$  dimerizes through the KIS/CBM domain and assembles into SnRK1 complexes. *FEBS Letters*, 583(12), 1887–1894.
- Loreti, E., Bellis, L. De, Alpi, A., & Perata, P. (2001). Why and how do plant cells sense sugars? *Annals of Botany*, 88(5), 803–812.
- Lu, X., Miao, J., Shen, D., & Dou, D. (2022). Proteinaceous Effector Discovery and Characterization in Plant Pathogenic Colletotrichum Fungi. *Frontiers in Microbiology*, 13, 914035. <https://doi.org/10.3389/FMICB.2022.914035/BIBTEX>

- Lucke, M., Correa, M. G., & Levy, A. (2020). The Role of Secretion Systems, Effectors, and Secondary Metabolites of Beneficial Rhizobacteria in Interactions With Plants and Microbes. *Frontiers in Plant Science*, *11*. <https://www.frontiersin.org/journals/plant-science/articles/10.3389/fpls.2020.589416>
- Ludwig, N., Reissmann, S., Schipper, K., Gonzalez, C., Assmann, D., Glatter, T., Moretti, M., Ma, L. S., Rexer, K. H., Snetselaar, K., & Kahmann, R. (2021). A cell surface-exposed protein complex with an essential virulence function in *Ustilago maydis*. *Nature Microbiology* *2021* *6*:6, 6(6), 722–730. <https://doi.org/10.1038/s41564-021-00896-x>
- Lunn, J. E., Feil, R., Hendriks, J. H. M., Gibon, Y., Morcuende, R., Osuna, D., Scheible, W.-R., Carillo, P., Hajirezaei, M.-R., & Stitt, M. (2006). Sugar-induced increases in trehalose 6-phosphate are correlated with redox activation of ADPglucose pyrophosphorylase and higher rates of starch synthesis in *Arabidopsis thaliana*. *Biochemical Journal*, *397*(1), 139–148.
- Ma, L. S., Wang, L., Trippel, C., Mendoza-Mendoza, A., Ullmann, S., Moretti, M., Carsten, A., Kahnt, J., Reissmann, S., Zechmann, B., Bange, G., & Kahmann, R. (2018). The *Ustilago maydis* repetitive effector Rsp3 blocks the antifungal activity of mannose-binding maize proteins. *Nature Communications* *2018* *9*:1, 9(1), 1–15. <https://doi.org/10.1038/s41467-018-04149-0>
- MacNeill, G. J., Mehrpouyan, S., Minow, M. A. A., Patterson, J. A., Tetlow, I. J., & Emes, M. J. (2017). Starch as a source, starch as a sink: the bifunctional role of starch in carbon allocation. *Journal of Experimental Botany*, *68*(16), 4433–4453. <https://doi.org/10.1093/jxb/erx291>
- Majeran, W., Cai, Y., Sun, Q., & van Wijk, K. J. (2005). Functional Differentiation of Bundle Sheath and Mesophyll Maize Chloroplasts Determined by Comparative Proteomics. *The Plant Cell*, *17*(11), 3111–3140. <https://doi.org/10.1105/tpc.105.035519>
- Matei, A., Ernst, C., Günl, M., Thiele, B., Altmüller, J., Walbot, V., Usadel, B., & Doehlemann, G. (2018). How to make a tumour: cell type specific dissection of *Ustilago maydis*-induced tumour development in maize leaves. *New Phytologist*, *217*(4), 1681–1695. <https://doi.org/10.1111/NPH.14960>
- Mayer, F. V., Heath, R., Underwood, E., Sanders, M. J., Carmena, D., McCartney, R. R., Leiper, F. C., Xiao, B., Jing, C., & Walker, P. A. (2011). ADP regulates SNF1, the *Saccharomyces cerevisiae* homolog of AMP-activated protein kinase. *Cell Metabolism*, *14*(5), 707–714.
- McKibbin, R. S., Muttucumar, N., Paul, M. J., Powers, S. J., Burrell, M. M., Coates, S., Purcell, P. C., Tiessen, A., Geigenberger, P., & Halford, N. G. (2006). Production of high-starch, low-glucose potatoes through over-expression of the metabolic regulator SnRK1. *Plant Biotechnology Journal*, *4*(4), 409–418.
- Meihls, L. N., Handrick, V., Glauser, G., Barbier, H., Kaur, H., Haribal, M. M., Lipka, A. E., Gershenzon, J., Buckler, E. S., & Erb, M. (2013). Natural variation in maize aphid resistance is associated with 2, 4-dihydroxy-7-methoxy-1, 4-benzoxazin-3-one glucoside methyltransferase activity. *The Plant Cell*, *25*(6), 2341–2355.
- Mendoza-Mendoza, A., Berndt, P., Djamei, A., Weise, C., Linne, U., Marahiel, M., Vraneš, M., Kämper, J., & Kahmann, R. (2009). Physical-chemical plant-derived signals induce differentiation in *Ustilago maydis*. *Molecular Microbiology*, *71*(4), 895–911. <https://doi.org/10.1111/J.1365-2958.2008.06567.X>

- Menzies, J. G. (2016). Virulence of isolates of *Ustilago tritici* collected in Manitoba and Saskatchewan, Canada, from 1999 to 2007. *Canadian Journal of Plant Pathology*, *38*(4), 470–475. <https://doi.org/10.1080/07060661.2016.1262901>
- Menzies, J. G., Nielsen, J., Thomas, P. L., & Knox, R. E. (2003). Virulence of Canadian isolates of *Ustilago tritici*: 1964–1998, and the use of the geometric rule in understanding host differential complexity. *Canadian Journal of Plant Pathology*, *25*(1), 62–72. <https://doi.org/10.1080/07060660309507050>
- Mesarich, C. H., Ökmen, B., Rovenich, H., Griffiths, S. A., Wang, C., Jashni, M. K., Mihajlovski, A., Collemare, J., Hunziker, L., Deng, C. H., Van Der Burgt, A., Beenen, H. G., Templeton, M. D., Bradshaw, R. E., & De Wit, P. J. G. M. (2018). Specific hypersensitive response-associated recognition of new apoplastic effectors from *Cladosporium fulvum* in wild tomato. *Molecular Plant-Microbe Interactions*, *31*(1), 145–162. [https://doi.org/10.1094/MPMI-05-17-0114-FI/ASSET/IMAGES/LARGE/MPMI-05-17-0114-FI\\_F5.JPG](https://doi.org/10.1094/MPMI-05-17-0114-FI/ASSET/IMAGES/LARGE/MPMI-05-17-0114-FI_F5.JPG)
- Mierziak, J., Kostyn, K., & Kulma, A. (2014). Flavonoids as Important Molecules of Plant Interactions with the Environment. *Molecules*, *19*(10), 16240. <https://doi.org/10.3390/MOLECULES191016240>
- Misas Villamil, J. C., Mueller, A. N., Demir, F., Meyer, U., Ökmen, B., Schulze Hüynck, J., Breuer, M., Dauben, H., Win, J., Huesgen, P. F., & Doehlemann, G. (2019). A fungal substrate mimicking molecule suppresses plant immunity via an inter-kingdom conserved motif. *Nature Communications* *2019 10:1*, *10*(1), 1–15. <https://doi.org/10.1038/s41467-019-09472-8>
- Mitchell, K. I., Michell, B. J., House, C. M., Stapleton, D., Dyck, J., Gamble, J., Ullrich, C., Witters, L. A., & Kemp, B. E. (1997). Posttranslational modifications of the 5'-AMP-activated protein kinase  $\beta$ 1 subunit. *Journal of Biological Chemistry*, *272*(39), 24475–24479.
- Miya, A., Albert, P., Shinya, T., Desaki, Y., Ichimura, K., Shirasu, K., Narusaka, Y., Kawakami, N., Kaku, H., & Shibuya, N. (2007). CERK1, a LysM receptor kinase, is essential for chitin elicitor signaling in Arabidopsis. *Proceedings of the National Academy of Sciences of the United States of America*, *104*(49), 19613. <https://doi.org/10.1073/PNAS.0705147104>
- Moore, J. W., Herrera-Foessel, S., Lan, C., Schnippenkoetter, W., Ayliffe, M., Huerta-Espino, J., Lillemo, M., Viccars, L., Milne, R., & Periyannan, S. (2015). A recently evolved hexose transporter variant confers resistance to multiple pathogens in wheat. *Nature Genetics*, *47*(12), 1494–1498.
- Mueller, A. N., Ziemann, S., Treitschke, S., Aßmann, D., & Doehlemann, G. (2013). Compatibility in the *Ustilago maydis*–Maize Interaction Requires Inhibition of Host Cysteine Proteases by the Fungal Effector Pit2. *PLOS Pathogens*, *9*(2), e1003177. <https://doi.org/10.1371/JOURNAL.PPAT.1003177>
- Nagl, W. (1976). DNA endoreduplication and polyteny understood as evolutionary strategies. *Nature*, *261*(5561), 614–615. <https://doi.org/10.1038/261614a0>
- Navarrete, F., Grujic, N., Stirnberg, A., Saado, I., Aleksza, D., Gallei, M., Adi, H., Alcântara, A., Khan, M., Bindics, J., Trujillo, M., & Djamei, A. (2021). The Pleiades are a cluster of

- fungual effectors that inhibit host defenses. *PLOS Pathogens*, 17(6), e1009641. <https://doi.org/10.1371/JOURNAL.PPAT.1009641>
- Nelson, T., & Dengler, N. G. (1992). Photosynthetic Tissue Differentiation in C4 Plants. *International Journal of Plant Sciences*, 153(3, Part 2), S93–S105. <https://doi.org/10.1086/297068>
- Nelson, T., & Langdale, J. A. (1992). Developmental Genetics of C4 Photosynthesis. *Http://Dx.Doi.Org/10.1146/Annurev.Pp.43.060192.000325*, 43(1), 25–47. <https://doi.org/10.1146/ANNUREV.PP.43.060192.000325>
- Ngou, B. P. M., Ahn, H. K., Ding, P., & Jones, J. D. G. (2021). Mutual potentiation of plant immunity by cell-surface and intracellular receptors. *Nature* 2021 592:7852, 592(7852), 110–115. <https://doi.org/10.1038/s41586-021-03315-7>
- Niks, R. E., Qi, X., & Marcel, T. C. (2015). Quantitative resistance to biotrophic filamentous plant pathogens: concepts, misconceptions, and mechanisms. *Annual Review of Phytopathology*, 53, 445–470.
- Nukarinen, E., Nägele, T., Pedrotti, L., Wurzinger, B., Mair, A., Landgraf, R., Börnke, F., Hanson, J., Teige, M., Baena-Gonzalez, E., Dröge-Laser, W., & Weckwerth, W. (2016). Quantitative phosphoproteomics reveals the role of the AMPK plant ortholog SnRK1 as a metabolic master regulator under energy deprivation. *Scientific Reports*, 6(1), 31697. <https://doi.org/10.1038/srep31697>
- Nunes, C., Primavesi, L. F., Patel, M. K., Martinez-Barajas, E., Powers, S. J., Sagar, R., Fevereiro, P. S., Davis, B. G., & Paul, M. J. (2013). Inhibition of SnRK1 by metabolites: Tissue-dependent effects and cooperative inhibition by glucose 1-phosphate in combination with trehalose 6-phosphate. *Plant Physiology and Biochemistry*, 63, 89–98. <https://doi.org/https://doi.org/10.1016/j.plaphy.2012.11.011>
- Oakhill, J. S., Scott, J. W., & Kemp, B. E. (2012). AMPK functions as an adenylate charge-regulated protein kinase. *Trends in Endocrinology & Metabolism*, 23(3), 125–132.
- Ökmen, B., & Doehlemann, G. (2014). Inside plant: biotrophic strategies to modulate host immunity and metabolism. *Current Opinion in Plant Biology*, 20, 19–25. <https://doi.org/10.1016/J.PBI.2014.03.011>
- Ökmen, B., Jaeger, E., Schilling, L., Finke, N., Klemd, A., Lee, Y. J., Wemhöner, R., Pauly, M., Neumann, U., & Doehlemann, G. (2022). A conserved enzyme of smut fungi facilitates cell-to-cell extension in the plant bundle sheath. *Nature Communications*, 13(1), 6003. <https://doi.org/10.1038/s41467-022-33815-7>
- Ökmen, B., Katzy, P., Huang, L., Wemhöner, R., & Doehlemann, G. (2023). A conserved extracellular Ribol with broad-spectrum cytotoxic activity enables smut fungi to compete with host-associated bacteria. *New Phytologist*, 240(5), 1976–1989. <https://doi.org/10.1111/NPH.19244>
- Ökmen, B., Kemmerich, B., Hilbig, D., Wemhöner, R., Aschenbroich, J., Perrar, A., Huesgen, P. F., Schipper, K., & Doehlemann, G. (2018). Dual function of a secreted fungalysin metalloprotease in *Ustilago maydis*. *New Phytologist*, 220(1), 249–261. <https://doi.org/10.1111/NPH.15265>
- Oliveira-Garcia, E., Tamang, T. M., Park, J., Dalby, M., Martin-Urdiroz, M., Herrero, C. R., Vu, A. H., Park, S., Talbot, N. J., & Valent, B. (2023). Clathrin-mediated endocytosis



- facilitates the internalization of *Magnaporthe oryzae* effectors into rice cells. *The Plant Cell*, 35(7), 2527–2551. <https://doi.org/10.1093/PLCELL/KOAD094>
- Pataky, J. K., & Chandler, M. A. (2003). Production of huitlacoche, *Ustilago maydis*: timing inoculation and controlling pollination. *Mycologia*, 95(6), 1261–1270. <https://doi.org/10.1080/15572536.2004.11833034>
- Paul, M. J., Gonzalez-Uriarte, A., Griffiths, C. A., & Hassani-Pak, K. (2018). The Role of Trehalose 6-Phosphate in Crop Yield and Resilience. *Plant Physiology*, 177(1), 12–23. <https://doi.org/10.1104/pp.17.01634>
- Paul, M. J., Oszvald, M., Jesus, C., Rajulu, C., & Griffiths, C. A. (2017). Increasing crop yield and resilience with trehalose 6-phosphate: targeting a feast–famine mechanism in cereals for better source–sink optimization. *Journal of Experimental Botany*, 68(16), 4455–4462.
- Paul, M. J., Primavesi, L. F., Jhurrea, D., & Zhang, Y. (2008). Trehalose metabolism and signaling. *Annu. Rev. Plant Biol.*, 59, 417–441.
- Peixoto, B., Moraes, T. A., Mengin, V., Margalha, L., Vicente, R., Feil, R., Höhne, M., Sousa, A. G. G., Lilue, J., Stitt, M., Lunn, J. E., & Baena-González, E. (2021). Impact of the SnRK1 protein kinase on sucrose homeostasis and the transcriptome during the diel cycle. *Plant Physiology*, 187(3), 1357–1373. <https://doi.org/10.1093/plphys/kiab350>
- Piattoni, C. V., Bustos, D. M., Guerrero, S. A., & Iglesias, A. Á. (2011). Nonphosphorylating glyceraldehyde-3-phosphate dehydrogenase is phosphorylated in wheat endosperm at serine-404 by an SNF1-related protein kinase allosterically inhibited by ribose-5-phosphate. *Plant Physiology*, 156(3), 1337–1350.
- Pierre, M., Traverso, J. A., Boisson, B., Domenichini, S., Bouchez, D., Giglione, C., & Meinel, T. (2007). N-Myristoylation Regulates the SnRK1 Pathway in Arabidopsis. *The Plant Cell*, 19(9), 2804–2821. <https://doi.org/10.1105/tpc.107.051870>
- Pieterse, C. M. J., Van Der Does, D., Zamioudis, C., Leon-Reyes, A., Van Wees, S. C. M., Ni, C. M. J. P., Ni, A. V., Ni, C. Z., & Ni, S. V. (2012). Hormonal Modulation of Plant Immunity. <https://doi.org/10.1146/annurev-cellbio-092910-154055>, 28, 489–521. <https://doi.org/10.1146/ANNUREV-CELLBIO-092910-154055>
- Plissonneau, C., Hartmann, F. E., & Croll, D. (2018). Pangenome analyses of the wheat pathogen *Zymoseptoria tritici* reveal the structural basis of a highly plastic eukaryotic genome. *BMC Biology*, 16(1), 1–16. <https://doi.org/10.1186/S12915-017-0457-4/FIGURES/6>
- Poland, J. A., Bradbury, P. J., Buckler, E. S., & Nelson, R. J. (2011). Genome-wide nested association mapping of quantitative resistance to northern leaf blight in maize. *Proceedings of the National Academy of Sciences*, 108(17), 6893–6898.
- Ponnu, J., Wahl, V., & Schmid, M. (2011). Trehalose-6-phosphate: connecting plant metabolism and development. *Frontiers in Plant Science*, 2, 70.
- Raffaele, S., Win, J., Cano, L. M., & Kamoun, S. (2010). Analyses of genome architecture and gene expression reveal novel candidate virulence factors in the secretome of *Phytophthora infestans*. *BMC Genomics* 2010 11:1, 11(1), 1–18. <https://doi.org/10.1186/1471-2164-11-637>
- Ramon, M., Dang, T. V. T., Broeckx, T., Hulsmans, S., Crepin, N., Sheen, J., & Rolland, F. (2019). Default Activation and Nuclear Translocation of the Plant Cellular Energy Sensor

- SnRK1 Regulate Metabolic Stress Responses and Development. *The Plant Cell*, 31(7), 1614–1632. <https://doi.org/10.1105/tpc.18.00500>
- Ramon, M., Rolland, F., & Sheen, J. (2008). The Arabidopsis Book. *American Society of Plant Biologists*, 6, e0117.
- Ramon, M., Ruelens, P., Li, Y., Sheen, J., Geuten, K., & Rolland, F. (2013). The hybrid four-CBS-Domain KIN  $\beta\gamma$  subunit functions as the canonical  $\gamma$  subunit of the plant energy sensor Sn RK 1. *The Plant Journal*, 75(1), 11–25.
- Redkar, A., Hoser, R., Schilling, L., Zechmann, B., Krzymowska, M., Walbot, V., & Doehlemann, G. (2015). A Secreted Effector Protein of *Ustilago maydis* Guides Maize Leaf Cells to Form Tumors. *The Plant Cell*, 27(4), 1332–1351. <https://doi.org/10.1105/TPC.114.131086>
- Rehmany, A. P., Gordon, A., Rose, L. E., Allen, R. L., Armstrong, M. R., Whisson, S. C., Kamoun, S., Tyler, B. M., Birch, P. R. J., & Beynon, J. L. (2005). Differential Recognition of Highly Divergent Downy Mildew Avirulence Gene Alleles by RPP1 Resistance Genes from Two Arabidopsis Lines. *The Plant Cell*, 17(6), 1839–1850. <https://doi.org/10.1105/TPC.105.031807>
- Rizzi, Y. S., Happel, P., Lenz, S., Urs Mounashree, J., Bonin, M., Cord-Landwehr, S., Singh, R., Moerschbacher Bruno, M., & Kahmann, R. (2021). Chitosan and Chitin Deacetylase Activity Are Necessary for Development and Virulence of *Ustilago maydis*. *MBio*, 12(2), 10.1128/mbio.03419-20. <https://doi.org/10.1128/mbio.03419-20>
- Robinson, M. D., McCarthy, D. J., & Smyth, G. K. (2010). edgeR: a Bioconductor package for differential expression analysis of digital gene expression data. *Bioinformatics*, 26(1), 139–140. <https://doi.org/10.1093/bioinformatics/btp616>
- Rodrigues, A., Adamo, M., Crozet, P., Margalha, L., Confraria, A., Martinho, C., Elias, A., Rabissi, A., Lumbreras, V., González-Guzmán, M., Antoni, R., Rodriguez, P. L., & Baena-González, E. (2013). ABI1 and PP2CA Phosphatases Are Negative Regulators of Snf1-Related Protein Kinase1 Signaling in Arabidopsis. *The Plant Cell*, 25(10), 3871–3884. <https://doi.org/10.1105/tpc.113.114066>
- Rodriguez-Moreno, L., Ebert, M. K., Bolton, M. D., & Thomma, B. P. H. J. (2018). Tools of the crook- infection strategies of fungal plant pathogens. *The Plant Journal*, 93(4), 664–674. <https://doi.org/10.1111/tpj.13810>
- Sambrook, J., Fritsch, E. F., & Maniatis, T. (1989). *Molecular cloning: a laboratory manual*. (Issue Ed. 2). Cold spring harbor laboratory press.
- Sánchez-Vallet, A., Fouché, S., Fudal, I., Hartmann, F. E., Soyer, J. L., Tellier, A., & Croll, D. (2018). The Genome Biology of Effector Gene Evolution in Filamentous Plant Pathogens. <https://doi.org/10.1146/Annurev-Phyto-080516-035303>, 56, 21–40. <https://doi.org/10.1146/ANNUREV-PHYTO-080516-035303>
- Sánchez-Vallet, A., Saleem-Batcha, R., Kombrink, A., Hansen, G., Valkenburg, D.-J., Thomma, B. P. H. J., & Mesters, J. R. (2013). Fungal effector Ecp6 outcompetes host immune receptor for chitin binding through intrachain LysM dimerization. *ELife*, 2, e00790. <https://doi.org/10.7554/eLife.00790>
- Sánchez-Vallet, A., Tian, H., Rodriguez-Moreno, L., Valkenburg, D. J., Saleem-Batcha, R., Wawra, S., Kombrink, A., Verhage, L., de Jonge, R., van Esse, H. P., Zuccaro, A., Croll,

- D., Mesters, J. R., & Thomma, B. P. H. J. (2020). A secreted LysM effector protects fungal hyphae through chitin-dependent homodimer polymerization. *PLoS Pathogens*, *16*(6), e1008652. <https://doi.org/10.1371/JOURNAL.PPAT.1008652>
- Santos Rezende, J., Zivanovic, M., Costa de Novaes, M. I., & Chen, Z. Y. (2020). The AVR4 effector is involved in cercosporin biosynthesis and likely affects the virulence of *Cercospora cf. flagellaris* on soybean. *Molecular Plant Pathology*, *21*(1), 53–65. <https://doi.org/10.1111/MPP.12879>
- Sauerzapfe, B., Engels, L., & Elling, L. (2008). Broadening the biocatalytic properties of recombinant sucrose synthase 1 from potato (*Solanum tuberosum* L.) by expression in *Escherichia coli* and *Saccharomyces cerevisiae*. *Enzyme and Microbial Technology*, *43*(3), 289–296.
- Saunders, D. G. O. (2023). Fine-tuning fungal effector secretion. *Nature Microbiology* *2023* *8*:9, *8*(9), 1613–1614. <https://doi.org/10.1038/s41564-023-01456-1>
- Savary, S., Willocquet, L., Pethybridge, S. J., Esker, P., McRoberts, N., & Nelson, A. (2019). The global burden of pathogens and pests on major food crops. *Nature Ecology & Evolution* *2019* *3*:3, *3*(3), 430–439. <https://doi.org/10.1038/s41559-018-0793-y>
- Saville, B. J., Donaldson, M. E., Doyle, C. E., Saville, B. J., Donaldson, M. E., & Doyle, C. E. (2012). Investigating Host Induced Meiosis in a Fungal Plant Pathogen. *Meiosis - Molecular Mechanisms and Cytogenetic Diversity*. <https://doi.org/10.5772/30032>
- Scherer, M., Heimel, K., Starke, V., & Kämper, J. (2006). The Clp1 Protein Is Required for Clamp Formation and Pathogenic Development of *Ustilago maydis*. *The Plant Cell*, *18*(9), 2388–2401. <https://doi.org/10.1105/TPC.106.043521>
- Schilling, L., Matei, A., Redkar, A., Walbot, V., & Doehlemann, G. (2014). Virulence of the maize smut *Ustilago maydis* is shaped by organ-specific effectors. *Molecular Plant Pathology*, *15*(8), 780–789. <https://doi.org/10.1111/MPP.12133/SUPPINFO>
- Schipper, K. (2009). *Charakterisierung eines Ustilago maydis Genclusters, das für drei neuartige sekretierte Effektoren kodiert*. Philipps-Universität Marburg.
- Schirawski, J., Böhnert, H. U., Steinberg, G., Snetselaar, K., Adamikowa, L., & Kahmann, R. (2005). Endoplasmic Reticulum Glucosidase II Is Required for Pathogenicity of *Ustilago maydis*. *The Plant Cell*, *17*(12), 3532–3543. <https://doi.org/10.1105/TPC.105.036285>
- Schirawski, J., Mannhaupt, G., Münch, K., Brefort, T., Schipper, K., Doehlemann, G., Di Stasio, M., Rössel, N., Mendoza-Mendoza, A., Pester, D., Müller, O., Winterberg, B., Meyer, E., Ghareeb, H., Wollenberg, T., Münsterkötter, M., Wong, P., Walter, M., Stukenbrock, E., ... Kahmann, R. (2010). Pathogenicity determinants in smut fungi revealed by genome comparison. *Science*, *330*(6010), 1546–1548. [https://doi.org/10.1126/SCIENCE.1195330/SUPPL\\_FILE/SCHIRAWSKI.SOM.PDF](https://doi.org/10.1126/SCIENCE.1195330/SUPPL_FILE/SCHIRAWSKI.SOM.PDF)
- Schurack, S., Depotter, J. R. L., Gupta, D., Thines, M., & Doehlemann, G. (2021). Comparative transcriptome profiling identifies maize line specificity of fungal effectors in the maize–*Ustilago maydis* interaction. *The Plant Journal*, *106*(3), 733–752.
- Schweighofer, A., Hirt, H., & Meskiene, I. (2004). Plant PP2C phosphatases: emerging functions in stress signaling. *Trends in Plant Science*, *9*(5), 236–243.

- Seitner, D., Uhse, S., Gallei, M., & Djamei, A. (2018). The core effector Cce1 is required for early infection of maize by *Ustilago maydis*. *Molecular Plant Pathology*, *19*(10), 2277–2287. <https://doi.org/10.1111/MPP.12698>
- Sekhon, R. S., Lin, H., Childs, K. L., Hansey, C. N., Buell, C. R., De Leon, N., & Kaeppler, S. M. (2011). Genome-wide atlas of transcription during maize development. *The Plant Journal*, *66*(4), 553–563.
- Shen, W., Reyes, M. I., & Hanley-Bowdoin, L. (2009). Arabidopsis protein kinases GRIK1 and GRIK2 specifically activate SnRK1 by phosphorylating its activation loop. *Plant Physiology*, *150*(2), 996–1005.
- Skibbe, D. S., Doehlemann, G., Fernandes, J., & Walbot, V. (2010). Maize tumors caused by *ustilago maydis* require organ-specific genes in host and pathogen. *Science*, *328*(5974), 89–92. <https://doi.org/10.1126/SCIENCE.1185775>
- Smith, L. G., Gerttula, S. M., Han, S., & Levy, J. (2001). Tangled1A Microtubule Binding Protein Required for the Spatial Control of Cytokinesis in Maize. *Journal of Cell Biology*, *152*(1), 231–236. <https://doi.org/10.1083/JCB.152.1.231>
- Smith, L. G., Hake, S., & Sylvester, A. W. (1996). The tangled-1 mutation alters cell division orientations throughout maize leaf development without altering leaf shape. *Development*, *122*(2), 481–489. <https://doi.org/10.1242/DEV.122.2.481>
- Snelders, N. C., Boshoven, J. C., Song, Y., Schmitz, N., Fiorin, G. L., Rovenich, H., van den Berg, G. C. M., Torres, D. E., Petti, G. C., Prockl, Z., Faino, L., Seidl, M. F., & Thomma, B. P. H. J. (2023). A highly polymorphic effector protein promotes fungal virulence through suppression of plant-associated Actinobacteria. *New Phytologist*, *237*(3), 944–958. <https://doi.org/10.1111/NPH.18576>
- Snelders, N. C., Rovenich, H., Petti, G. C., Rocafort, M., van den Berg, G. C. M., Vorholt, J. A., Mesters, J. R., Seidl, M. F., Nijland, R., & Thomma, B. P. H. J. (2020). Microbiome manipulation by a soil-borne fungal plant pathogen using effector proteins. *Nature Plants* *2020 6:11*, *6*(11), 1365–1374. <https://doi.org/10.1038/s41477-020-00799-5>
- Snetselaar, K. M., Bölker, M., & Kahmann, R. (1996). *Ustilago maydis* Mating Hyphae Orient Their Growth toward Pheromone Sources. *Fungal Genetics and Biology*, *20*(4), 299–312. <https://doi.org/10.1006/FGBI.1996.0044>
- Snetselaar, K. M., & Mims, C. W. (1992). Sporidial Fusion and Infection of Maize Seedlings by the Smut Fungus *Ustilago maydis*. *Mycologia*, *84*(2), 193. <https://doi.org/10.2307/3760250>
- Snetselaar, K. M., & Mims, C. W. (1994). Light and electron microscopy of *Ustilago maydis* hyphae in maize. *Mycological Research*, *98*(3), 347–355. [https://doi.org/10.1016/S0953-7562\(09\)80463-2](https://doi.org/10.1016/S0953-7562(09)80463-2)
- Sosso, D., Luo, D., Li, Q.-B., Sasse, J., Yang, J., Gendrot, G., Suzuki, M., Koch, K. E., McCarty, D. R., & Chourey, P. S. (2015). Seed filling in domesticated maize and rice depends on SWEET-mediated hexose transport. *Nature Genetics*, *47*(12), 1489–1493.
- Sosso, D., van der Linde, K., Bezruczyk, M., Schuler, D., Schneider, K., Kämper, J., & Walbot, V. (2019). Sugar Partitioning between *Ustilago maydis* and Its Host *Zea mays* L during Infection. *Plant Physiology*, *179*(4), 1373–1385. <https://doi.org/10.1104/pp.18.01435>

- Southern, E. M. (1975). Detection of specific sequences among DNA fragments separated by gel electrophoresis. *J Mol Biol*, *98*(3), 503–517.
- Sperschneider, J., & Dodds, P. N. (2022). EffectorP 3.0: prediction of apoplastic and cytoplasmic effectors in fungi and oomycetes. *Molecular Plant-Microbe Interactions*, *35*(2), 146–156.
- Stein, O., & Granot, D. (2019). An overview of sucrose synthases in plants. *Frontiers in Plant Science*, *10*, 435701.
- Steinberg, G., & Gurr, S. J. (2020). Fungi, fungicide discovery and global food security. *Fungal Genetics and Biology*, *144*, 103476. <https://doi.org/10.1016/J.FGB.2020.103476>
- Stergiopoulos, I., Collemare, J., Mehrabi, R., & De Wit, P. J. G. M. (2013). Phytotoxic secondary metabolites and peptides produced by plant pathogenic Dothideomycete fungi. *FEMS Microbiology Reviews*, *37*(1), 67–93. <https://doi.org/10.1111/J.1574-6976.2012.00349.X>
- Stergiopoulos, I., Van Den Burg, H. A., Ökmen, B., Beenen, H. G., Van Liere, S., Kema, G. H. J., & De Wit, P. J. G. M. (2010). Tomato Cf resistance proteins mediate recognition of cognate homologous effectors from fungi pathogenic on dicots and monocots. *Proceedings of the National Academy of Sciences of the United States of America*, *107*(16), 7610–7615. <https://doi.org/10.1073/PNAS.1002910107>
- Stirnberg, A., & Djamei, A. (2016). Characterization of ApB73, a virulence factor important for colonization of *Zea mays* by the smut *Ustilago maydis*. *Molecular Plant Pathology*, *17*(9), 1467–1479.
- Stitt, M., Wilke, I., Feil, R., & Heldt, H. W. (1988). Coarse control of sucrose-phosphate synthase in leaves: Alterations of the kinetic properties in response to the rate of photosynthesis and the accumulation of sucrose. *Planta*, *174*(2), 217–230. <http://www.jstor.org/stable/23379205>
- Strand, Å., Zrenner, R., Trevanion, S., Stitt, M., Gustafsson, P., & Gardeström, P. (2000). Decreased expression of two key enzymes in the sucrose biosynthesis pathway, cytosolic fructose-1, 6-bisphosphatase and sucrose phosphate synthase, has remarkably different consequences for photosynthetic carbon metabolism in transgenic *Arabidopsis thaliana*. *The Plant Journal*, *23*(6), 759–770.
- Sugden, C., Crawford, R. M., Halford, N. G., & Hardie, D. G. (1999). Regulation of spinach SNF1-related (SnRK1) kinases by protein kinases and phosphatases is associated with phosphorylation of the T loop and is regulated by 5'-AMP. *The Plant Journal*, *19*(4), 433–439.
- Sun, B., Zhong, F.-J., Xu, C., Li, Y.-M., Zhao, Y.-R., Cao, M.-M., & Yang, L.-Y. (2021). Programmed cell death 10 promotes metastasis and epithelial-mesenchymal transition of hepatocellular carcinoma via PP2Ac-mediated YAP activation. *Cell Death & Disease*, *12*(9), 849. <https://doi.org/10.1038/s41419-021-04139-z>
- Sun, N., Liu, Y., Xu, T., Zhou, X., Xu, H., Zhang, H., Zhan, R., & Wang, L. (2023). Genome-wide analysis of sugar transporter genes in maize (*Zea mays* L.): identification, characterization and their expression profiles during kernel development. *PeerJ*, *11*, e16423. <https://doi.org/10.7717/PEERJ.16423/SUPP-6>

- Sylvester, A. W., Cande, W. Z., & Freeling, M. (1990). Division and differentiation during normal and liguleless-1 maize leaf development. *Development*, *110*(3), 985–1000. <https://doi.org/10.1242/DEV.110.3.985>
- Szczesny, R., Büttner, D., Escolar, L., Schulze, S., Seiferth, A., & Bonas, U. (2010). Suppression of the AvrBs1-specific hypersensitive response by the YopJ effector homolog AvrBsT from *Xanthomonas* depends on a SNF1-related kinase. *New Phytologist*, *187*(4), 1058–1074.
- Tanaka, S., Brefort, T., Neidig, N., Djamei, A., Kahnt, J., Vermerris, W., Koenig, S., Feussner, K., Feussner, I., & Kahmann, R. (2014). A secreted *Ustilago maydis* effector promotes virulence by targeting anthocyanin biosynthesis in maize. *ELife*, *3*. <https://doi.org/10.7554/ELIFE.01355>
- Tapke, VF. (1945). Physiologic races of *Ustilago hordei*. *Phytopathology*, *35*, 970–976.
- Teufel, F., Almagro Armenteros, J. J., Johansen, A. R., Gíslason, M. H., Pihl, S. I., Tsirigos, K. D., Winther, O., Brunak, S., von Heijne, G., & Nielsen, H. (2022). SignalP 6.0 predicts all five types of signal peptides using protein language models. *Nature Biotechnology*, *40*(7), 1023–1025.
- Tiessen, A., Prescha, K., Branscheid, A., Palacios, N., McKibbin, R., Halford, N. G., & Geigenberger, P. (2003). Evidence that SNF1-related kinase and hexokinase are involved in separate sugar-signalling pathways modulating post-translational redox activation of ADP-glucose pyrophosphorylase in potato tubers. *The Plant Journal*, *35*(4), 490–500.
- Todd, J. N. A., Carreón-Anguiano, K. G., Islas-Flores, I., & Canto-Canché, B. (2022). Fungal Effectoromics: A World in Constant Evolution. *International Journal of Molecular Sciences* *2022*, Vol. *23*, Page *13433*, *23*(21), 13433. <https://doi.org/10.3390/IJMS232113433>
- Tollot, M., Assmann, D., Becker, C., Altmüller, J., Duthel, J. Y., Wegner, C. E., & Kahmann, R. (2016). The WOPR Protein Ros1 Is a Master Regulator of Sporogenesis and Late Effector Gene Expression in the Maize Pathogen *Ustilago maydis*. *PLoS Pathogens*, *12*(6). <https://doi.org/10.1371/JOURNAL.PPAT.1005697>
- Toroser, D., Plaut, Z., & Huber, S. C. (2000). Regulation of a plant SNF1-related protein kinase by glucose-6-phosphate. *Plant Physiology*, *123*(1), 403–412.
- Toruño, T. Y., Stergiopoulos, I., & Coaker, G. (2016). Plant-Pathogen Effectors: Cellular Probes Interfering with Plant Defenses in Spatial and Temporal Manners. <https://doi.org/10.1146/Annurev-Phyto-080615-100204>, *54*, 419–441. <https://doi.org/10.1146/ANNUREV-PHYTO-080615-100204>
- Valverde, M. E., Paredes-Lopez, O., Guevara-Lara, F., & Pataky, J. K. (1995). Huitlacoche (*Ustilago maydis*) as a Food Source — Biology, Composition, and Production. *Critical Reviews in Food Science and Nutrition*, *35*(3), 191–229. <https://doi.org/10.1080/10408399509527699>
- van der Linde, K., Kastner, C., Kumlehn, J., Kahmann, R., & Doehlemann, G. (2011). Systemic virus-induced gene silencing allows functional characterization of maize genes during biotrophic interaction with *Ustilago maydis*. *New Phytologist*, *189*(2), 471–483. <https://doi.org/https://doi.org/10.1111/j.1469-8137.2010.03474.x>

- Van Dingenen, J., De Milde, L., Vermeersch, M., Maleux, K., De Rycke, R., De Bruyne, M., Storme, V., Gonzalez, N., Dhondt, S., & Inzé, D. (2016). Chloroplasts Are Central Players in Sugar-Induced Leaf Growth. *Plant Physiology*, *171*(1), 590–605. <https://doi.org/10.1104/pp.15.01669>
- Van Dingenen, J., Vermeersch, M., De Milde, L., Hulsmans, S., De Winne, N., Van Leene, J., Gonzalez, N., Dhondt, S., De Jaeger, G., & Rolland, F. (2019). The role of HEXOKINASE1 in Arabidopsis leaf growth. *Plant Molecular Biology*, *99*, 79–93.
- van Kan, J. A. L. (2006). Licensed to kill: the lifestyle of a necrotrophic plant pathogen. *Trends in Plant Science*, *11*(5), 247–253. <https://doi.org/10.1016/j.tplants.2006.03.005>
- Van Leene, J., Eeckhout, D., Gadeyne, A., Matthijs, C., Han, C., De Winne, N., Persiau, G., Van De Slijke, E., Persyn, F., Mertens, T., Smagghe, W., Crepin, N., Broucke, E., Van Damme, D., Pleskot, R., Rolland, F., & De Jaeger, G. (2022). Mapping of the plant SnRK1 kinase signalling network reveals a key regulatory role for the class II T6P synthase-like proteins. *Nature Plants*, *8*(11), 1245–1261. <https://doi.org/10.1038/s41477-022-01269-w>
- Varden, F. A., De la Concepcion, J. C., Maidment, J. H. R., & Banfield, M. J. (2017). Taking the stage: effectors in the spotlight. *Current Opinion in Plant Biology*, *38*, 25–33. <https://doi.org/https://doi.org/10.1016/j.pbi.2017.04.013>
- Villagrán, Z., Martínez-Reyes, M., Gómez-Rodríguez, H., Ríos-García, U., Montalvo-González, E., Ortiz-Basurto, R. I., Anaya-Esparza, L. M., & Pérez-Moreno, J. (2023). Huitlacoche (*Ustilago maydis*), an Iconic Mexican Fungal Resource: Biocultural Importance, Nutritional Content, Bioactive Compounds, and Potential Biotechnological Applications. *Molecules* *2023*, Vol. *28*, Page *4415*, *28*(11), 4415. <https://doi.org/10.3390/MOLECULES28114415>
- Wang, B.-T., Hu, S., Yu, X.-Y., Jin, L., Zhu, Y.-J., & Jin, F.-J. (2020). Studies of cellulose and starch utilization and the regulatory mechanisms of related enzymes in fungi. *Polymers*, *12*(3), 530.
- Wang, F., Ye, Y., Chen, X., Wang, J., Chen, Z., & Zhou, Q. (2017). A sucrose non-fermenting-1-related protein kinase 1 gene from potato, StSnRK1, regulates carbohydrate metabolism in transgenic tobacco. *Physiology and Molecular Biology of Plants*, *23*, 933–943.
- Wang, Wang, S., Wang, W., Xu, L., Welsh, L. R. J., Gierlinski, M., Whisson, S. C., Hemsley, P. A., Boevink, P. C., & Birch, P. R. J. (2023). Uptake of oomycete RXLR effectors into host cells by clathrin-mediated endocytosis. *The Plant Cell*, *35*(7), 2504–2526. <https://doi.org/10.1093/PLCELL/KOAD069>
- Wang, Weiberg, A., Dellota, E., Yamane, D., & Jin, H. (2017). Botrytis small RNA Bc-siR37 suppresses plant defense genes by cross-kingdom RNAi. *RNA Biology*, *14*(4), 421–428. <https://doi.org/10.1080/15476286.2017.1291112>
- Wang, Y., Li, W., Qu, J., Li, F., Du, W., & Weng, J. (2023). Genome-Wide Characterization of the Maize (*Zea mays* L.) WRKY Transcription Factor Family and Their Responses to *Ustilago maydis*. *International Journal of Molecular Sciences*, *24*(19), 14916.
- Wang, Y., Pruitt, R. N., Nürnberger, T., & Wang, Y. (2022). Evasion of plant immunity by microbial pathogens. *Nature Reviews Microbiology* *2022* *20*:8, *20*(8), 449–464. <https://doi.org/10.1038/s41579-022-00710-3>

- Wang, Y., & Wang, Y. (2018). Trick or treat: Microbial pathogens evolved apoplast effectors modulating plant susceptibility to infection. *Molecular Plant-Microbe Interactions*, *31*(1), 6–12. [https://doi.org/10.1094/MPMI-07-17-0177-FI/ASSET/IMAGES/LARGE/MPMI-07-17-0177-FI\\_F1.JPG](https://doi.org/10.1094/MPMI-07-17-0177-FI/ASSET/IMAGES/LARGE/MPMI-07-17-0177-FI_F1.JPG)
- Warden, S. M., Richardson, C., O'Donnell Jr, J., Stapleton, D., Kemp, B. E., & Witters, L. A. (2001). Post-translational modifications of the  $\beta$ -1 subunit of AMP-activated protein kinase affect enzyme activity and cellular localization. *Biochemical Journal*, *354*(2), 275–283.
- Weiberg, A., Wang, M., Lin, F. M., Zhao, H., Zhang, Z., Kaloshian, I., Huang, H. Da, & Jin, H. (2013). Fungal small RNAs suppress plant immunity by hijacking host RNA interference pathways. *Science*, *342*(6154), 118–123. [https://doi.org/10.1126/SCIENCE.1239705/SUPPL\\_FILE/WEIBERG-SM.PDF](https://doi.org/10.1126/SCIENCE.1239705/SUPPL_FILE/WEIBERG-SM.PDF)
- Wenzler, H., & Meins, F. (1987). Persistent changes in the proliferative capacity of maize leaf tissues induced by Ustilago infection. *Physiological and Molecular Plant Pathology*, *30*(2), 309–319. [https://doi.org/10.1016/0885-5765\(87\)90044-0](https://doi.org/10.1016/0885-5765(87)90044-0)
- Wildermuth, M. C. (2010). Modulation of host nuclear ploidy: a common plant biotroph mechanism. *Current Opinion in Plant Biology*, *13*(4), 449–458. <https://doi.org/10.1016/J.PBI.2010.05.005>
- Willmann, R., Lajunen, H. M., Erbs, G., Newman, M. A., Kolb, D., Tsuda, K., Katagiri, F., Fliegmann, J., Bono, J. J., Cullimore, J. V., Jehle, A. K., Götz, F., Kulik, A., Molinaro, A., Lipka, V., Gust, A. A., & Nürnberger, T. (2011). Arabidopsis lysin-motif proteins LYM1 LYM3 CERK1 mediate bacterial peptidoglycan sensing and immunity to bacterial infection. *Proceedings of the National Academy of Sciences of the United States of America*, *108*(49), 19824–19829. [https://doi.org/10.1073/PNAS.1112862108/SUPPL\\_FILE/SAPP.PDF](https://doi.org/10.1073/PNAS.1112862108/SUPPL_FILE/SAPP.PDF)
- Wlodarchak, N., & Xing, Y. (2016). PP2A as a master regulator of the cell cycle. *Critical Reviews in Biochemistry and Molecular Biology*, *51*(3), 162–184. <https://doi.org/10.3109/10409238.2016.1143913>
- Worrell, A. C., Bruneau, J.-M., Summerfelt, K., Boersig, M., & Voelker, T. A. (1991). Expression of a maize sucrose phosphate synthase in tomato alters leaf carbohydrate partitioning. *The Plant Cell*, *3*(10), 1121–1130.
- Wurzinger, B., Nukarinen, E., Nägele, T., Weckwerth, W., & Teige, M. (2018). The SnRK1 Kinase as Central Mediator of Energy Signaling between Different Organelles . *Plant Physiology*, *176*(2), 1085–1094. <https://doi.org/10.1104/pp.17.01404>
- Yang, F., Li, W., Jiang, N., Yu, H., Morohashi, K., Ouma, W. Z., Morales-Mantilla, D. E., Gomez-Cano, F. A., Mukundi, E., & Prada-Salcedo, L. D. (2017). A maize gene regulatory network for phenolic metabolism. *Molecular Plant*, *10*(3), 498–515.
- Yang, Q., He, Y., Kabahuma, M., Chaya, T., Kelly, A., Borrego, E., Bian, Y., El Kasmi, F., Yang, L., & Teixeira, P. (2017). A gene encoding maize caffeoyl-CoA O-methyltransferase confers quantitative resistance to multiple pathogens. *Nature Genetics*, *49*(9), 1364–1372.
- Yang, X., Deng, F., & Ramonell, K. M. (2012). Receptor-like kinases and receptor-like proteins: Keys to pathogen recognition and defense signaling in plant innate immunity. *Frontiers in Biology*, *7*(2), 155–166. <https://doi.org/10.1007/S11515-011-1185-8/METRICS>



- Yuan, M., Jiang, Z., Bi, G., Nomura, K., Liu, M., Wang, Y., Cai, B., Zhou, J. M., He, S. Y., & Xin, X. F. (2021). Pattern-recognition receptors are required for NLR-mediated plant immunity. *Nature* 2021 592:7852, 592(7852), 105–109. <https://doi.org/10.1038/s41586-021-03316-6>
- Yuan, P., Jauregui, E., Du, L., Tanaka, K., & Poovaiah, B. W. (2017). Calcium signatures and signaling events orchestrate plant–microbe interactions. *Current Opinion in Plant Biology*, 38, 173–183. <https://doi.org/10.1016/J.PBI.2017.06.003>
- Zhang, J., Coaker, G., Zhou, J. M., & Dong, X. (2020). Plant Immune Mechanisms: From Reductionistic to Holistic Points of View. *Molecular Plant*, 13(10), 1358–1378. <https://doi.org/10.1016/J.MOLP.2020.09.007>
- Zhang, R., Isozumi, N., Mori, M., Okuta, R., Singkaravanit-Ogawa, S., Imamura, T., Kurita, J.-I., Gan, P., Shirasu, K., Ohki, S., & Takano, Y. (2021). Fungal effector SIB1 of *Colletotrichum orbiculare* has unique structural features and can suppress plant immunity in *Nicotiana benthamiana*. *Journal of Biological Chemistry*, 297(6), 101370. <https://doi.org/https://doi.org/10.1016/j.jbc.2021.101370>
- Zheng, Y., Kief, J., Auffarth, K., Farfsing, J. W., Mahlert, M., Nieto, F., & Basse, C. W. (2008). The *Ustilago maydis* Cys2His2-type zinc finger transcription factor Mzr1 regulates fungal gene expression during the biotrophic growth stage. *Molecular Microbiology*, 68(6), 1450–1470. <https://doi.org/10.1111/J.1365-2958.2008.06244.X>
- Zhou, Z., Bi, G., & Zhou, J. (2018). Luciferase complementation assay for protein-protein interactions in plants. *Current Protocols in Plant Biology*, 3(1), 42–50.
- Zipfel, C. (2014). Plant pattern-recognition receptors. *Trends in Immunology*, 35(7), 345–351. <https://doi.org/10.1016/J.IT.2014.05.004>
- Zipfel, C., Kunze, G., Chinchilla, D., Caniard, A., Jones, J. D. G., Boller, T., & Felix, G. (2006). Perception of the Bacterial PAMP EF-Tu by the Receptor EFR Restricts Agrobacterium-Mediated Transformation. *Cell*, 125(4), 749–760. <https://doi.org/10.1016/J.CELL.2006.03.037>
- Zuo, W., Depotter, J. R. L., Gupta, D. K., Thines, M., & Doehlemann, G. (2021). Cross-species analysis between the maize smut fungi *Ustilago maydis* and *Sporisorium reilianum* highlights the role of transcriptional change of effector orthologs for virulence and disease. *New Phytologist*, 232(2), 719–733. <https://doi.org/10.1111/NPH.17625>
- Zuo, W., Depotter, J. R. L., Stolze, S. C., Nakagami, H., & Doehlemann, G. (2023). A transcriptional activator effector of *Ustilago maydis* regulates hyperplasia in maize during pathogen-induced tumor formation. *Nature Communications* 2023 14:1, 14(1), 1–12. <https://doi.org/10.1038/s41467-023-42522-w>
- Zuo, W., Oekmen, B., Depotter, J. R. L., Ebert, M. K., Redkar, A., Misas Villamil, J., & Doehlemann, G. (2019). Molecular Interactions Between Smut Fungi and Their Host Plants. <https://doi.org/10.1146/Annurev-Phyto-082718-100139>, 57, 411–430. <https://doi.org/10.1146/ANNUREV-PHYTO-082718-100139>

## 6. Supplementary figures and tables



**Fig. S1A) Multiple alignment sequence of Hap2, Hap3, and UMAG\_00794 using T-Coffee.** Protein sequences were obtained from the maize genome database (<https://www.maizedb.org/>). Hap2: 174aa; Hap3: 160aa; UMAG\_00794, 110aa. The percentage shown represents the amino acid percent match between Hap2 and UMAG\_00794, using Hap3 as the reference for comparison.

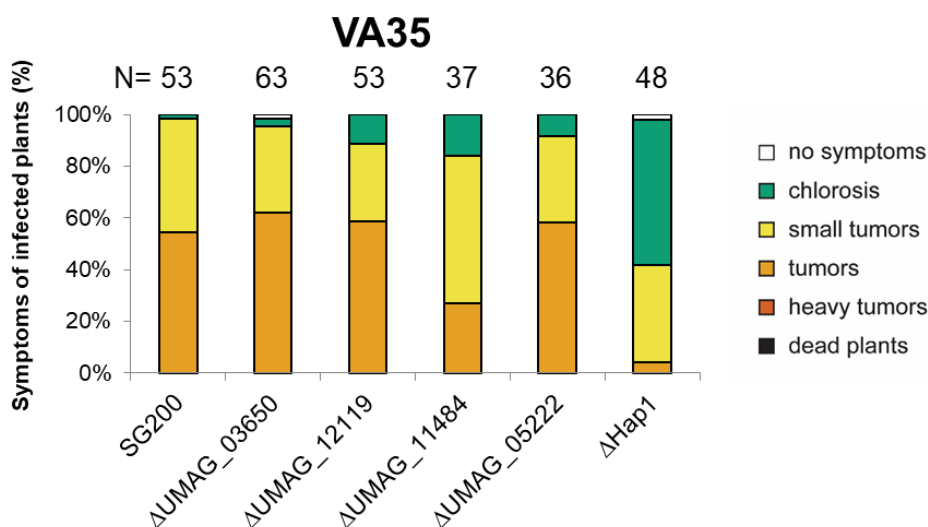


**Fig. S1B) UMAG\_11484 and Hap1 effectors show maize line-specificity in Ustilago maydis virulence.** Disease symptoms of frameshift knockout mutants that did not show virulence reduction in GB maize line were infected in more resistant VA35 maize line compared to *U. maydis* SG200 at 12 dpi. n = number of infected plants

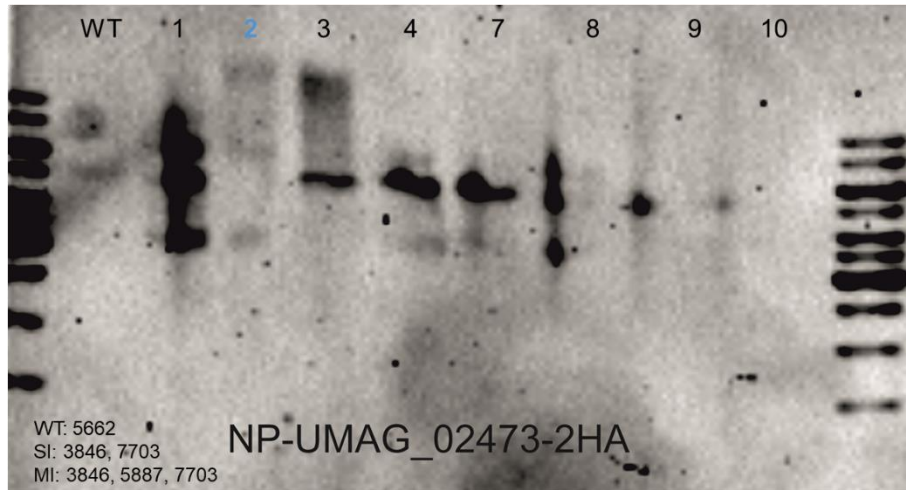


**Fig. S1C) Southern blot analysis of the *U. maydis*  $\Delta Hap1$  complementation strain.** Genomic DNA was extracted from the indicated strains, digested with the BamHI restriction enzymes, and separated on a 0.9% agarose gel. A DNA probe specific to the *ip* locus was hybridized to the southern blot, which was performed according to the standard protocol. Lanes 1 and 10 contain a molecular weight marker (unlabeled). Lanes 2-9 correspond to the following strains: Lane 2, SG200 strain (WT); Lanes 3-9, different transformants of  $\Delta Hap1$  complementation strains. The ladder sizes of the bands are indicated on the left. The expected sizes for the *ip* locus are written on the figure. Colonies with a single integration based on band size is bolded and colored with Blue.

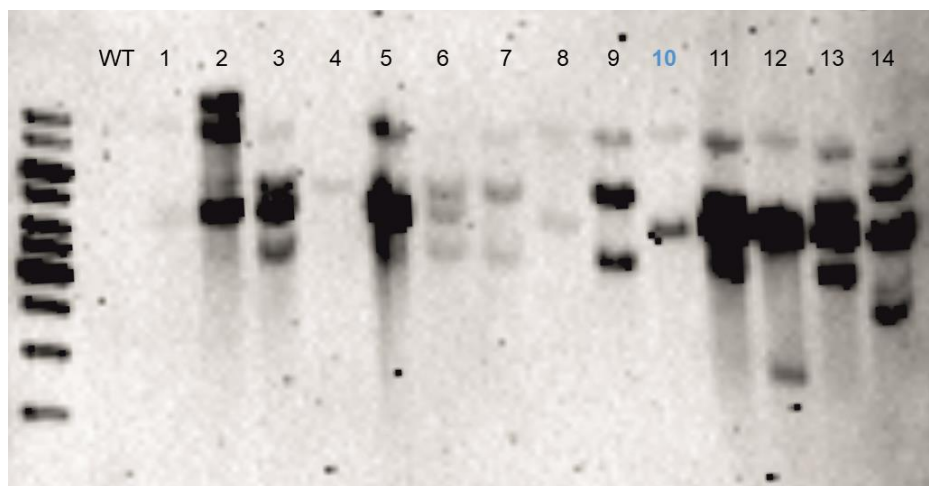


**Fig. S1D) Southern blot analysis of the *U. maydis*  $\Delta Hap2$  complementation strain.** Genomic DNA was extracted from the indicated strains, digested with the HindIII restriction enzymes, and separated on a 0.9% agarose gel. A DNA probe specific to the *ip* locus was hybridized to the southern blot, which was performed according to the standard protocol. Lanes 1 contains a molecular weight marker (unlabeled). Lanes 2-15 correspond to the following strains: Lane 2, SG200 strain (WT); Lanes 3-15, different transformants of  $\Delta Hap2$  complementation strains. The ladder sizes of the bands are indicated on the left. The expected sizes for the *ip* locus are written on the figure. Colonies with a single integration based on band size is bolded and colored with Blue.

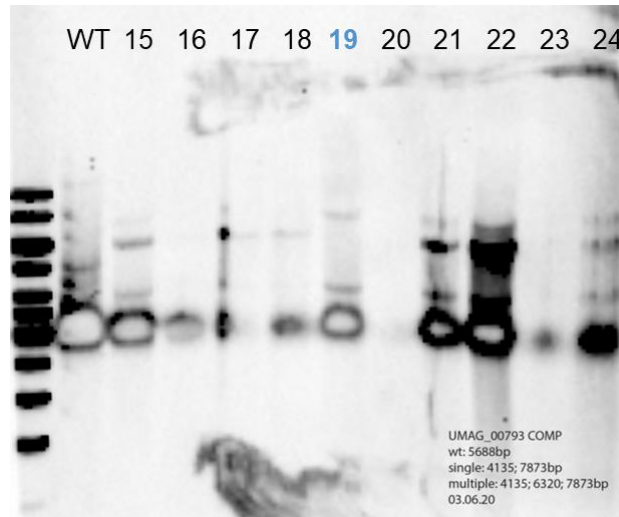


**Fig. S1E) Southern blot analysis of the *U. maydis*  $\Delta Hap3$  complementation strain.** Genomic DNA was extracted from the indicated strains, digested with the HindIII restriction enzymes, and separated on a 0.9% agarose gel. A DNA probe specific to the *ip* locus was hybridized to the southern blot, which was performed according to the standard protocol. Lanes 1 contains a molecular weight marker (unlabeled). Lanes 2-11 correspond to the following strains: Lane 2, SG200 strain (WT); Lanes 3-11, different transformants of  $\Delta Hap3$  complementation strains. The ladder sizes of the bands are indicated on the left. The expected sizes for the *ip* locus are written on the figure. Colonies with a single integration based on band size is bolded and colored with Blue.

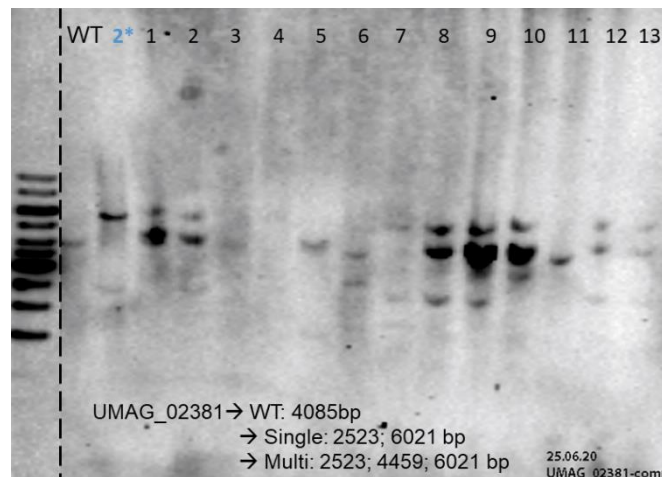


**Fig. S1F) Southern blot analysis of the *U. maydis*  $\Delta umag\_02381$  complementation strain.** Genomic DNA was extracted from the indicated strains, digested with the EcoRV and HindIII restriction enzymes, and separated on a 0.9% agarose gel. A DNA probe specific to the *ip* locus was hybridized to the southern blot, which was performed according to the standard protocol. Lanes 1 contains a molecular weight marker (unlabeled). Lanes 2-15 correspond to the following strains: Lane 2, SG200 strain (WT); Lanes 3-15, different transformants of  $\Delta umag\_02381$  complementation strains. The ladder sizes of the bands are indicated on the left. The expected sizes for the *ip* locus are written on the figure. Colonies with a single integration based on band size is bolded and colored with Blue.

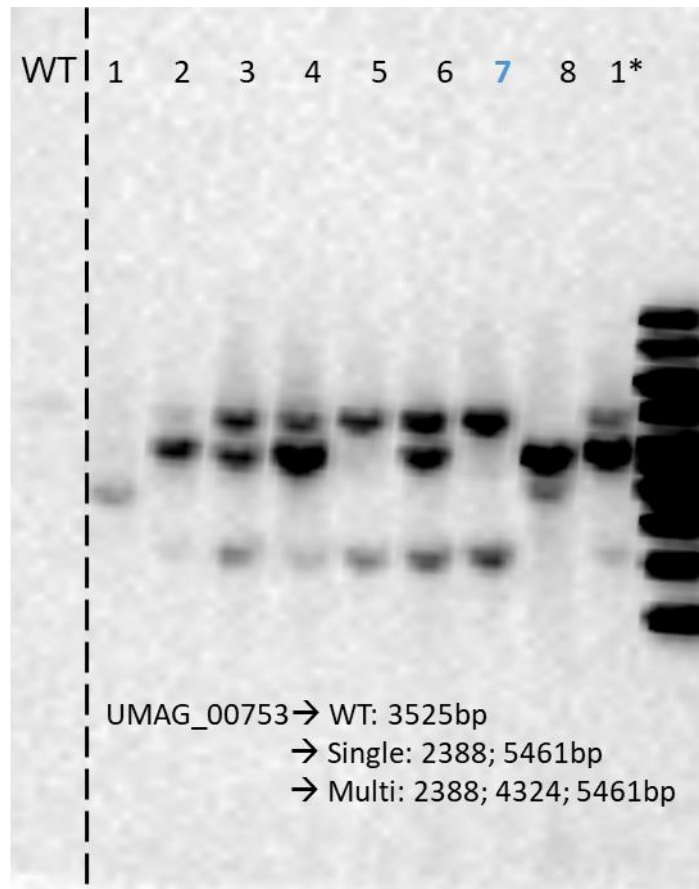


**Fig. S1G) Southern blot analysis of the *U. maydis*  $\Delta$ *umag\_00753* complementation strain.** Genomic DNA was extracted from the indicated strains, digested with the EcoRV and PvuII restriction enzymes, and separated on a 0.9% agarose gel. A DNA probe specific to the *ip* locus was hybridized to the southern blot, which was performed according to standard protocols. Lanes 11 contains a molecular weight marker (unlabeled). Lanes 1-9 correspond to the following strains: Lane 1, SG200 strain (WT); Lanes 1-8, different transformants of  $\Delta$ *umag\_00753* complementation strains. The ladder sizes of the bands are indicated on the left. The expected sizes for the *ip* locus are written on the figure. Colonies with a single integration based on band size is bolded and colored with Blue.

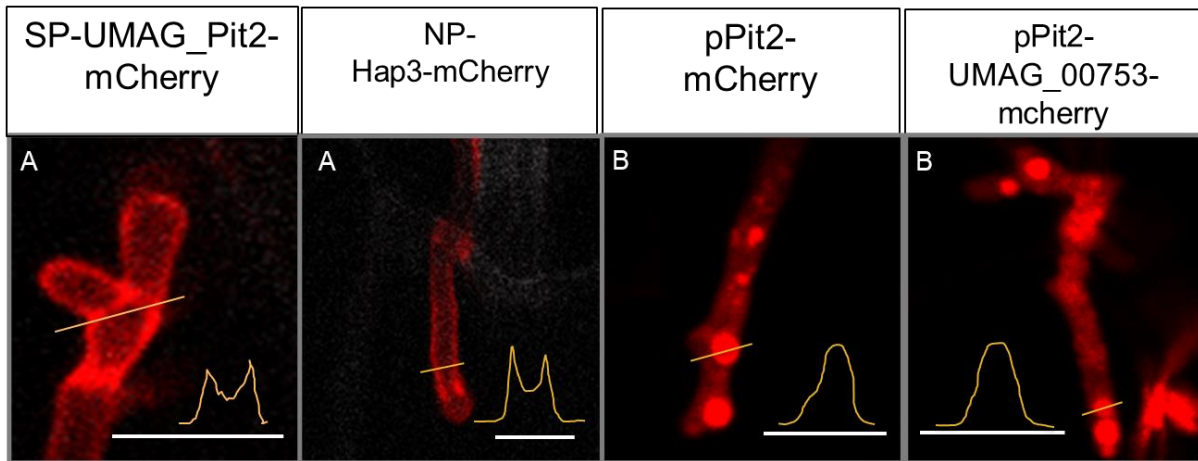


**Fig. S1H) UMAG\_00753 is not secreted, but Hap3 is a secreted effector. A)** *U. maydis* hyphae expressing Pit2-mCherry at 2dpi **B)** *U. maydis* hyphae expressing Hap3-mCherry at 2dpi. **C)** *U. maydis* hyphae expressing cytoplasmic Pit2-mCherry at 2dpi. **D)** *U. maydis* hyphae expressing Pit2-mCherry at 2dpi. The plots are the mCherry intensities measured from the solid lines indicated in the photos. The experiments were repeated two times. Representative photos are shown. Scale bar = 50 $\mu$ m.

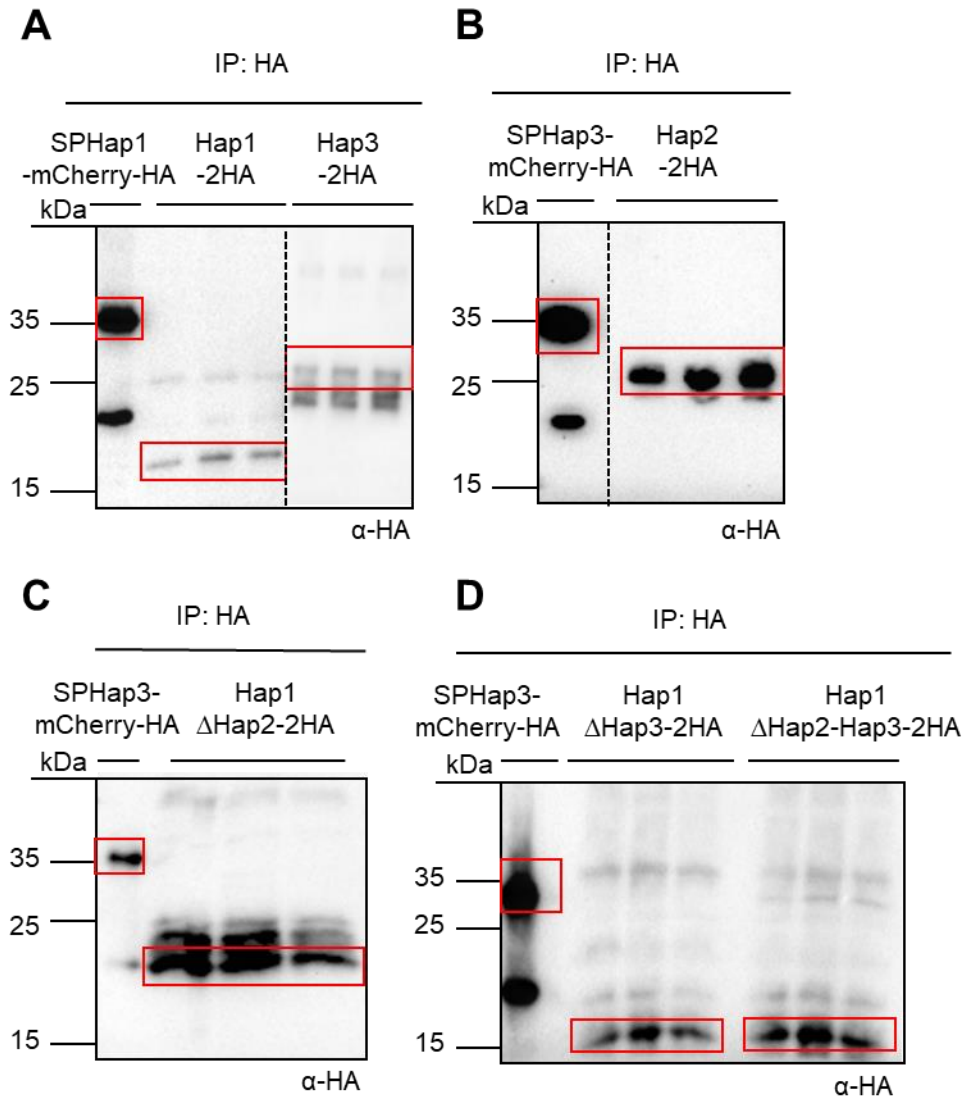


**Fig. S2) Expression of effector proteins sent for IP/MS-MS to identify interacting effector and host target(s).** **A**) 7-day-old maize plants were infected with SG200-p*Pit2*::*SPHap1*-mCherry-HA (control), SG200-p*Pit2*::*Hap1*-mCherry-HA, and SG200-p*Pit2*::*Hap3*-mCherry-HA. **B**) 7-day-old maize plants were infected with SG200-p*Pit2*::*SPHap1*-mCherry-HA (control) and SG200-p*Pit2*::*Hap2*-mCherry-HA. **C**) 7-day-old maize plants were infected with SG200-p*Pit2*::*SPHap1*-mCherry-HA (control) and SG200 $\Delta$ Hap1-p*Pit2*::*Hap1*-2xHA $\Delta$ Hap2. **D**) SG200-p*Pit2*::*SPHap1*-mCherry-HA (control), SG200 $\Delta$ Hap1-p*Pit2*::*Hap1*-2xHA $\Delta$ Hap3 and SG200 $\Delta$ Hap1-p*Pit2*::*Hap1*-2xHA $\Delta$ Hap2-3. Infected leaves were collected at 3 dpi. Total proteins were extracted and immunoprecipitated using HA magnetic beads. Western blot analysis was performed using an anti-HA antibody.

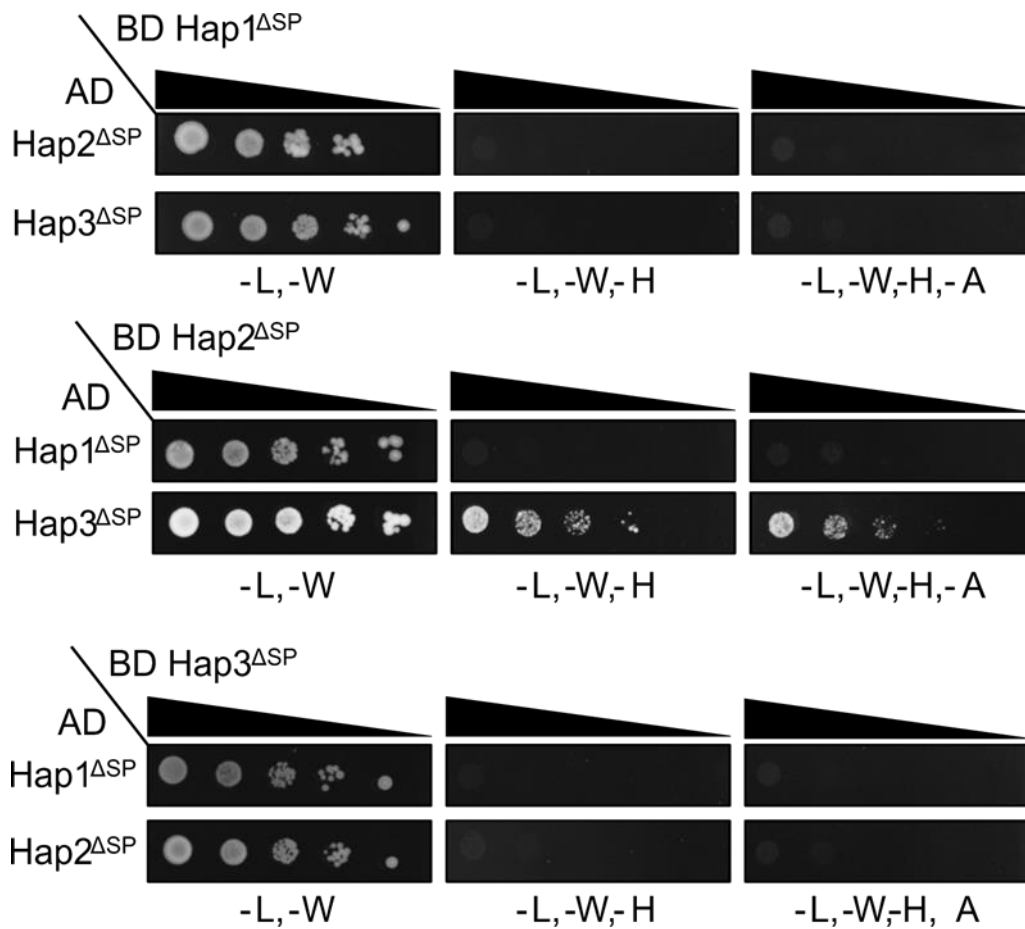


**Fig. S3) Hap2 and Hap3 interact in Yeast-two-hybrid assay.** Yeast cells were co-transformed with plasmids carrying pGBKT7-Hap1<sup>ΔSP</sup>, -Hap2<sup>ΔSP</sup>, or -Hap2<sup>ΔSP</sup> with pGADT7-Hap1<sup>ΔSP</sup>, -Hap2<sup>ΔSP</sup>, or -Hap3<sup>ΔSP</sup>. The resulting transformants were serially diluted ten times and plated onto nutrition-deficient synthetic defined (SD) media, SD/-Leu/-Trp, SD/-Leu/-Trp/-His, or SD/-Leu/-Trp/-His/-Ade. The plates were incubated for 5 days and images were captured. The experiment was repeated three times.



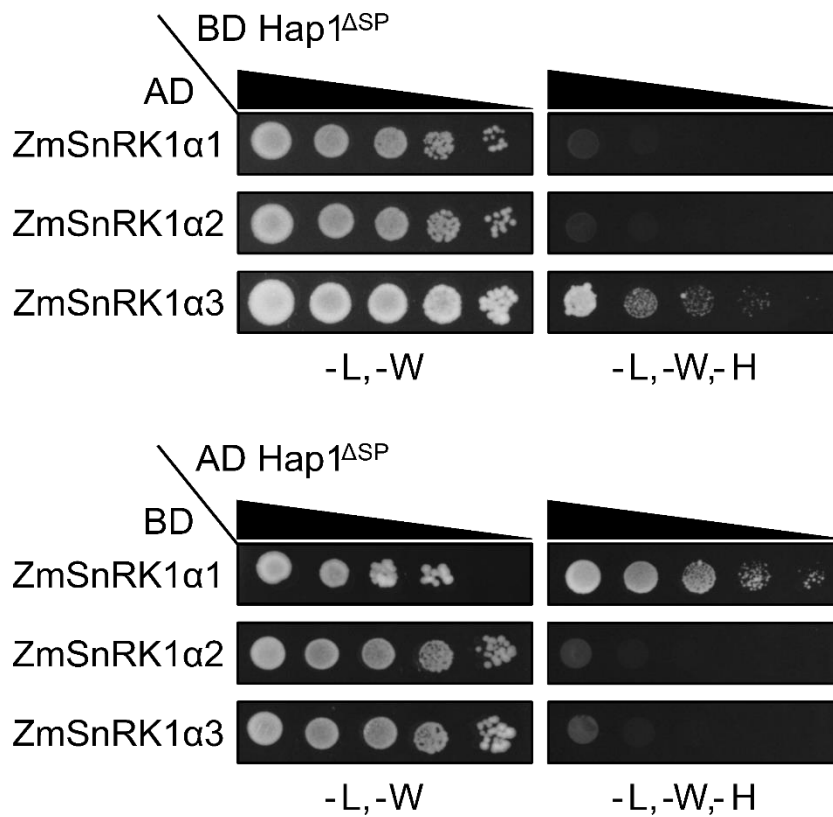


**Fig. S4) ZmSnRK1 $\alpha$ 1 and ZmSnRK1 $\alpha$ 3 interact weakly with Hap1 in Yeast-two-hybrid assay.** Yeast cells were co-transformed with plasmids carrying pGBKT7-Hap1 $\Delta$ SP with pGADT7-ZmSnRK1 $\alpha$ 1, -ZmSnRK1 $\alpha$ 1, or -ZmSnRK1 $\alpha$ 1. The resulting transformants were serially diluted ten times and plated onto nutrition-deficient synthetic defined (SD) media, SD/-Leu/-Trp, and SD/-Leu/-Trp/-His. The plates were incubated for 5 days and images were captured. The experiment was repeated three times.

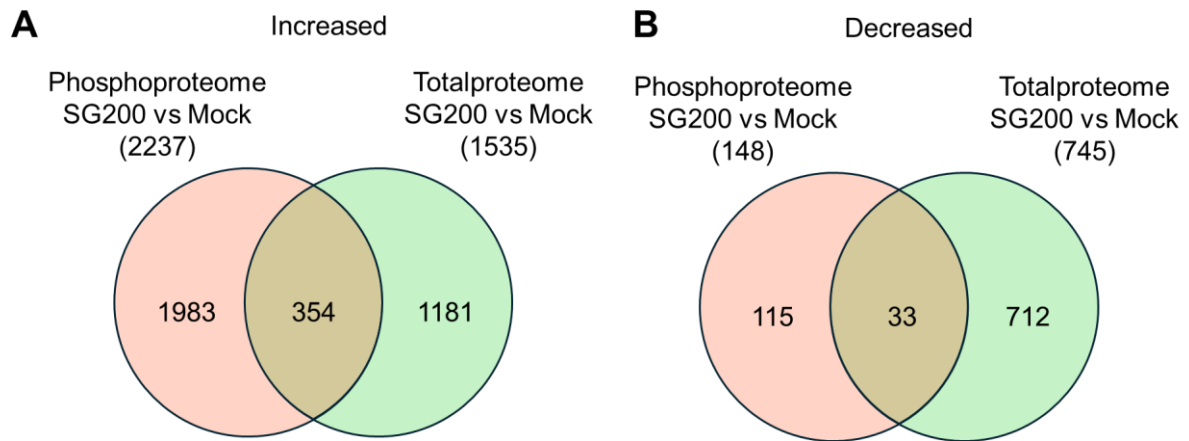


**Fig. S5) Venn diagram analysis showing the unique and overlapping proteins between phosphoproteomics and total proteomics in SG200 compared to mock. A)** Comparison of proteins with increased phosphorylation to proteins that are enriched in SG200 relative to mock. **B)** Comparison of proteins with decreased phosphorylation to proteins that are depleted in SG200 relative to mock. The terms 'increased', 'decreased', 'enriched', and 'depleted' describe relative changes in SG200 compared to the mock condition.

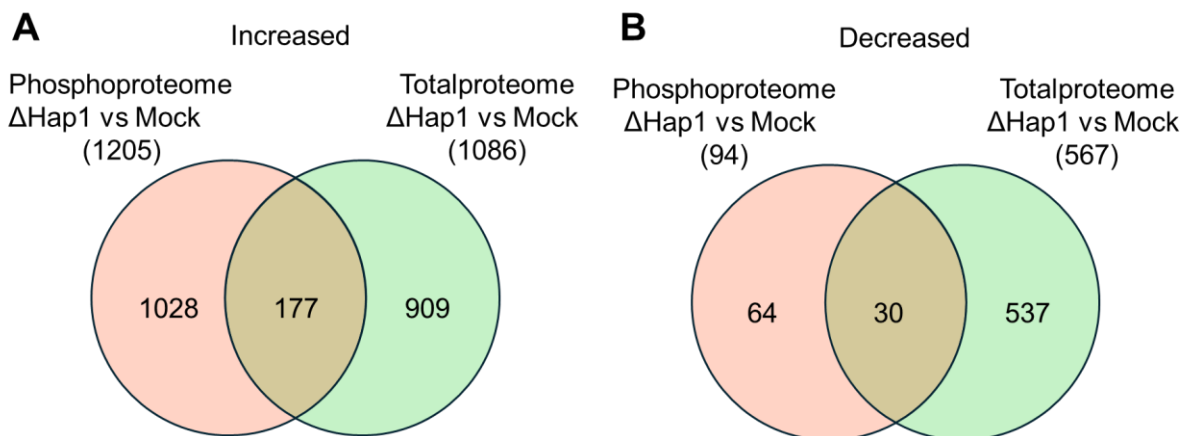


**Fig. S6) Venn diagram analysis showing the unique and overlapping proteins between phosphoproteomics and total proteomics in ΔHap1 compared to mock. A)** Comparison of proteins with increased phosphorylation to proteins that are enriched in ΔHap1 relative to mock. **B)** Comparison of proteins with decreased phosphorylation to proteins that are depleted in ΔHap1 relative to mock. The terms 'increased', 'decreased', 'enriched', and 'depleted' describe relative changes in ΔHap1 compared to the mock condition.

**Table S1) Effector proteins detected in Hap1 IP-MS analysis**

SP= signal peptide; TPMmax= the highest Transcripts Per Million, representing the highest expression level of *U. maydis* effector candidates observed at plant associated time points throughout the growth stages (Lanver et al., 2018). EffectorP\_Fungi 3.0 was used to predict whether fungal effectors are apoplastic or cytoplasmic with a minimal change in already characterized effector proteins. Dual-localization is predicted for both cytoplasmic (cytoplasmic/apoplastic) and apoplastic (apoplastic/cytoplasmic) effectors. was predicted using InterProScan.

Annotation	Protein ID	EffectorP_Fungi 3.0	TPMmax	Domain	SP
Hypothetical protein	UMAG_01501	Non-effector	0.5 dpi	Y	Y
Hypothetical protein	UMAG_04641	Non-effector	0.5 dpi	N	Y
Septin3	UMAG_03449	Cytoplasmic effector	1 dpi	Y	N
Putative cyclophilin b	UMAG_01018	Cytoplasmic/apoplastic effector	2 dpi	Y	Y
Hypothetical protein	UMAG_05352	Cytoplasmic effector	2 dpi	Y	Y
Putative disulfide-isomerase precursor	UMAG_01802	Cytoplasmic effector	2 dpi	Y	Y
Tin3	UMAG_10556	Cytoplasmic effector	2 dpi	N	Y
Hap3	UMAG_00793	Cytoplasmic/apoplastic effector	2 dpi	N	Y
Hap2	UMAG_00792	Apoplastic/cytoplasmic effector	2 dpi	N	Y
Hypothetical protein	UMAG_10823	Apoplastic/cytoplasmic effector	2 dpi	N	Y
Hypothetical protein	UMAG_01820	Apoplastic/cytoplasmic effector	2 dpi	N	Y
Cce1	UMAG_12197	Apoplastic effector	2 dpi	N	Y
Hypothetical protein	UMAG_03201	Apoplastic effector	2 dpi	N	Y
Hypothetical protein	UMAG_02474	Apoplastic effector	2 dpi	N	Y
Hypothetical protein	UMAG_01301	Apoplastic effector	2 dpi	N	Y
Egl3	UMAG_04816	Apoplastic effector	2 dpi	N	Y
Egl1	UMAG_06332	Apoplastic effector	2 dpi	N	Y
Putative exochitinase	UMAG_00695	Non-effector	2 dpi	Y	Y
Hypothetical protein	UMAG_01512	Non-effector	2 dpi	Y	Y
Metal ion binding	UMAG_01130	Non-effector	2 dpi	Y	Y
Stp1	UMAG_02475	Apoplastic effector	2 dpi	N	Y
Hypothetical protein	UMAG_05173	Non-effector	2 dpi	Y	Y
Hypothetical protein	UMAG_00628	Non-effector	2 dpi	N	Y
Hypothetical protein	UMAG_12216	Non-effector	2 dpi	N	Y
Hypothetical protein	UMAG_05929	Cytoplasmic effector	4 dpi	N	Y
Hypothetical protein	UMAG_10418	Apoplastic effector	4 dpi	N	Y
Hypothetical protein	UMAG_01977	Non-effector	4 dpi	N	Y
Hypothetical protein	UMAG_05928	Non-effector	4 dpi	N	Y
Hypothetical protein	UMAG_12217	Non-effector	4 dpi	N	Y
Putative disulfate isomerase	UMAG_10156	Non-effector	2/6 dpi	Y	Y
Afu3	UMAG_04309	Non-effector	2/12 dpi	Y	Y
Hypothetical protein	UMAG_11763	Non-effector	12 dpi	Y	Y

**Table S2) Effector proteins detected in Hap2 IP-MS analysis**

SP= signal peptide; TPMmax= the highest Transcripts Per Million, representing the highest expression level of *U. maydis* effector candidates observed at plant associated time points throughout the growth stages (Lanver et al., 2018). EffectorP\_Fungi 3.0 was used to predict whether fungal effectors are apoplastic or cytoplasmic with a minimal change in already characterized effector proteins. Dual-localization is predicted for both cytoplasmic (cytoplasmic/apoplastic) and apoplastic (apoplastic/cytoplasmic) effectors. was predicted using InterProScan.

Annotation	Protein ID	EffectorP_Fungi 3.0	TPMmax	Domain	SP
Hypothetical protein	UMAG_01690	Cytoplasmic effector	2 dpi	N	Y
Hap3	UMAG_00793	Cytoplasmic/apoplastic effector	2 dpi	N	Y
Hap1	UMAG_02473	Cytoplasmic effector	2 dpi	N	Y
Mig2-2	UMAG_06179	Cytoplasmic effector	4 dpi	N	Y

**Table S3) Effector proteins detected in Hap3 IP-MS analysis**

SP= signal peptide; TPMmax= the highest Transcripts Per Million, representing the highest expression level of *U. maydis* effector candidates observed at plant associated time points throughout the growth stages (Lanver et al., 2018). EffectorP\_Fungi 3.0 was used to predict whether fungal effectors are apoplastic or cytoplasmic with a minimal change in already characterized effector proteins. Dual-localization is predicted for both cytoplasmic (cytoplasmic/apoplastic) and apoplastic (apoplastic/cytoplasmic) effectors. was predicted using InterProScan.

Annotation	Protein ID	EffectorP_Fungi 3.0	TPMmax	Domain	SP
Hypothetical protein	UMAG_01690	Cytoplasmic effector	2 dpi	N	Y
Hap1	UMAG_02473	Cytoplasmic effector	2 dpi	N	Y
Rsp3	UMAG_03274	Apoplastic effector	2 dpi	N	Y
Egl3	UMAG_04816	Apoplastic effector	2 dpi	N	Y
Hypothetical protein	UMAG_03201	Apoplastic effector	2 dpi	N	Y
Hypothetical protein	UMAG_05528	Non-effector	2 dpi	N	Y
Hypothetical protein	UMAG_10030	Non-effector	2 dpi	N	Y
Mig2-2	UMAG_06179	Cytoplasmic effector	4 dpi	N	Y
Hypothetical protein	UMAG_05929	Cytoplasmic effector	4 dpi	N	Y
Hypothetical protein	UMAG_12217	Non-effector	4 dpi	N	Y
Hypothetical protein	UMAG_03105	Cytoplasmic effector	2/6 dpi	N	Y
Hypothetical protein	UMAG_05495	Cytoplasmic effector	6 dpi	N	Y
Hypothetical protein	UMAG_00538	Non-effector	12 dpi	N	Y

# Erklärung zur Dissertation

gemäß der Promotionsordnung vom 12. März 2020

Hiermit versichere ich an Eides statt, dass ich die vorliegende Dissertation selbstständig und ohne die Benutzung anderer als der angegebenen Hilfsmittel und Literatur angefertigt habe. Alle Stellen, die wörtlich oder sinngemäß aus veröffentlichten und nicht veröffentlichten Werken dem Wortlaut oder dem Sinn nach entnommen wurden, sind als solche kenntlich gemacht. Ich versichere an Eides statt, dass diese Dissertation noch keiner anderen Fakultät oder Universität zur Prüfung vorgelegen hat; dass sie - abgesehen von unten angegebenen Teilpublikationen und eingebundenen Artikeln und Manuskripten - noch nicht veröffentlicht worden ist sowie, dass ich eine Veröffentlichung der Dissertation vor Abschluss der Promotion nicht ohne Genehmigung des Promotionsausschusses vornehmen werde. Die Bestimmungen dieser Ordnung sind mir bekannt. Darüber hinaus erkläre ich hiermit, dass ich die Ordnung zur Sicherung guter wissenschaftlicher Praxis und zum Umgang mit wissenschaftlichem Fehlverhalten der Universität zu Köln gelesen und sie bei der Durchführung der Dissertation zugrundeliegenden Arbeiten und der schriftlich verfassten Dissertation beachtet habe und verpflichte mich hiermit, die dort genannten Vorgaben bei allen wissenschaftlichen Tätigkeiten zu beachten und umzusetzen. Ich versichere, dass die eingereichte elektronische Fassung der eingereichten Druckfassung vollständig entspricht.

Datum: 06.05.2024

Unterschrift:

## **Delimitation of own contribution**

The results presented in this study were obtained independently by me without any assistance other than that stated here. The conception of the experiments was done in collaboration with my supervisor Prof. Dr. Gunther Döhlemann. The experimental contributions of others who participated in this study are listed below:

Dr. Malaika Ebert generated plasmid of pCas9HF1\_pU6::sgRNA\_Hap3 and *U. maydis* strain of  $\Delta Hap3$

Dr. Selma Schurack generated plasmid of pCas9HF1\_pU6::sgRNA\_UMAG\_00753 as a part of her Doctoral thesis.

Dr. Hirofumi Nakagami, Sara Christina Stolze, and Anne Harzen performed liquid chromatography-mass spectrometry/ mass spectrometry protein identification for proteomics and phosphoproteomics and original raw data analysis. (Protein Mass Spectrometry Facility, Max-Planck Institute for Plant Breeding Research, Cologne, Germany).

Dr. Georgios Saridis analyzed the raw RNA-Seq data and produced the count files for differential gene expression analyses, providing the final list of DEGs.

Mrs. Ute Myer and Mr. Muelhoefer assisted with grinding and processing samples for enzymatic quantification of starch and soluble sugars.

## Acknowledgement

First of all, I wish to express my profound gratitude to my supervisor, Prof. Dr. Gunther Döhlemann, for providing me with the freedom to pursue my research interests and for his invaluable support and guidance throughout my PhD journey. Thank you, Gunther, for your mentorship and trust, especially during moments of hardship. Your expertise and insights have been crucial in shaping both my research and my development as a scholar.

I am thankful to my thesis advisory committee members, Prof. Dr. Martin Hülkamp and Dr. Takaki Maekawa, for their insightful scientific discussions and feedback throughout my PhD journey. My gratitude extends to Prof. Dr. Bart Thomma for serving as the second reviewer on my thesis defense committee and to Prof. Dr. Kay Hoffmann for chairing my thesis defense committee. I am also thankful to Dr. Isabell Witt and GSfBS for their support and organizing constructive and beneficial workshops. I would like to thank Dr. Hirofumi Nakagami, Dr. Sara Christina Stolze, and Anne Harzen for their indispensable support in proteomics and phosphoproteomics performed in my study. Their expertise was crucial to the success of my studies.

My heartfelt thanks go to all my colleagues from AG Döhlemann, with whom I have spent the majority of my PhD journey. Special thanks to Bilal, Wei, and Weiliang for their countless contributions to project discussions and experimental suggestions, which were especially helpful during challenging times. I am thankful to Sina for her friendship, encouragement, and the many pleasant conversations we've shared. I am also thankful to Luyao for the valuable project discussion and for the late nights we spent together in the lab working on experiments. Our random conversations and spontaneous dinners added much enjoyment to my time in the lab. I am grateful to have met both of you, Sina and Luyao during my PhD. The friendship we shared will forever hold a special place in my heart. I am thankful to my lab mates Philipp and Laura for listening to my lighthearted grumbles and for our meaningful conversations, both scientific and beyond. Thanks to Maurice for the enriching conversations, we've shared. From our days in Bonn to Oxford and finally in Köln, our paths crossing has been truly remarkable. I wish you all the best and great successes in the future. I am also thankful to Janina for her kindness and invaluable support in the lab, as well as for her company while waiting for Gunther's availability. The time we spent together in Asilomar and San Francisco, including our memorable journey through the infamous Tenderloin, will be cherished in my memories. I would like to thank Daniel and Georgios for their support in bioinformatics and all the fun

conversations in the lab. Thanks to Nina, Rutchi, Zarah, and Niklas for nice casual conversations. Thanks to Andrea and Anna for being my supportive next-door neighbor and staying as a fellow PhD student with nice random chats. I wish you the best for your family. I am also grateful to Gudrun, Johana, Ute, Rapha and Jan for all their help and support throughout my time in the lab.

I would like to express my gratitude to the friends I met in Germany, who have made my time here truly memorable. I especially want to thank Vadim for his support, encouragement, and companionship during our trips to sushi restaurants, as well as for the challenge of selecting from countless identical selfies for his social media. I would like to thank Nino for his great support throughout the ups and downs of my PhD years. Nino, I really appreciate your understanding and patience when lab experiments kept me late and your positive affirmations. I'm grateful for your efforts to travel to Cologne every weekend since we've met, even though it meant spending endless hours on trains. I'm lucky to have you in my life. Finally, I wish to extend a heartfelt thanks to my family. Mom and Dad, your great support for every decision I've made and your encouragement to always strive for better have deeply shaped who I am. My journeys abroad and education, from the Philippines to the USA, England, and Germany, would not have been possible without your enduring support and trust. Thank you for everything and I love you. My brother, Ki Sang, thanks for always being there for me and for the laughs over the phone when I needed a pick-me-up. I miss you a lot and see you soon!



## Curriculum Vitae

Yoon Joo Lee

born on 20. April 1996 in Incheon, Korea

Education	<p>09/2019-05/2024      PhD candidate <i>Universität zu Köln, Köln, Germany</i></p> <p>PhD thesis:</p> <ul style="list-style-type: none"> <li>• “Characterization of hypertrophy-related effectors in <i>Ustilago maydis</i> induced tumor formation”</li> </ul> <p>Supervisor: Prof. Dr. Gunther Doehlemann</p> <p>09/2017-07/2019      MS in Plant Sciences <i>Rheinische Friedrich-Wilhelms-Universität Bonn, Bonn, Germany</i></p> <p>Master thesis:</p> <ul style="list-style-type: none"> <li>• “Investigate the Broader Role of BGAL in Plant Immunity”</li> </ul> <p>Supervisor: Prof. Dr. Renier van der Hoorn at Oxford University</p> <p>08/2015-05/2017      BS in Plant Sciences, (Genetics and Breeding Concentration) <i>Cornell University, College of Agriculture and Life Sciences, Ithaca, NY</i></p> <p>09/2013-05/2015      AS in Biotechnology <i>Jamestown Community College, State University of New York, Jamestown, NY</i></p>
Honors/ Awards/ Scholarship	<p>4 years of Dean's list Phi Theta Kappa Honor Society Penn York American Chemical Society Award Sophomore Chemistry Award CALS Alumni Association Grant Erasmus+ scholarship</p>
Publications	<p>Oekmen B, Jaeger E, Schilling L, Finke N, Klemd A, <b>Lee YJ</b>, Wemhöner R, Pauly M, Neumann U, Doehlemann G. A conserved enzyme of smut fungi facilitates cell-to-cell extension in the plant bundle sheath. <i>Nat Commun.</i> 2022 Oct 12;13(1):6003. doi: 10.1038/s41467-022-33815-7.</p> <p>Buscaill P, Sanguankiattichai N, <b>Lee YJ</b>, Kourelis J, Preston G, van der Hoorn RAL. Agromonas: a rapid disease assay for <i>Pseudomonas syringae</i> growth in agroinfiltrated leaves. <i>Plant J.</i> 2021 Feb;105(3):831-840. doi: 10.1111/tpj.15056.</p>